

DISSERTATION

FORCE FIELD MODELS IN HALOGEN BONDING

Submitted by

Mardi Marie Billman

Department of Chemistry

In partial fulfillment of the requirements

For the Degree of Doctor of Philosophy

Colorado State University

Fort Collins, Colorado

Spring 2019

Doctoral Committee:

Advisor: Anthony Rappé

Amy Prieto
Stephen Strauss
Pui Shing Ho

Copyright by Mardi Marie Billman 2019

All Rights Reserved

ABSTRACT

FORCE FIELD MODELS IN HALOGEN BONDING

Halogen bonding schemes have been proposed to replace those of hydrogen bonding in biomolecules, such as proteins and DNA, because halogens can counter-intuitively attract a Lewis base. Unlike hydrogen bonding, halogen bonding strength is dependent on a number of factors, such as electrostatics, exchange repulsion, dispersion, and charge transfer. Understanding the underlying energetic components of halogen bonding at a fundamental level, defined herein to mean the subatomic level, is necessary to utilize halogen bonding in a biomolecular context. Our aspiration throughout this research has not been to quantify the strength of the underlying interactions. Instead, it has been to identify and explain the interactions as dependent on the uneven distribution of valence electrons inherent to the halogens, and apply our findings to developing force field models.

Chapter 2: The Cambridge Structural Database was used to show that crystals of halogen bonding structures exhibit a distance-angle correlation. The correlation is similar to that present in crystals of hydrogen bonding structures, though with a diminished angular dependence beyond the sum of the van der Waals radii. Halogen bonding strength, approximated by bonding frequency, was found to be inversely proportional to non-bonding distance. The shape of the distance-angle correlation would continue to be studied in Chapters 3–4.

Chapter 3: An angular dependence was illustrated in Chapter 2 at short non-bonding distances; the interaction energy must have been dependent on anisotropic, short-range components such as electrostatics and exchange repulsion. The electronic structure of halogen-containing

compounds was studied independently as a function of distance and then as a function of angle. Electron-withdrawing and -donating moieties were used to observe the dependence of electrostatics, exchange repulsion, and dispersion on the polarizability of the halogen. Both substituent and periodic trends were observed, where halogen bonding strength increased with σ -hole and aspherical shape of the halogen atom.

Chapter 4: Atomic halogens were used to study the anisotropic electrostatic potential and exchange repulsion directly, without influence of the substituent groups present in Chapter 3. Our hypothesis was that theoretical models of the electrostatic potential and exchange repulsion would display an angular dependence because of the inherent $s^2p_x^2p_y^2p_z^1$ valence electron configuration. The halogen atoms were defined as a linear combination of core and valence s and p wavefunctions, fitted simultaneously to Hartree-Fock calculations of the orbital shapes, electrostatic potential, and exchange repulsion. The shape of the exchange repulsion model as a function of distance and angle, in conjunction with dispersion, could explain the distance-angle correlation of experimental and theoretical halogen bonding. The electrostatic potential, associated with the σ -hole model of halogen bonding, did not vanish at long distance. Instead, it was found that the presence of a dipole-dipole interaction was necessary to recreate experimental results.

Chapter 5: The purpose of this study was to begin development on a multimolecular system to model solvent interactions with halogen bonding structures. We found that halogen bonding trimer systems have a cooperative non-bonding energy due to the electrostatics, dispersion, and partial charge transfer from Lewis base to halogen. The polarization of the model hydrogen-bond enhanced halogen bonds increased the electrostatic attraction within the trimer systems. The charge transfer stabilized the structure and lead to decrease in bond distances relative to the corresponding dimers. Because attractive dispersion interactions are inversely

dependent on interaction distance, the overall dispersive attraction increased in the trimer system as well.

Chapter 6: A novel model was created to examine the process of charge transfer as a function of distance in halogen bonding dimers. Two molecular models of borane with ammonia and diatomic bromine with ammonia were developed and fitted to computational calculations. The results of the models showed that the cross-term of the charge transfer interaction between reactant and product components contributes to the attraction between Lewis acids and bases.

ACKNOWLEDGEMENTS

First and foremost, I would like to thank Dr. Anthony Rappé for his constant support and guidance through the years. I can say with confidence that if it were not for his persistent encouragement, I would not have received my doctorate. In addition, I would like to thank my thesis committee: Dr. Amy Prieto, Dr. Rick Finke, Dr. Steven Strauss, and Dr. Shing Ho. They gave me incredible advice and unwarranted patience, particularly in my third year when I felt myself slipping. To all of my peers in graduate school, especially Joseph Allison, Collette and Jake Nite, and Jake Anderson. We were all in this together, though I am sad to admit that “Movie Fridays” never became a thing. Finally, to those who set the bar for my career as a professor, Dr. Brian Johnson, Dr. T. Nicholas Jones, Dr. Bret Benesh, Dr. Kris Nairn, and Dr. Richard Scott, you taught me more than chemistry and calculus. You taught me perseverance, patience, and how to harness my passions; for that I am eternally grateful.

I would also like to acknowledge Marty Billman and Karen Bird, my parents, along with Bee Billman, my sibling, whom has pioneered our incessant journey of self-discovery; Shannon O’Neill, my best friend, whom always picked up the phone when I needed to vent; Grant Backes, whom joined me in most of my math classes and pushed the boundaries of my personal philosophies; and Katherine Sheehan, whom came to Colorado with me looking for adventure. Life has led us all to strange and wonderful places. Last but not least, thank you to the online content creators I subscribe to, notably CinnamonToastKen, CreepsMcPasta, Cryaotic, the Game Grumps, Markiplier, PeanutButterGamer (and the rest of Normal Boots), the Scary Game Squad, and SpaceHamster (and the rest of Hidden Block); though you don’t know me, you kept me sane in the darkest of times. A million times to all those mentioned and beyond, thank you.

TABLE OF CONTENTS

Abstract.....	ii
Acknowledgements.....	v
CHAPTER 1: INTRODUCTION.....	1
The History of Halogen Bonding.....	2
The σ -Hole Model.....	4
Force Field Models of Non-Bonding Interactions.....	8
I. The AMBER Force Field and PEP Model.....	9
II. The Force Field for Biological Halogen Bonds.....	12
Thesis Overview.....	16
REFERENCES.....	18
CHAPTER 2: HALOGEN BONDING IN CRYSTAL STRUCTURES.....	22
Experimental Evidence for the Geometry of Halogen Bonding.....	25
Analysis of the Experimental Angular Dependence of Halogen Bonding.....	30
REFERENCES.....	34
CHAPTER 3: DIMER SYSTEMS.....	37
Electronic Structure Studies as a Function of Distance.....	40
Electronic Structure Studies as a Function of Angle.....	51
Electronic Structure Studies as a Function of Distance and Angle.....	59
Illustrating the Dispersive Component of Halogen Bonding.....	61
REFERENCES.....	64
CHAPTER 4: MODEL HALOGEN BONDING VIA ORBITAL OVERLAP.....	67
Model Potential Studies.....	67

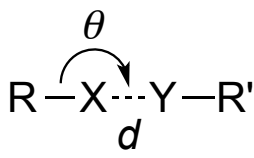
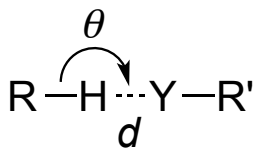
I. The Heitler-London Model.....	68
II. Modeling the Exchange Repulsion of a Halogen Atom.....	74
III. Modeling the Electrostatics of a Halogen Atom.....	83
Further Analysis of the Exchange Repulsion and Electrostatic Potential Models.....	92
REFERENCES.....	96
CHAPTER 5: TRIMER SYSTEMS.....	98
Cooperativity of Model Hydrogen-Bond Enhanced Halogen Bonds.....	101
Electronic Structure Studies of Model Hydrogen-Bond Enhanced Halogen Bonds.....	102
Charge Transfer in Model Hydrogen-Bond Enhanced Halogen Bonds.....	107
Distinguishing the Electron Correlation.....	112
References.....	116
CHAPTER 6: MODEL HALOGEN BONDING VIA CHARGE TRANSFER.....	118
Model Charge Transfer Between Borane and Ammonia.....	120
Model Charge Transfer Between Bromine and Ammonia.....	125
REFERENCES.....	132
CHAPTER 7: CONCLUSION.....	134
Future Work.....	137
REFERENCES.....	139
APPENDIX 1.....	141
REFERENCES.....	146
APPENDIX 2.....	148
APPENDIX 3.....	151
APPENDIX 4.....	157
APPENDIX 5.....	191

REFERENCES.....	194
APPENDIX 6.....	195

CHAPTER 1: INTRODUCTION

Halogen bonding has been incorporated into supramolecular and biomolecular chemistry, specifically photovoltaics, organic magnets, anion transport, protein and ligand modification, and drug design, since the turn of the 21st century.¹⁻⁴ Halogen bonding can be concisely described as a counterintuitive attraction between a halogen and Lewis base, such as oxygen or nitrogen.^{3,5-13} The phenomenon is similar to hydrogen bonding geometrically and energetically, except that the strength of a halogen bond is reported to increase with the polarizability of the atom from chlorine to iodine.^{1,14-17} The interaction distance (d) is shorter than the sum of the species' van der Waals radii (Σr_{vdW}), and the bond angle (θ) is approximately 180° (Table 1.1).^{13,17-23} The binding affinity and selectivity of halogen bonding can be more finely tuned than hydrogen bonding due to these geometric factors,^{3,5-13,24-30} whereas the strength of hydrogen bonding increases with charge separation.^{31,32}

Table 1.1. The geometric definitions of halogen and hydrogen bonding.^{14,32} The bond distance between atoms X and Y is less than the sum of the van der Waals radii, and the bond angle is approximately 180°. The Lewis acid (X or H) is covalently bound to some group (R), and the Lewis base (Y) is covalently bound to some group (R').

Structural Geometry	d (Å)	θ (°)
	Shorter than the sum of the X—Y van der Waals radii	155-180
	Generally shorter than the sum of the H—Y van der Waals radii	110-180

The History of Halogen Bonding

The earliest known report of what would come to be known as a halogen bond was published by J. Colin in 1814,² but the initial discovery is often credited to F. Guthrie for his work in 1863.^{2,33,34} Guthrie reported that colorless solutions of iodine and ammonia in a 1:1 mixture changed to dark brown, signifying a chemical change,^{33–35} and reasoned that I₂ and NH₃ combined as a charge transfer complex^{35–37} in a geometry close to that of halogen bonding structures known today. Similar results were reported by I. Remsen and J. F. Norris in 1896^{34,38} upon mixing bromine and trimethylamine, except that the solution did not just change color; a product crystallized as well. Crystallized complexes comprised of hypothesized charge transfer complexes were further studied in the 20th century using spectroscopic techniques such as X-ray or electron diffraction.³⁵ For example, X-ray diffraction was used on a crystal structure of bromine and dioxane by Hassel et al. in 1954³⁹ to determine the molecular arrangement of halogen bonding (Fig. 1.1).

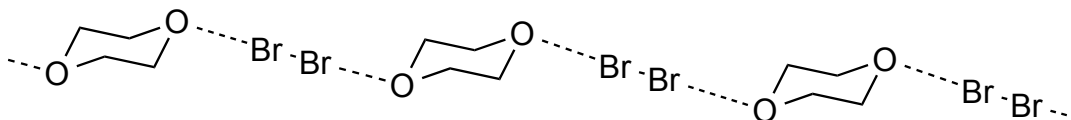


Figure 1.1. A crystallized chain of bromine and dioxane. The Br—O bond distance was 2.71 Å, whereas the sum of the van der Waals radii is 3.35 Å. The apparent Br-Br—O bond angle was 180° (adapted from *Q. Rev. Chem. Soc.* **1962**, 16, 1).

Diatomic bromine was found to interact with the oxygen of dioxane at a distance of only 2.71 Å.^{34,39,40} Hassel et al. commented, “This is the most striking feature of the whole structure as it indicates a very strong interaction between the bromine and oxygen atoms.”³⁹ The remaining halogens were then incorporated and yielded similar results. It was concluded that the unexpected attraction between bromine and oxygen was an example of a “charge transfer bond.”^{34,40–42} The term was coined in reference to the research of R. S. Mulliken published not long before,^{35,41} wherein Mulliken stated that a previously forbidden absorption was allowed, “...due to an *intermolecular charge transfer process* during the light absorption;”⁴³ italics added for emphasis.

In more recent research, the charge transfer interaction is said to be caused by electron donation from a Lewis base in close proximity to the σ^* -orbital of the R–X bond.^{7,44,45}

Modern understanding of halogen bonding has moved beyond a pure charge transfer model with the discovery of halogen bonds in supramolecular complexes and biosystems.^{1,7,25,35} The interactions have been attributed primarily to electrostatics as opposed to charge transfer due to the reported structural similarities to hydrogen bonding complexes,^{37,46} which can at times be solely attributed to electrostatic effects.³¹ For example, a screening of biological halogen bonding crystal structures was performed by Auffinger et al. in 2004.¹ The search was narrowed to halogenated complexes containing C–Cl, C–Br, and C–I bonds arranged in a halogen bonding configuration near oxygen (*Ref. 1; Fig. 1*). The average non-bonding distances were found to be less than the sum of the van der Waals radii of the interacting atoms. The shortest interactions were found to occur at C–X—O angles between 160° and 180°, though another group of structures were found at smaller angles between 145° and 150°. The latter group was attributed to additional polarization effects induced by the Lewis base, the researchers arguing that when working with “complex environments, like those encountered in biomolecular systems... some deviation from linearity for halogen bonds can be expected.”

Electrostatic potential maps were created by Auffinger et al. to gauge the polarizability of model halogenated compounds at the 3-21G(*) level. A partially positive electrostatic potential was found on the halogen atoms, increasing with atomic polarizability from Cl to I. In addition, the presence of an electron withdrawing substituent group, such as an aromatic moiety, resulted in an increased positive potential on the halogen. The partially positive electrostatic potential on each halogen was observed extending from the C–X covalent bond, which would cause an interaction angle of 180° via electrostatic attraction in the vicinity of a Lewis base. It was therefore concluded that the halogen bonding interactions observed were primarily driven by electrostatics, and, to a

lesser extent, charge transfer. The research group has since worked to perform statistical analyses on the geometry and energy of biological halogen bonds, such as those found in Holliday junctions and enzymes.^{1,4,26,37,47–52}

The σ -Hole Model

The discovery of biological halogen bonding structures shifted the focus of research from a model solely dependent on charge transfer to one that incorporated electrostatics, due to the structural similarities shared with hydrogen bonding.^{26,31,35,37,53} With that shift came the proposal of an electrostatic halogen bonding model: the σ -hole model. Researchers Politzer et al. wrote in a 2008 paper, “We wish... to draw attention to a common fallacy related to atomic charges; they are typically viewed as global. The entire atom is assigned a single numerical positive or negative charge; in effect, it is being treated as a point charge,”⁵⁴ disregarding non-uniform electron density across atoms in molecules. The partially positive electrostatic potential exposed on halogen atoms, like those demonstrated by Auffinger et al.¹ using molecular electrostatic potential maps, result from the half-filled valence p-orbital participating in a covalent bond. The electron deficiency extending from the R–X bond allows positive charge from the nucleus to attract excess electron density (negative) regions on nearby Lewis bases, where *R* is an organic functional group attached to the halogen, *X*. This area of partially positive charge on the halogen is called the σ -hole (Fig. 1.2).^{53,55} The partially negative excess electron density on a halogen is distributed around an, “equatorial belt... coaxial with the [R]–X bond.”⁹

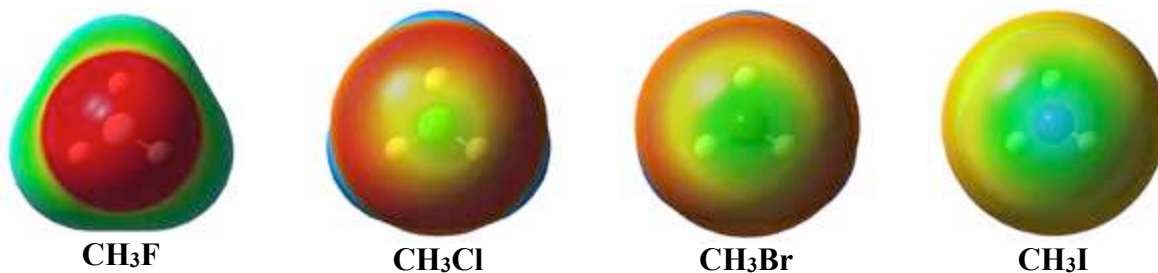


Figure 1.2. The σ -hole is seen to increase in size from F to I when looking down the C–X bond of CH_3X . Red represents a negative electrostatic potential (-15.7 kcal/mol) and blue represents a positive electrostatic potential (15.7 kcal/mol) between a negative point charge probe and the molecule evaluated at grid point points on the 0.0004 electron density isosurface (adapted from *PNAS*, **2004**, *101*, 16789).

Currently, the σ -hole model is the most prominent theoretical model in the literature used to explain the behavior of halogen bonds.^{54,56–59} It was developed by Politzer et al.,⁵⁶ who reported in 2007 that the magnitude of positive electrostatic potential on a halogen is proportional to the strength of a non-bonding interaction with a Lewis base.^{54,56–58} The focus of the study was the source of attraction between electrostatically driven non-bonding interactions between molecules that would be expected to repel one another. Molecular electrostatic potential (MEP) maps were also utilized, wherein the electrostatic potential, V_{esp} (Eqn. 1.1), is calculated over a set of points, d , to display the interaction between a negative point charge probe and the nuclear point charge and electron density of a molecule.^{54,58,60}

$$V_{esp} = \sum_X \frac{Z_X}{|d_X - d|} - \int \frac{\rho dd'}{|d' - d|} \quad (1.1)$$

V_{esp} is generated using a point charge as a probe at a set of positions, d . A negative point charge probe is attracted to the nuclear charges (Z_X) on atoms (X) at a positions (d_X) and repelled by the electron density (ρ) distributed over the system. The interaction with electron density is integrated over all space. Both terms in V_{esp} increase with decreasing distance between the nucleus and the probe as well as the electron density and the probe (d_X-d and $d'-d$, respectively).^{54,56–58}

The effectiveness of the MEP model was demonstrated by Politzer et al. in their early work by mapping both the BrOH and SCl₂ electrostatic potential surfaces.⁵⁴ The electrostatic potential surfaces illustrated a region of positive potential on bromine extending from the O–Br covalent bond, and two regions of positive potential on sulfur extending from the Cl–S covalent bonds. The electrostatic potential on the surface of a halogen in a molecule was not “global” but rather non-uniform, with a positive polar crown extending from each R–X covalent bond.^{15,54,56–58} Once the electrostatic potential surfaces (*Ref. 54; Fig. 2 and Fig. 3*) were analyzed, two pairwise complexes, HOBr–BrOH and Cl₂S–SCl₂, were optimized by Politzer et al. The HOBr dimer oriented in a conformation that optimizes halogen bonding with a Br–Br distance of 3.21 Å, such that the partially positive region on one Br aligned with the partially negative region on the other. The Cl₂S dimer adopted a conformation that maximizes chalcogen bonding with an S–S distance of 3.17 Å, such that the partially positive and negative regions on adjacent sulfurs aligned. The interaction energies were calculated to be -3.5 kcal/mol and -5.5 kcal/mol in the complexes, respectively.

The necessity of a covalent bond in the formation of a σ -hole has been a point of contention in the halogen bonding literature; the σ -hole is said to result from the positive nucleus of the halogen becoming more exposed as electron density shifts away from the atom and toward the covalent bond.^{15,16,57,61} However, two articles were published by Politzer et al. in 2013 and 2014 that illustrated the presence of a σ -hole on free fluorine and chlorine atoms, respectively.^{57,58} The singly-occupied p_z-orbital of a halogen that is directly involved in a covalent bond remains singly-occupied in the absence of a covalent bond. This results in two partially positive σ -holes on the surface of a halogen atom, corresponding to the $-z$ and $+z$ directions as the positive charge of the protons in the nucleus become more prominent on an electron density isosurface. As is true for the halogens when covalently bound, the intrinsic σ -holes increase in size with the polarizability of the atom.

The electrostatic description of halogen bonding was so widely accepted that in 2013, the International Union of Pure and Applied Chemistry defined a halogen bond as, “a net attractive interaction between an electrophilic region associated with a halogen atom in a molecular entity and a nucleophilic region in another, or the same, molecular entity.”⁵⁹ This is not to say that additional energetic components, such as charge transfer, are not present, although electrostatics is often reported to be the primary component.^{31,62–64} In fact, at times the electrostatic component is reported to be the sole contributing factor toward a stable halogen bond.^{57,59} In response to this, Wang et al. stated in a 2014 publication *On the Nature of Halogen Bonds*, “The current discussions of experimental and theoretical studies of [halogen] bonds are virtually dominated by the ‘ σ -hole’ notion and its electrostatic effects, sometimes to the exclusion of other effects.”³⁵ To this end, researchers employ energy decomposition analysis methods to observe the relative contributions of halogen bonding energetic components, including but not limited to electrostatics, exchange repulsion, dispersion, and charge transfer.^{15,19,45}

For instance, Symmetry Adapted Perturbation Theory (SAPT) was used by K. E. Riley and P. Hobza¹⁹ to observe the underlying electrostatic contributions as well as exchange in halogen bonding dimers. SAPT⁶⁵ assesses the magnitudes of the various intermolecular interactions, such as electrostatics (*elec*), induction (*ind*), dispersion (*disp*), and exchange (*exch*). Hartree-Fock and MP2 methods were also used to compare the total SAPT energy calculated (Table 1.2). As reported by Riley and Hobza,¹⁹ the differences between the Hartree-Fock (HF) and Møller-Plesset 2nd Order Perturbation (MP2) results signified a considerable electron correlation component to the halogen bonding interactions, increasing from chloromethane to iodomethane. The SAPT energies were of the same magnitude as those found at the MP2 level, although the deviation increases from chloromethane to iodomethane. The electrostatic component was found to contribute toward the interaction energy increasingly as a periodic trend from chloromethane to iodomethane. The

dispersive component (*disp*) also increased as a periodic trend, and can be seen to contribute to the interaction energy more than electrostatics in the chloro- and bromomethane dimers. Charge transfer contributes little to the interaction energy in these dimer models, whereas exchange repulsion is of a greater magnitude than the total energy, balanced by the attractive components. These trends are consistent with other literature reports.^{31,45,62,66,67}

Table 1.2. The interaction energies and underlying electrostatic (*elec*), inductive (*ind*), dispersive (*disp*), and exchange repulsion (*exch*) components of the halomethanes with formaldehyde using SAPT method, reported by Riley and Hobza.¹⁹

ΔE_{METHOD}	CH ₃ Cl—OCH ₂ (kcal/mol)	CH ₃ Br—OCH ₂ (kcal/mol)	CH ₃ I—OCH ₂ (kcal/mol)
HF	0.66	0.36	0.27
MP2	-1.11	-1.61	-1.68
CCSD(T)	-1.05	-1.49	-1.57
SAPT	-0.98	-1.70	-2.67
elec	-0.96	-1.47	-2.61
ind	-0.23	-0.37	-0.78
disp	-1.81	-1.98	-2.31
exch	2.02	2.12	3.01

A recent publication by Thirman et al. observed halogen bonding between methylhalides and fluoride ion using an energy decomposition analysis.⁴⁵ Similarly to Riley and Hobza, the research group found a large electrostatic contribution as a function of distance. However, the charge transfer component was near-equal to the electrostatic component (*Ref. 45; Fig. 7*). The researchers concluded that “All of [the energetic components] are important for determining the overall interaction, so each needs to be considered separately.”

Force Field Models of Non-Bonding Interactions

Understanding the underlying energetic components of halogen bonding as dependent on d and θ is necessary to accurately predict the energy of a biomolecular system.^{1,23} For example, the binding interaction of ligands within the active site of proteins is dependent on intermolecular

attractions between molecules, including biological halogen bonds (BXBs).^{47,68} Due to the geometric and energetic specificity of halogen bonding as introduced above, BXBs can be used to design novel drugs in medicinal chemistry.^{1,10,12,13,26,69} A new drug is estimated to take over a decade and nearly \$2 billion to develop and launch, so the methodology throughout the process should be as cost efficient as possible.^{12,23,70} The primary method for calculating the theoretical energy of biomolecular systems, like proteins or DNA, is to use a force field to approximate the interaction energy using simple potential expressions within molecular mechanics/dynamics suites.^{68,71-79}

I. The AMBER Force Field and PEP Model

Force fields approximate the energy of large and complex biomolecular systems using simple potential expressions.^{68,71-80} One such force field is called Assisted Model Building with Energy Refinement (AMBER), and was developed by Kollman et al.⁷² The goal when developing AMBER was to create a molecular mechanics program that could calculate the optimized structure and interaction energy of small molecules as well as larger polymers. In AMBER, the interaction energy, ΔE_{AMBER} (Eqn. 1.2), is calculated via interatomic bonding and non-bonding terms that are dependent on the distances, angles, and dihedrals (torsions) between atoms.

$$\begin{aligned}
 \Delta E_{AMBER} = & \sum_{\text{bonds}} K_r (r - r_{eq})^2 + \sum_{\text{angles}} K_\theta (\theta - \theta_{eq})^2 \\
 & + \sum_{\text{torsions}} \frac{1}{2} V_n (1 + \cos(n\phi - \gamma)) \\
 & + \sum_{\substack{\text{nonbonds,} \\ i < j}} \left(\frac{A_{ij}}{R_{ij}^{12}} - \frac{B_{ij}}{R_{ij}^6} + \frac{q_i q_j}{\epsilon R_{ij}} \right) + \sum_{\text{H-bonds}} \left(\frac{C_{ij}}{R_{ij}^{12}} - \frac{D_{ij}}{R_{ij}^{10}} \right)
 \end{aligned} \tag{1.2}$$

The bonding distance (bonds) and angle terms are approximated by harmonic equations, and the dihedral (torsion) term by a cosine expansion, where a force constant (K_r , K_θ , and V_n , respectively) is multiplied by the variance of the terms from their equilibrium values ($r-r_{eq}$, $\theta-\theta_{eq}$, and $n\phi-\gamma$, respectively) within each term.⁷⁵ The equilibrium terms (r_{eq} , θ_{eq} , and γ) were parameterized relative to experimental structural data. The non-bonding terms are described by Lennard-Jones and Coulombic potentials, where A_{ij} and B_{ij} derive from the well depths and van der Waals interaction distances. Hydrogen bonding term is approximated by a 12-10 potential, where C_{ij} and D_{ij} also derive from well depths and interaction distances; R_{ij} is equal to the interaction distance in both the non-bonding and hydrogen bonding terms. The atomic charges (q_i and q_j) are calculated from small molecular models using restrained electrostatic potentials (RESPs) at the HF/6-31G* level.^{72,75,81} A non-additive approximation to the polarizability has been subsequently added to ΔE_{AMBER} to improve computational results.^{72,75}

AMBER yields halogen-bonding interaction energies comparable to experimental and quantum mechanical results for moderately sized molecular systems.^{71,72} For example, in a study completed by M. A. A. Ibrahim,⁷¹ the halogen-bond bond distances and interaction energies between the halobenzenes and biologically applicable Lewis bases resulted in rms differences of 0.18 Å and 0.49 kcal/mol relative to MP2 results, respectively (Table 1.3). The AMBER non-bonding distances were consistently longer than MP2, and the interaction energies were weaker than the MP2 results.^{71,82} The longer distances predicted by AMBER suggest that the force field underestimated the dispersive component of the halogen bonding strength, or overestimated the exchange repulsion.^{72,82}

Table 1.3. Distances and interaction energies presented by M. M. A. Ibrahim,⁷¹ demonstrating that AMBER overestimates the non-bonding distances and underestimates the halogen bonding attraction for chlorobenzene, bromobenzene, and iodobenzene interacting with furan, pyridine, and ammonia when compared to the results at the MP2 level.

Lewis Acid	Lewis Base	d_{AMBER} (Å)	d_{MP2} (Å)	ΔE_{AMBER} (kcal/mol)	ΔE_{MP2} (kcal/mol)
chlorobenzene	furan	3.30	3.15	-0.77	-1.15
	pyridine	3.26	3.17	-0.90	-1.42
	ammonia	3.34	3.33	-0.44	-0.71
bromobenzene	furan	3.43	3.14	-1.38	-1.72
	pyridine	3.29	3.07	-2.59	-2.80
	ammonia	3.31	3.21	-1.82	-1.83
iodobenzene	furan	3.53	3.23	-1.65	-2.21
	pyridine	3.36	3.07	-3.29	-4.36
	ammonia	3.38	3.22	-2.37	-3.03

Force field electrostatic approximations are currently being developed based on the σ -hole model to improve the structural and energetic halogen bonding calculations in large molecules. One such approach was developed by Ibrahim,⁸² where a positive extra point (PEP) was added to the halogen corresponding to the location of its σ -hole.^{71,76} The PEP is meant to replicate the partially positive electrostatic potential of the σ -hole and establish an electrostatic potential gradient from polar cap to negative perpendicular axes.^{23,76} Ibrahim calculated the partial charge of the PEP using RESP's at the HF/6-31G* level, which is the same method used in AMBER to approximate partial charges. The PEP was placed within the valence electron density of the halogen (Fig. 1.3), at a selected distance of $\sqrt[6]{2}r_{vdW}$ from the nucleus.

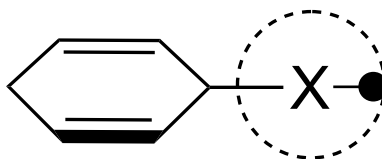


Figure 1.3. The location of the positive extra point (PEP) within the electron density (dotted line) of a halogen (X), where the PEP is positively charged and the halogen negatively charged. This is meant to model the charge of the σ -hole (adapted from *J. Mol. Model* **2012**, 18, 4625).

Bond distances and interaction energies between the halobenzenes and model Lewis bases, including formaldehyde and ammonia, using the AMBER-PEP method yielded rms differences of

0.09 Å and 0.37 kcal/mol relative to the MP2 method, respectively (Table 1.4). These results are an improvement over AMBER without the PEP. Lastly, the interaction energy via AMBER-PEP was consistently underestimated when ammonia was the Lewis base. Charge transfer has been reported to be a significant contribution for halogen bonding involving ammonia,^{36,83,84} an underlying attraction not addressed by the PEP model.

Table 1.4. Distances and interaction energies presented by M. M. A. Ibrahim⁸² for chlorobenzene, bromobenzene, and iodobenzene interacting with formaldehyde and ammonia at the AMBER-PEP and MP2 level. The non-bonding distances calculated by AMBER-PEP were consistently overestimated when compared to the MP2 results, though the estimated interaction energies showed a decreased root mean square difference compared to the previous AMBER results in Table 1.3.

Lewis Acid	Lewis Base	$d_{AMBER-PEP}$ (Å)	d_{MP2} (Å)	$\Delta E_{AMBER-PEP}$ (kcal/mol)	ΔE_{MP2} (kcal/mol)
chlorobenzene	formaldehyde	3.26	3.21	-0.27	-0.53
	ammonia	3.34	3.33	-0.44	-0.71
bromobenzene	formaldehyde	3.28	3.18	-1.51	-1.14
	ammonia	3.31	3.21	-1.82	-1.83
iodobenzene	formaldehyde	3.35	3.27	-2.05	-1.72
	ammonia	3.38	3.22	-2.37	-3.03

II. The Force Field for Biological Halogen Bonds

The development of a comprehensive halogen bond force field term, one that incorporates exchange repulsion and dispersive interactions as well as electrostatics would assist researchers in predicting the binding interaction of ligands within the active site of proteins that incorporate BXBs. A force field was published by Carter et al. in 2012, which they refer to as a force field for biological halogen bonds (ffBxB).⁶⁸ Focus was on the interaction potential of bromine because experimental and theoretical halogen bonding interactions have been published in the literature for bromine-containing BXBs. The potential terms within the ffBxB were developed from trends in experimental structural and energetic data as well as select electronic structure computations.

The ffBxB potential term consisted of a sum of modified Lennard-Jones, V_{LJ} (Eqn. 1.3), and electrostatic, V_{elect} (Eqn. 1.4), contributions.

$$V_{LJ} = \sqrt{\varepsilon_A \varepsilon_{Br}} \left[\left(\frac{r_{vdW(A)} + \langle r_{vdW(Br)} \rangle - \Delta r_{Br} \cos(\nu\alpha)}{d} \right)^{12} - 2 \left(\frac{r_{vdW(A)} + \langle r_{vdW(Br)} \rangle}{d} \right)^6 \right] \quad (1.3)$$

$$V_{elect} = \frac{(A \cos(\nu\alpha) + B) Z_A e^2}{D d^n} \quad (1.4)$$

The repulsive term in V_{LJ} is calculated by summing the van der Waals radii of the interacting atom ($r_{vdW(A)}$) and bromine ($\langle r_{vdW(Br)} \rangle - \Delta r_{Br} \cos(\nu\alpha)$), divided by the interaction distance (d) raised to the power of 12. The anisotropic van der Waals radius of bromine is equal to the difference of the average radius ($\langle r_{vdW(Br)} \rangle$) and the angularly dependent polar flattening ($\Delta r_{Br} \cos(\nu\alpha)$). The cosine function provides a dependence on period (ν) and angle (α). The dispersive term in V_{LJ} is calculated by summing the van der Waals radii of the interacting atom and bromine, divided by d raised to the power of 6. There is no angular dependence in the dispersive term because Carter et al. showed, using a combination of MP2 and HF methods, that the angular dependence resides within the exchange repulsion. The repulsive and attractive terms are scaled by the root of the multiple of the well depths (ε).

V_{elect} is a Coulombic potential term. The research team used the same cosine function to model the angular dependence of the charge distribution of bromine as they did when modeling the aspherical exchange repulsion shape. Carter et al. explain, "... although the σ -hole model for [halogen] bonds does not explicitly consider the steric and dispersion terms, we show that the size and shape of the halogen is aspherical, which we [attribute] to the depopulation of the atomic p_z -orbital, a hallmark of the σ -hole model." In other words, the same singly-occupied p_z -orbital that results in the atom's aspherical shape also gives rise to its σ -hole. The amplitude (A) of the cosine function and its baseline (B) were scaled to fit the maximum and minimum potential values

calculated using the MP2 method. The remaining parameters include the partial charge (Z_A) on the interacting atom (A), the charge of a proton (e), the dielectric constant of the medium (D), and the interaction distance (d). The 7 parameters, between V_{LJ} and V_{elect} (see Table 1.5), were parameterized from a model bromouracil-phosphate interaction.

Table 1.5. The 7 unique parameters of the ffBXB, presented by Carter et al,⁶⁸ which were parametrized from a model bromouracil-phosphate interaction.

$\langle r_{vdW(Br)} \rangle$ (Å)	Δr (Å)	ϵ_{Br} (kcal/mol)	A	B	n	ν
2.04	0.060 ± 0.022	0.019 ± 0.002	2.84 ± 0.82	1.53 ± 0.45	2.29 ± 0.29	2.31 ± 0.02

The energies and structures obtained using the parameterized ffBXB for the DNA junction configurations Br1J and Br2J, examples of experimental biological halogen bond structures, were then compared to experimental results from the literature and QM methods (Table 1.6). Bromouracil and either hypophosphite ($H_2PO_2^-$) or dimethylphosphate (DMP^-) were used to model Br1J and Br2J in the QM calculations because the DNA junctions would be too large for the MP2 method directly. It was reported by Carter et al. that both the QM and ffBXB calculations resulted in interaction energies within the errors of the experimentally determined energies, so the bromouracil pairwise interaction effectively modeled Br1J and Br2J. The ffBXB energies correlated with the MP2 results “very well” with an R value of 0.96. In conclusion, the ffBXB replicated both the experimental and theoretical model results.

Table 1.6. Experimental energies of Br1J and Br2J in comparison to theoretical interaction energies of bromine-containing model BXBs, presented by Carter et al.⁶⁸

Geometry	Experimental (kcal/mol)		Theoretical (kcal/mol)	
	Crystal Assay	Calorimetric	QM ($H_2PO_2^-/DMP^-$)	ffBXB ($H_2PO_2^-/DMP^-$)
Br1J	-2.0 ± 0.5		-1.44/-1.53	-1.97/-2.47
Br2J		-3.5 ± 1.3	-3.02/-3.06	-2.86/-4.63

The ffBxB was not developed like AMBER-PEP, in which a positive extra point was added to a halogen in the AMBER force field.⁸² Instead, a new force field term was designed by modeling anisotropic shapes and electrostatic potentials.⁶⁸ Both force fields yielded comparative results to QM calculation, as is evident by the rms differences between AMBER-PEP and MP2 (0.09 Å, 0.37 kcal/mol), and the R value of 0.96 between ffBxB and MP2. As such, two PEP models were constructed by Carter et al. to directly compare the predictive capabilities of AMBER-PEP and ffBxB. The first was referred to as PEP-a and the second PEP-f. PEP-a was constructed using parameters from the AMBER ff99 force field, and PEP-f was constructed using parameters from the ffBxB (*Ref. 68; Table 3*).

The ffBxB, PEP-a, and PEP-f all predicted similar potential wells between bromine and anionic oxygen (*Ref. 68; Fig. 8c, Fig. 10a, Fig. 10d, respectively*), although the PEP-a well was narrower and the PEP-f well broader than what was predicted by the ffBxB. PEP-a was then tested using model Br1J and Br2J junctions and found that the BXB interactions were all positive, i.e. repulsive (Table 1.7). It was concluded by Carter et al. that the standard AMBER parameters did not model the van der Waals interactions of more complex systems, leading to incorrect theoretical predictions. The same experiments were conducted using PEP-f, and the attractive results were interpreted to mean, “... that the size of the halogen and energy terms for the van der Waals interaction need to be reduced relative to the standard AMBER definitions in order to properly describe the interactions in the experimental X-bonded DNA junction system.”

Table 1.7. PEP-a and PEP-f interaction energies (kcal/mol) for bromine-containing model BXBs of Br1J and Br2J, presented by Carter et al.⁶⁸

Geometry	PEP-a (H ₂ PO ₂ ⁻ /DMP ⁻)	PEP-f (H ₂ PO ₂ ⁻ /DMP ⁻)
Br1J	1.57/3.88	-3.40/-4.96
Br2J	5.66/6.12	-4.15/-5.99

As of 2012, ffBXB was only parameterized for BXBs that contained bromine. In 2015, another article was published by the Ho group, titled *Force Field Model of Periodic Trends in Biomolecular Halogen Bonds*,⁸⁰ which outlined the parameterization of the force field for chlorine and iodine, as well as improving that of bromine. My contribution to this work can be found in Appendix 1; in summary, a combination of anisotropic exchange repulsion and isotropic dispersion was found to model the van der Waals component of chlorine-, bromine-, and iodine-containing BXBs.

Thesis Overview

The application and history of halogen bonding has been introduced herein along with the geometric and energetic components of halogen bonding. Throughout this thesis, structural data from crystal structures were extracted containing halogen bonds reported in the Cambridge Structural Database. The data was used to determine correlations in crystal frequency based on the halogen present, interaction distance, and interaction angle (Chapter 2). The strength of the attractive components of halogen bonding was identified to increase with the depth of the σ -hole, dependent on the polarizability of the halogen as well as the electron-withdrawing capabilities of the substituent group, while exchange repulsion decreased (Chapter 3). Exchange repulsion and electrostatic potential models were developed, which show both the van der Waals and electrostatic components have an angular dependence of $\cos^2(\theta)$ (Chapter 4). Halogen bonding trimer systems were found to have a cooperative non-bonding energy due to underlying energetic components of the interaction energy, resulting in more contracted bond distances (Chapter 5). Lastly, novel charge transfer models were developed, which examined the process of charge transfer as a function of distance in halogen bonding dimers. The cross-term between reactant and

product components was primarily found to contribute to the attraction between Lewis acid and base (Chapter 6). A summary of findings and future works will conclude this thesis (Chapter 7).

REFERENCES

- (1) Auffinger, P.; Hays, F. A.; Westhof, E.; Ho, P. S. Halogen Bonds in Biological Molecules. *Proc. Natl. Acad. Sci.* **2004**, *101*, 16789–16794.
- (2) Erdelyi, M. A Big Hello to Halogen Bonding: Scientific Conferences. *Nat. Chem.* **2014**, *6*, 762–764.
- (3) Priimagi, A.; Cavallo, G.; Metrangolo, P.; Resnati, G. The Halogen Bond in the Design of Functional Supramolecular Materials: Recent Advances. *Acc. Chem. Res.* **2013**, *46*, 2686–2695.
- (4) Carlsson, A.-C. C.; Scholfield, M. R.; Rowe, R. K.; Ford, M. C.; Alexander, A. T.; Mehl, R. A.; Ho, P. S. Increasing Enzyme Stability and Activity through Hydrogen Bond-Enhanced Halogen Bonds. *Biochemistry* **2018**, *57*, 4135–4147.
- (5) Aakeröy, C. B.; Wijethunga, T. K.; Desper, J. Practical Crystal Engineering Using Halogen Bonding: A Hierarchy Based on Calculated Molecular Electrostatic Potential Surfaces. *J. Mol. Struct.* **2014**, *1072*, 20–27.
- (6) Zordan, F.; Brammer, L.; Sherwood, P. Supramolecular Chemistry of Halogens: Complementary Features of Inorganic (M–X) and Organic (C–X′) Halogens Applied to M–X⋯X′–C Halogen Bond Formation. *J. Am. Chem. Soc.* **2005**, *127*, 5979–5989.
- (7) Metrangolo, P.; Resnati, G. Halogen Bonding: A Paradigm in Supramolecular Chemistry. *Chem. - Eur. J.* **2001**, *7*, 2511–2519.
- (8) Wilcken, R.; Zimmermann, M. O.; Lange, A.; Zahn, S.; Boeckler, F. M. Using Halogen Bonds to Address the Protein Backbone: A Systematic Evaluation. *J. Comput. Aided Mol. Des.* **2012**, *26*, 935–945.
- (9) Parisini, E.; Metrangolo, P.; Pilati, T.; Resnati, G.; Terraneo, G. Halogen Bonding in Halocarbon–Protein Complexes: A Structural Survey. *Chem. Soc. Rev.* **2011**, *40*, 2267.
- (10) Ibrahim, M. A. A. Molecular Mechanical Study of Halogen Bonding in Drug Discovery. *J. Comput. Chem.* **2011**, *32*, 2564–2574.
- (11) Chudzinski, M. G.; McClary, C. A.; Taylor, M. S. Anion Receptors Composed of Hydrogen- and Halogen-Bond Donor Groups: Modulating Selectivity With Combinations of Distinct Noncovalent Interactions. *J. Am. Chem. Soc.* **2011**, *133*, 10559–10567.
- (12) Xu, Z.; Yang, Z.; Liu, Y.; Lu, Y.; Chen, K.; Zhu, W. Halogen Bond: Its Role beyond Drug–Target Binding Affinity for Drug Discovery and Development. *J. Chem. Inf. Model.* **2014**, *54*, 69–78.
- (13) Wilcken, R.; Zimmermann, M. O.; Lange, A.; Joerger, A. C.; Boeckler, F. M. Principles and Applications of Halogen Bonding in Medicinal Chemistry and Chemical Biology. *J. Med. Chem.* **2013**, *56*, 1363–1388.
- (14) Desiraju, G. R.; Ho, P. S.; Kloo, L.; Legon, A. C.; Marquardt, R.; Metrangolo, P.; Politzer, P.; Resnati, G.; Rissanen, K. Definition of the Halogen Bond (IUPAC Recommendations 2013). *Pure Appl. Chem.* **2013**, *85*, 1711–1713.
- (15) Riley, K. E.; Murray, J. S.; Fanfrlík, J.; Řezáč, J.; Solá, R. J.; Concha, M. C.; Ramos, F. M.; Politzer, P. Halogen Bond Tunability II: The Varying Roles of Electrostatic and Dispersion Contributions to Attraction in Halogen Bonds. *J. Mol. Model.* **2013**, *19*, 4651–4659.
- (16) Politzer, P.; Murray, J. S.; Clark, T. Halogen Bonding and Other σ -Hole Interactions: A Perspective. *Phys. Chem. Chem. Phys.* **2013**, *15*, 11178.
- (17) Shields, Z. P.; Murray, J. S.; Politzer, P. Directional Tendencies of Halogen and Hydrogen Bonds. *Int. J. Quantum Chem.* **2010**, *110*, 2823–2832.
- (18) Politzer, P.; Riley, K. E.; Bulat, F. A.; Murray, J. S. Perspectives on Halogen Bonding and Other σ -Hole Interactions: Lex Parsimoniae (Occam’s Razor). *Comput. Theor. Chem.* **2012**, *998*, 2–8.
- (19) Riley, K. E.; Hobza, P. Investigations into the Nature of Halogen Bonding Including Symmetry Adapted Perturbation Theory Analyses. *J. Chem. Theory Comput.* **2008**, *4*, 232–242.
- (20) Riley, K. E.; Merz, K. M. Insights into the Strength and Origin of Halogen Bonding: The Halobenzene–Formaldehyde Dimer. *J. Phys. Chem. A* **2007**, *111*, 1688–1694.

- (21) Peebles, S. A.; Fowler, P. W.; Legon, A. C. Anisotropic Repulsion in Complexes B--Cl₂ and B--HCl: The Shape of the Chlorine Atom-in-a-Molecule. *Chem. Phys. Lett.* **1995**, *240*, 130–134.
- (22) Riley, K. E.; Murray, J. S.; Fanfrlík, J.; Řezáč, J.; Solá, R. J.; Concha, M. C.; Ramos, F. M.; Politzer, P. Halogen Bond Tunability I: The Effects of Aromatic Fluorine Substitution on the Strengths of Halogen-Bonding Interactions Involving Chlorine, Bromine, and Iodine. *J. Mol. Model.* **2011**, *17*, 3309–3318.
- (23) Kolář, M.; Hobza, P. On Extension of the Current Biomolecular Empirical Force Field for the Description of Halogen Bonds. *J. Chem. Theory Comput.* **2012**, *8*, 1325–1333.
- (24) Pérez-Torralba, M.; García, M. Á.; López, C.; Torralba, M. C.; Torres, M. R.; Claramunt, R. M.; Elguero, J. Structural Investigation of Weak Intermolecular Interactions (Hydrogen and Halogen Bonds) in Fluorine-Substituted Benzimidazoles. *Cryst. Growth Des.* **2014**, *14*, 3499–3509.
- (25) Rissanen, K. Halogen Bonded Supramolecular Complexes and Networks. *CrystEngComm* **2008**, *10*, 1107.
- (26) Lu, Y.; Shi, T.; Wang, Y.; Yang, H.; Yan, X.; Luo, X.; Jiang, H.; Zhu, W. Halogen Bonding-A Novel Interaction for Rational Drug Design? *J. Med. Chem.* **2009**, *52*, 2854–2862.
- (27) Zhou, P.; Lv, J.; Zou, J.; Tian, F.; Shang, Z. Halogen–Water–Hydrogen Bridges in Biomolecules. *J. Struct. Biol.* **2010**, *169*, 172–182.
- (28) Matter, H.; Nazaré, M.; Güssregen, S.; Will, D. W.; Schreuder, H.; Bauer, A.; Urmann, M.; Ritter, K.; Wagner, M.; Wehner, V. Evidence for C-Cl/C-Br... π Interactions as an Important Contribution to Protein-Ligand Binding Affinity. *Angew. Chem. Int. Ed.* **2009**, *48*, 2911–2916.
- (29) Kolář, M.; Hobza, P.; Bronowska, A. K. Plugging the Explicit σ -Holes in Molecular Docking. *Chem. Commun.* **2013**, *49*, 981–983.
- (30) Riel, A. M. S.; Decato, D. A.; Sun, J.; Massena, C. J.; Jessop, M. J.; Berryman, O. B. The Intramolecular Hydrogen Bonded–Halogen Bond: A New Strategy for Preorganization and Enhanced Binding. *Chem. Sci.* **2018**, *9*, 5828–5836.
- (31) Stone, A. J. Are Halogen Bonded Structures Electrostatically Driven? *J. Am. Chem. Soc.* **2013**, *135*, 7005–7009.
- (32) Arunan, E.; Desiraju, G. R.; Klein, R. A.; Sadlej, J.; Scheiner, S.; Alkorta, I.; Clary, D. C.; Crabtree, R. H.; Dannenberg, J. J.; Hobza, P.; et al. Definition of the Hydrogen Bond (IUPAC Recommendations 2011). *Pure Appl. Chem.* **2011**, *83*.
- (33) Guthrie, F. XXVIII.—On the Iodide of Iodammonium. *J. Chem. Soc.* **1863**, *16*, 239–244.
- (34) Bent, H. A. Structural Chemistry of Donor-Acceptor Interactions. *Chem. Rev.* **1968**, *68*, 587–648.
- (35) Wang, C.; Danovich, D.; Mo, Y.; Shaik, S. On The Nature of the Halogen Bond. *J. Chem. Theory Comput.* **2014**, *10*, 3726–3737.
- (36) Karpfen, A. Charge-Transfer Complexes between NH₃ and the Halogens F₂, ClF, and Cl₂: An Ab Initio Study on the Intermolecular Interaction. *J. Phys. Chem. A* **2000**, *104*, 6871–6879.
- (37) Zhou, P.; Tian, F.; Zou, J.; Shang, Z. Rediscovery of Halogen Bonds in Protein-Ligand Complexes. *Mini Rev. Med. Chem.* **2010**, *10*, 309–314.
- (38) Remsen, I. Action of the Halogens on the Methylamines. *Am. Chem. J.* **1896**, *18*, 90–95.
- (39) Hassel, O.; Hvosllef, J. The Structure of Bromine 1,4-Dioxanate. *Acta Chem. Scand.* **1954**, *8*, 873.
- (40) Hassel, O.; Rømming, C. Direct Structural Evidence for Weak Charge-Transfer Bonds in Solids Containing Chemically Saturated Molecules. *Q. Rev. Chem. Soc.* **1962**, *16*, 1–18.
- (41) Hassel, O. Structural Aspects of Interatomic Charge-Transfer Bonding. *Science* **1970**, *170*, 497–502.
- (42) Nguyen, H. L.; Horton, P. N.; Hursthouse, M. B.; Legon, A. C.; Bruce, D. W. Halogen Bonding: A New Interaction for Liquid Crystal Formation. *J. Am. Chem. Soc.* **2004**, *126*, 16–17.
- (43) Mulliken, R. S. Structures of Complexes Formed by Halogen Molecules with Aromatic and with Oxygenated Solvents¹. *J. Am. Chem. Soc.* **1950**, *72*, 600–608.
- (44) Torii, H.; Yoshida, M. Properties of Halogen Atoms for Representing Intermolecular Electrostatic Interactions Related to Halogen Bonding and Their Substituent Effects. *J. Comput. Chem.* **2010**, *31*, 107–116.
- (45) Thirman, J.; Engelage, E.; Huber, S. M.; Head-Gordon, M. Characterizing the Interplay of Pauli Repulsion, Electrostatics, Dispersion and Charge Rransfer in Halogen Bonding with Energy Decomposition Analysis. *Phys. Chem. Chem. Phys.* **2018**, *20*, 905–915.

- (46) Amezaga, N. J. M.; Pamies, S. C.; Peruchena, N. M.; Sosa, G. L. Halogen Bonding: A Study Based on the Electronic Charge Density. *J. Phys. Chem. A* **2010**, *114*, 552–562.
- (47) Carter, M.; Ho, P. S. Assaying the Energies of Biological Halogen Bonds. *Cryst. Growth Des.* **2011**, *11*, 5087–5095.
- (48) Voth, A. R.; Hays, F. A.; Ho, P. S. Directing Macromolecular Conformation Through Halogen Bonds. *Proc. Natl. Acad. Sci.* **2007**, *104*, 6188–6193.
- (49) Voth, A. R.; Khuu, P.; Oishi, K.; Ho, P. S. Halogen Bonds as Orthogonal Molecular Interactions to Hydrogen Bonds. *Nat. Chem.* **2009**, *1*, 74–79.
- (50) Scholfield, M. R.; Zanden, C. M. V.; Carter, M.; Ho, P. S. Halogen Bonding (X-Bonding): A Biological Perspective. *Protein Sci.* **2013**, *22*, 139–152.
- (51) Carter, M.; Voth, A. R.; Scholfield, M. R.; Rummel, B.; Sowers, L. C.; Ho, P. S. Enthalpy–Entropy Compensation in Biomolecular Halogen Bonds Measured in DNA Junctions. *Biochemistry* **2013**, *52*, 4891–4903.
- (52) Vander Zanden, C. M.; Carter, M.; Ho, P. S. Determining Thermodynamic Properties of Molecular Interactions from Single Crystal Studies. *Methods* **2013**, *64*, 12–18.
- (53) Zou, W. S.; Han, J.; Jin, W. J. Concentration-Dependent Br \cdots O Halogen Bonding between Carbon Tetrabromide and Oxygen-Containing Organic Solvents. *J. Phys. Chem. A* **2009**, *113*, 10125–10132.
- (54) Politzer, P.; Murray, J. S.; Concha, M. C. σ -Hole Bonding Between Like Atoms; A Fallacy of Atomic Charges. *J. Mol. Model.* **2008**, *14*, 659–665.
- (55) Grabowski, S. J. Halogen Bond and Its Counterparts: Bent’s Rule Explains the Formation of Nonbonding Interactions. *J. Phys. Chem. A* **2011**, *115*, 12340–12347.
- (56) Clark, T.; Hennemann, M.; Murray, J. S.; Politzer, P. Halogen Bonding: The σ -Hole: Proceedings of “Modeling Interactions in Biomolecules II”, Prague, September 5th–9th, 2005. *J. Mol. Model.* **2007**, *13*, 291–296.
- (57) Politzer, P.; Murray, J. S.; Clark, T. σ -Hole Bonding: A Physical Interpretation. In *Halogen Bonding I*; Metrangolo, P., Resnati, G., Eds.; Springer International Publishing: Cham, 2014; Vol. 358, pp 19–42.
- (58) Politzer, P.; Murray, J. S. Halogen Bonding: An Interim Discussion. *ChemPhysChem* **2013**, *14*, 278–294.
- (59) Clark, T.; Heßelmann, A. The Coulombic σ -Hole Model Describes Bonding in CX₃I \cdots Y⁻ Complexes Completely. *Phys. Chem. Chem. Phys.* **2018**.
- (60) Politzer, P.; Murray, J. S.; Clark, T. Halogen Bonding: An Electrostatically-Driven Highly Directional Noncovalent Interaction. *Phys. Chem. Chem. Phys.* **2010**, *12*, 7748.
- (61) Clark, T.; Politzer, P.; Murray, J. S. Correct Electrostatic Treatment of Noncovalent Interactions: The Importance of Polarization. *Wiley Interdiscip. Rev. Comput. Mol. Sci.* **2015**, *5*, 169–177.
- (62) Jabłoński, M.; Palusiak, M. Nature of a Hydride–Halogen Bond. A SAPT-, QTAIM-, and NBO-Based Study. *J. Phys. Chem. A* **2012**, *116*, 2322–2332.
- (63) Mohan, N.; Suresh, C. H. Accurate Binding Energies of Hydrogen, Halogen, and Dihydrogen Bonded Complexes and Cation Enhanced Binding Strengths. *Int. J. Quantum Chem.* **2014**, *114*, 885–894.
- (64) Schneider, W. B.; Bistoni, G.; Sparta, M.; Saitow, M.; Riplinger, C.; Auer, A. A.; Neese, F. Decomposition of Intermolecular Interaction Energies within the Local Pair Natural Orbital Coupled Cluster Framework. *J. Chem. Theory Comput.* **2016**, *12*, 4778–4792.
- (65) Jeziorski, B.; Moszynski, R.; Szalewicz, K. Perturbation Theory Approach to Intermolecular Potential Energy Surfaces of van Der Waals Complexes. *Chem. Rev.* **1994**, *94*, 1887–1930.
- (66) Lommerse, J. P. M.; Stone, A. J.; Taylor, R.; Allen, F. H. The Nature and Geometry of Intermolecular Interactions Between Halogens and Oxygen or Nitrogen. *J. Am. Chem. Soc.* **1996**, *118*, 3108–3116.
- (67) Sladek, V.; Punyain, K.; Ilčin, M.; Lukeš, V. Substitution Effect on the Intermolecular Halogen and Hydrogen Bonds of the σ -Bonded Fluorinated Pyridine \cdots XY/HX Complexes (XY = F₂, Cl₂, ClF; HX = HF, HCl). *Int. J. Quantum Chem.* **2014**, *114*, 869–878.
- (68) Carter, M.; Rappé, A. K.; Ho, P. S. Scalable Anisotropic Shape and Electrostatic Models for Biological Bromine Halogen Bonds. *J. Chem. Theory Comput.* **2012**, *8*, 2461–2473.

- (69) Ford, M. C.; Ho, P. S. Computational Tools to Model Halogen Bonds in Medicinal Chemistry. *J. Med. Chem.* **2016**, *59*, 1655–1670.
- (70) Lu, Y.; Li, H.; Zhu, X.; Zhu, W.; Liu, H. How Does Halogen Bonding Behave in Solution? A Theoretical Study Using Implicit Solvation Model. *J. Phys. Chem. A* **2011**, *115*, 4467–4475.
- (71) Ibrahim, M. A. A. AMBER Empirical Potential Describes the Geometry and Energy of Noncovalent Halogen Interactions Better than Advanced Semiempirical Quantum Mechanical Method PM6-DH2X. *J. Phys. Chem. B* **2012**, *116*, 3659–3669.
- (72) Pearlman, D. A.; Case, D. A.; Caldwell, J. W.; Wilson, R. S.; Cheatham III, T. E.; DeBolt, S.; Ferguson, D.; Seibel, G.; Kollman, P. A. AMBER, A Package of Computer Programs for Applying Molecular Mechanics, Normal Mode Analysis, Molecular Dynamics and Free Energy Calculations to Simulate the Structural and Energetic Properties of Molecules. *Comput. Phys. Commun.* **1995**, *91*, 1–41.
- (73) Weiner, S. J.; Kollman, P. A.; Case, D. A.; Singh, U. C.; Ghio, C.; Alagona, G.; Profeta, S.; Weiner, P. A New Force Field for Molecular Mechanical Simulation of Nucleic Acids and Proteins. *J. Am. Chem. Soc.* **1984**, *106*, 765–784.
- (74) Weiner, S. J.; Kollman, P. A.; Nguyen, D. T.; Case, D. A. An All Atom Force Field for Simulations of Proteins and Nucleic Acids: An All Atom Force Field. *J. Comput. Chem.* **1986**, *7*, 230–252.
- (75) Wang, J.; Wolf, R. M.; Caldwell, J. W.; Kollman, P. A.; Case, D. A. Development and Testing of a General Amber Force Field. *J. Comput. Chem.* **2004**, *25*, 1157–1174.
- (76) Jorgensen, W. L.; Schyman, P. Treatment of Halogen Bonding in the OPLS-AA Force Field: Application to Potent Anti-HIV Agents. *J. Chem. Theory Comput.* **2012**, *8*, 3895–3901.
- (77) Jorgensen, W. L.; Tirado-Rives, J. The OPLS Potential Functions for Proteins. Energy Minimizations for Crystals of Cyclic Peptides and Crambin. *J. Am. Chem. Soc.* **1988**, *110*, 1657–1666.
- (78) Brooks, B. R.; Brucoleri, R. E.; Olafson, B. D.; States, D. J.; Swaminathan, S.; Karplus, M. CHARMM: A Program for Macromolecular Energy, Minimization, and Dynamics Calculations. *J. Comput. Chem.* **1983**, *4*, 187–217.
- (79) Brooks, B. R.; Brooks, C. L.; Mackerell, A. D.; Nilsson, L.; Petrella, R. J.; Roux, B.; Won, Y.; Archontis, G.; Bartels, C.; Boresch, S.; et al. CHARMM: The Biomolecular Simulation Program. *J. Comput. Chem.* **2009**, *30*, 1545–1614.
- (80) Scholfield, M. R.; Ford, M. C.; Vander Zanden, C. M.; Billman, M. M.; Ho, P. S.; Rappé, A. K. Force Field Model of Periodic Trends in Biomolecular Halogen Bonds. *J. Phys. Chem. B* **2015**, *119*, 9140–9149.
- (81) Wang, J.; Cieplak, P.; Kollman, P. A. How Well Does a Restrained Electrostatic Potential (RESP) Model Perform in Calculating Conformational Energies of Organic and Biological Molecules? *J. Comput. Chem.* **2000**, *21*, 1049–1074.
- (82) Ibrahim, M. A. A. Molecular Mechanical Perspective on Halogen Bonding. *J. Mol. Model.* **2012**, *18*, 4625–4638.
- (83) Mo, Y.; Gao, J.; Peyerimhoff, S. D. Energy Decomposition Analysis of Intermolecular Interactions Using a Block-Localized Wave Function Approach. *J. Chem. Phys.* **2000**, *112*, 5530–5538.
- (84) Esrafil, M. D.; Vakili, M. Halogen Bonds Enhanced by σ -Hole and π -Hole Interactions: A Comparative Study on Cooperativity and Competition Effects Between $X\cdots N$ and $S\cdots N$ Interactions in $H_3N\cdots XCN\cdots SF_2$ and $H_3N\cdots XCN\cdots SO_2$ Complexes ($X = F, Cl, Br$ and I). *J. Mol. Model.* **2014**, *20*, 2291.

CHAPTER 2: HALOGEN BONDING IN CRYSTAL STRUCTURES

A delicate balance of intermolecular non-bonding interactions, such as hydrogen and halogen bonding, contributes to the binding of a ligand within the active site of a protein.¹⁻³ The nature and magnitude of these interactions can be studied using computational approaches, including molecular dynamics and quantum mechanical calculations. Direct electronic structure calculations on biomolecular systems is not routinely feasible, but small molecular models that retain important characteristics of the biological systems can be used in place of the larger structures,⁴ as demonstrated by Carter et al.⁵ If crystal structures of larger molecules are found to have a consistent intermolecular contact geometry, then it logically follows that studies on small molecular dimers in similar geometric orientations should be able to examine the electronic basis of the effect found in the larger molecules. Our results on geometric trends in hydrogen and halogen bonding crystal structures are presented throughout this Chapter.

The Cambridge Structural Database (CSD)⁶ was used to obtain a visual representation of the distance-angle correlations in hydrogen and halogen bonding crystal structure data. Version 5.38 of the CSD was scanned for structures with a hydroxyl hydrogen in close contact with a carbonyl oxygen (Fig. 2.1) using selected general geometric parameters within crystal structures, including the elements present, non-bonding distance, d , and angle, θ . The non-bonding H—O distance and two angles were collected: the first (θ_1) around the hydrogen, O—H—O (Lewis acid), and the second (θ_2) around the carbonyl oxygen, H—O=C (Lewis base). The CSD was then scanned for structures with a halogen in close contact with a carbonyl oxygen, discussed in the following section.

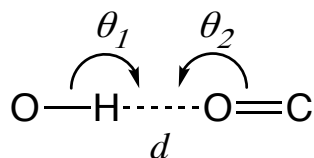


Figure 2.1. The general geometric parameters used to search the Cambridge Structural Database for model hydrogen bonding crystal structures containing an alcohol and a carbonyl oxygen, where non-bonding distance (d) and angles (θ_1 , θ_2) were allowed to vary.

The collected distances were normalized by Σr_{vdW} , which allows hydrogen bonding results to be compared to other non-bonding interactions, such as halogen bonding.⁴ It is a long-recognized issue that surface area contracts near the polar axis (θ of 180°) of an sphere, providing distorted statistics of the number of interactions at a given angle. In other words, the decreasing surface area near a linear bonding configuration causes a falsely perceived decrease in interaction frequency (*Ref. 7; Fig. 1*). The use of $1-\cos(\theta)$ reweights the frequency distribution to one evenly spaced in surface area.^{7,8} As stated by Kanters et al., “This factor, [the redistribution], does not affect the observed bond angle in any single case, but only affects the frequency distribution of the whole set of bond angles,”⁷ which then causes angularly dependent results to be more consistent with intrinsic property.⁷⁻¹⁰

A program was written to count the number of interactions found by the CSD search as a function of normalized distance and $1-\cos(\theta)$. The data was then organized in a 2-dimensional histogram with boxes equal-sized in distance and $\cos(\theta)$, accounting for the decreased surface area near the polar axis. The results were graphed in 3-dimensions (Fig. 2.2), where the x-axis corresponds to bond angle, the y-axis to normalized bond length, and the z-axis to number of interactions found with a given distance/angle combination. As would be expected, a pronounced distance-angle dependence of the hydrogen bond can be seen around the hydrogen, with the surface maximum correlating to a d of 1.64 \AA (0.6 in fractional space) and a θ_1 of 180° . The sharp peak of the distribution suggests a significant attractive interaction between the hydrogen and oxygen that

pulls molecular fragments together, dependent on the electrostatic component of the interaction.^{4,11,12}

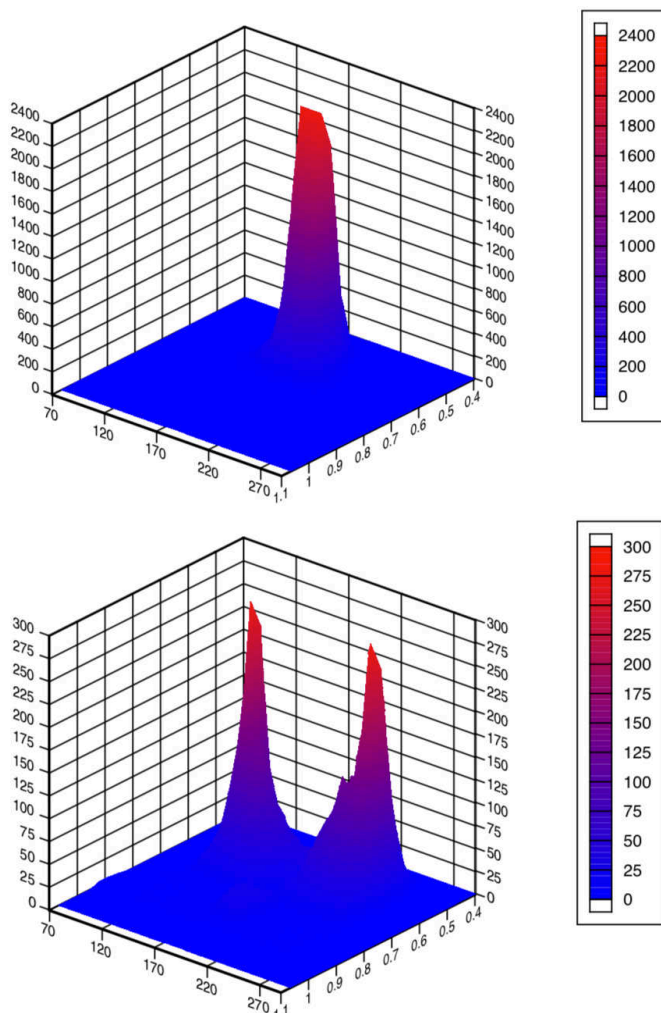


Figure 2.2. A 3-D histogram plot of hydrogen bonding crystal structures found in the CSD, displaying a correlation between normalized non-bonding distance and angle around the hydrogen, θ_1 (top) and lone pair of the carbonyl oxygen, θ_2 (bottom).

Two maxima were found around the carbonyl oxygen correlating to a normalized d of 1.64 Å and θ_2 values of 124° and 236°. These correlate to locations in space where the carbonyl oxygen acts as a Lewis base;^{13,14} the maxima illustrate the lone pairs on carbonyl oxygen. The angles were found to deviate from previous studies that focused on the lone pair interactions surrounding

oxygen of specific carbonyls, such as esters, amides, or ketones.^{10,13} For example, it was reported by Vedani and Dunitz that hydrogen bonds incorporating a ketone as the Lewis base are the most stable with an H—O=C bond angle of 135°.¹³ The CSD results presented in Fig. 2.2 instead demonstrates that carbonyls have different angular characteristics due to auxiliary interactions, and the aggregate H—O=C hydrogen bonding angles are 124° and 236° (Fig. 2.3). That is not to say that the angular dependence of specific carbonyls is not important, but rather that it was not the focus of this study.

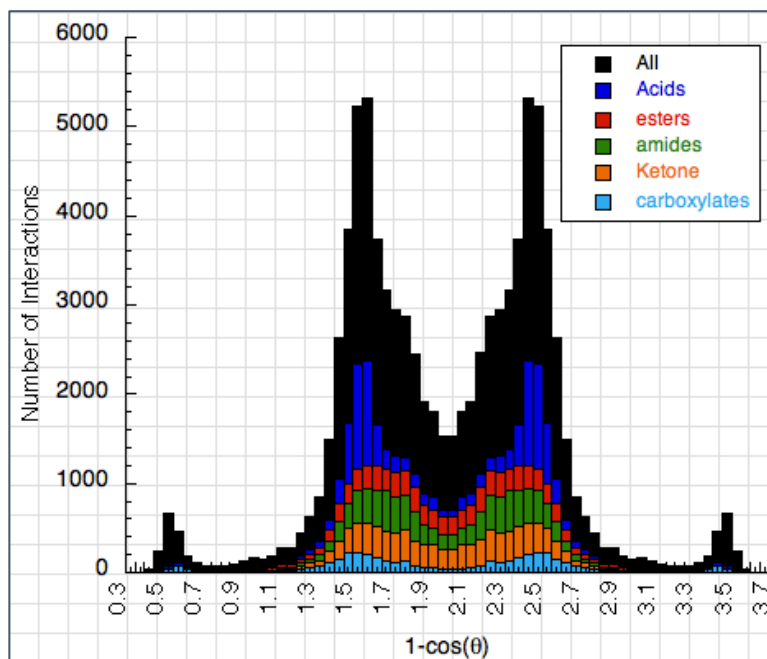


Figure 2.3. A 1-D histogram plot of hydrogen bonding crystal structures found in the CSD, displaying the stable lone pair interactions surrounding carbonyls acting as Lewis bases.

Experimental Evidence for the Geometry of Halogen Bonding

The CSD was scanned for structures with short R—X—O=C contacts to observe the distance-angle correlation of halogen bonding crystal structures (Fig. 2.4).⁶ A generic carbonyl group was chosen as the Lewis base to model biological halogen bonds,^{4,15} as well as parallel the hydrogen bonding results presented above. The distance was allowed to range from 0.0 Å to the sum of the van der Waals radii plus 10% ($\Sigma r_{vdw} \times 1.1$), and the R—X—O angle from 50° to 180°.

Of the near 800,000 crystal structures in the database,^{6,7,9,10,16,17} approximately 12,000 structures were found to have short X—O non-bonding distances. A number of these structures contained multiple short X—O non-bonding distances, bringing the total number of interactions found to approximately 18,000. The aggregate X—O=C data is presented in Appendix 2, Figures A2.1a–b.

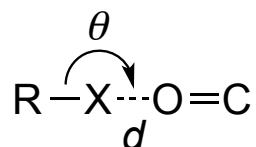


Figure 2.4. The general geometric parameters used to search the Cambridge Structural Database for known model halogen bonding crystal structures containing a carbonyl oxygen.

The aggregate R—X—O data was mirrored across the 180° plane to obtain a symmetric plot from 50° to 310° around X . The collected distances were normalized by Σr_{vdW} , and the distance-angle pairs were plotted (Fig. 2.5, top). The bond angles were then redistributed over $1-\cos(\theta)$, as was done for the alcohol-carbonyl hydrogen bonding interaction above, to show the impact of variable polar surface area (Fig. 2.5, bottom). The scatterplots corresponding to each halogen bonding case, $X = \text{F, Cl, Br, or I}$, can be found in Appendix 2, Figures A2.2a–d.

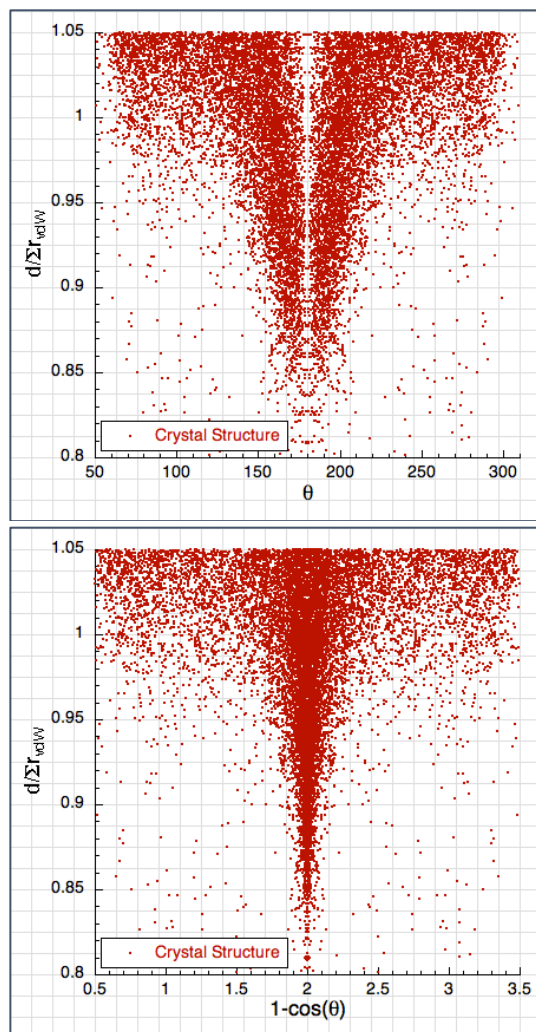


Figure 2.5. Scatterplots of the halogenated crystal structures displaying the correlation between normalized non-bonding distance versus angle (top) and redistributed angle by $1-\cos(\theta)$ (bottom); $1-\cos(\theta)$ evenly spaces the data around the surface of the halogen.

The distance versus angle dot density illustrates the high number of interactions within the region characteristic of halogen bonding. The program was again used to count the number of interactions as a function of distance and angle, using equal-sized surface area boxes to account for the decreased surface area near the polar axis (Fig. 2.6). The histogram-derived surfaces demonstrate that the highest concentration of halogen bonding geometries does in fact reside within the sum of the van der Waals radii for Cl, Br, and I. This is evidenced by the peak location at less than a normalized distance of 1. The total frequency of the interactions in the crystal

structures was also broken down by halogen ($X = \text{F}, \text{Cl}, \text{Br}, \text{I}$) to illustrate the contribution of each halogen to the maximum. The maximum for I occurs at a normalized distance of 0.88, Br resides at 0.91, Cl resides at 0.93, and F resides at 1.01, each at an angle of 180° . Halogen bonding strength is inversely proportional to non-bonding distance,^{18–21} therefore, the maxima of frequencies suggest that non-bonding interaction energy increases as a function of atomic size, which is directly proportional to polarizability and in agreement with the literature.^{21–24}

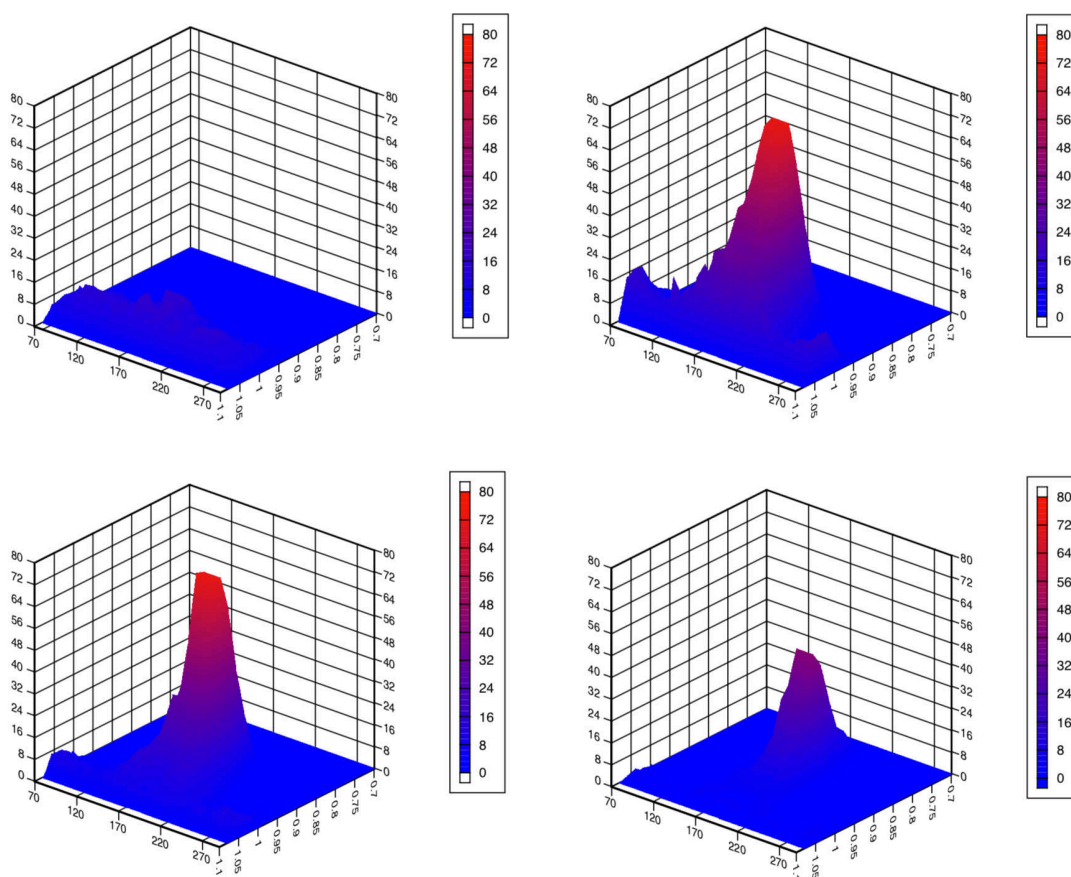


Figure 2.6. A 3-D histogram plot of the halogenated crystal structures of fluorine (top left), chlorine (top right), bromine (bottom left), and iodine (bottom right) found in the CSD displaying the correlation between normalized non-bonding distance and angle.

The aggregate distance-angle data was plotted in 3-D (Fig. 2.7), similarly to the hydrogen bonding 3-D plots in Fig. 2.2. The halogen bonding peak corresponds to the high frequency of model halogen bonding interactions with a $d < \Sigma r_{vdW}$ and $\theta = 180^\circ$. The two smaller clusters in the

Cl and Br plots of Fig. 2.6 as well as Fig. 2.7, which appear as high-density regions in Fig. 2.5, seen at d greater than Σr_{vdW} and θ approximately equal to 90° and 270° are the result of stable non-bonding interactions, though they are not geometrically defined as halogen bonding interactions. The maximum of the major peak aligns with the location of the σ -hole at short distance and its wider distribution can be attributed to environmentally induced distortions.⁴ The fact that there is a peak suggests that a significant attraction exists between halogen and oxygen.

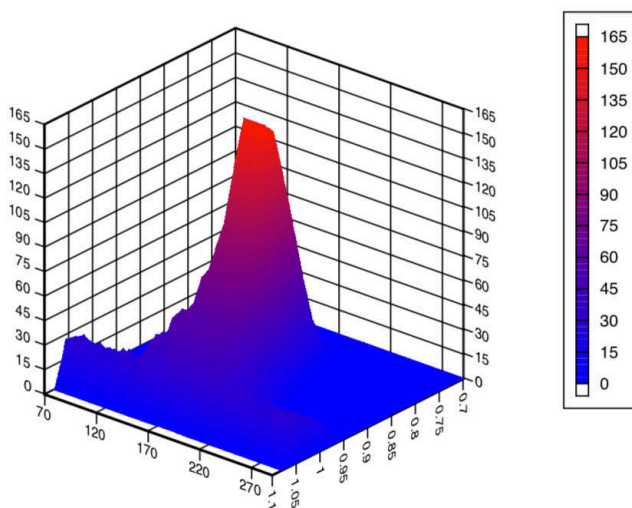


Figure 2.7. An aggregate 3-D histogram plot of the halogenated crystal structures found in the CSD displaying the correlation between normalized non-bonding distance and angle.

The angular dependence of halogen bonding is reported to be dependent on electrostatics, much like hydrogen bonding.^{1-3,15,20,25-35} The long-range interaction demonstrated in Fig. 2.7 does not have a significant angular dependence, signifying that the halogen bond does not project significant angular preference beyond the sum of the van der Waals radii, relative to the surface maximum. This is in contrast to the electrostatic potential contour plots of the halogens (Fig. 2.8), which illustrate an angular dependence that does not die off at the van der Waals radii of the atom.

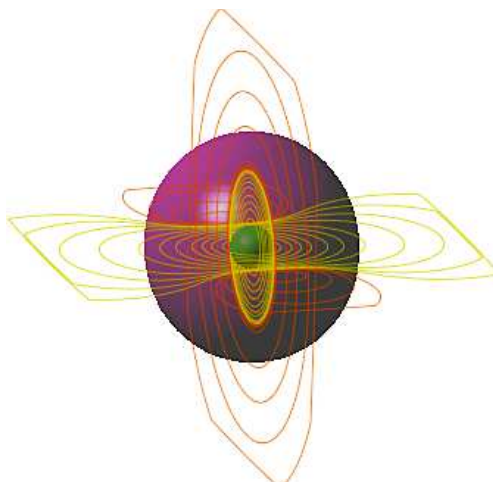


Figure 2.8. The electrostatic potential contours of chlorine atom mapped with its electron density surface, located at an isovalue of 0.0004. The orange contours represent negative electrostatic potentials, and the yellow contours the positive electrostatic potential, where the contours occur at isovalues of 0.002, 0.004, 0.008, 0.02, 0.04, 0.08, 0.2, 0.4, 0.8, 2, 4, 8, and 20. Chlorine was selected for clarity; the remaining halogens exhibit similar trends.

Analysis of the Experimental Angular Dependence of Halogen Bonding

A random statistical analysis was performed on the histogram data used to generate Figure 2.6 in order to draw quantitative conclusions on the nature of the trends observed (adapted from a private communication with Dr. P. S. Ho). The number of interactions that fit the geometric criteria of a halogen bond (N_{X-Bond}) in Fig. 2.7 were summed: $d/\Sigma r_{vdW} < 1.0$ and $155^\circ < \theta < 180^\circ$. The total number of interactions (N_{TOT}) in Fig. 2.7 were also summed (Table 2.1).

Table 2.1. The number of crystal structures found within our CSD results that demonstrate a halogen bonding geometry (N_{X-Bond}) in comparison to the total number found (N_{TOT}) per halogen, X . Those found with a halogen bonding geometry exhibited a normalized bond distance equal to or less than unity, and a bond angle between 155° and 180° .

X	N_{X-Bond}	N_{TOT}
F	102	4524
Cl	1396	8047
Br	1224	3850
I	585	1204

The percentage, P_{X-Bond} (Eqn. 2.1), of N_{X-Bond} in N_{TOT} was calculated and normalized by the expected values, N_{exp} (Eqn. 2.2). N_{exp} corrects P_{X-Bond} by scaling it to the contracted surface area

experienced near $\theta = 180^\circ$, and was found to equal 0.159 for each halogen. The van der Waals radii were reported by Bondi ($F = 2.99 \text{ \AA}$, $Cl = 3.25 \text{ \AA}$, $Br = 3.35 \text{ \AA}$, $I = 3.48 \text{ \AA}$).³⁷

$$P_{X-Bond} = \left(\frac{N_{X-Bond}}{N_{TOT}N_{exp}} \right) \times 100 \quad (2.1)$$

$$N_{exp} = \frac{2\pi r_{vdW}(\cos(180^\circ) - \cos(155^\circ))}{4\pi^2(r_{vdW}(\cos(180^\circ) - \cos(155^\circ))(\cos(180^\circ) - \cos(90^\circ)))} \quad (2.2)$$

The results of the analysis (Table 2.2) show that carbonyl oxygen is biased away from a halogen bonding configuration when in contact with fluorine (14.1%). It has an approximately random bias toward a halogen bonding configuration when in contact with chlorine (109%), and an increasing bias when in contact with bromine (200%) and then iodine (305%). The data also provide quantitative support for the frequency-distance correlation illustrated in Fig. 2.6 and suggest that the electronic structure of iodine leads to more stable halogen bonding than smaller elements like fluorine. The increase in number of model halogen bonds from fluorine to iodine correlates with non-bonding strength as reported in the literature.^{10,18,38-41}

Table 2.2. The results of the random statistical analysis (Dr. P. S. Ho), showing the bias away from the formation of a halogen bond ($P_{X-Bond} < 100\%$) or toward the formation of a halogen bond ($P_{X-Bond} > 100\%$). Percentages near 100% represent a random bias.

X	$P_{X-Bond} (\%)$
F	14.1
Cl	109
Br	200
I	305

Two additional percentages were calculated in order to understand halogen bonding trends at distances shorter than Σr_{vdW} and distances longer than Σr_{vdW} . P_{X-Bond}^{In} was calculated by taking the number of interactions found between $155^\circ < \theta < 180^\circ$ at $d/\Sigma r_{vdW} < 1.0$ (N_{X-Bond}^{In}) over the

total number found at $d/\Sigma r_{vdW} < 1.0$ (N_{TOT}^{In}), normalized by N_{exp} (Table 2.3). P_{X-Bond}^{Out} was calculated by taking the number of interactions found between $155^\circ < \theta < 180^\circ$ at $d/\Sigma r_{vdW} > 1.0$ (N_{X-Bond}^{Out}) over the total number found at $d/\Sigma r_{vdW} > 1.0$ (N_{TOT}^{Out}), normalized by N_{exp} .

Table 2.3. The number of crystal structures found within the sum of the van der Waals radii (*In*) in comparison to beyond the sum of the van der Waals radii (*Out*) per halogen, *X*. Those found with a halogen bonding geometry exhibited a bond angle between 155° and 180° .

<i>X</i>	N_{X-Bond}^{In}	N_{TOT}^{In}	N_{X-Bond}^{Out}	N_{TOT}^{Out}
F	102	640	375	3884
Cl	1396	2074	914	5973
Br	1224	1568	357	2282
I	585	738	48	466

The percentages, P_{X-Bond}^{In} and P_{X-Bond}^{Out} (Table 2.4), were determined using equations analogous to Eqn. 2.1 and 2.2. The results show that carbonyl oxygen interacts with fluorine at distances less the sum of the van der Waals radii randomly (99.9%), and then has an increasing bias toward halogen bonding as a periodic trend to iodine (498%). This signifies the increase in angular dependence of halogen bonding at a non-bonding distance shorter than the sum of the van der Waal's radii. The trend illustrated by P_{X-Bond}^{In} also matches that of P_{X-Bond} , where the number of stable halogen bonding structures increases from $X = F$ to I .

Table 2.4. The results of the random statistical analysis (Dr. P. S. Ho), showing the bias away from the formation of a halogen bond ($P_{X-Bond}^{In,Out} < 100\%$) or toward the formation of a halogen bond ($P_{X-Bond}^{In,Out} > 100\%$). Percentages near 100% represent a random bias.

<i>X</i>	P_{X-Bond}^{In} (%)	P_{X-Bond}^{Out} (%)
F	99.9	60.6
Cl	423	96.1
Br	490	98.0
I	498	64.7

The carbonyl oxygen is biased away from a halogen bonding configuration with fluorine (60.6%) and iodine (64.7%) at distances greater than the sum of the van der Waals radii. The Lewis base interacts with chlorine (96.1%) and bromine (98.0%) randomly beyond the sum of the van

der Waals radii. The results of these calculations provide quantifiable evidence of the distinct angular dependence of model halogen bonds at short and long non-bonding distances. In summary, the bias against a R–F—O non-bonding angle of 180° corresponds to long-range interactions, suggesting an electrostatic effect. The anisotropy of such short-range interactions appears to be random. In comparison, the anisotropy of long-range chlorinated and brominated halogen bonding structures appears to be random. It is the short-range interactions that show bias toward R–Cl—O and R–Br—O non-bonding angles of 180° , suggesting non-electrostatic effects. A bias can be seen against R–I—O halogen bonding for long-range interactions, but a strong bias toward halogen bonding for short-range interactions, suggesting a combination of electrostatics and non-electrostatic effects.

The CSD was used to observe the geometry of hydrogen and halogen bonding interactions in experimental crystal structures. Scatterplots and 3-D histogram plots were generated that illustrated a clear distance-angle correlation of the non-bonding geometry and the shapes of the Lewis acids and bases studied. The surface maxima were found to correlate with bond distances and angles that fit the geometric definition of hydrogen and halogen bonds, as seen in Table 1.1.^{15,18,24,42–46} The atomic shapes were then studied using various quantum mechanical methods to better understand the components of the interaction energy and their dependence on the electronic structure of X ,^{6,7,10,16,17,30} which will be discussed in the following Chapters.

REFERENCES

- (1) Wilcken, R.; Zimmermann, M. O.; Lange, A.; Zahn, S.; Boeckler, F. M. Using Halogen Bonds to Address the Protein Backbone: A Systematic Evaluation. *J. Comput. Aided Mol. Des.* **2012**, *26*, 935–945.
- (2) Parisini, E.; Metrangolo, P.; Pilati, T.; Resnati, G.; Terraneo, G. Halogen Bonding in Halocarbon–Protein Complexes: A Structural Survey. *Chem. Soc. Rev.* **2011**, *40*, 2267.
- (3) Matter, H.; Nazaré, M.; Güssregen, S.; Will, D. W.; Schreuder, H.; Bauer, A.; Urmann, M.; Ritter, K.; Wagner, M.; Wehner, V. Evidence for C-Cl/C-Br $\cdots\pi$ Interactions as an Important Contribution to Protein-Ligand Binding Affinity. *Angew. Chem. Int. Ed.* **2009**, *48*, 2911–2916.
- (4) Auffinger, P.; Hays, F. A.; Westhof, E.; Ho, P. S. Halogen Bonds in Biological Molecules. *Proc. Natl. Acad. Sci.* **2004**, *101*, 16789–16794.
- (5) Carter, M.; Rappé, A. K.; Ho, P. S. Scalable Anisotropic Shape and Electrostatic Models for Biological Bromine Halogen Bonds. *J. Chem. Theory Comput.* **2012**, *8*, 2461–2473.
- (6) Allen, F. H. The Cambridge Structural Database: A Quarter of a Million Crystal Structures and Rising. *Acta Crystallogr. B* **2002**, *58*, 380–388.
- (7) Kroon, J.; Kanters, J. A. Non-Linearity of Hydrogen Bonds in Molecular Crystals. *Nature* **1974**, *248*, 667–668.
- (8) McGaughey, G. B.; Gagné, M.; Rappé, A. K. π -Stacking Interactions. Alive and Well in Proteins. *J. Biol. Chem.* **1998**, *273*, 15458–15463.
- (9) Ouvard, C.; Le Questel, J.-Y.; Berthelot, M.; Laurence, C. Halogen-Bond Geometry: A Crystallographic Database Investigation of Dihalogen Complexes. *Acta Crystallogr. B* **2003**, *59*, 512–526.
- (10) Lommerse, J. P. M.; Stone, A. J.; Taylor, R.; Allen, F. H. The Nature and Geometry of Intermolecular Interactions Between Halogens and Oxygen or Nitrogen. *J. Am. Chem. Soc.* **1996**, *118*, 3108–3116.
- (11) Arunan, E.; Desiraju, G. R.; Klein, R. A.; Sadlej, J.; Scheiner, S.; Alkorta, I.; Clary, D. C.; Crabtree, R. H.; Dannenberg, J. J.; Hobza, P.; et al. Definition of the Hydrogen Bond (IUPAC Recommendations 2011). *Pure Appl. Chem.* **2011**, *83*.
- (12) Stone, A. J. Are Halogen Bonded Structures Electrostatically Driven? *J. Am. Chem. Soc.* **2013**, *135*, 7005–7009.
- (13) Vedani, A.; Dunitz, J. D. Lone-Pair Directionality in Hydrogen Bond Potential Functions for Molecular Mechanics Calculations: The Inhibition of Human Carbonic Anhydrase II by Sulfonamides. *J. Am. Chem. Soc.* **1985**, *107*, 7653–7658.
- (14) Lommerse, J. P. M.; Price, S. L.; Taylor, R. Hydrogen Bonding of Carbonyl, Ether, and Ester Oxygen Atoms with Alkanol Hydroxyl Groups. *J. Comput. Chem.* **1997**, *18*, 757–774.
- (15) Wilcken, R.; Zimmermann, M. O.; Lange, A.; Joerger, A. C.; Boeckler, F. M. Principles and Applications of Halogen Bonding in Medicinal Chemistry and Chemical Biology. *J. Med. Chem.* **2013**, *56*, 1363–1388.
- (16) Mooibroek, T. J.; Gamez, P. Halogen Bonding Versus Hydrogen Bonding: What Does the Cambridge Database Reveal? *CrystEngComm* **2013**, *15*, 4565.
- (17) Eramian, H.; Tian, Y.-H.; Fox, Z.; Beneberu, H. Z.; Kertesz, M. On the Anisotropy of van Der Waals Atomic Radii of O, S, Se, F, Cl, Br, and I. *J. Phys. Chem. A* **2013**, *117*, 14184–14190.
- (18) Riley, K. E.; Hobza, P. Investigations into the Nature of Halogen Bonding Including Symmetry Adapted Perturbation Theory Analyses. *J. Chem. Theory Comput.* **2008**, *4*, 232–242.
- (19) Thirman, J.; Engelage, E.; Huber, S. M.; Head-Gordon, M. Characterizing the Interplay of Pauli Repulsion, Electrostatics, Dispersion and Charge Rransfer in Halogen Bonding with Energy Decomposition Analysis. *Phys. Chem. Chem. Phys.* **2018**, *20*, 905–915.
- (20) Metrangolo, P.; Resnati, G. Halogen Bonding: A Paradigm in Supramolecular Chemistry. *Chem. - Eur. J.* **2001**, *7*, 2511–2519.

- (21) Riley, K. E.; Murray, J. S.; Fanfrlík, J.; Řezáč, J.; Solá, R. J.; Concha, M. C.; Ramos, F. M.; Politzer, P. Halogen Bond Tunability II: The Varying Roles of Electrostatic and Dispersion Contributions to Attraction in Halogen Bonds. *J. Mol. Model.* **2013**, *19*, 4651–4659.
- (22) Desiraju, G. R.; Ho, P. S.; Kloo, L.; Legon, A. C.; Marquardt, R.; Metrangolo, P.; Politzer, P.; Resnati, G.; Rissanen, K. Definition of the Halogen Bond (IUPAC Recommendations 2013). *Pure Appl. Chem.* **2013**, *85*, 1711–1713.
- (23) Politzer, P.; Murray, J. S.; Clark, T. Halogen Bonding and Other σ -Hole Interactions: A Perspective. *Phys. Chem. Chem. Phys.* **2013**, *15*, 11178.
- (24) Shields, Z. P.; Murray, J. S.; Politzer, P. Directional Tendencies of Halogen and Hydrogen Bonds. *Int. J. Quantum Chem.* **2010**, *110*, 2823–2832.
- (25) Priimagi, A.; Cavallo, G.; Metrangolo, P.; Resnati, G. The Halogen Bond in the Design of Functional Supramolecular Materials: Recent Advances. *Acc. Chem. Res.* **2013**, *46*, 2686–2695.
- (26) Aakeröy, C. B.; Wijethunga, T. K.; Desper, J. Practical Crystal Engineering Using Halogen Bonding: A Hierarchy Based on Calculated Molecular Electrostatic Potential Surfaces. *J. Mol. Struct.* **2014**, *1072*, 20–27.
- (27) Zordan, F.; Brammer, L.; Sherwood, P. Supramolecular Chemistry of Halogens: Complementary Features of Inorganic (M–X) and Organic (C–X') Halogens Applied to M–X \cdots X'–C Halogen Bond Formation. *J. Am. Chem. Soc.* **2005**, *127*, 5979–5989.
- (28) Ibrahim, M. A. A. Molecular Mechanical Perspective on Halogen Bonding. *J. Mol. Model.* **2012**, *18*, 4625–4638.
- (29) Chudzinski, M. G.; McClary, C. A.; Taylor, M. S. Anion Receptors Composed of Hydrogen- and Halogen-Bond Donor Groups: Modulating Selectivity With Combinations of Distinct Noncovalent Interactions. *J. Am. Chem. Soc.* **2011**, *133*, 10559–10567.
- (30) Xu, Z.; Yang, Z.; Liu, Y.; Lu, Y.; Chen, K.; Zhu, W. Halogen Bond: Its Role beyond Drug–Target Binding Affinity for Drug Discovery and Development. *J. Chem. Inf. Model.* **2014**, *54*, 69–78.
- (31) Pérez-Torralba, M.; García, M. Á.; López, C.; Torralba, M. C.; Torres, M. R.; Claramunt, R. M.; Elguero, J. Structural Investigation of Weak Intermolecular Interactions (Hydrogen and Halogen Bonds) in Fluorine-Substituted Benzimidazoles. *Cryst. Growth Des.* **2014**, *14*, 3499–3509.
- (32) Rissanen, K. Halogen Bonded Supramolecular Complexes and Networks. *CrystEngComm* **2008**, *10*, 1107.
- (33) Lu, Y.; Shi, T.; Wang, Y.; Yang, H.; Yan, X.; Luo, X.; Jiang, H.; Zhu, W. Halogen Bonding-A Novel Interaction for Rational Drug Design? *J. Med. Chem.* **2009**, *52*, 2854–2862.
- (34) Zhou, P.; Lv, J.; Zou, J.; Tian, F.; Shang, Z. Halogen–Water–Hydrogen Bridges in Biomolecules. *J. Struct. Biol.* **2010**, *169*, 172–182.
- (35) Kolář, M.; Hobza, P.; Bronowska, A. K. Plugging the Explicit σ -Holes in Molecular Docking. *Chem. Commun.* **2013**, *49*, 981–983.
- (36) Riley, K. E.; Murray, J. S.; Politzer, P.; Concha, M. C.; Hobza, P. Br \cdots O Complexes as Probes of Factors Affecting Halogen Bonding: Interactions of Bromobenzenes and Bromopyrimidines with Acetone. *J. Chem. Theory Comput.* **2009**, *5*, 155–163.
- (37) Bondi, A. Van Der Waals Volumes and Radii. *J. Phys. Chem.* **1964**, *68*, 441–451.
- (38) Sladek, V.; Punyain, K.; Ilčin, M.; Lukeš, V. Substitution Effect on the Intermolecular Halogen and Hydrogen Bonds of the σ -Bonded Fluorinated Pyridine \cdots XY/HX Complexes (XY = F₂, Cl₂, ClF; HX = HF, HCl). *Int. J. Quantum Chem.* **2014**, *114*, 869–878.
- (39) Jabłoński, M.; Palusiak, M. Nature of a Hydride–Halogen Bond. A SAPT-, QTAIM-, and NBO-Based Study. *J. Phys. Chem. A* **2012**, *116*, 2322–2332.
- (40) Politzer, P.; Murray, J. S.; Clark, T. σ -Hole Bonding: A Physical Interpretation. In *Halogen Bonding I*; Metrangolo, P., Resnati, G., Eds.; Springer International Publishing: Cham, 2014; Vol. 358, pp 19–42.
- (41) Politzer, P.; Murray, J. S. Halogen Bonding: An Interim Discussion. *ChemPhysChem* **2013**, *14*, 278–294.
- (42) Politzer, P.; Riley, K. E.; Bulat, F. A.; Murray, J. S. Perspectives on Halogen Bonding and Other σ -Hole Interactions: Lex Parsimoniae (Occam's Razor). *Comput. Theor. Chem.* **2012**, *998*, 2–8.

- (43) Riley, K. E.; Merz, K. M. Insights into the Strength and Origin of Halogen Bonding: The Halobenzene–Formaldehyde Dimer. *J. Phys. Chem. A* **2007**, *111*, 1688–1694.
- (44) Peebles, S. A.; Fowler, P. W.; Legon, A. C. Anisotropic Repulsion in Complexes B–Cl₂ and B–HCl: The Shape of the Chlorine Atom-in-a-Molecule. *Chem. Phys. Lett.* **1995**, *240*, 130–134.
- (45) Riley, K. E.; Murray, J. S.; Fanfrlík, J.; Řezáč, J.; Solá, R. J.; Concha, M. C.; Ramos, F. M.; Politzer, P. Halogen Bond Tunability I: The Effects of Aromatic Fluorine Substitution on the Strengths of Halogen-Bonding Interactions Involving Chlorine, Bromine, and Iodine. *J. Mol. Model.* **2011**, *17*, 3309–3318.
- (46) Kolář, M.; Hobza, P. On Extension of the Current Biomolecular Empirical Force Field for the Description of Halogen Bonds. *J. Chem. Theory Comput.* **2012**, *8*, 1325–1333.

CHAPTER 3: DIMER SYSTEMS

The first image of a halogen bonding structure was reported by Hassel et al. in 1954 when an X-ray diffraction structure of a Br_2 —1,4-dioxane adduct was obtained.^{1,2} The interaction distance (d) between bromine and oxygen was reported to be 2.71 Å (Fig. 3.1). The bond angle (θ) was reported to be near 180° (*Ref. 1; Fig. 1*). Hassel et al. did not provide an explanation for the unexpected short distance between halogen and oxygen, saying instead that “work [had] been started” on analogous halogenated compounds, and “the consequences of these findings [would] be discussed in a forthcoming, more detailed publication.”¹⁻³ Subsequent publications provided the structures for I_2 —1,4-dioxane⁴ and Cl_2 —1,4-dioxane.⁵ For each system the X—O interaction distance was reported to be roughly 80% of the van der Waals distance. The shorter-than-expected interaction distance near 180° is attributed to the positive polar cap on the halogen, and its ability to attract electron rich elements, such as oxygen, according to the modern σ -hole model.⁶⁻¹⁰

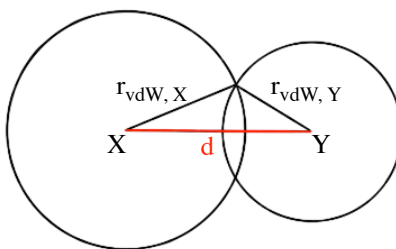


Figure 3.1. A halogen bond is said to exist between a halogen acting as a Lewis acid (X) and Lewis base (Y) if the interaction distance, d , is shorter than the sum of the two atom's van der Waals radii, $r_{vdW,X}$ and $r_{vdW,Y}$.

The σ -hole on a halogen is said to result from its singly-occupied p_z -orbital participating in a covalent bond, of which electron density shifts toward the covalent bond.^{8,11-13} This shift in density exposes the positive charge of the nucleus. The magnitude of the shift is correlated to the polarizability of the atom and the electron-withdrawing strength of the substituent group on the

halogen atom.^{11,14,15} For example, fluorine withdraws electron density from bromine in the molecule BrF (Fig. 3.2), increasing the partially positive σ -hole on bromine when compared to the σ -hole on diatomic Br₂. Whether a covalent bond is necessary to form a σ -hole has been a point of contention, but the existence of positive polar caps on neutral fluorine and chlorine atoms have been reported, where the lack of a covalent bond leads to two, smaller σ -holes on the surface of a halogen, corresponding to the $-z$ and $+z$ directions.^{8,9}

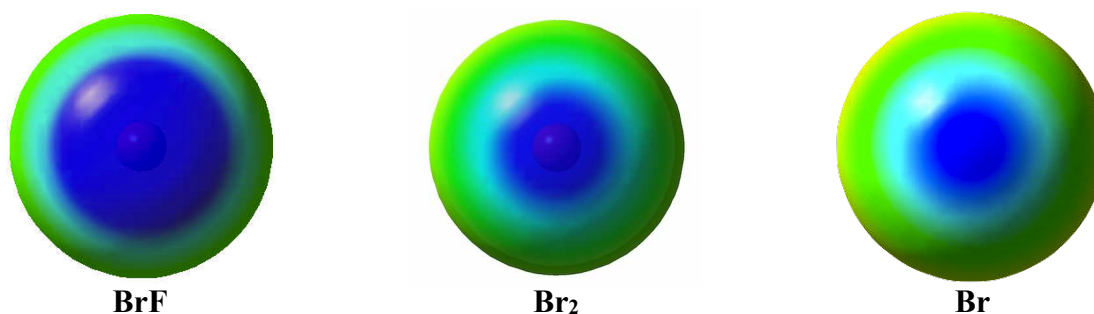


Figure 3.2. The σ -hole is seen to decrease in size from BrF > Br₂ > Br when looking down the covalent bond or free, singly-occupied p_z-orbital. Red represents a negative electrostatic potential (-15.7 kcal/mol) and blue represents a positive electrostatic potential (15.7 kcal/mol) between a negative point charge probe and the molecule evaluated at grid point points on the 0.0004 electron density isosurface.

In a study completed by K. E. Riley and P. Hobza in 2008,¹⁶ the results of four different quantum methods determined that iodomethane consistently had a larger binding energy (ΔE) to formaldehyde than bromomethane, which was larger than chloromethane. The strength of the attraction was correlated with the polarizability of the atom, associated with an electrostatic component.¹⁷⁻²¹ However, the strength of the attraction was also correlated to the percent contraction of the non-bonding X—O distance (Table 3.1), and if alternate energetic components are considered to exist within halogen bonding structures,^{16,22-26} this finding implies a strong dispersive contribution as the halogen increased in size. Dispersion strengthens non-bonding interactions at short distances, so the percent contraction of non-bonding distance (d) from the sum of the van der Waals radii (Σr_{vdW}) was used as a proportional approximation of the dispersive

component. A similar measure of bond distances normalized by the sum of the van der Waals radii was used in Chapter 2 of this thesis to compare distance-dependence between halogenated species. Such scaled distances ($d/\Sigma r_{vdW}$) are also presented in Table 3.1, and will continue to be used throughout this chapter.

Table 3.1. The MP2 binding energies, ΔE , and non-bonding distances, d , presented by Riley and Hobza¹⁶ at the optimized geometries of the halomethanes and formaldehyde. Van der Waals radii determined by Bondi.²⁷ Riley and Hobza calculated a percent contraction of the bond from the sum of the van der Waals radii; our normalizations are presented for comparison.

	ΔE (kcal/mol)	d (Å)	Σr_{vdW} (Å)	Contraction (%)	$d/\Sigma r_{vdW}$
CH ₃ Cl—OCH ₂	-1.11	3.26	3.27	0.31	0.997
CH ₃ Br—OCH ₂	-1.68	3.29	3.37	2.37	0.976
CH ₃ I—OCH ₂	-2.34	3.30	3.50	5.71	0.943

Energetic components of non-bonding interactions also have an angular dependence along with a distance dependence.^{16,18,19,28,29} In Chapter 2, the maximum on the 3-D surface generated using experimental crystal structures shown in Fig. 2.6 demonstrated a clear angular dependence at short distances. The reported angular dependence of halogen bonding must therefore be dependent on its anisotropic components, such as electrostatics and exchange repulsion. However, the angular dependence drastically decreases at long-range, signifying that the energetic components that are responsible for initial attraction must also be approximately isotropic at long-range, such as dispersion. The focus of this chapter will be the distance and angle dependence of the total interaction energy between small halogen bonding dimers, and the relative contributions of the energetic components: electrostatic potential, exchange repulsion, and dispersion.

Electronic Structure Studies as a Function of Distance

Acetone was selected to as a model carbonyl functional group; methyl and phenyl halides were used as representative electron donating and withdrawing organic frameworks, respectively, to model the geometric dependence of biological halogen bonds.^{15,30,31} The underlying attractive components of the interaction energy were expected to increase in magnitude relative to the polarizability of the atom and electron-withdrawing strength of the organic substituent group, whereas the repulsive forces would decrease. Both factors are known to increase the size of the partially positive electrostatic potential of the σ -hole,^{15,18,20} leading to a greater ΔE between acetone and the organic halides. The distance-dependence of the interaction energy of the phenyl halide was calculated, where the organic moiety is a slightly electron-withdrawing functional group. Then, the interaction energy of the methyl halides was calculated, where methyl is an electron-donating functional group. Finally, ΔE of diatomic halogens was calculated as a control.

The halogen-containing monomers were optimized at the HF/6-31G level and placed in a halogen bonding orientation, where the C-X—O bond angle was held constant at 180°. The X—O=C angle was set to 130°. In this way, the Lewis base aligned with the σ -hole on the Lewis acid. For reference, the X—O=C angle in the crystal structure of Br₂—acetone is 124°.³² The electrostatic potential was mapped onto the electron density of the present models in order to compare the sizes of the σ -holes (Fig. 3.3). As expected, the relative size and strength of the phenyl halide σ -holes were larger than those of the methyl halides due to the electron-withdrawing nature of the substituent.

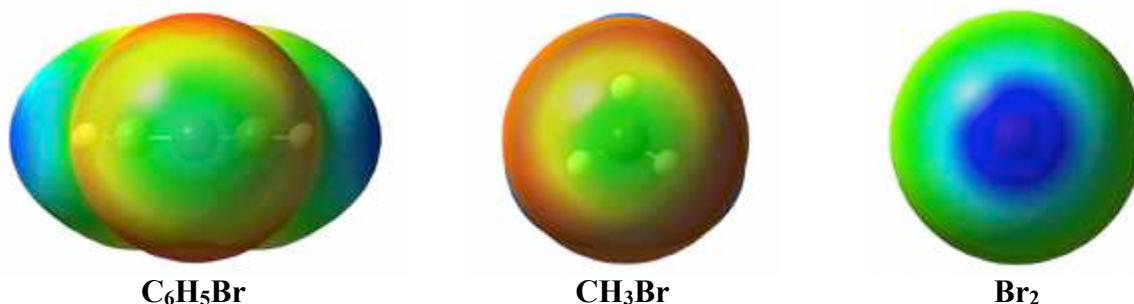


Figure 3.3. The σ -hole on bromobenzene, bromomethane, and bromine can be visualized using electrostatic potential maps. Red represents a negative electrostatic potential (-15.7 kcal/mol) and blue represents a positive electrostatic potential (15.7 kcal/mol) between a negative point charge probe and the molecule evaluated at grid point points on the 0.0004 electron density isosurface.

The interaction energy, ΔE (Eqn. 3.1), of the model dimers was calculated as a function of the non-bonding distance at a constant θ of 180° .

$$\Delta E = E_{X-Y} - (E_X + E_Y) \quad (3.1)$$

The sum of the halogen (E_X) and Lewis base (E_Y) monomer energies was subtracted from the single point energy of the dimer (E_{X-Y}). The ΔE was calculated as a function of d in 0.1 Å steps. Once ΔE was calculated as a function of distance, the halogen bonding strength was computed as a function of angle at the non-bonding minimum (Fig. 3.4), which will be the focus of the following section. The small molecular dimer calculations were performed at the HF/aug-cc-pVTZ and MP2/aug-cc-pVTZ levels for $X = \text{F, Cl, and Br}$, and at the HF/aug-cc-pVTZ-PP and MP2/aug-cc-pVTZ-PP levels for $X = \text{I}$.

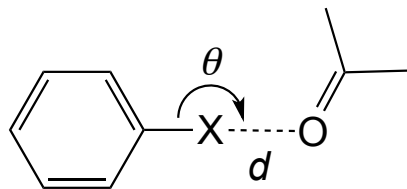


Figure 3.4. The model halogen bond between a halobenzene and acetone, where halogen, X , and O were placed in close-proximity. Non-bonding distance, d , was increased in 0.1 \AA steps while angle, θ , was initially held constant. Then, d was held constant at the energetic minimum and θ increased from 90° to 180° in 10° steps. The $X\text{---}O\text{---}C$ bond angle was held constant at 130° . The substituent group was first exchanged for a methyl group and then an additional X , and the distance dependent and angle dependent calculations repeated.

These methods, Hartree-Fock (HF) and Møller-Plesset 2nd Order Perturbation (MP2), were used to qualitatively probe the energetic components of ΔE . HF provides an estimate of the electrostatic interaction and exchange repulsion, and the difference in ΔE between the HF and MP2 dominantly estimates the dispersive component.³³ Computational methodology is limited by the size and complexity of molecular structures,^{34,35} but Dunning's augmented correlation consistent triple zeta basis set was able to be used due to our focus on small molecular dimers limited to no more than 12 atoms per molecule.³⁶ Dunning's suite of cc-pVXZ basis sets are advantageous because they include polarization, diffuse exponents, and optional pseudo-potential extensions to account for relativistic core effects in heavy atoms like iodine.³⁶⁻³⁸ A counterpoise correction was also included to address basis set superposition error (BSSE).³⁹

Locations of energetic minima were identified for $X = \text{Cl}$, Br , and I at the HF and MP2 levels as a function of d between acetone and the phenyl halides (Fig. 3.5). For $X = \text{F}$, there is not a minimum on either potential curve.

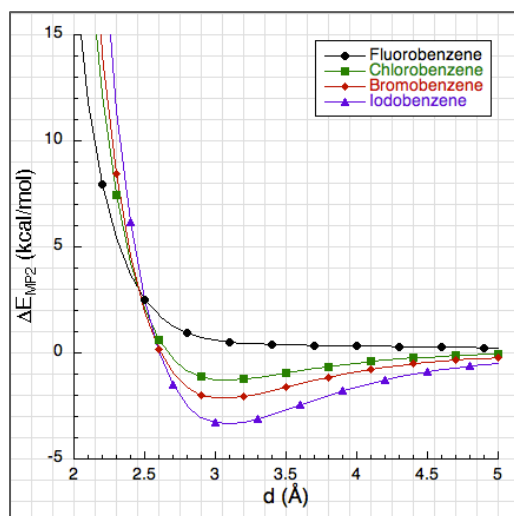
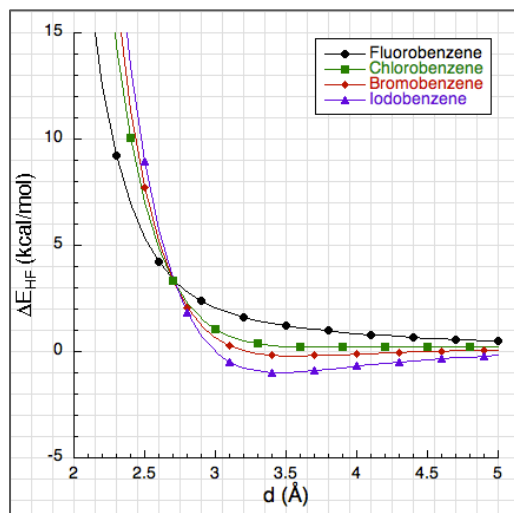


Figure 3.5. The interaction energy of the halobenzenes as a function of distance with acetone using HF (top) and MP2 (bottom). The well depths are seen to increase from fluorobenzene to iodobenzene, signifying a more stable interaction with acetone as a periodic trend.

Consider the results for acetone with bromobenzene, for example. The potential curves were visually inspected to find energetic minima at well depths of -0.2 kcal/mol at 3.6 Å and -2.1 kcal/mol at 3.1 Å using the HF and MP2 methods, respectively. The HF results suggest that the electrostatic attraction is not strong enough to overcome exchange repulsion because the minimum in ΔE occurs at a d larger than $\sum r_{vdW}$, which is equal to 3.37 Å for Br—O. The MP2 results suggest that the decreased exchange repulsion near 180° , which is due to the aspherical shape of bromine (Fig. 3.6), enables acetone to approach the halogen more closely than the sum of the van der Waals

radii and interact attractively through dispersion. The dispersion, found to be -2.6 kcal/mol at the energy minimum, was calculated by subtracting the HF interaction energy from the MP2 interaction energy. Similar conclusions could be drawn for the remaining halobenzenes; dispersion was stronger at the well minimum than electrostatic attraction.

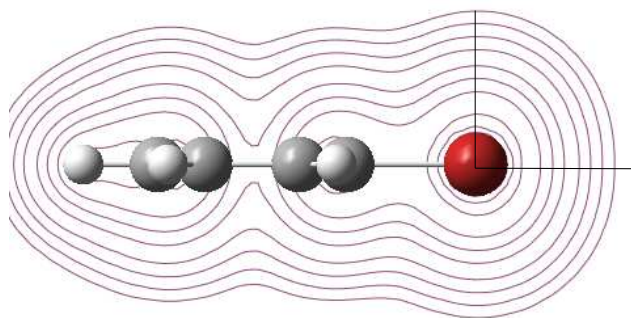


Figure 3.6. The electron density contour plot of bromobenzene. The solid axes are the same size, illustrating the aspherical shape of the halogen that results from the singly-occupied p_z -orbital. The decrease in electron density extending from the covalent bond in bromobenzene leads to a decrease in the exchange repulsion experienced by acetone at an angle of 180° .

The well depths were also observed to increase from fluorobenzene to iodobenzene in both the HF and MP2 curves. The σ -hole of a halogen increases in size from F to I, leading to the greater electrostatic attraction illustrated by the HF results. The interaction distances, on the other hand, remained approximately the same between each X—O while the normalized van der Waals distances shortened (Table 3.2). This can be explained by the polarizability of each halogen, where iodine is most susceptible to the electron-withdrawing substituent, enabling a stronger attraction at a shorter relative distance. The HF results, along with the MP2 results, for acetone with the halobenzenes, suggest that the contraction of d is due to a combination of electrostatics and dispersion, not solely the electrostatics.

Table 3.2. The non-bonding distances as estimated from the MP2 interaction curves, which were then normalized by the sum of the van der Waals radii to approximate the relative contraction of non-bonding distances for acetone in close proximity to the halobenzenes.

Lewis Acid	d (Å)	Σr_{vdW} (Å)	$d/\Sigma r_{vdW}$
Fluorobenzene	-	2.99	-
Chlorobenzene	3.1	3.27	0.95
Bromobenzene	3.1	3.37	0.92
Iodobenzene	3.1	3.50	0.88

Our hypothesis stated at the beginning of this section was that the underlying attractive components would increase in magnitude with the electron-withdrawing strength of the substituent. Similarly, the repulsive component, exchange repulsion, would decrease. The opposite, therefore, was expected to be true when observing halogen bonding strength in the presence of an electron-donating moiety. This hypothesis was tested by considering the interaction energy between acetone and the methyl halides as a function of d at the HF and MP2 levels (Fig. 3.7). The locations of energetic minima were visually identified for $X = \text{Cl}$, Br , and I . As with the phenyl halides no minimum was found for $X = \text{F}$.

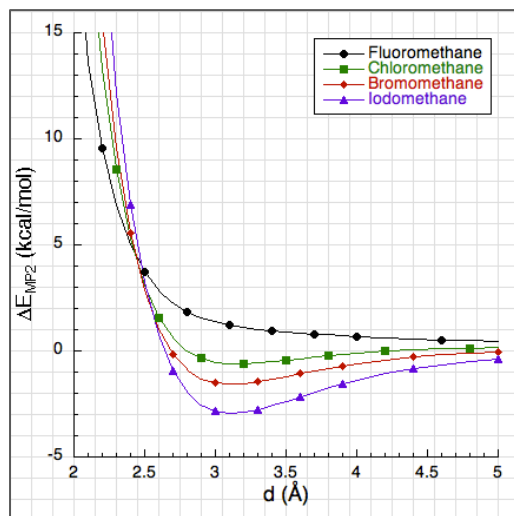
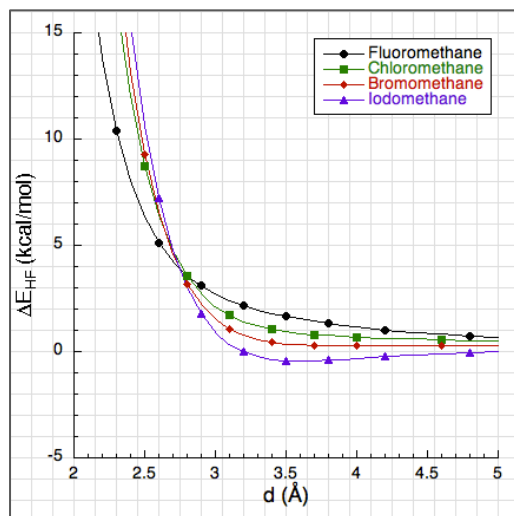


Figure 3.7. The interaction energy of the halomethanes as a function of distance with acetone using HF (top) and MP2 (bottom). The well depths are seen to increase from fluoromethane to iodomethane, signifying a more stable interaction with acetone as a periodic trend.

Consider the results for acetone with bromomethane, where no energetic minimum was found using HF in contrast to an approximate well depth of -1.6 kcal/mol at 3.1 Å using MP2. The interaction energy is smaller than that of bromobenzene with acetone because the underlying electrostatic attraction has decreased. This is further evidenced by the lack of energetic minima for $X = \text{F}$, Cl , and Br and a very shallow minimum for $X = \text{I}$ at the HF level, which is consistent with the decrease in size of bromomethane's σ -hole in Figure 3.3 relative to bromobenzene. Exchange repulsion was calculated as a function of distance for both bromobenzene and -methane using a

helium probe at the HF/aug-cc-pVTZ level to compare the energetic components. Exchange repulsion was 0.48 kcal/mol between acetone and bromobenzene, and 0.51 kcal/mol between acetone and bromomethane at 3.0 Å, which is not a significant difference.

Dispersion at the energetic minimum, calculated by subtracting the interaction energy at the HF level from the MP2 level, was equal to -2.7 kcal/mol. The dispersion between acetone and bromomethane unexpectedly increased by 0.1 kcal/mol in comparison to that of bromobenzene, although this could be attributed to slight differences in geometry. Just as with the halobenzenes, ΔE was found to increase as a function of distance from fluoromethane to iodomethane, although d from the MP2 interaction energy curve slightly decreased. The finding is consistent with the phenyl halide results in that iodine is the most polarizable halogen and can accommodate interacting with a Lewis base, such as acetone, enabling a stronger attraction at a shorter relative distance than chlorine or bromine (Table 3.3). The magnitude of the interaction was not as large due to the shift in electron density toward the Lewis base, however.

Table 3.3. The non-bonding distances as estimated from the MP2 interaction curves, which were then normalized by the sum of the van der Waals radii to approximate the relative contraction of non-bonding distances for acetone in close proximity to the halomethanes.

Lewis Acid	d (Å)	Σr_{vdW} (Å)	$d/\Sigma r_{vdW}$
Fluoromethane	-	2.99	-
Chloromethane	3.2	3.27	0.98
Bromomethane	3.1	3.37	0.92
Iodomethane	3.1	3.50	0.89

As discussed above, crystal structures of molecular halogen-dioxane adducts have been reported and the X—O interaction distances are shorter than the van der Waals distances, roughly 80% of the van der Waals distances. The interaction energy of acetone was calculated with the diatomic halogens as a control against the electron-withdrawing and -donating results. For the diatomic halogens, a substituent with equal electronegativity led to an aspherical atom shape and

partially positive σ -hole due to the involvement of the halogen singly-occupied p_z -orbital in a nonpolar covalent bond (Fig. 3.8).

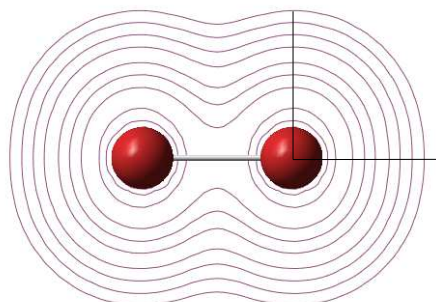


Figure 3.8. The electron density contour of bromine, which illustrates the aspherical shape of the halogens. The solid axes are the same size, relative to the perpendicular axes of bromine. The decrease in electron density opposite the covalent bond in bromine leads to a decrease in the exchange repulsion experienced by acetone at an angle of 180° .

ΔE was calculated as a function of d at the HF and MP2 levels (Fig. 3.9), and the locations of energetic minima were identified for $X = \text{F, Cl, Br, and I}$. In contrast to the above results for methyl and phenyl halides, there is a minimum for fluorine here. Consider the results for acetone with bromine, where energetic minima were found at well depths of -2.2 kcal/mol at 3.1 \AA and -5.4 kcal/mol at 2.8 \AA using the HF and MP2 methods, respectively. The HF results suggest that electrostatic attraction increases when compared to the organic bromine models, and/or exchange repulsion decreases. Even though aryls are thought of as being electron-withdrawing and alkyls as being electron-donating relative to an organic “standard”, the electronegativity of halogen relative to carbon promotes electron transfer toward the halogen for organic halides in general. There is no such charge transfer in diatomic bromine, leading to an increase in σ -hole size, decrease in interaction distance, and increase in halogen bonding strength.

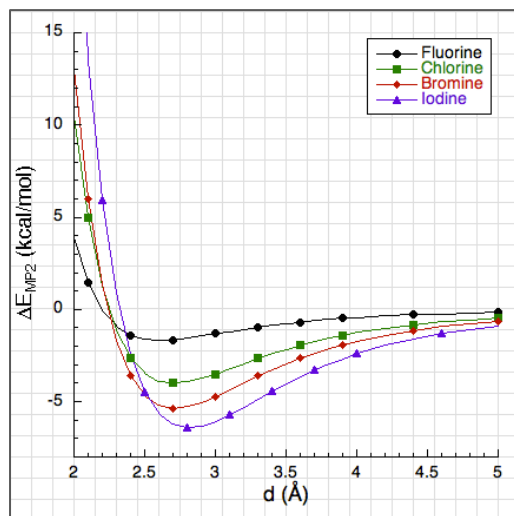
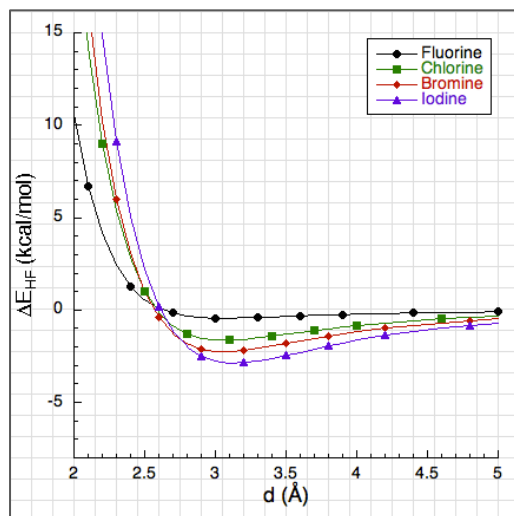


Figure 3.9. The interaction energy of the molecular halogens as a function of distance with acetone using HF (top) and MP2 (bottom). The well depths are seen to increase from fluorine to iodine, signifying a more stable interaction with acetone as a periodic trend.

The interaction energy is stronger than that of bromobenzene or bromomethane with acetone by 3.3 kcal/mol and 3.6 kcal/mol, respectively. Dispersion, calculated by subtracting the interaction energy at the HF level from the MP2 level, was found to equal -3.9 kcal/mol at 2.8 Å. This component was larger than when compared to that of bromobenzene or bromomethane with acetone by 1.2 kcal/mol and 1.1 kcal/mol, respectively, which is consistent with our hypothesis of charge transfer due to electronegativity differences with the substituent group not existing in the diatomic halogens. Exchange repulsion decreased when compared to the organic bromine models

and the attractive dispersion, therefore, increased. Similar conclusions could be drawn for the remaining diatomic halogens. In addition, ΔE and d from the MP2 curves increased from F₂ to I₂. The polarizability of iodine made it more susceptible to the impact of the nonpolar covalent bond, as evident by $d/\Sigma r_{vdW}$ (Table 3.4).

Table 3.4. The non-bonding distances as estimated from the MP2 interaction curves, which were then normalized by the sum of the van der Waals radii to approximate the relative contraction of non-bonding distances for acetone in close proximity to the diatomic halogens.

Lewis Acid	d (Å)	Σr_{vdW} (Å)	$d/\Sigma r_{vdW}$
Fluorine	2.6	2.99	0.87
Chlorine	2.7	3.27	0.83
Bromine	2.7	3.37	0.80
Iodine	2.8	3.50	0.80

The scaled van der Waals distances for organic halides were found to be roughly 90% of the standard distances whereas for molecular halides the distances were as low as 80% of the standard distances. Difference curves, calculated by subtracting the binding energy of X₂—acetone from that of RX—acetone at the MP2 level, were used order to explicitly determine the source of the differentiation between molecular halogens and organic halides (Fig. 3.10). In general, the phenyl and methyl binding energies are more repulsive than X₂, as expected given the observed stronger and shorter binding curves for X₂. The electron donating methyl group is consistently more repulsive than electron withdrawing phenyl group. The difference between the halogen atom, X, and corresponding X₂ is quite small for F and Cl. In fact, acetone is more attracted to monoatomic fluorine than diatomic fluorine at all distances, and acetone is as attracted to monoatomic chlorine as it is to diatomic chlorine. This is in contrast to acetone being more attracted to diatomic bromine and iodine than it is to monoatomic bromine and iodine.

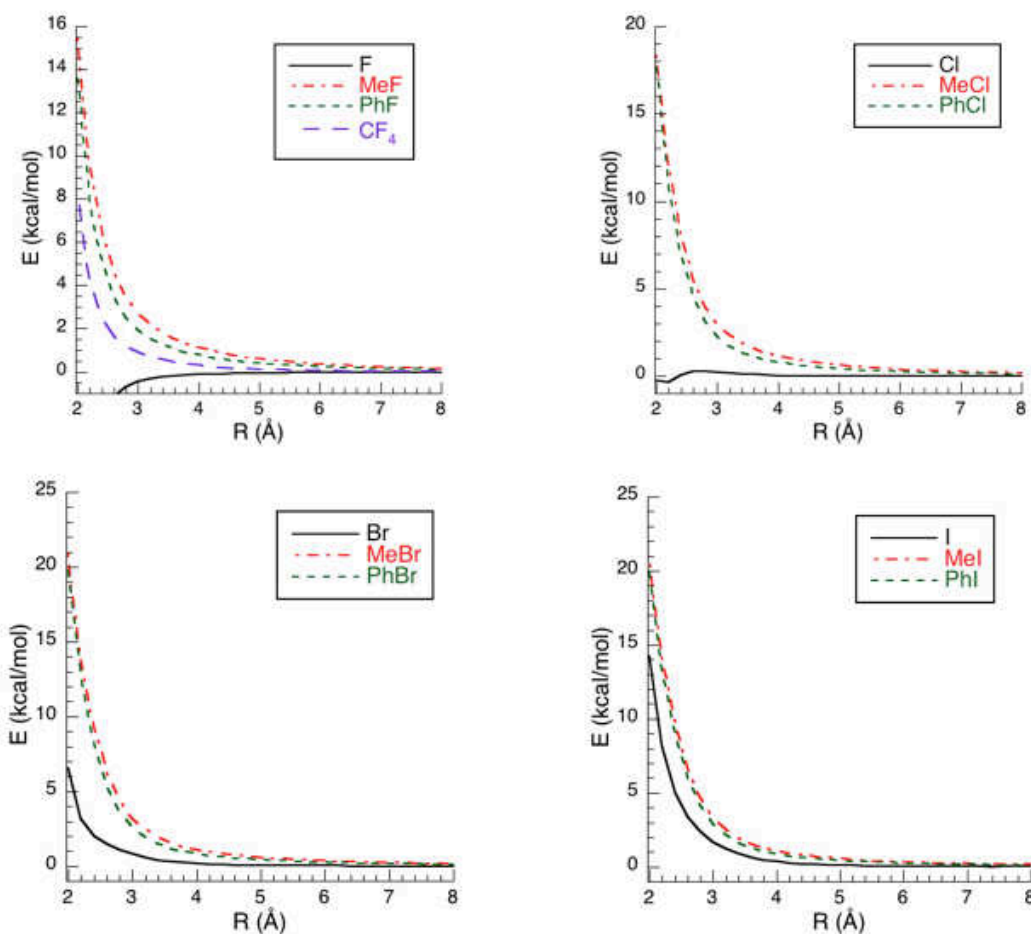


Figure 3.10. Difference curves of the interaction energies between phenyl- and methylhalogens and acetone as a function of distance. The organic moieties were found to consistently result in more repulsive model halogen bonds than the diatomic halogens with acetone.

Thus far, we have analyzed the distance-dependence of the energetic components of ΔE in three halogen bonding model dimers, and have reported both substituent and periodic trends.

Electronic Structure Studies as a Function of Angle

The focus of the previous section was the interaction energy and relative contributions of the electrostatics, exchange repulsion, and dispersion to the binding energy as a function of distance. The interaction energies in this section will be calculated as a function of angle at a constant distance. Our hypothesis was that the electrostatics and exchange repulsion would

demonstrate an angular dependence. The electrostatic component was expected to be attractive and the exchange repulsion component expected to be weaker at $\theta = 180^\circ$ due to the alignment of the carbonyl oxygen with the halogen's σ -hole. The dimers would interact more repulsively as the angle rotated away from 180° , as the exchange repulsion is stronger near the doubly-occupied p-orbital, assuming constant distance.^{19,22,30,40,41} The attraction was also expected to increase with the polarizability of the halogen and electron-withdrawing capability of the substituent group, as it did as a function of distance.^{11,13,22,42-46}

ΔE was calculated at the HF/aug-cc-pVTZ and MP2/aug-cc-pVTZ levels for $X = \text{F}, \text{Cl},$ and Br , and at the HF/aug-cc-pVTZ-PP and MP2/aug-cc-pVTZ-PP levels for $X = \text{I}$ as a function of angle using Eqn. 3.1 in 1° steps near 90° and in 10° steps near 180° , as illustrated in Fig. 3.4. The interaction distance was held constant at 3.1 \AA , the energetic minima for the aryl halogens that was determined in the previous section. The angle was varied such that the acetone rotated in the plane of the phenyl ring. Similar results were found when the acetone was rotated perpendicular to the aromatic ring, which suggest that the halogen atom is angularly symmetric about the σ -hole.

Energetic minima as a function of angle were found at a θ of 180° for $X = \text{Cl}, \text{Br},$ and I using both the HF and MP2 methods (Fig. 3.11); the dependence on the non-bonding angle was inverted for $X = \text{F}$. A suggestion on the differentiation for fluorine will be given in Chapter 4. The HF results showed that for $X = \text{Cl}$ and Br , the interaction was repulsive overall with energetic minima at 180° . The minima can be attributed to an electrostatic attraction caused by the σ -holes on chlorine and bromine, but the exchange repulsion remains dominant due to the relatively short interaction distance. An energetic well was present for $X = \text{I}$, although the exchange repulsion increases to a magnitude larger than that of Br as θ approaches 90° or 270° .

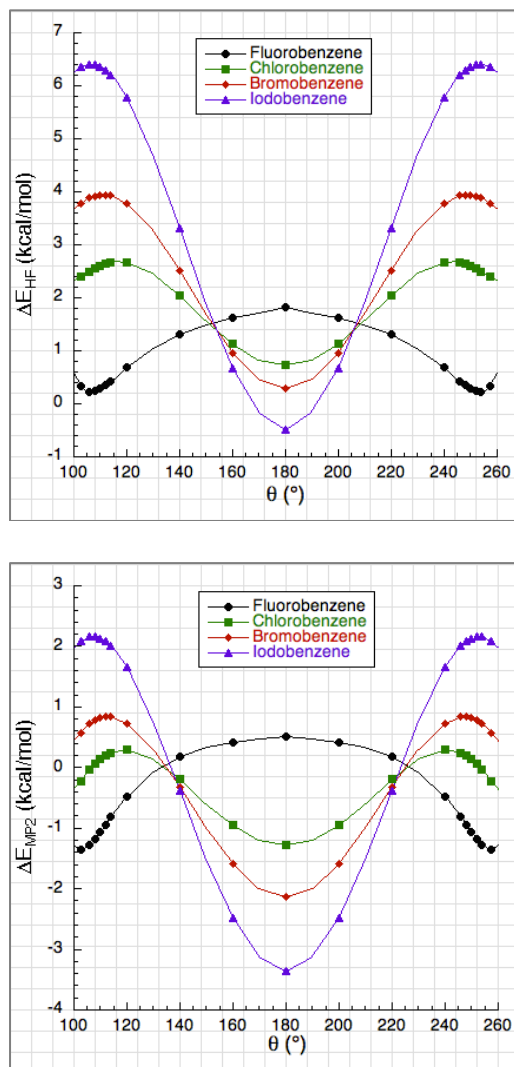


Figure 3.11. The interaction energies versus bond angle of the halobenzenes with acetone using the HF (top) and MP2 methods (bottom). The well depths at 180° are seen to increase from fluorobenzene to iodobenzene, consistent with the distance-dependent findings.

The energetic well of approximately -0.5 kcal/mol for $X = I$ can be attributed to a dominant electrostatic attraction at 180° caused by the large σ -hole on iodine.^{8,9} The repulsion maxima occur near 110° and 250° , where the periodic trend inverts and iodine is the most repulsive, fluorine the least repulsive. The larger σ -hole on iodobenzene increases the attraction for acetone, but its larger aspherical shape also increases the exchange repulsion experienced as acetone rotates away from a 180° alignment at a constant distance.

The MP2 curves display a similar angular anisotropy. The energetic minima for $X = \text{Cl}$, Br , and I aligned with those of the wells in Figure 3.5, and the repulsion near 110° and 250° decreased relative to the HF results. A similar periodic trend is illustrated in the MP2 curves, where $X = \text{I}$ is the most attractive at 180° but the most repulsive at 110° and 250° . Both the HF and MP2 results illustrated inflection points that intersect at the same angles: 155° and 215° in the HF curves and 140° and 220° in the MP2 curves. This observation was attributed to the orbital overlap as a function of angle, explained in Chapter 4.

The difference between the HF and MP2 curves provides an illustration for how dispersion varies with interaction angle (Figure 3.12). Dispersion is an isotropic attraction,^{11,47-50} and the calculated dispersion curves between the halobenzenes and acetone are consistent with this description. There is an apparent increasing angular dependence from $X = \text{F}$ to I , which can be attributed to a dispersive attraction between acetone and the phenyl substituent approaching 90° in each model dimer. There are not any inflection points that intersect, however, and the angular dependence is relatively constant between dispersion curves. This leads to a consistent lowering of the interaction energy in the MP2 curves, retaining the periodic trend presented at the HF level. This was true in all of the model halogen bonding dimers tested throughout Chapter 3.

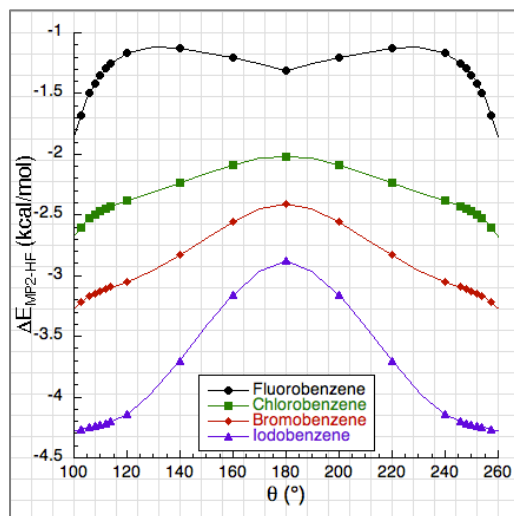


Figure 3.12. The dispersion (MP2–HF) versus bond angle of the halobenzenes with acetone. The attraction increases from fluorobenzene to iodobenzene, demonstrating that dispersion as measured by the electron correlation is relatively isotropic and increases as a periodic trend.

The angular dependence presented by the phenyl halides was dependent on the electrostatic attraction and exchange repulsion, as evident by the anisotropy of the HF interaction energy curves. The methyl halides had smaller σ -holes relative to those of the phenyl halides, so a decrease in the angular dependence of both the electrostatic attraction and exchange repulsion should be expected. Energetic minima were again found at a θ of 180° for $X = \text{Cl}, \text{Br},$ and I using both the HF and MP2 methods and a maximum found for $X = \text{F}$ (Fig. 3.13). The HF results showed that electrostatic attraction is still present when $X = \text{Cl}, \text{Br},$ and I , but that exchange repulsion has increased due to greater electron-donation from the methyl substituent group. There are energetic minima but no attractive wells. The previous interaction between acetone and iodobenzene resulted in an approximate -0.5 kcal/mol attraction, but that between acetone and iodomethane result in an approximate 0.4 kcal/mol repulsion at 180° and 3.1 \AA .

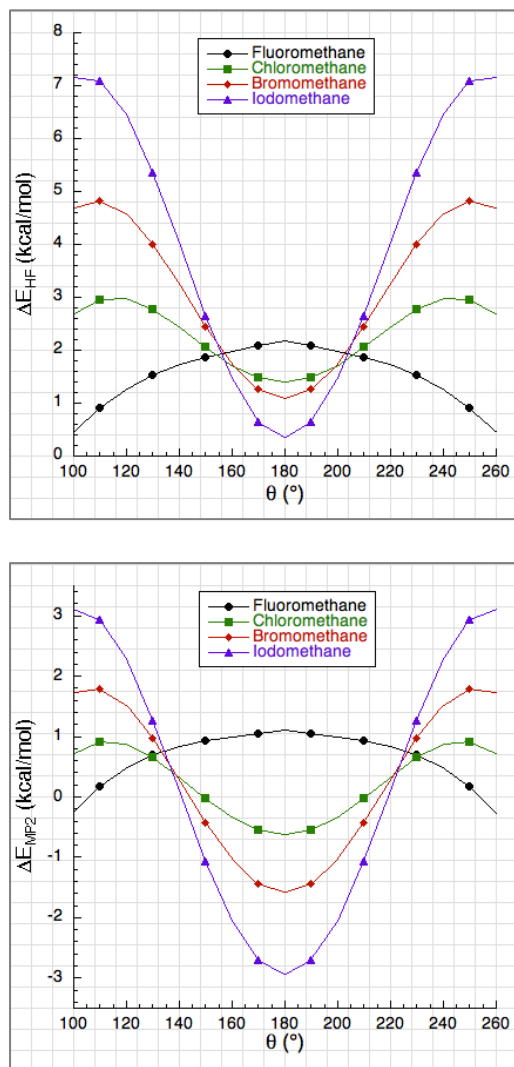


Figure 3.13. The interaction energy of the halomethanes as a function of non-bonding angle with acetone using HF (top) and MP2 (bottom). The well depths at 180° are seen to increase from fluoromethane to iodomethane, consistent with the distance-dependent findings.

The energetic minima at the MP2 level are aligned with the wells in Figure 3.7. A similar periodic trend is illustrated in the MP2 curves as in the HF curves, resulting from the dispersive attraction increasing between acetone and each methyl halide independent of angle. Both HF and MP2 results illustrated inflection points that intersect at the same angles: 165° and 205° in the HF curves and 135° and 225° in the MP2 curves, a 20° decrease and 10° increase from their phenyl counterparts, respectively. The repulsion maxima occur near 100° and 260° in both the HF and

MP2 curves, a 20° increase in width relative to the maxima presented in the phenyl halides. These differences suggest that the magnitude of electron-donation from the methyl substituent to the halogen alters the physical shape of the halogen, thereby altering the exchange repulsion experienced as a function of angle.

ΔE between acetone and the diatomic halogens was calculated as a function of angle as a control for the organic substituent groups (Fig. 3.14), to observe the angular dependence of the model dimers in the absence of charge transfer. Energetic minima were present for $X = \text{F, Cl, Br,}$ and I , where energetic wells were present for the latter three halogens. The magnitude of the interaction energy was correlated to the polarizability of the halogen, evident by acetone being the most strongly attracted to molecular iodine. ΔE was approximately equal to -2.0 kcal/mol between acetone and molecular iodine, which is 1.5 kcal/mol stronger than that between acetone and iodobenzene. The electrostatic minimum present between acetone and molecular fluorine was attributed to the removal of the bond polarization observed in the organic moieties, as discussed above.

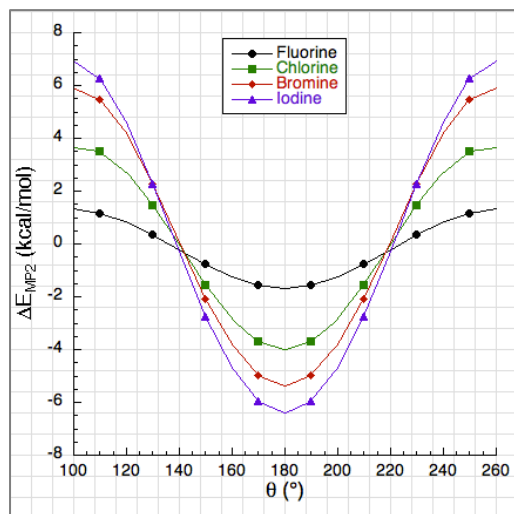
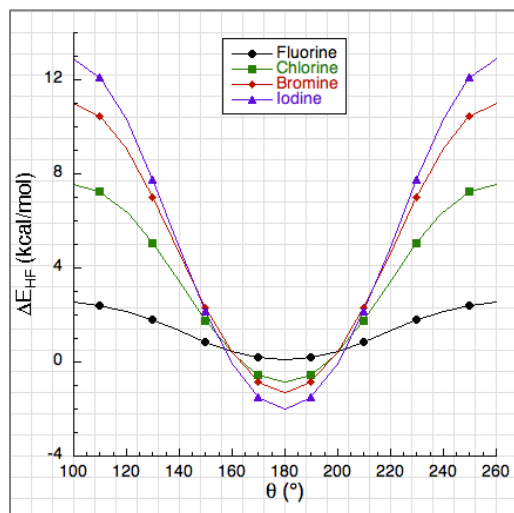


Figure 3.14. The interaction energy of the diatomic halogens as a function of non-bonding angle with acetone using HF (top) and MP2 (bottom). The well depths at 180° are seen to increase from fluorine to iodine, consistent with the distance-dependent findings.

The energetic wells of the MP2 curves align with those in Figure 3.9. The angular dependence was caused by the anisotropic electrostatic attraction and exchange repulsion, as the dispersion lowered the interaction energy independent of angle. The magnitude of dispersion experienced between acetone and the halogens was inversely proportional to the normalized bond distances in Table 3.4. The repulsion experienced as acetone rotates away from a 180° alignment is the greatest in the molecular halogen dimers when compared to the previous model dimers, however. This can be explained in that the diminished exchange repulsion at 180° is caused by the

greater aspherical shape of the halogen. Acetone is then stabilized in the energetic well at close distance by dispersion. As the Lewis base then rotates away at a constant distance, it encounters the doubly-occupied p-orbitals near $90^\circ/270^\circ$ and experiences an even greater exchange repulsion. This increases the angular dependence of the interaction, consistent with our hypothesis.

Electronic Structure Studies as a Function of Distance and Angle

A major objective of these model studies was to provide an explanation for the experimental data presented in Figure 2.6 and 2.7. That is, to provide an explanation for the pronounced distance and angle dependence for halogen bonding interactions. The plots of the two previous sections provided slices through the distance/angle/energy 3-D space. The MP2 3-D potential curve for I_2 —acetone (Fig. 3.15) demonstrates that there is a minimum in the 3-D potential surface near 180° and a scaled d around 0.85, consistent with there being a maximum in the experimental probability histogram from Chapter 2. The MP2 potential curve for F_2 —acetone in Figure 3.15 suggests analogous behavior for all the halogens. It could be concluded that the reason crystalized halogen bonding structures exhibit such similar geometries is because they all experience attractive electrostatics and dispersion at an angle of 180° and non-bonding distances within the sum of the species' van der Waals radii. Rotating away from 180° causes a sharp increase in exchange repulsion at short distances, but the exchange repulsion approaches 0 kcal/mol at long distances, allowing for less of an angular dependence. These interactions lead to the signature shape seen in the aggregate data presented in Figure 2.7.

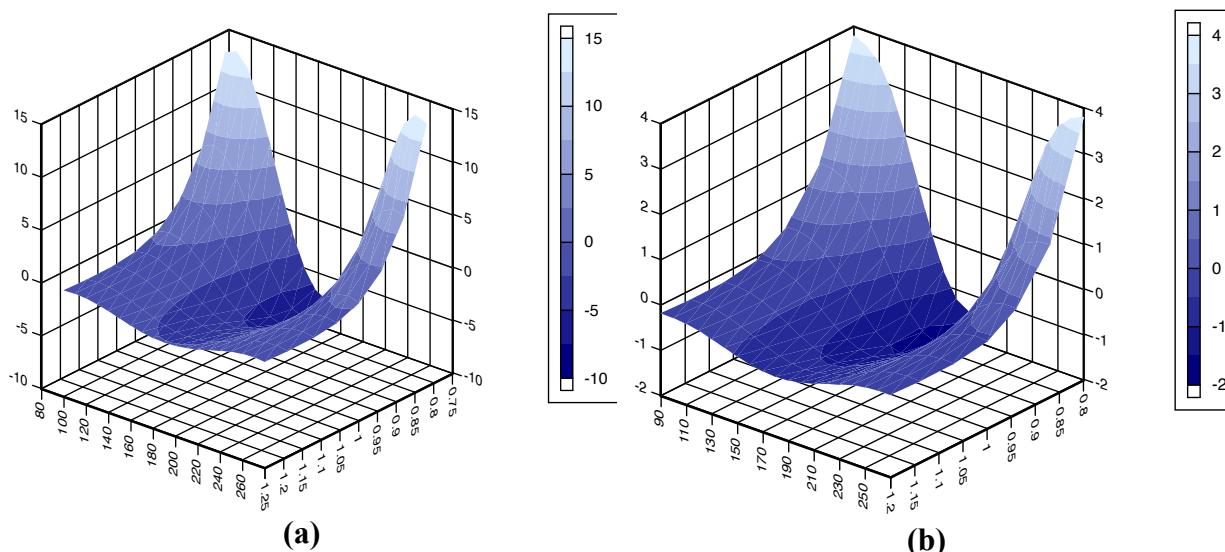


Figure 3.15. The interaction energy at the MP2 level between acetone and (a) diatomic iodine and (b) diatomic fluorine as a function of distance and angle.

3-dimensional difference curves were calculated by subtracting the binding energy of X_2 —acetone from that of MeX —acetone (Fig. 3.16) as a function of distance and angle, for $X = I$ and F , to illustrate the shape associated with alkyl substitution in distance/angle/energy space. It had been shown in Figure 3.10 that the methyl binding energies were more repulsive than X_2 as a function of distance held constant at 180° . The repulsion in the difference surfaces can be seen to decrease as the bond angle varied to 90° or 270° as well as with increasing distance. The decrease in magnitude near 90° or 270° implies that acetone interacts with the co-axial region of MeX similarly to how it does X_2 . This finding signifies that altering the substituent group of the halogen primarily affects the shape of the σ -hole, where an electron-donating moiety results in an increased repulsion near an interaction angle of 180° .

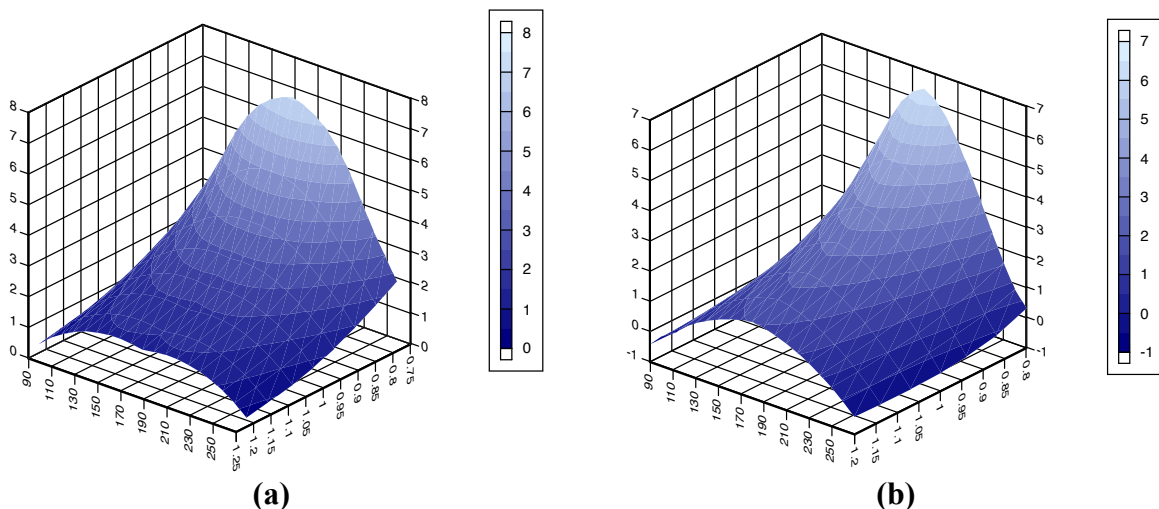


Figure 3.16. 3-dimensional difference plots of the interaction energy at the MP2 level between X_2 —acetone and MeX—acetone as a function of distance and angle for (a) $X = I$ and (b) $X = F$.

In addition, the long-distance shape correlates with the fluorine data in Figures 3.11 and 3.13. A more detailed suggestion for the source of this differentiation will be developed in Chapter 4.

Illustrating the Dispersive Component of Halogen Bonding

The aspherical shape of the halogen atom was found to positively correlate with the strength of the halogen bonding interaction via electrostatics, exchange repulsion, dispersion, and intra-bond charge transfer. The dependence of the atomic shape on the valence electronic configuration of the halogen will be the focus of Chapter 4, wherein mathematical models will be used to predict the atomic electrostatic interaction and exchange repulsion as a function of distance and angle. Before demonstrating the dependence that halogen bonding has on the electron configuration, it is worthwhile to illustrate the dispersive capabilities of the atomic halogens, much like how it is for the electrostatic potential.

The cubegen utility with the Gaussian 09 suite of programs was modified in order to graphically illustrate the density-dependence of the dispersive component. Dispersion, ΔE_{disp} ,

between two atoms X and Y (Eqn. 3.2) was approximated using the attractive term of a Lennard-Jones van der Waals potential as a function of distance, d .

$$\Delta E_{\text{disp}} = -(\varepsilon_X + \varepsilon_Y) \left(\frac{0.5(\rho_X + \rho_Y)}{d} \right)^6 \quad (3.2)$$

UFF⁵⁰ well depths for the interacting atoms (ε_X and ε_Y) and respective van der Waals radii (ρ_X and ρ_Y) were used in Eqn. 3.2. The aspherical electron density calculated by Gaussian 09 provided a measure of the relative repulsion. The monoatomic halogens were selected to represent X , and a helium atom was chosen as the van der Waals probe, Y , due to its small size and high energetic resolution, despite a weaker interaction with the atoms (Fig. 3.17). The lack of repulsion near the region of polar flattening corresponding to the location of the singly-occupied p-orbital allowed helium to approach the halogen more closely and interact attractively through dispersion. The strength and angular dependence of the angular attraction can be seen to increase from atomic fluorine to iodine. This signifies that, although dispersion is an isotropic attraction, the exchange repulsion modeled here by the electron density is anisotropic.

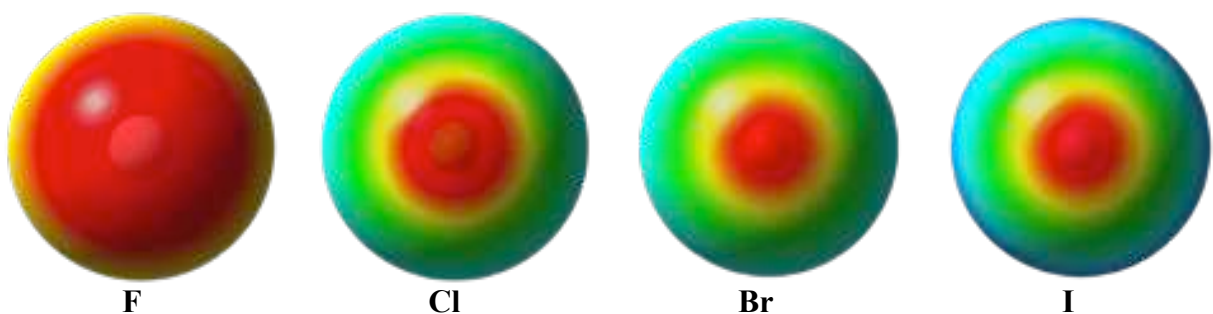


Figure 3.17. An illustration of the dispersive ability of the atomic halogens, where red represents an area of stronger attraction to a helium probe (-2.51 kcal/mol), and blue an area of weaker attraction to a helium probe (-1.41 kcal/mol).

The strength of the dispersive component is inversely proportional to that of the exchange repulsion, where the repulsive component was modeled by the electron density. The physical shape

of the halogen is, therefore, a component that should be considered when studying halogen bonds. Force fields most commonly incorporate the angularly symmetric van der Waals radii of Pauling or Bondi,^{1,2,21} despite the fact that elements are not perfectly spherical. In Chapter 4, we will consider how the electronic structure of the halogen atom leads to both the σ -hole and physical polar flattening, which in turn causes the defining electrostatic and exchange repulsion components of a halogen bond.

In this chapter, acetone was used to model electron-withdrawing and –donating groups to study the geometric dependence of model halogen bonds. The distance dependence was observed of the X—O halogen bonding interaction as a function of halogen and the organic moiety bound to the halogen. Small molecular models were prepared to better understand the distance dependence of halogen bonding strength on the electron-withdrawing and electron-donating groups. A correlation was found between the aspherical shape of the halogen and strength of the interaction energy in each of the molecular models. This correlation accrues from the underlying energetic components, which are dependent on the electronic structure of the halogen atom.^{49,51}

REFERENCES

- (1) Hassel, O.; Hvoslef, J. The Structure of Bromine 1,4-Dioxanate. *Acta Chem. Scand.* **1954**, *8*, 873.
- (2) Bent, H. A. Structural Chemistry of Donor-Acceptor Interactions. *Chem. Rev.* **1968**, *68*, 587–648.
- (3) Hassel, O. Structural Aspects of Interatomic Charge-Transfer Bonding. *Science* **1970**, *170*, 497–502.
- (4) Bock, H.; Holl, S. Interaction in Molecular Crystals, 167. Crystallization and Structure Determination of s-Donor/Acceptor Complexes between 1,4-Dioxane and the Polyiodine Molecules I₂, I₂C=Cl₂, (IC)₄S and (IC)₄NR (R = H, CH₃). *Z. Für Naturforschung B* **2001**, *56*, 111–121.
- (5) Hassel, O.; Strømme, K. O. Crystal Structure of the Addition Compound 1,4-Dioxan-Chlorine. *Acta Chem. Scand.* **1959**, *13*, 1775–1780.
- (6) Politzer, P.; Murray, J. S.; Concha, M. C. σ -Hole Bonding Between Like Atoms; A Fallacy of Atomic Charges. *J. Mol. Model.* **2008**, *14*, 659–665.
- (7) Clark, T.; Hennemann, M.; Murray, J. S.; Politzer, P. Halogen Bonding: The σ -Hole: Proceedings of “Modeling Interactions in Biomolecules II”, Prague, September 5th–9th, 2005. *J. Mol. Model.* **2007**, *13*, 291–296.
- (8) Politzer, P.; Murray, J. S.; Clark, T. σ -Hole Bonding: A Physical Interpretation. In *Halogen Bonding I*; Metrangolo, P., Resnati, G., Eds.; Springer International Publishing: Cham, 2014; Vol. 358, pp 19–42.
- (9) Politzer, P.; Murray, J. S. Halogen Bonding: An Interim Discussion. *ChemPhysChem* **2013**, *14*, 278–294.
- (10) Clark, T.; Heßelmann, A. The Coulombic σ -Hole Model Describes Bonding in CX₃I \cdots Y⁻ Complexes Completely. *Phys. Chem. Chem. Phys.* **2018**.
- (11) Riley, K. E.; Murray, J. S.; Fanfrlík, J.; Řezáč, J.; Solá, R. J.; Concha, M. C.; Ramos, F. M.; Politzer, P. Halogen Bond Tunability II: The Varying Roles of Electrostatic and Dispersion Contributions to Attraction in Halogen Bonds. *J. Mol. Model.* **2013**, *19*, 4651–4659.
- (12) Clark, T.; Politzer, P.; Murray, J. S. Correct Electrostatic Treatment of Noncovalent Interactions: The Importance of Polarization. *Wiley Interdiscip. Rev. Comput. Mol. Sci.* **2015**, *5*, 169–177.
- (13) Politzer, P.; Murray, J. S.; Clark, T. Halogen Bonding and Other σ -Hole Interactions: A Perspective. *Phys. Chem. Chem. Phys.* **2013**, *15*, 11178.
- (14) Nguyen, H. L.; Horton, P. N.; Hursthouse, M. B.; Legon, A. C.; Bruce, D. W. Halogen Bonding: A New Interaction for Liquid Crystal Formation. *J. Am. Chem. Soc.* **2004**, *126*, 16–17.
- (15) Auffinger, P.; Hays, F. A.; Westhof, E.; Ho, P. S. Halogen Bonds in Biological Molecules. *Proc. Natl. Acad. Sci.* **2004**, *101*, 16789–16794.
- (16) Riley, K. E.; Hobza, P. Investigations into the Nature of Halogen Bonding Including Symmetry Adapted Perturbation Theory Analyses. *J. Chem. Theory Comput.* **2008**, *4*, 232–242.
- (17) Politzer, P.; Murray, J. S. Halogen Bonding and Beyond: Factors Influencing the Nature of CN–R and SiN–R Complexes with F–Cl and Cl₂. *Theor. Chem. Acc.* **2012**, *131*, 1114.
- (18) Riley, K. E.; Murray, J. S.; Fanfrlík, J.; Řezáč, J.; Solá, R. J.; Concha, M. C.; Ramos, F. M.; Politzer, P. Halogen Bond Tunability I: The Effects of Aromatic Fluorine Substitution on the Strengths of Halogen-Bonding Interactions Involving Chlorine, Bromine, and Iodine. *J. Mol. Model.* **2011**, *17*, 3309–3318.
- (19) Shields, Z. P.; Murray, J. S.; Politzer, P. Directional Tendencies of Halogen and Hydrogen Bonds. *Int. J. Quantum Chem.* **2010**, *110*, 2823–2832.
- (20) Politzer, P.; Murray, J. S.; Clark, T. Halogen Bonding: An Electrostatically-Driven Highly Directional Noncovalent Interaction. *Phys. Chem. Chem. Phys.* **2010**, *12*, 7748.
- (21) Politzer, P.; Murray, J. S.; Lane, P. σ -Hole Bonding and Hydrogen Bonding: Competitive Interactions. *Int. J. Quantum Chem.* **2007**, *107*, 3046–3052.
- (22) Stone, A. J. Are Halogen Bonded Structures Electrostatically Driven? *J. Am. Chem. Soc.* **2013**, *135*, 7005–7009.

- (23) Lommerse, J. P. M.; Stone, A. J.; Taylor, R.; Allen, F. H. The Nature and Geometry of Intermolecular Interactions Between Halogens and Oxygen or Nitrogen. *J. Am. Chem. Soc.* **1996**, *118*, 3108–3116.
- (24) Sladek, V.; Punyain, K.; Ilčin, M.; Lukeš, V. Substitution Effect on the Intermolecular Halogen and Hydrogen Bonds of the σ -Bonded Fluorinated Pyridine \cdots XY/HX Complexes (XY = F₂, Cl₂, ClF; HX = HF, HCl). *Int. J. Quantum Chem.* **2014**, *114*, 869–878.
- (25) Jabłoński, M.; Palusiak, M. Nature of a Hydride–Halogen Bond. A SAPT-, QTAIM-, and NBO-Based Study. *J. Phys. Chem. A* **2012**, *116*, 2322–2332.
- (26) Wang, C.; Danovich, D.; Mo, Y.; Shaik, S. On The Nature of the Halogen Bond. *J. Chem. Theory Comput.* **2014**, *10*, 3726–3737.
- (27) Bondi, A. Van Der Waals Volumes and Radii. *J. Phys. Chem.* **1964**, *68*, 441–451.
- (28) Peebles, S. A.; Fowler, P. W.; Legon, A. C. Anisotropic Repulsion in Complexes B–Cl₂ and B–HCl: The Shape of the Chlorine Atom-in-a-Molecule. *Chem. Phys. Lett.* **1995**, *240*, 130–134.
- (29) Kolář, M.; Hobza, P. On Extension of the Current Biomolecular Empirical Force Field for the Description of Halogen Bonds. *J. Chem. Theory Comput.* **2012**, *8*, 1325–1333.
- (30) Riley, K. E.; Murray, J. S.; Politzer, P.; Concha, M. C.; Hobza, P. Br \cdots O Complexes as Probes of Factors Affecting Halogen Bonding: Interactions of Bromobenzenes and Bromopyrimidines with Acetone. *J. Chem. Theory Comput.* **2009**, *5*, 155–163.
- (31) Wilcken, R.; Zimmermann, M. O.; Lange, A.; Joerger, A. C.; Boeckler, F. M. Principles and Applications of Halogen Bonding in Medicinal Chemistry and Chemical Biology. *J. Med. Chem.* **2013**, *56*, 1363–1388.
- (32) Jones, R. H.; Knight, K. S.; Marshall, W. G.; Coles, S. J.; Horton, P. N.; Pitak, M. B. The Competition Between Halogen Bonds (Br \cdots O) and C–H \cdots O Hydrogen Bonds: The Structure of the Acetone–Bromine Complex Revisited. *CrystEngComm* **2013**, *15*, 8572–8577.
- (33) Su, P.; Li, H. Energy Decomposition Analysis of Covalent Bonds and Intermolecular Interactions. *J. Chem. Phys.* **2009**, *131*, 014102.
- (34) Mohan, N.; Suresh, C. H. Accurate Binding Energies of Hydrogen, Halogen, and Dihydrogen Bonded Complexes and Cation Enhanced Binding Strengths. *Int. J. Quantum Chem.* **2014**, *114*, 885–894.
- (35) Schneider, W. B.; Bistoni, G.; Sparta, M.; Saitow, M.; Riplinger, C.; Auer, A. A.; Neese, F. Decomposition of Intermolecular Interaction Energies within the Local Pair Natural Orbital Coupled Cluster Framework. *J. Chem. Theory Comput.* **2016**, *12*, 4778–4792.
- (36) Woon, D. E.; Dunning, T. H. Gaussian Basis Sets for Use in Correlated Molecular Calculations. IV. Calculation of Static Electrical Response Properties. *J. Chem. Phys.* **1994**, *100*, 2975–2988.
- (37) Woon, D. E. Benchmark Calculations with Correlated Molecular Wave Functions. V. The Determination of Accurate *Ab Initio* Intermolecular Potentials for He₂, Ne₂, and Ar₂. *J. Chem. Phys.* **1994**, *100*, 2838–2850.
- (38) Peterson, K. A.; Shepler, B. C.; Figgen, D.; Stoll, H. On the Spectroscopic and Thermochemical Properties of ClO, BrO, IO, and Their Anions. *J. Phys. Chem. A* **2006**, *110*, 13877–13883.
- (39) Boys, S. F.; Bernardi, F. The Calculation of Small Molecular Interactions by the Differences of Separate Total Energies. Some Procedures with Reduced Errors. *Mol. Phys.* **1970**, *19*, 553–566.
- (40) Wu, W.; Lu, Y.; Liu, Y.; Li, H.; Peng, C.; Liu, H.; Zhu, W. Weak Energetic Effects Between X– π and X–N Halogen Bonds: CSD Search and Theoretical Study. *Chem. Phys. Lett.* **2013**, *582*, 49–55.
- (41) Priimagi, A.; Cavallo, G.; Metrangolo, P.; Resnati, G. The Halogen Bond in the Design of Functional Supramolecular Materials: Recent Advances. *Acc. Chem. Res.* **2013**, *46*, 2686–2695.
- (42) Desiraju, G. R.; Ho, P. S.; Kloo, L.; Legon, A. C.; Marquardt, R.; Metrangolo, P.; Politzer, P.; Resnati, G.; Rissanen, K. Definition of the Halogen Bond (IUPAC Recommendations 2013). *Pure Appl. Chem.* **2013**, *85*, 1711–1713.
- (43) Murray, J. S.; Lane, P.; Clark, T.; Riley, K. E.; Politzer, P. σ -Holes, π -Holes and Electrostatically-Driven Interactions. *J. Mol. Model.* **2012**, *18*, 541–548.
- (44) Ibrahim, M. A. A. Molecular Mechanical Perspective on Halogen Bonding. *J. Mol. Model.* **2012**, *18*, 4625–4638.

- (45) Ji, J.; Meng, D.; Zhang, X.; Meng, L.; Zeng, Y. Enhancing Effects of Hydrogen/Halogen Bonds on σ -Hole Interactions Involving Ylide. *J. Mol. Model.* **2014**, *20*, 2282.
- (46) Aakeröy, C. B.; Wijethunga, T. K.; Desper, J. Practical Crystal Engineering Using Halogen Bonding: A Hierarchy Based on Calculated Molecular Electrostatic Potential Surfaces. *J. Mol. Struct.* **2014**, *1072*, 20–27.
- (47) Kolář, M.; Kubař, T.; Hobza, P. On the Role of London Dispersion Forces in Biomolecular Structure Determination. *J. Phys. Chem. B* **2011**, *115*, 8038–8046.
- (48) Martin, J. M. What Can We Learn about Dispersion from the Conformer Surface of N-Pentane? *J. Phys. Chem. A* **2013**, *117*, 3118–3132.
- (49) Carter, M.; Rappé, A. K.; Ho, P. S. Scalable Anisotropic Shape and Electrostatic Models for Biological Bromine Halogen Bonds. *J. Chem. Theory Comput.* **2012**, *8*, 2461–2473.
- (50) Rappé, A. K.; Casewit, C. J.; Colwell, K. S.; Goddard III, W. A.; Skiff, W. M. UFF, A Full Periodic Table Force Field for Molecular Mechanics and Molecular Dynamic Simulations. *J. Am. Chem. Soc.* **1992**, *114*, 10024–10035.
- (51) Scholfield, M. R.; Ford, M. C.; Vander Zanden, C. M.; Billman, M. M.; Ho, P. S.; Rappé, A. K. Force Field Model of Periodic Trends in Biomolecular Halogen Bonds. *J. Phys. Chem. B* **2015**, *119*, 9140–9149.

CHAPTER 4: MODEL HALOGEN BONDING VIA ORBITAL OVERLAP

Two underlying components of halogen bonding, the electrostatic potential and exchange repulsion, will be modeled in this chapter using a linear combination of atomic orbitals. The purpose of this study is to understand the source of the observed distance-angle dependence of halogen bonding introduced in Chapters 2 and 3 at the most fundamental level. Understanding the electrostatic and exchange repulsion components of the interaction will help to improve current molecular models of halogen bonding.^{1,2}

Model Potential Studies

Two underlying components of halogen bonding, electrostatic potential (E_{ES}) and exchange repulsion (E_{XR}), were constructed to further understand their contribution to the distance dependence and angular dependence of a model halogen bonds. Atomic halogens were selected as the model in order to remove the effects of substituents and study the electronic structure directly. Our hypothesis was that both theoretical models would display an angular dependence because the $s^2p_x^2p_y^2p_z^1$ valence electron configuration leads to both the σ -hole and polar flattening. In addition, the models would assist in demonstrating the differences in the electrostatic potential and exchange repulsion components as a function of halogen,³⁻¹⁰ as well as provide a basis for the anomalous nature of molecular halogen bonds and the paucity of halogen bonds for fluorine. Lastly, the models suggest a means of accounting for substituent effects in force field halogen bond models.

I. The Heitler-London Model

Our theoretical model of the E_{XR} was inspired by the Heitler-London (H-L) derivations that outlined the impact of the Pauli Principle on chemical bonding.¹¹⁻¹⁴ The H-L derivations are summarized below for the small molecules of H_2^+ (Fig. 4.1), H_2 , He_2^+ , and He_2 to demonstrate how exchange repulsion depends on orbital overlap.

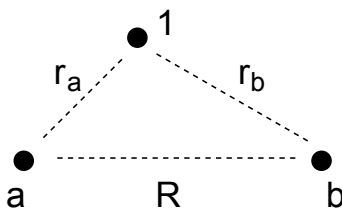


Figure 4.1. An illustration of the possible attractive and repulsive interactions between protons (a and b) and electron (1), separated by distances (R , r_a , and r_b) (adapted from *Nature of the Chemical Bond* by *W. A. Goddard III*).

W. Heitler and F. London began with the energy, E (Eqn. 4.1), resulting from the expectation value with respect to the Hamiltonian (\hat{H}). A wavefunction (Ψ) was constructed from a linear combination of atomic orbitals.¹⁴⁻¹⁶

$$E = \frac{\langle \Psi | \hat{H} | \Psi \rangle}{\langle \Psi | \Psi \rangle} \quad (4.1)$$

The Hamiltonian, \hat{H} (Eqn. 4.2), written in atomic units and comprised of the kinetic operator (∇_1^2) and potential terms ($\frac{1}{r_a}$ and $\frac{1}{r_b}$), distances of which are illustrated in Figure 4.1, can be written such that the electronic terms ($h^{(1)}$) are separated from the nuclear repulsion ($\frac{1}{R}$) (Eqn. 4.3).

$$\hat{H} = \left(-\frac{1}{2} \nabla_1^2 - \frac{1}{r_a} - \frac{1}{r_b} \right) + \frac{1}{R} \quad (4.2)$$

$$\hat{H} = h^{(1)} + \frac{1}{R} \quad (4.3)$$

The bonding wavefunction, $|\Psi_g\rangle$ (Eqn. 4.4), written in Dirac notation, was defined as a positive linear combination of the atomic orbitals (ϕ_a and ϕ_b) centered on the nuclei of H_2^+ .

$$|\Psi_g\rangle = |\phi_a\rangle + |\phi_b\rangle \quad (4.4)$$

The antibonding wavefunction, $|\Psi_u\rangle$ (Eqn. 4.5), was defined as a negative linear combination of the same atomic orbitals.

$$|\Psi_u\rangle = |\phi_a\rangle - |\phi_b\rangle \quad (4.5)$$

The bonding wavefunction of Eqn. 4.4 was inserted into the energy expression of Eqn. 4.1 to derive the bonding energy, E_g (Eqn. 4.6), of H_2^+ . The electronic term was distributed to the linear combination of atomic orbitals (Eqn. 4.7) and rearranged such that the electronic terms were separated from the nuclear repulsion (Eqn. 4.8), as in the Hamiltonian of Eqn. 4.3. \mathcal{S} is the overlap of orbitals ϕ_a and ϕ_b .

$$E_g = \frac{\langle \Psi_g | h^{(1)} | \Psi_g \rangle}{\langle \Psi_g | \Psi_g \rangle} + \frac{1}{R} \quad (4.6)$$

$$E_g = \frac{\langle \phi_a | h^{(1)} | \phi_a \rangle + \langle \phi_b | h^{(1)} | \phi_b \rangle + 2\langle \phi_a | h^{(1)} | \phi_b \rangle}{2 + 2\langle \phi_a | \phi_b \rangle} + \frac{1}{R} \quad (4.7)$$

$$E_g = \frac{h_{aa}^{(1)} + h_{ab}^{(1)}}{1 + \mathcal{S}} + \frac{1}{R} \quad (4.8)$$

The bonding energy expression in Eqn. 4.8 was rearranged (Eqn. 4.9) such that the terms combined into classical (E^{Cl}) and bonding exchange (E_g^X) energy terms (Eqn. 4.10).

$$E_g = \left(h_{aa}^{(1)} + \frac{1}{R} \right) + \left(\frac{h_{ab}^{(1)} - \mathcal{S}h_{aa}^{(1)}}{1 + \mathcal{S}} \right) \quad (4.9)$$

$$E_g = E^{Cl} + E_g^X \quad (4.10)$$

The antibonding wavefunction of Eqn. 4.5 was inserted into the energy expression of Eqn. 4.1 to derive the antibonding energy, E_u , of H_2^+ , which was rearranged (Eqn. 4.11) such that the terms combined into classical and antibonding exchange (E_u^X) energy terms (Eqn. 4.12).

$$E_u = \left(h_{aa}^{(1)} + \frac{1}{R} \right) + \left(\frac{-(h_{ab}^{(1)} - \mathcal{S}h_{aa}^{(1)})}{1 - \mathcal{S}} \right) \quad (4.11)$$

$$E_u = E^{Cl} + E_u^X \quad (4.12)$$

The classical energy, which describes the energy of the system as if ϕ_a and ϕ_b do not superimpose (*Ref. 14; Fig. 2.7*), was found to be identical in the bonding and antibonding cases, seen in Eqns. 4.9 and 4.11. The exchange terms E_g^X and E_u^X were concluded to contain the characteristic energies that define the chemical bond in H_2^+ because they differed in the energy expressions.

Heitler and London also derived the exchange energy for a slightly larger model, H_2 , and drew similar results. The ground state wavefunction (Eqn. 4.13) consisted of the symmetric exchange of the spatial coordinates of the two electrons combined with an antisymmetric spin function.

$$|\Psi_g\rangle = |\phi_a\phi_b\rangle + |\phi_b\phi_a\rangle \quad (4.13)$$

Orthogonality of the spin functions permits the spatial wavefunctions to overlap. Similarly, the antisymmetric wavefunction (Eqn. 4.14) was combined with a symmetric spin function.

$$|\Psi_u\rangle = |\phi_a\phi_b\rangle - |\phi_b\phi_a\rangle \quad (4.14)$$

The antisymmetric spatial combination is mathematically identical to the wave function that places one electron in ϕ_g and one electron in the orthogonal ϕ_u . Eqn. 4.13 and Eqn. 4.14 were each inserted into the energy expression of Eqn. 4.1. The bonding (Eqn. 4.15) and antibonding (Eqn. 4.16) energy expressions were derived and rearranged into classical and exchange terms (Eqn. 4.17 and 4.18), respectively.

$$E_g = \left(h_{aa}^{(1)} + h_{bb}^{(2)} + \langle \phi_a\phi_b \left| \frac{1}{r_{12}} \right| \phi_a\phi_b \rangle + \frac{1}{R} \right) + \left(\frac{\langle \phi_a\phi_b | \hat{H}^{(1,2)} | \phi_b\phi_a \rangle - S^2 \langle \phi_a\phi_b | \hat{H}^{(1,2)} | \phi_a\phi_b \rangle}{1 + S^2} \right) \quad (4.15)$$

$$E_u = \left(h_{aa}^{(1)} + h_{bb}^{(2)} + \langle \phi_a\phi_b \left| \frac{1}{r_{12}} \right| \phi_a\phi_b \rangle + \frac{1}{R} \right) + \left(\frac{-\langle \phi_a\phi_b | \hat{H}^{(1,2)} | \phi_b\phi_a \rangle - S^2 \langle \phi_a\phi_b | \hat{H}^{(1,2)} | \phi_a\phi_b \rangle}{1 - S^2} \right) \quad (4.16)$$

$$E_g = E^{Cl} + E_g^X \quad (4.17)$$

$$E_u = E^{Cl} + E_u^X \quad (4.18)$$

The derivations again resulted in an identical classical energy and different exchange energies between the bonding and antibonding expressions. E^{Cl} is only slightly attractive at long distance for H_2 , so the chemical bond of H_2 is attributed to the symmetric exchange of electrons 1 and 2.

This analysis can be extended to three-electron and four-electron systems, modeled by He^+ and He. The three (Eqn. 4.19) and four electron (Eqn. 4.20) wavefunctions are provided and the corresponding one-electron energy terms (Eqn. 4.21), derived similarly to those above.

$$\Psi_3 = \phi_a \phi_a \phi_b - \phi_b \phi_b \phi_a \quad (4.19)$$

$$\Psi_4 = \phi_a \phi_a \phi_b \phi_b \quad (4.20)$$

$$\begin{aligned} E_1 &\propto \frac{\mathbf{S}\tau}{1 - \mathbf{S}} \\ E_2 &\propto \frac{2\mathbf{S}^2\tau}{1 - \mathbf{S}^2} \\ E_3 &\propto \frac{3\mathbf{S}^2\tau}{1 - \mathbf{S}^2} \\ E_4 &\propto \frac{4\mathbf{S}^2\tau}{1 - \mathbf{S}^2} \end{aligned} \quad (4.21)$$

τ in Eqn. 4.21 is an energy term (Eqn. 4.22), which can be further simplified using the Mulliken approximation for h_{ab} (Eqn. 4.23), where κ is taken to be 1.75.

$$\tau = h_{ab} - \frac{1}{2}S_{ab}(h_{aa} + h_{bb}) \quad (4.22)$$

$$h_{ab} = \frac{1}{2}\kappa S_{ab}(h_{aa} + h_{bb}) \quad (4.23)$$

Inserting Eqn. 4.23 into 4.22 yields a simplified version of τ (Eqn. 4.24).

$$\tau \approx \frac{1}{2}(\kappa - 1)S_{ab}(h_{aa} + h_{bb}) \quad (4.24)$$

Eqn. 4.24 can be defined as ε_{ab} , and when inserted back into Eqn 4.24 yields four simplified energy terms (Eqn. 4.25).

$$\begin{aligned}
E_1 &\approx \frac{\mathbf{S}\varepsilon_{ab}}{1 - \mathbf{S}} \\
E_2 &\approx \frac{2\mathbf{S}^2\varepsilon_{ab}}{1 - \mathbf{S}^2} \\
E_3 &\approx \frac{3\mathbf{S}^2\varepsilon_{ab}}{1 - \mathbf{S}^2} \\
E_4 &\approx \frac{4\mathbf{S}^2\varepsilon_{ab}}{1 - \mathbf{S}^2}
\end{aligned}
\tag{4.25}$$

The impact of orthogonality on the total energy is contained in Eqn. 4.25, which we used for our exchange repulsion model (Eqn. 4.26). E_{XR} is proportional to the orbital overlap (\mathbf{S}) between two atoms, squared,^{13,14} and one-electron energies, ε_{ab} of Eqn 4.24, were incorporated to improve the accuracy of the model.

$$E_{XR} \propto \frac{\mathbf{S}^2}{1 - \mathbf{S}^2} \tag{4.26}$$

When a probe comes into close contact with a molecular system containing a bond between orbitals a and b , squaring the overlap of the wavefunctions (Eqn. 4.27 and Eqn. 4.28) results in an approximation that contains both the atomic ($\mathbf{S}_{He,a}^2, \mathbf{S}_{He,b}^2$) and exchange ($\mathbf{S}_{He,a}\mathbf{S}_{He,b}$) terms of the interaction.

$$\mathbf{S}^2 = \frac{\langle \Psi_{He} | \Psi_a \rangle^2 - 2\langle \Psi_{He} | \Psi_a \rangle \langle \Psi_{He} | \Psi_b \rangle - \langle \Psi_{He} | \Psi_b \rangle^2}{2 - 2\langle \Psi_a | \Psi_b \rangle} \tag{4.27}$$

$$\mathbf{S}^2 = \frac{\mathbf{S}_{He,a}^2 - 2\mathbf{S}_{He,a}\mathbf{S}_{He,b} - \mathbf{S}_{He,b}^2}{2 - 2\mathbf{S}_{a,b}} \tag{4.28}$$

E_{ES} and E_{XR} are admittedly not a part of any valid electronic structure energy expression but they do provide a measure of the impact of orthogonality and electrostatic potential on structure

and binding. Discussions of Density Functional Theory and the Hellman-Feynman theorem focus on the dependence of energy and physical properties on electron density,¹⁷⁻¹⁹ but discount the preamble to a proper electronic structure analysis wherein the Pauli Principle states that electrons are fermions. As such, the wavefunction of the electrons must change sign when the coordinates of said electrons are interchanged. This antisymmetric property of electronic wavefunctions is the source of exchange repulsion. Exchange repulsion may generally correlate with electron density, but it is not caused by electron density. Consider the interaction of a p_π -orbital with an s-orbital (Fig. 4.2a). The overlap between the two orbitals is zero due to equal positive and negative contributions to the overlap, and hence there is not exchange repulsion between the p_π -orbital and s-orbital. When the interaction between the p_π -orbital density, equal to the wavefunction squared, and the s-orbital is considered, the interaction is not zero (Fig. 4.2b).



Figure 4.2. An illustration of the difference between (a) wavefunction/orbital overlap and (b) electron density interaction. The former is orthogonal, and therefore results in no repulsion. The latter is not orthogonal, and the model results in a measure of repulsion.

II. Modeling the Exchange Repulsion of a Halogen Atom

Our exchange model was developed in order to understand the underlying anisotropic E_{XR} near a halogen atom as dependent on the occupation of the valence atomic orbitals. The derivations and results of the anisotropic E_{XR} will be discussed first, and then E_{ES} in the following section. The halogen atoms were defined as a linear combination of two wavefunctions, which represented the core-corrected valence s- and p-orbitals (Eqn. 4.29 and 4.30, respectively).

$$|\Psi_s\rangle = |\phi_{2s}\rangle - \mathcal{S}|\phi_{2s}^{cc}\rangle \quad (4.29)$$

$$|\Psi_p\rangle = |\phi_{2p}\rangle - \mathcal{S}|\phi_{2p}^{cc}\rangle \quad (4.30)$$

The wavefunctions were written such that the atomic orbitals, ϕ_{2s} and ϕ_{2p} (Eqn. 4.31 and 4.32, respectively), could be adjusted via Slater exponents (ζ_{2s} and ζ_{2p}), where r is in Bohrs.^{16,20–22}

$$\phi_{2s} = \sqrt{\frac{(2\zeta_{2s})^5}{96\pi}} r e^{-\zeta_{2s}r} \quad (4.31)$$

$$\phi_{2p} = \sqrt{\frac{3(2\zeta_{2p})^5}{96\pi}} r e^{-\zeta_{2p}r} \quad (4.32)$$

The core-correction orbitals (ϕ_{2s}^{cc} and ϕ_{2p}^{cc}) were adjusted independently using the Slater exponents (ζ_{2s}^{cc} , ζ_{2p}^{cc}), and subtracted from the valence orbitals (ϕ_{2s} and ϕ_{2p}) by a factor of their overlap (\mathcal{S}) in Eqn. 4.29 and Eqn. 4.30. The purpose of the core correction was to approximate the effect of the core electrons, improve the shape of valence orbitals, and achieve more accurate energy approximations.

Reference atomic orbital wavefunction amplitudes were calculated at the HF/6-31G level for F, Cl, and Br, and at the HF/aug-cc-pVTZ-PP level for I, including additional 5D and 7F functions with a radial step size that varies from 0.05 Å to 0.20 Å. The Slater exponents of the models were adjusted until the shape of the model wavefunctions reproduced the radial distribution of the HF wavefunctions, which can be seen in Appendix 3, Figures A3.1a–d. The Simplex algorithm, developed by J. A. Nelder and R. Mead,²³ was used to obtain the Slater exponents by minimizing the sum of least squares between our model and the HF orbital amplitudes. Data for the distance dependence of exchange repulsion and electrostatic potential were also included in optimization.

Optimization of the model wavefunctions yielded reasonable Slater exponents (Table 4.1). Larger exponents correspond to smaller orbitals, and smaller exponents to larger more diffuse orbitals. For example, ζ_{2s}^{cc} equals 14.04 for fluorine, suggesting a tightly contracted core correction s-orbital relative to the valence s-orbital, where ζ_{2s} equals 2.11. ζ_{2s} is also smaller than ζ_{2p} , suggesting that the valence p-orbital is more contracted than the valence s-orbital. A ζ_{2p}^{cc} was not included for fluorine because there is not a 1p electron configuration.

Table 4.1. The optimized Slater exponents corresponding to the valence and core-corrected orbitals found for Equations 4.29 – 4.32.

	ζ_{2s}	ζ_{2p}	ζ_{2s}^{cc}	ζ_{2p}^{cc}
Fluorine	2.11	2.18	14.04	-
Chlorine	2.08	1.37	5.41	6.09
Bromine	1.90	1.27	4.36	4.36
Iodine	1.74	1.17	3.77	3.20

The prominence of the p-orbital increased down the periodic table, attributed here to the electronic structure of the halogen. The amplitude maximum of fluorine’s s-orbital for F was at $r = 0.40 \text{ \AA}$, and that of the p-orbital was at $r = 0.35 \text{ \AA}$. The isotropic s-orbital dominated the p-orbital, creating a more spherical valence electron density in the smaller halogen, decreasing the size of the σ -hole despite the singly-occupied p_z -orbital. In contrast, the amplitude maximum of iodine’s s-orbital was at $r = 0.90 \text{ \AA}$, and that of the p-orbital was at $r = 1.00 \text{ \AA}$. The anisotropic p-orbitals dominated the s-orbital, creating a more aspherical valence electron distribution in the larger halogen, increasing the size of the σ -hole. The Slater exponents of our model therefore suggest that the aspherical shape of a halogen is inherent to the atom (Table 4.2), in agreement with the σ -hole model by Politzer et al.^{24,25}

Table 4.2. The locations of the amplitude maxima of the radial distributions of the valence wavefunctions as a function of atomic radius at the HF level.

	$r^*\Psi_s$ (Å)	$r^*\Psi_p$ (Å)
Fluorine	0.40	0.35
Chlorine	0.70	0.75
Bromine	0.80	0.90
Iodine	0.90	1.00

The model E_{XR} was calculated for the optimized core-corrected valence orbitals using a model He probe (Ψ_{He}) as a function of atomic radius and angle, relative to the singly occupied p_z-orbital (ϕ_{2p_σ}) of the halogen (Fig. 4.3). Helium is an ideal probe for modeling E_{XR} , as it is a closed-shell atom that contains an electron of both +1/2 and -1/2 spins. The low polarizability of helium causes it to behave as a model electron pair, while contributing little to the attractive van der Waals.

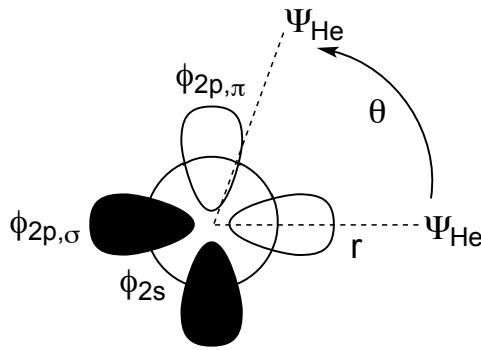


Figure 4.3. The E_{XR} was calculated using a helium atom in close proximity to the model ϕ_{2s} , ϕ_{2p_σ} , and ϕ_{2p_π} orbitals versus atomic radius and angle, relative to ϕ_{2p_σ} .

The orbital overlaps between Ψ_{He} and Ψ_{2s} (Eqn. 4.33) and Ψ_{He} and Ψ_{2p} (Eqn. 4.34) were defined using overlap expressions derived by C. C. J. Roothaan, where $\langle \Psi_{He} | \Psi_{2p} \rangle = \langle \Psi_{He} | \Psi_{2p_\sigma} \rangle$ and $\langle \Psi_{He} | \Psi_{2p_\pi} \rangle = 0$.²⁰⁻²² The terms τ and ρ were considered to be independent variables by Roothaan, written in terms of ζ and defined in Eqn. 15 of *Ref. 20*. The term κ was written in terms of τ and ζ , defined in Eqn. 16 of *Ref. 20*.

$$\langle \Psi_{\text{He}} | \Psi_{2s} \rangle = \left(\frac{\sqrt{1-\tau^2}}{\sqrt{3\tau\rho}} \right) \left((1+\kappa)(2(1-\kappa)(2-3\kappa) + 4(1-\kappa)\rho_{2s} + \rho_{2s}^2)e^{-\rho_{2s}} - (1-\kappa)(2(1+\kappa)(2-3\kappa) + (1-2\kappa)\rho_{\text{He}})e^{-\rho_{\text{He}}} \right) \quad (4.33)$$

$$\langle \Psi_{\text{He}} | \Psi_{2p} \rangle = \left(\frac{\sqrt{1+\tau}}{\tau\rho^2\sqrt{1-\tau}} \right) \left((1+\kappa)(6(1-\kappa)^2(1+\rho_{2p}) + 4(1-\kappa)\rho_{2p}^2 + \rho_{2p}^3)e^{-\rho_{2p}} - (1-\kappa)^2(6(1+\kappa)(1+\rho_{\text{He}}) + 2\rho_{\text{He}}^2)e^{-\rho_{\text{He}}} \right) \quad (4.34)$$

The model E_{XR} (Eqn. 4.35) was written as a sum of the exchange repulsion calculated between the probe and each orbital present in our model, where the leading coefficients are proportional to the number of electrons occupying the orbital. A coefficient of 8 was not present on the third term because one of the $\phi_{2p\pi}$ orbitals was orthogonal to the rotation of the He probe and contributes zero exchange repulsion to the sum as illustrated in Fig. 4.2.

$$E_{\text{XR}} = 4E_{\text{XR},2s} + 3E_{\text{XR},2p\sigma} + 4E_{\text{XR},2p\pi} \quad (4.35)$$

When calculating E_{XR} with the original model, expanded in Equations 4.36 and 4.37, it was found that the model underestimated the energy relative to that as a function of atomic radius at the HF/aug-cc-pVTZ level for F, Cl, and Br, and at the HF/aug-cc-pVTZ-PP level for I with step sizes of 0.20 Å. Additional energetic factors, ε_{ab} , were added to the model in order to improve accuracy, based on Eqn. 4.15 and Eqn. 4.16 in the H-L derivations.¹²⁻¹⁴

$$E_{\text{XR}} = \left(4 \left(\frac{-\varepsilon_{2s} \langle \Psi_{\text{He}} | \Psi_{2s} \rangle^2}{1 - \langle \Psi_{\text{He}} | \Psi_{2s} \rangle^2} \right) + 3 \frac{-\varepsilon_{2p\sigma} \langle \Psi_{\text{He}} | \Psi_{2p\sigma} \rangle^2}{1 - \langle \Psi_{\text{He}} | \Psi_{2p\sigma} \rangle^2} + 4 \left(\frac{-\varepsilon_{2p\pi} \langle \Psi_{\text{He}} | \Psi_{2p\pi} \rangle^2}{1 - \langle \Psi_{\text{He}} | \Psi_{2p\pi} \rangle^2} \right) \right) \quad (4.36)$$

$$E_{\text{XR}} = \left(4 \left(\frac{-\varepsilon_{2s} \mathbf{S}_{\text{He},2s}^2}{1 - \mathbf{S}_{\text{He},2s}^2} \right) + 3 \frac{-\varepsilon_{2p\sigma} \mathbf{S}_{\text{He},2p\sigma}^2}{1 - \mathbf{S}_{\text{He},2p\sigma}^2} + 4 \left(\frac{-\varepsilon_{2p\pi} \mathbf{S}_{\text{He},2p\pi}^2}{1 - \mathbf{S}_{\text{He},2p\pi}^2} \right) \right) \quad (4.37)$$

The HF probe approach results as a function of distance along $\phi_{2p\sigma}$ and $\phi_{2p\pi}$ in Fig. 4.3 were used to fit ε_{ab} using the Simplex minimization algorithm according to the sum of least squares.²³ The previously described optimized Slater exponents of the model wavefunctions were held fixed. The ε_{ab} results are related to the underlying energy of the valence alpha electrons found at the HF level (Table 4.3).

Table 4.3. The energetic scaling factors (ε) of the optimized model exchange repulsions.

	ε_{2s}	$\varepsilon_{2p\sigma}$	$\varepsilon_{2p\pi}$
Fluorine	-0.2837	-0.0946	-0.3369
Chlorine	-0.5449	-0.0903	-0.2336
Bromine	-0.613	-0.0669	-0.2233
Iodine	-0.6194	-0.0884	-0.2135

The updated model E_{XR} was then able to reproduce the HF results as a function of r along $\phi_{2p\sigma}$ and $\phi_{2p\pi}$ (Fig. 4.4). Fluorine had the smallest orbitals of the halogens according to the optimized Slater exponents and wavefunction maxima locations. The small valence orbitals of fluorine led to a smaller overlap with Ψ_{He} , which was illustrated by the repulsive wall at a short atomic radius. Iodine, in contrast, had the largest orbitals of the halogens studied, evidenced again by the optimized Slater exponents. The large valence orbitals of iodine led to a greater overlap with Ψ_{He} , which was illustrated by the repulsive wall being located at long atomic radius.^{3,24,26–30} The model can be used to approximate the orbital contributions to the overall exchange repulsion, which can be seen in Appendix 3, Figures A3.2a–d. The contribution of $E_{XR,2p\sigma}$ is smaller than that of $E_{XR,2p\pi}$ due to $\phi_{2p\sigma}$ containing only one electron instead of two. The orbital contributions illustrate the angular dependence of the E_{XR} on the valence wavefunctions.

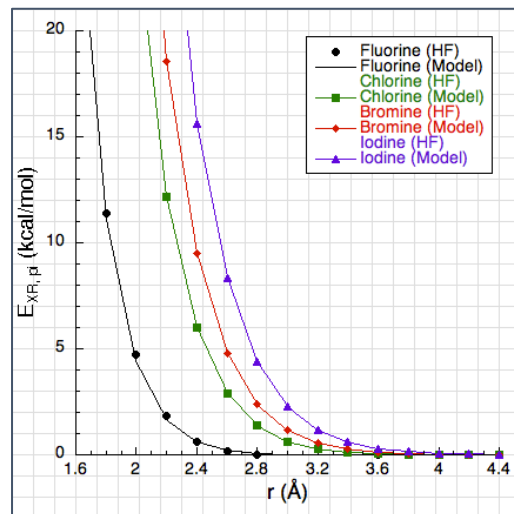
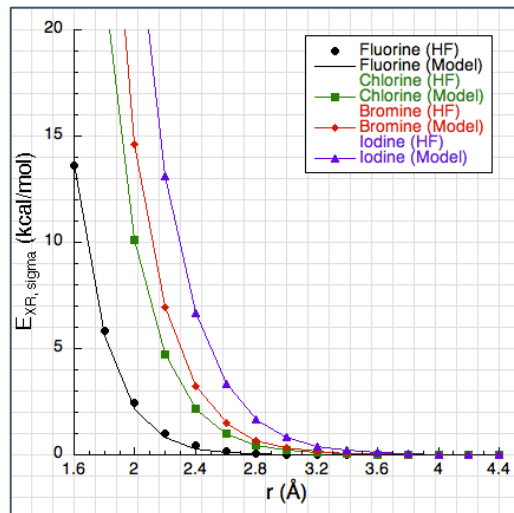


Figure 4.4. The Hartree-Fock (dots) and model (curves) E_{XR} versus radii of the halogen atoms for σ and π approach of helium. The model can be seen to fit the HF results very well as a function of distance approaching both the singly- and doubly-filled p-orbitals.

A rotation matrix was applied to the model exchange repulsion (Eqn. 4.38 and Eqn. 4.39) to calculate E_{XR} as a function of angle.

$$\langle \Psi_{He} | \Psi_{2p_\sigma} \rangle = \cos(\theta) \langle \Psi_{He} | \Psi_{2p_\sigma} \rangle + \sin(\theta) \langle \Psi_{He} | \Psi_{2p_\pi} \rangle \quad (4.38)$$

$$\langle \Psi_{He} | \Psi_{2p_\pi} \rangle = \sin(\theta) \langle \Psi_{He} | \Psi_{2p_\sigma} \rangle + \cos(\theta) \langle \Psi_{He} | \Psi_{2p_\pi} \rangle \quad (4.39)$$

Eqn. 4.38 and Eqn. 4.39 were simplified such that only the trigonometric contributions of $\Psi_{2p\sigma}$ were considered (Eqn. 4.40 and Eqn. 4.41, respectively) because $\langle \Psi_{He} | \Psi_{2p\pi} \rangle = 0$.²⁰ The exchange repulsion was found to have an angular dependence of exactly $\cos^2(\theta)$ when Eqn. 4.40 and Eqn. 4.41 were inserted into Eqn. 4.37, and the overlaps squared. This finding is consistent with the repulsive van der Waals potential in the Empirical Force Field for Biological Halogen Bonds (ffBXB).^{31,32} The ffBXB contains a $\cos(\nu\theta)$ term to model the angular dependent exchange repulsion component of halogen bonding, where ν represents the period of the cosine function. Once parameterized, $\nu \approx 2$ for $X = \text{Cl}, \text{Br}, \text{and I}$, signifying that the angular dependence can be said to approximately be equal to $\cos^2(\theta)$.^{31,32}

$$\langle \Psi_{He} | \Psi_{2p\sigma} \rangle = \cos(\theta) \langle \Psi_{He} | \Psi_{2p\sigma} \rangle \quad (4.40)$$

$$\langle \Psi_{He} | \Psi_{2p\pi} \rangle = \sin(\theta) \langle \Psi_{He} | \Psi_{2p\sigma} \rangle \quad (4.41)$$

Three-dimensional potential surfaces for E_{XR} were generated (Fig. 4.5) for each of the atomic models as a function of angle (x-axis) and atomic radius normalized by its respective van der Waals radius (y-axis). The distance dependence was adjusted to match at an angle of 90° and a normalized distance of 0.8. The model E_{XR} exhibited a clear angular dependence as expected, providing a measure of the orbital overlap per halogen. The E_{XR} surfaces for Cl, Br, and I are quite similar, while the well for fluorine is shallower due to the relative extension of the 2s orbital. A distinct angular dependence can be seen in each of the 3-D E_{XR} plots within the van der Waals at a normalized distance of 0.8. The magnitude of the dependence can be seen to increase from fluorine to iodine, consistent with Figure 2.6 and Table 2.1. The size of the repulsive well illustrates the relative increase in size of the σ -hole due to the singly-occupied valence p_z -orbital.

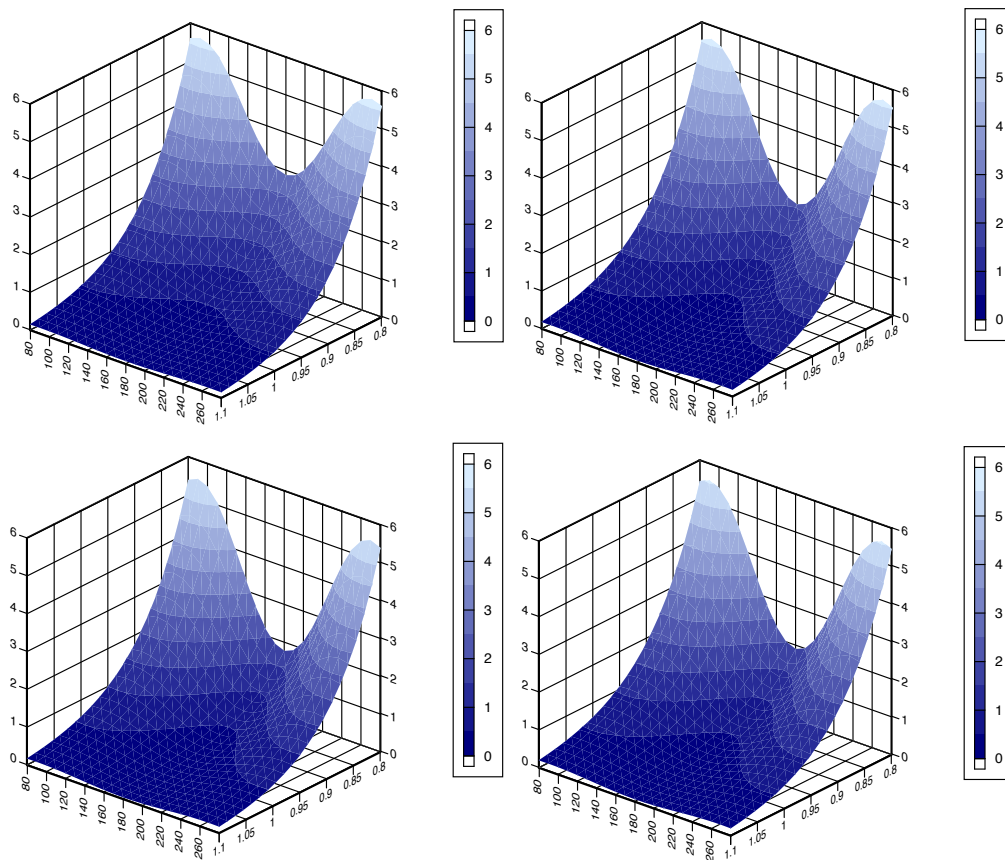


Figure 4.5. The E_{XR} versus normalized radii and angle for the model halogen atoms F (top left), Cl (top right), Br (bottom left), and I (bottom right). The shapes of the surfaces partially account for the repulsion near non-bonding angles near 90° and 270° in Figure 3.15.

The angular dependence rapidly goes to zero at a normalized distance of one and greater, implying that the exchange repulsion vanishes beyond the atomic radius of the halogen. The experimental 3-D CSD surfaces presented in Chapter 2 also lacked angular dependence beyond the sum of the van der Waals radii of the interacting halogen and carbonyl. This suggests that the electronic structure of our exchange repulsion model is consistent with experimental reports. The shape of the angular dependence of halogen bonding is correlated to the shape of E_{XR} both within and beyond the van der Waals distance. Attraction caused by dispersion, an isotropic component of halogen bonding, occurs where there is a lack of exchange repulsion and its strength is inversely proportional to non-bonding distance to the sixth power.

The model exchange repulsion as a function of r and θ described thus far has been incorporated into a series of Fortran 77 programs pertaining to F, Cl, Br, and I, which can be found in Appendix 4, Program A4.1.

III. Modeling the Electrostatics of a Halogen Atom

According to the σ -hole model, it is the region of partially positive charge on a halogen (Fig. 4.6) that attracts a partially negative Lewis base.^{4,24,33} The σ -hole model approximates the electrostatic potential by a Coulombic derivation of the Hellman-Feynman Theorem.^{17,18} The electrostatic potential is a model of the interaction between the electron density and nuclear charge of one molecule and a net negative point charge for another. The electrostatic potential excludes electron-electron interactions, and hence should not be expected to provide a precise description of the interaction energy of halogen bonding.

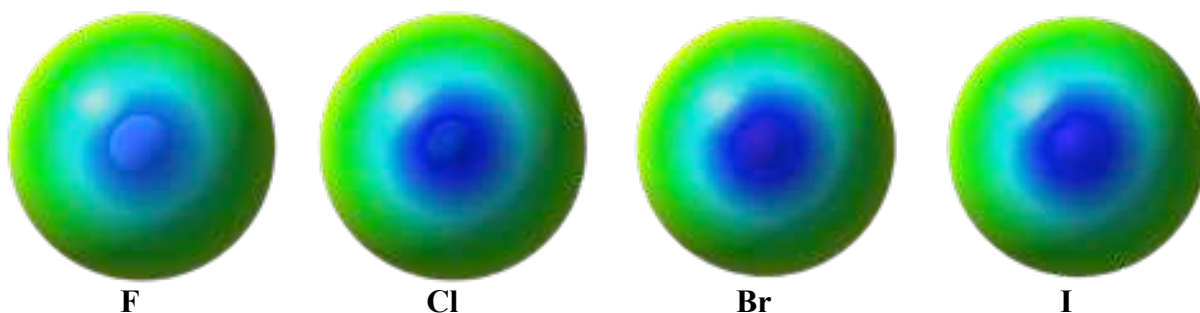


Figure 4.6. The σ -hole on the atomic halogens illustrated by the electrostatic potential. Red represents a negative electrostatic potential (-15.7 kcal/mol) and blue represents a positive electrostatic potential (15.7 kcal/mol) between a negative point charge probe and the molecule evaluated at grid point points on the 0.0004 electron density isosurface.

Our theoretical E_{ES} was modeled using a linear combination of atomic orbitals, much like the E_{XR} , to better understand the anisotropy of the halogen bonding components. The same atomic model was used to calculate the electrostatic potential as presented in Fig. 4.3, except that a negative point charge (q_n) was inserted in place of the helium probe.

The electrostatic attractions between q_n and Ψ_{2s}^2 (Eqn. 4.42), q_n and $\Psi_{2p\sigma}^2$ (Eqn. 4.43), and q_n and $\Psi_{2p\pi}^2$ (Eqn. 4.44) were modeled using expressions derived by Roothaan,²⁰ where ρ' is dependent on averages of ζ and defined in Eqn. 29 of *Ref. 20*. Notice that the first terms in Eqn. 4.42, Eqn. 4.43, and Eqn. 4.44, corresponding to the radial component, are identical. The second terms in Eqn. 4.43 and Eqn. 4.44, corresponding to the angular component, are also identical, save the leading coefficients (+3 or -3/2). The implication of these similarities will be discussed in the following section.

$$[q_n|\Psi_{2s}^2] = (1 + \tau)^{2.5}(1 - \tau)^{2.5} \left(\frac{\rho'}{\rho} \right) \left(1 - \left(1 + \frac{3}{2}\rho + \rho^2 + \frac{1}{3}\rho^3 \right) e^{-2\rho} \right) \quad (4.42)$$

$$[q_n|\Psi_{2p\sigma}^2] = (1 + \tau)^{2.5}(1 - \tau)^{2.5} \left(\left(\frac{\rho'}{\rho} \right) \left(1 - \left(1 + \frac{3}{2}\rho + \rho^2 + \frac{1}{3}\rho^3 \right) e^{-2\rho} \right) + 3 \left(\frac{\rho'}{\rho} \right) \left(1 - \left(1 + 2\rho + 2\rho^2 + \frac{4}{3}\rho^3 + \frac{2}{3}\rho^4 + \frac{2}{9}\rho^5 \right) e^{-2\rho} \right) \right) \quad (4.43)$$

$$[q_n|\Psi_{2p\pi}^2] = (1 + \tau)^{2.5}(1 - \tau)^{2.5} \left(\left(\frac{\rho'}{\rho} \right) \left(1 - \left(1 + \frac{3}{2}\rho + \rho^2 + \frac{1}{3}\rho^3 \right) e^{-2\rho} \right) - \frac{3}{2} \left(\frac{\rho'}{\rho} \right) \left(1 - \left(1 + 2\rho + 2\rho^2 + \frac{4}{3}\rho^3 + \frac{2}{3}\rho^4 + \frac{2}{9}\rho^5 \right) e^{-2\rho} \right) \right) \quad (4.44)$$

The model E_{ES} was then written as a sum of the electrostatic potential calculated between the probe and each orbital present in our model (Eqn. 4.45), expanded in Equations 4.46 and 4.47, where the leading coefficients correspond to the number of electrons that occupy the orbital.

$$E_{ES} = 2E_{ES,2s} + E_{ES,2p\sigma} + 2E_{ES,2p\pi} + 2E_{ES,2p'\pi} \quad (4.45)$$

$$E_{ES} = 2 \langle \Psi_{2s} | \frac{1}{r} | \Psi_{2s} \rangle + \langle \Psi_{2p\sigma} | \frac{1}{r} | \Psi_{2p\sigma} \rangle + 2 \langle \Psi_{2p\pi} | \frac{1}{r} | \Psi_{2p\pi} \rangle + 2 \langle \Psi_{2p'\pi} | \frac{1}{r} | \Psi_{2p'\pi} \rangle \quad (4.46)$$

$$E_{ES} = 2[q_n|\Psi_{2s}^2] + [q_n|\Psi_{2p\sigma}^2] + 2[q_n|\Psi_{2p\pi}^2] + 2[q_n|\Psi_{2p'\pi}^2] + \frac{-7}{r} \quad (4.47)$$

The model E_{ES} incorporated the third p-orbital ($\phi_{2p'_\pi}$) due to its contribution toward the partially negative perpendicular axes of the atom, whereas ϕ_{2p_π} was not included in the model E_{XR} due to its orthogonality to Ψ_{He} . The third p-orbital was notated differently to signify its symmetry about the rotation of the negative point charge, and the effective nuclear charge of 7 was selected to balance the seven valence electrons in the electronically neutral model atoms.

The electrostatic potential was then calculated as a function of the atomic radius at the HF/6-31G* level for F, Cl, and Br, and at the HF/aug-cc-pVTZ-PP level for I along ϕ_{2p_σ} (Fig. 4.7). The model E_{ES} visually matched the electrostatics using the same Slater exponents that had been fit using the Simplex minimization, discussed previously. The results illustrate the weak attraction of q_n to fluorine as a function of r along ϕ_{2p_σ} . The aspherical shape of the atom is caused by an uneven electron distribution, which directly results in the partially positive charge of the σ -hole; the more spherical the atom, the smaller the σ -hole. The weak partially positive charge on fluorine results from the shielding of its protons along ϕ_{2p_σ} , and the similar size of its valence s- and p-orbitals. The opposite is also true, as we found that iodine had the strongest attraction to q_n , explained by the prominence of its protons along ϕ_{2p_σ} , and contraction of its valence s-orbitals relative to its p-orbitals.

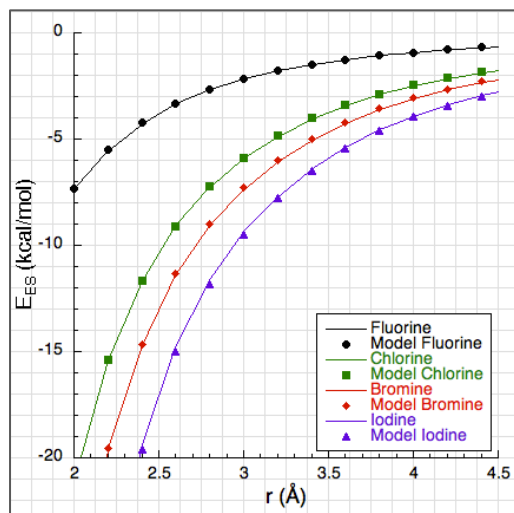


Figure 4.7. The Hartree-Fock (line) and model (dots) E_{ES} versus atomic radii of the halogens. The model can be seen to fit the HF results very well as a function of distance.

A rotation matrix was applied to the model electrostatic potential (Eqn. 4.48 and Eqn. 4.49) to calculate the model E_{ES} as a function of angle.

$$[q_n|\Psi_{2p\sigma}^2] = \cos^2(\theta) [q_n|\Psi_{2p\sigma}^2] + \sin^2(\theta) [q_n|\Psi_{2p\pi}^2] \quad (4.48)$$

$$[q_n|\Psi_{2p\pi}^2] = \sin^2(\theta) [q_n|\Psi_{2p\sigma}^2] + \cos^2(\theta) [q_n|\Psi_{2p\pi}^2] \quad (4.49)$$

The rotation was applied twice due to the wavefunctions in the expression being squared and $\Psi_{2p\pi}^2$ was not included because it is symmetric to the rotation of the negative point charge. The model E_{ES} exhibited clear angular dependence (Fig. 4.8), providing a relative measure of the σ -hole per halogen as a function of distance and angle. The model electrostatic potential as a function of r and θ has been incorporated into a series of Fortran 77 programs, which can be found in Appendix 4, Program A4.2.

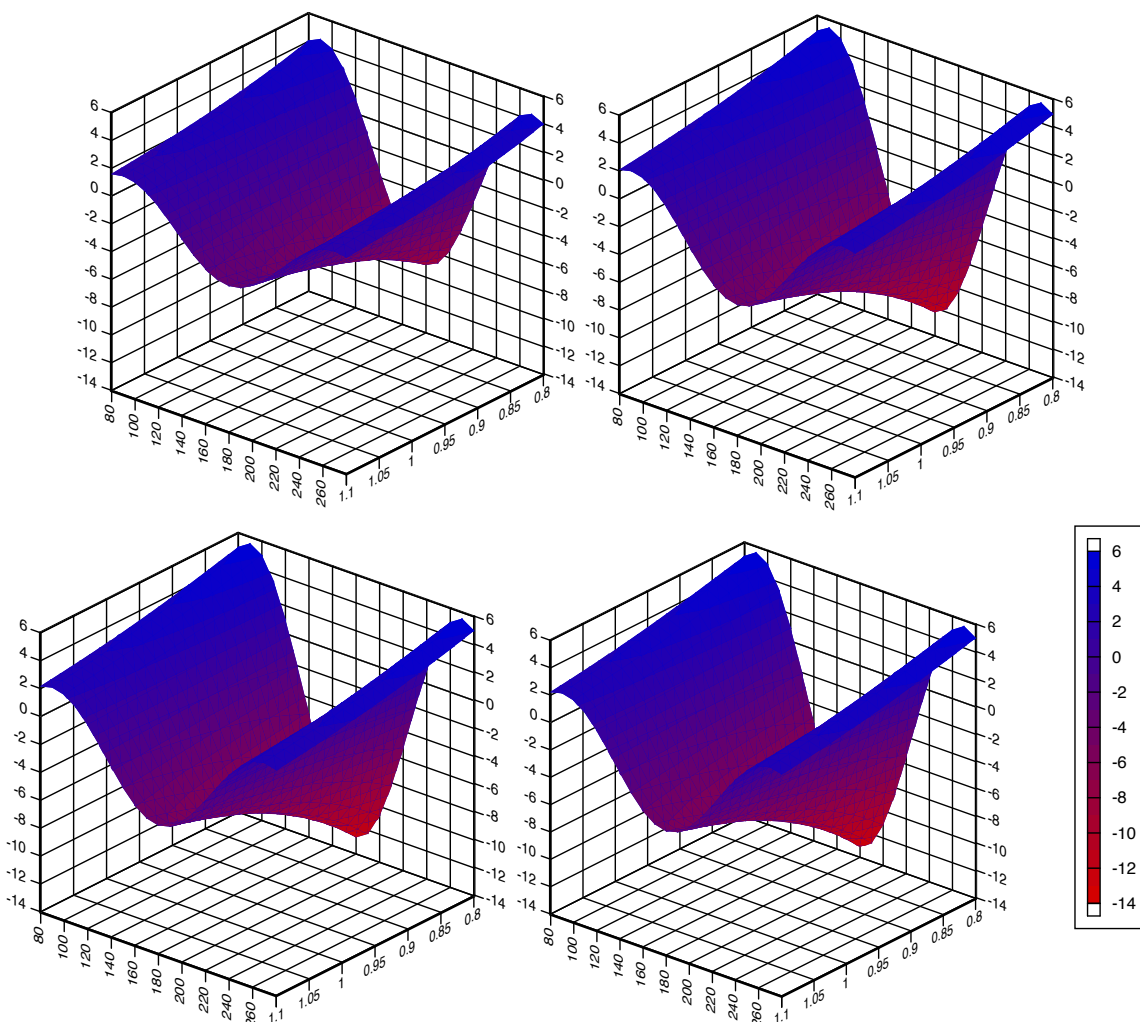


Figure 4.8. The E_{ES} versus scaled radii and angle for the model halogen atoms F (top left), Cl (top right), Br (bottom left), and I (bottom right). The shapes of the surfaces partially account for the repulsion near non-bonding angles of 90° and 270° in Figure 3.15, as well as the energetic wells at distances less than the sum of the van der Waals radii of the interacting species.

The 3-D E_{ES} plots illustrate a distinct angular dependence within the van der Waals radius at a normalized distance of 0.8. Unlike the E_{XR} plots, an attraction between the halogen and negative point probe can be seen, increasing the strength from fluorine to iodine. The angular dependence of the electrostatic potential does not go to zero at a normalized distance of one or greater, which is consistent with the electrostatic contour map presented in Figure 2.8, but inconsistent with the 3-D CSD plot in Figure 2.7. where the angular dependence had vanished by

the sum of the van der Waals radii. This discrepancy can be accounted for by observing how the electrostatics are affected by dipole interactions.

The CSD crystal structures were primarily comprised of halogen bonds that had charge transferred to the halogen from carbon, forming a polar bond. In Chapter 3, it was found that the inclusion of organic substituent groups increased the exchange repulsion component of the interaction energy by changing the shape of the halogen atom. The phenyl halide dimers were slightly lower in energy due to the electron-withdrawing nature of the substituent relative to the methyl halide dimers. Considering this information, 3-D E_{ES} plots were generated for three additional scenarios: 1) addition of a partial charge to the model, 2) addition of a dipole-charge interaction to the model, and 3) replacement of the electrostatic potential model with a dipole-dipole model, (Fig. 4.9). The first two scenarios both display a distinct angular dependence at short normalized distances, with decreasing angular dependence at long normalized distances, and remaining repulsive outside the van der Waals distance. The third scenario, a dipole-dipole model precisely reproduces the shape of the MeX-X₂ difference plots from Figure 3.16.

The model electrostatic potential as a function of r and θ pertaining to these three additional scenarios has also been incorporated into a series of Fortran 77 programs, which can be found in Appendix 4, Program A4.3.

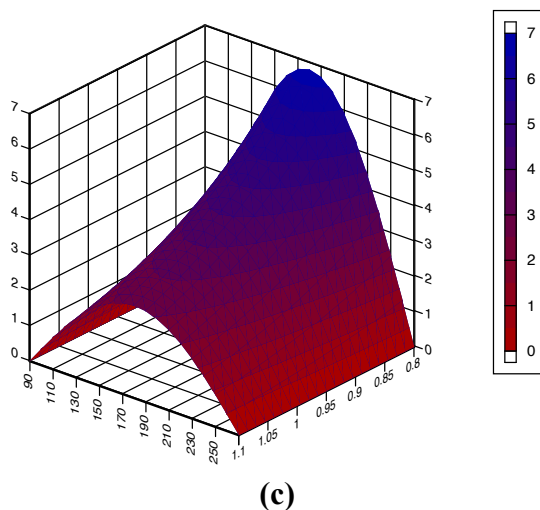
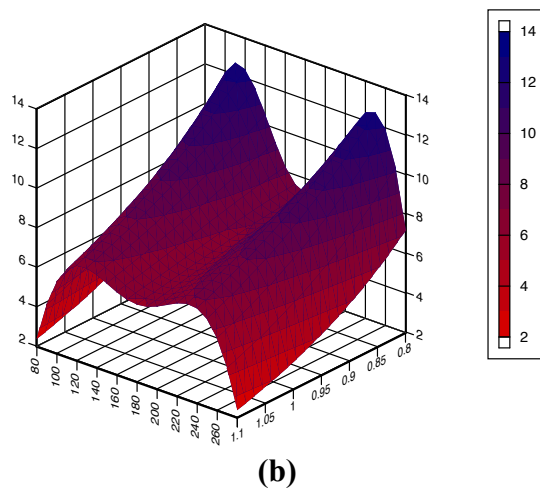
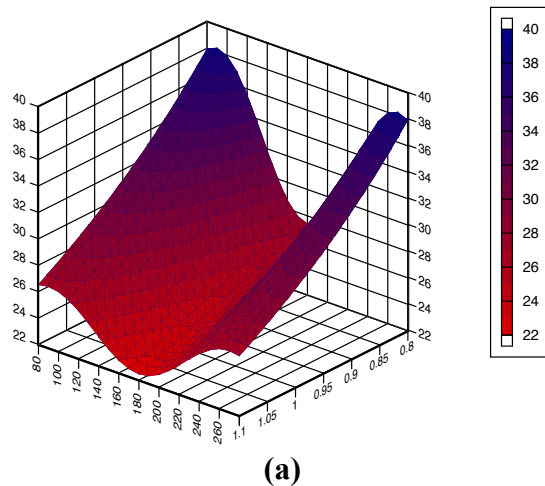


Figure 4.9. Model electrostatic potential of fluorine as a function of angle and normalized bond distance after the addition of (a) a partial charge, (b) a charge-dipole, and (c) a dipole-dipole interaction.

The surfaces above show that our model is consistent with experimental and theoretical results, which has profound implications for halogen bonding. The C-X bond dipole is aligned opposite the O=C bond dipole, providing a repulsive interaction between the halogen bond acceptor and donor. Therefore, dipole-dipole interactions with a distance dependence of $1/r^3$ should be largest for the smallest halogen, fluorine, selected to demonstrate the suggested implication. A model energy (E) was calculated as a function of distance (Eqn. 4.50).

$$E = \frac{e_{ES}}{r^n} + \frac{e_{XR}S_{ab}^2}{1 - S_{ab}^2} \quad (4.50)$$

The Slater exponents (ζ) decrease with increasing halogen size, as expected (Table 4.4). The exponents (n) and energy values (e_x) were fit to the MeX-X₂ acetone data of Figure 3.16 using the Simplex minimization algorithm according to the sum of least squares.²³

Table 4.4. The energetic scaling factors of the model dipole-dipole interaction presented in Equation 4.50, as well as the quadrupole-dipole interaction discussed below.

	ζ	$1/r^n$ (\AA^{-1})	e_{ES} (kcal/mol)	e_{XR} (kcal/mol)
Fluorine	2.162	3.007	86.7	134.4
Chlorine	1.817	3.014	94.4	124.6
Bromine	1.712	3.062	93.4	125.7
Iodine	1.701	3.074	86.2	136.5
CF ₄	2.087	4.105	78.4	171.0

E was calculated as a function of distance and laid overtop MeX-X₂ difference curves at the HF level (Fig. 4.10). It was found that the difference curves for $X = \text{F, Cl, Br, and I}$ could be accurately modeled using the combination of $1/r^3$ dipole-dipole repulsion (E_{ES}) and exchange repulsion (E_{XR}), combined in Eqn. 4.50. In other words, halogen bonds bound to an organic moiety are more repulsive than their nonpolar counterparts due to the introduction of a repulsive dipole-dipole interaction as well as exchange repulsion.

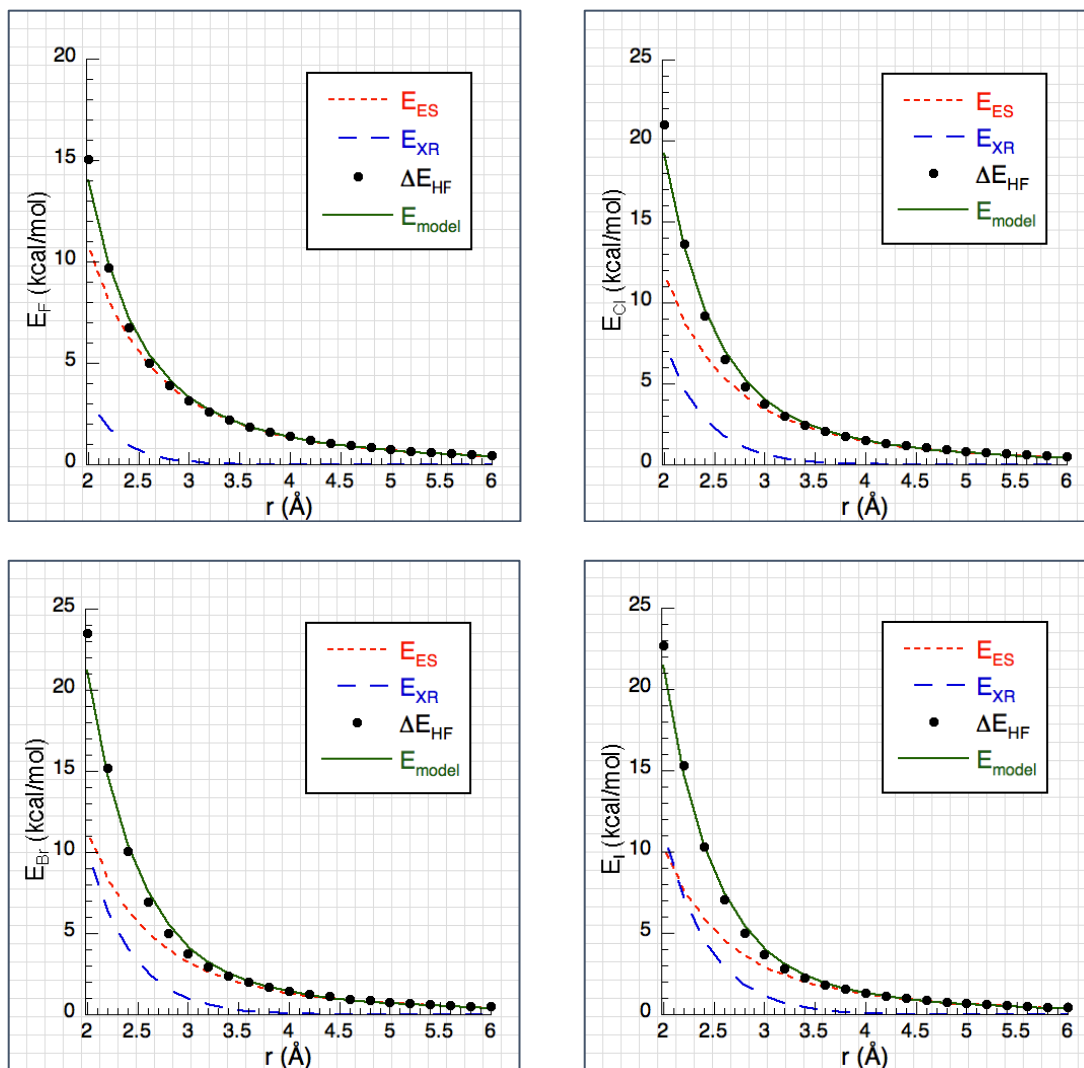


Figure 4.10. Model energy as a function of distance in comparison to the MeX-X₂—acetone difference curves for the model halogen atoms F (top left), Cl (top right), Br (bottom left), and I (bottom right).

This model further suggests that if fluoromethane were substituted by CF₄—acetone, the interaction would be a quadrupole-dipole and have a distance dependence of $1/r^4$. The fit of the CF₄-F₂ acetone data (Fig. 4.11) is consistent with quadrupole-dipole interaction. The fit variables are also presented in Table 4.4.

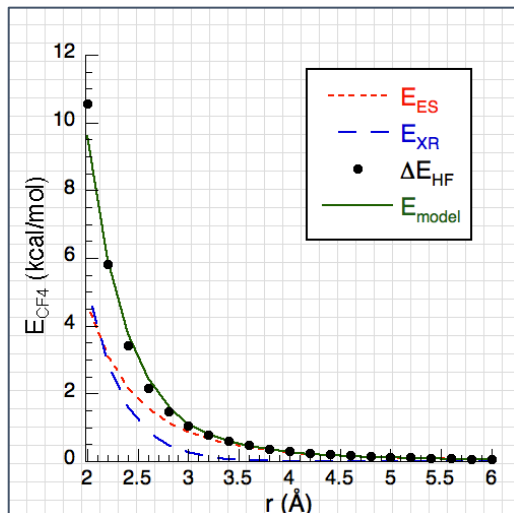


Figure 4.11. Model energy as a function of distance in comparison to the CF₄-F₂—acetone difference curve for the model halogen atoms F.

Further Analysis of the Exchange Repulsion and Electrostatic Potential Models

The electrostatic potential expressions from Eqn. 4.42, 4.43, and 4.44 can be simplified (Eqn. 4.51, Eqn. 4.52, and Eqn. 4.53, respectively) in order to more closely observe the angular dependence of the electrostatic potential on the first and second terms of these equations. The first terms within Eqn. 4.42, Eqn. 4.43, and Eqn. 4.44 were identical, call them *A*. Eqn. 4.42, representing the electrostatic attraction between a point charge and Ψ_{2s} , lacks a second term due to the isotropic angular momentum of s-orbitals. The second terms of Eqn. 4.43 and 4.44, which represent the electrostatic attraction between a point charge and $\Psi_{2p\sigma}$, and $\Psi_{2p\pi}$, respectively, were also identical, save the leading coefficients (3 or -3/2), call them *B*. The variation in electrostatics due to the angular component vanishes at an atomic radius where the electrostatics are comparable at 180°.

$$[q_n|\Psi_{2s}^2] = A \quad (4.51)$$

$$[q_n|\Psi_{2p\sigma}^2] = A + 3B \quad (4.52)$$

$$[q_n|\Psi_{2p\pi}^2] = A - \frac{3}{2}B \quad (4.53)$$

The sum of the terms as a probe moves along the directions of $\Psi_{2p\sigma}$ (Eqn. 4.54) and $\Psi_{2p\pi}$ (Eqn. 4.55) yields a general potential expression, V (Eqn. 4.56), when Eqn. 4.54 and 4.55 are inserted into Eqn. 4.45 and a rotation matrix is applied.

$$V_\sigma = 7A - 3B \quad (4.54)$$

$$V_\pi = 7A + \frac{3}{2}B \quad (4.55)$$

$$V = 7A - 3B\cos^2(\theta) + \frac{3}{2}B\sin^2(\theta) \quad (4.56)$$

If unity is subtracted (Eqn. 4.57) from Eqn. 4.56, the resulting expression (Eqn. 4.58) suggests that the electrostatic potential has an angular dependence of $\cos^2(\theta)$.

$$1 = \frac{3}{2}B\cos^2(\theta) + \frac{3}{2}B\sin^2(\theta) \quad (4.57)$$

$$V - 1 = 7A - \frac{9}{2}\cos^2(\theta) \quad (4.58)$$

In other words, as derived using these simpler expressions, the electrostatic potential was found to have an angular dependence of exactly $\cos^2(\theta)$ when Eqn. 4.48 and Eqn. 4.49 were inserted into Eqn. 4.47. This is true for all the halogens and is consistent with the electrostatic interaction in the ffBXB.^{31,32} Like the exchange repulsion, the ffBXB contains a $\cos(\nu\theta)$ term to model the angular dependent electrostatic component of halogen bonding, where ν represents the period of the cosine

function. Once parameterized, $\nu \approx 2$ for $X = \text{Cl}, \text{Br}, \text{and I}$, signifying that the angular dependence can be said to approximately be equal to $\cos^2(\theta)$.^{31,32}

The simpler expressions can also be used to describe the affect an electron-donating substituent has on the shape of the atom based on the valence p-orbitals. Our models have provided further evidence suggesting that the aspherical shape of a halogen is inherent to the atom and dependent on the relative sizes of the valence s- and p-orbitals. If a net charge representing electron transfer from a substituent to the halogen atom is added, an expression, V_σ (Eqn. 4.59), is found representing the relative shape of p_σ-orbital from Eqn. 4.54 and another expression, V_π (Eqn. 4.60), representing the shape of the p_π-orbital from Eqn. 4.47.

$$V_\sigma = (7 - q_n)A - (1 + q_n)3B \quad (4.59)$$

$$V_\pi = (7 - q_n)A + (1 + q_n)\frac{3}{2}B \quad (4.60)$$

The angularly dependent B terms from Eqn. 4.59 and Eqn. 4.60 go to zero in the event that a full electron charge ($q_n = -1$) is transferred to the halogen from the electron-donating substituent. This results in V being dependent on a spherical potential term A , resulting in an isotropic electrostatic potential on the outer electron density contour, diminishing any E_{ES} attraction to a Lewis base. In summary, we have derived simple expressions showing that an additional charge on a halogen atom via electron-donating substituent removes the angular dependency from the underlying energetic components of halogen bonding.

Just as the electrostatic potential was affected by the charge transfer from the covalent bond of the substituent group, so too was the exchange repulsion. Charge dependence for our E_{XR} model follows from the linear dependence on number of electrons in the energy expression. Consider intra-bond charge transfer, i.e. bond polarization, in a bond between carbon, C , and fluorine, F . The valence bond wavefunction, Ψ , for such an interaction is provided (Eqn. 4.61).

$$\Psi = c_{\text{covalent}}(\phi_{\text{C}}\phi_{\text{F}} + \phi_{\text{F}}\phi_{\text{C}}) + c_{\text{ionic}}\phi_{\text{F}}\phi_{\text{F}} \quad (4.61)$$

The covalent contribution, c_{cov} , would interact with a Lewis base through a 3-electron interaction, see Eqn. 4.21 while the ionic contribution, c_{ionic} , would utilize the 4-electron interaction term. In going from a halogen atom toward a halide ion the exchange repulsion increases from 3 to $3-q_n$, where q_n is c_{ionic}^2 .

The electrostatic potential and exchange repulsion were modeled using a linear combination of atomic orbitals to understand the source of the observed distance-angle dependence at the most fundamental level. Based on the findings presented in Chapters 2–4, it is proposed that the attraction in halogen bonding occurs through a balance of electrostatics, exchange repulsion, and dispersion. The initial, long-range interaction of a halogen bonding dimers is caused by net attractive electrostatics, weakened and made more angularly independent by bond polarization to the halogen by its organic substituent group and repulsive dipole-dipole interaction. As the Lewis base draws closer to the halogen it is funneled to an interaction angle of 180° by the increasing angular dependence of the electrostatics and exchange repulsion. Due to the diminished exchange repulsion at 180° , the Lewis base stabilizes at a distance shorter than the sum of the two species van der Waals radii through electrostatics and dispersion. The impact of charge transfer, an additional energetic component, on dimer binding energy will be discussed in Chapter 5.

REFERENCES

- (1) Pearlman, D. A.; Case, D. A.; Caldwell, J. W.; Wilson, R. S.; Cheatham III, T. E.; DeBolt, S.; Ferguson, D.; Seibel, G.; Kollman, P. A. AMBER, A Package of Computer Programs for Applying Molecular Mechanics, Normal Mode Analysis, Molecular Dynamics and Free Energy Calculations to Simulate the Structural and Energetic Properties of Molecules. *Comput. Phys. Commun.* **1995**, *91*, 1–41.
- (2) Wang, J.; Wolf, R. M.; Caldwell, J. W.; Kollman, P. A.; Case, D. A. Development and Testing of a General Amber Force Field. *J. Comput. Chem.* **2004**, *25*, 1157–1174.
- (3) Stone, A. J. Are Halogen Bonded Structures Electrostatically Driven? *J. Am. Chem. Soc.* **2013**, *135*, 7005–7009.
- (4) Desiraju, G. R.; Ho, P. S.; Kloo, L.; Legon, A. C.; Marquardt, R.; Metrangolo, P.; Politzer, P.; Resnati, G.; Rissanen, K. Definition of the Halogen Bond (IUPAC Recommendations 2013). *Pure Appl. Chem.* **2013**, *85*, 1711–1713.
- (5) Riley, K. E.; Murray, J. S.; Fanfrlík, J.; Řezáč, J.; Solá, R. J.; Concha, M. C.; Ramos, F. M.; Politzer, P. Halogen Bond Tunability II: The Varying Roles of Electrostatic and Dispersion Contributions to Attraction in Halogen Bonds. *J. Mol. Model.* **2013**, *19*, 4651–4659.
- (6) Politzer, P.; Murray, J. S.; Clark, T. Halogen Bonding and Other σ -Hole Interactions: A Perspective. *Phys. Chem. Chem. Phys.* **2013**, *15*, 11178.
- (7) Murray, J. S.; Lane, P.; Clark, T.; Riley, K. E.; Politzer, P. σ -Holes, π -Holes and Electrostatically-Driven Interactions. *J. Mol. Model.* **2012**, *18*, 541–548.
- (8) Ibrahim, M. A. A. Molecular Mechanical Perspective on Halogen Bonding. *J. Mol. Model.* **2012**, *18*, 4625–4638.
- (9) Ji, J.; Meng, D.; Zhang, X.; Meng, L.; Zeng, Y. Enhancing Effects of Hydrogen/Halogen Bonds on σ -Hole Interactions Involving Ylide. *J. Mol. Model.* **2014**, *20*, 2282.
- (10) Aakeröy, C. B.; Wijethunga, T. K.; Desper, J. Practical Crystal Engineering Using Halogen Bonding: A Hierarchy Based on Calculated Molecular Electrostatic Potential Surfaces. *J. Mol. Struct.* **2014**, *1072*, 20–27.
- (11) Heitler, W.; London, F. Wechselwirkung Neutraler Atome Und Homoopolare Bindung Nach Der Quatenmechanik. *Z. Phys.* **1927**, *44*, 455.
- (12) Muller, R. P.; Goddard III, W. A. Valence Bond Theory. In *The Encyclopedia of Physical Science and Technology*; Academic Press, 2002; pp 1–8.
- (13) Wilson Jr., C. W.; Goddard III, W. A. Exchange Kinetic Energy, Contragradience, and Chemical Binding. *Chem. Phys. Lett.* **1970**, *5*, 45–49.
- (14) Goddard III, W. A. *Nature of the Chemical Bond*; California Institute of Technology: Pasadena, CA, 1986; Vol. 1.
- (15) Pauling, L. *The Nature of the Chemical Bond*; Cornell University Press: New York, 1942.
- (16) McQuarrie, D. A. *Quantum Chemistry*, 2nd ed.; University Science Books: Sausalito, CA, 2008.
- (17) Slater, J. C. Hellmann-Feynman and Virial Theorems in the X_α Method. *J. Chem. Phys.* **1972**, *57*, 2389–2396.
- (18) Politzer, P.; Murray, J. S.; Concha, M. C. σ -Hole Bonding Between Like Atoms; A Fallacy of Atomic Charges. *J. Mol. Model.* **2008**, *14*, 659–665.
- (19) Ziegler, T. Approximate Density Functional Theory as a Practical Tool in Molecular Energetics and Dynamics. *Chem. Rev.* **1991**, *91*, 651–667.
- (20) Roothaan, C. C. J. A Study of Two-Center Integrals Useful in Calculations on Molecular Structure. I. *J. Chem. Phys.* **1951**, *19*, 1445–1458.
- (21) Wahl, A. C. Analytic Self-Consistent Field Wavefunctions and Computed Properties for Homonuclear Diatomic Molecules. *J. Chem. Phys.* **1964**, *41*, 2600–2611.
- (22) Rüdénberg, K. A Study of Two-Center Integrals Useful in Calculations on Molecular Structure. II. The Two-Center Exchange Integrals. *J. Chem. Phys.* **1951**, *19*, 1459–1477.
- (23) Nelder, J. A.; Mead, R. A Simplex Method for Function Minimization. *Comput. J.* **1965**, *7*, 308–313.

- (24) Politzer, P.; Murray, J. S.; Clark, T. σ -Hole Bonding: A Physical Interpretation. In *Halogen Bonding I*; Metrangolo, P., Resnati, G., Eds.; Springer International Publishing: Cham, 2014; Vol. 358, pp 19–42.
- (25) Politzer, P.; Murray, J. S. Halogen Bonding: An Interim Discussion. *ChemPhysChem* **2013**, *14*, 278–294.
- (26) Mohan, N.; Suresh, C. H. Accurate Binding Energies of Hydrogen, Halogen, and Dihydrogen Bonded Complexes and Cation Enhanced Binding Strengths. *Int. J. Quantum Chem.* **2014**, *114*, 885–894.
- (27) Pérez-Torralba, M.; García, M. Á.; López, C.; Torralba, M. C.; Torres, M. R.; Claramunt, R. M.; Elguero, J. Structural Investigation of Weak Intermolecular Interactions (Hydrogen and Halogen Bonds) in Fluorine-Substituted Benzimidazoles. *Cryst. Growth Des.* **2014**, *14*, 3499–3509.
- (28) Nguyen, H. L.; Horton, P. N.; Hursthouse, M. B.; Legon, A. C.; Bruce, D. W. Halogen Bonding: A New Interaction for Liquid Crystal Formation. *J. Am. Chem. Soc.* **2004**, *126*, 16–17.
- (29) Esrafil, M. D.; Mohammadian-Sabet, F. Halogen-Bond Interactions Enhanced by Charge-Assisted Hydrogen Bonds: An Ab Initio Study. *Bull. Chem. Soc. Jpn.* **2014**, *87*, 882–889.
- (30) Esrafil, M. D.; Vakili, M. Halogen Bonds Enhanced by σ -Hole and π -Hole Interactions: A Comparative Study on Cooperativity and Competition Effects Between $X\cdots N$ and $S\cdots N$ Interactions in $H_3N\cdots XCN\cdots SF_2$ and $H_3N\cdots XCN\cdots SO_2$ Complexes ($X = F, Cl, Br$ and I). *J. Mol. Model.* **2014**, *20*, 2291.
- (31) Carter, M.; Rappé, A. K.; Ho, P. S. Scalable Anisotropic Shape and Electrostatic Models for Biological Bromine Halogen Bonds. *J. Chem. Theory Comput.* **2012**, *8*, 2461–2473.
- (32) Scholfield, M. R.; Ford, M. C.; Vander Zanden, C. M.; Billman, M. M.; Ho, P. S.; Rappé, A. K. Force Field Model of Periodic Trends in Biomolecular Halogen Bonds. *J. Phys. Chem. B* **2015**, *119*, 9140–9149.
- (33) Arunan, E.; Desiraju, G. R.; Klein, R. A.; Sadlej, J.; Scheiner, S.; Alkorta, I.; Clary, D. C.; Crabtree, R. H.; Dannenberg, J. J.; Hobza, P.; et al. Definition of the Hydrogen Bond (IUPAC Recommendations 2011). *Pure Appl. Chem.* **2011**, *83*.

CHAPTER 5: TRIMER SYSTEMS

Non-additivity is a measure of the increased stability in a multimolecular, non-bonding structure due to a synergistic interaction of the components.^{1,2} The purpose of the research presented herein was to determine the underlying energetic contributions to the non-additivity of multimolecular halogen bonding systems. The presence of non-additivity has been shown to increase the difficulty of theoretically predicting the interaction energy of multimolecular systems, such as halogenated molecules in polar solvents.^{3,4} For example, the results of a SAMPL2 Blind Prediction Challenge were published in 2010,⁵ wherein transfer energies between gas phase and aqueous solutions were calculated to benchmark the accuracy and applicability of novel theoretical methods. The transfer energies were calculated “blind,” meaning that the participants were not given reported experimental results, creating an environment free of bias for a controlled comparison between the methods. The transfer energies were underestimated between gas phase and aqueous solution of the 5-halouracils with an absolute mean raw error of 6 kcal/mol across the series of solvents with a standard deviation of only 0.4 kcal/mol. Due to the inaccurate yet precise predictions, a systematic error was concluded to have been present in the theoretical methods. One contributing factor to the systematic error could be the non-additivity, which the methods did not account for.

Model trimers can be used to study simplified versions of multimolecular halogen bonding systems. For instance, Voth et al.⁶ placed bromobenzene near a carbonyl oxygen that had already formed a hydrogen bond (Fig. 5.1) to model a halogen bond interacting with a peptide chain. Voth et al. found that the halogen bonding bromobenzene and hydrogen bonding *N*-ethylpropanimide on a peptide chain were separated by an average bond angle of 88.2°, making them approximately geometrically orthogonal.

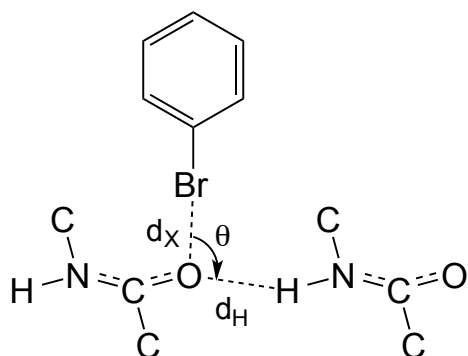


Figure 5.1. The trimer system used to test the effect a halogen bond would have on an already existed hydrogen bond, where the distances (d_X and d_H) were varied and the angle (θ) was found to be 88.2° on average (adapted from *Nat. Chem.* **2009**, 1, 74).

Voth et al. calculated the interaction energies as a function of non-bonding distances (d_X and d_H) (Ref. 6; Fig. 5). It was discovered that the presence of bromobenzene did not greatly affect the already-present hydrogen bond as d_X was varied, nor did the presence of *N*-ethylpropanamide affect the halogen bond as d_H was varied, so the two interactions were concluded to be energetically orthogonal. Non-additivity was not reported for the trimer.

However, in a more recent study presented by Carlsson et al.,⁷ it was hypothesized that an intramolecular hydrogen bond would polarize the electron density of a halogen, enhancing its σ -hole (Ref. 7; Fig. 7) and increase corresponding halogen bonding strength. A pseudo-wild-type (WT*) T4 lysozyme was crystallized as well as structures in which Y18 is halogenated at the *meta* position by chlorine, bromine, or iodine to test this hypothesis. Differential scanning calorimetry was used to determine the thermal stability of the WT* and halogenated constructs. Melting temperatures and enthalpies of the structures showed that the chlorinated lysozyme was more stable than WT*, the brominated lysozyme is approximately as stable as WT*, and the iodized lysozyme was less stable than WT* (Ref. 7; Table 2). The increased stability of the chlorinated structure was said to be dependent on its ability to form a halogen bond with the G28 oxygen, further enhanced by an intramolecular hydrogen bond. Molecular models of *N*-methylacetamide

with chlorobenzene or 2-chlorophenol were created (Fig. 5.2), and energetic calculations at the MP2/aug-cc-pVTZ in a cyclohexane solvent showed that the presence of an intramolecular hydrogen bond resulted in a more stable halogen bond (*Ref. 7; Fig. 8*).

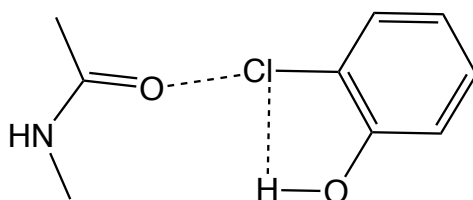


Figure 5.2. The model of *N*-methylacetamide in a halogen bonding configuration with 2-chlorophenol. The Cl—O halogen bonding strength is enhanced by the hydroxyl group, which forms an intramolecular hydrogen bond with chlorine. The Cl—O interaction energy was reported to be -1.43 kcal/mol, OH—Cl was reported to be -1.84 kcal/mol, and the complex interaction energy was reported to be -3.24 kcal/mol. The interaction could be considered as a trimer-like interaction due to the presence of three interacting species (adapted from *Biochemistry*. **2018**, 57, 4135).

The energetic orthogonality reported by Voth et al.⁶ in contrast to the halogen bonding strength being enhanced by an intramolecular hydrogen bond reported by Carlsson et al.⁷ is not necessarily surprising. Researchers Riel et al.⁸ have also published an article on hydrogen-bond enhanced halogen bonds, the purpose of which was to discern whether halogen bonding could be used to practically pre-organize biomolecular structures. The researchers confirmed after modeling the halogen bonding capabilities of 1,3-bis(4-ethynylpyridinium) that simultaneous pre-organization and enhancement of the halogen bond is possible; however, Riel et al. also state that “computational reports of intermolecular hydrogen bonding to halogen bonding donors suggest that hydrogen bonds can have both a cooperative and non-cooperative effect on halogen bonding strength.”⁸ This provides motivation to study the non-additivity as dependent on the underlying energetic components of the interaction energy.

Cooperativity of Model Hydrogen-Bond Enhanced Halogen Bonds

One way to quantify the non-additivity of a trimer system is to calculate the cooperativity, ΔE_{COOP} (Eqn. 5.1), by adding the optimized dimer energies (ΔE_{AB}^{opt} and ΔE_{BC}^{opt}) and single point energy of the indirectly interacting molecules (ΔE_{AC}^{sp}), and subtracting the sum from the optimized trimer energy (ΔE_{ABC}^{opt}).^{1,2,9-11}

$$\Delta E_{COOP} = \Delta E_{ABC}^{opt} - (\Delta E_{AB}^{opt} + \Delta E_{BC}^{opt} + \Delta E_{AC}^{sp}) \quad (5.1)$$

For instance, Solimannejad et al.² demonstrated the effectiveness of using the ΔE_{COOP} as a measure of the non-additivity of trimer systems for halogen bonding pyridine-acetonitrile derivatives (Ref. 2; Table 2), including 4-nitropyridine-cyanogen bromide-cyanogen bromide (Fig. 5.3).

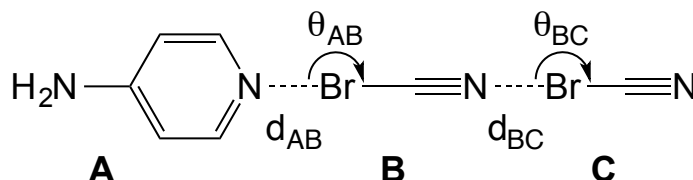


Figure 5.3. An example of one trimer studied by Solimannejad et al.² where the pyridine and acetonitrile derivatives were arranged in series such that angles θ_{AB} and θ_{BC} equaled 180° . The pyridine was labeled as molecule A, the central cyanogen bromide as molecule B, and the outermost cyanogen bromide as molecule C. The non-bonding distances, d_{AB} and d_{BC} , were minimized during optimization (adapted from *J. Phys. Chem. A* **2013**, *117*, 5551).

The non-additivity of halogen bonding trimers has been found to be dependent not only on the dimer interactions, but also on the molecular arrangement and composition.^{12,13} A collection of reports in the literature focus on what can be referred to as “linear trimers,” an arrangement of three molecules linked in series, like that of the structures studied by Solimannejad et al.^{2,10,13-15} Linear trimers have been of interest because ΔE_{COOP} generally varies consistently as a function of non-bonding distance, as A and C are far enough apart to interact negligibly. Alternate reports focus on what can be referred to as “cluster trimers,” an arrangement in which the three molecules

are bound in a geometrically orthogonal configuration, like that of the structure studied by Voth et al.^{9,16,17} ΔE_{COOP} in cluster trimers appears to vary less as a function of distance; molecules *A* and *C* are close enough to attract one another through van der Waals interactions, which appears to decrease the calculated cooperativity according to Eqn. 5.1. Cluster trimers are still of interest because they provide a reasonable representation of how solvents, such as water, would behave in close contact with halogen bonds in solution.^{13,14,16}

Electronic Structure Studies of Model Hydrogen-Bond Enhanced Halogen Bonds

Our aspiration throughout this project was to identify the energetic components of halogen bonding trimers as a function of distance to gain preliminary understanding of the behavior of halogen bonding in multimolecular systems. Electrostatic, exchange repulsion, and dispersive components were each expected to play a role based on the results presented in Chapters 2–4. The non-additivity of halogen bonding structures was also expected to be partially caused by charge transfer interactions, a non-bonding component originally suggested by Mulliken.¹⁸ Molecular bromine was chosen as the model halogen in order to test the dependence of the non-additivity, as is the most abundant halogen bonding case reported in the literature.^{19,20} Two small molecules were used as solvents in the model trimers: water and ammonia. Water is a ubiquitous solvent in biomolecular systems,^{4,5,21,22} and nitrogen is an important element in biomolecules that can be modeled via ammonia.^{3,23,24}

The trimers were arranged in a cluster configuration (Fig. 5.4), where the non-bonding distances (d_{AB} and d_{BC}) were allowed to minimize during optimization, and the angles (θ_{AB} and θ_{BC}) were constrained to 180° and 90° (respectively) to maintain a cluster-configuration. The interaction energies of the trimer systems were calculated using separate hybrid methods like those presented by Mohan et al.^{12,24–26} A hybrid method splits the geometric optimization and

counterpoise correction calculations into two steps. The optimizations of the water-containing cluster trimer ($\text{Br}_2\text{-2H}_2\text{O}$) and ammonia-containing cluster trimer ($\text{Br}_2\text{-2NH}_3$) were performed at the MP2/aug-cc-pVTZ level, and the counterpoise corrected single point energy calculations at the MP2/aug-cc-pV5Z and APFD/aug-cc-pVTZ levels, notated MP2/aug-cc-pVTZ//MP2/aug-cc-pV5Z and MP2/aug-cc-pVTZ//APFD/aug-cc-pVTZ, respectively. A counterpoise correction addressed the basis set superposition error,²⁷ which is caused by incomplete basis sets, leading to an overestimation of a dimer's interaction energy by up to 20%,^{17,25-28} and Dunning's expansive aug-cc-pV5Z basis set was used to calculate the electron correlation accurately.

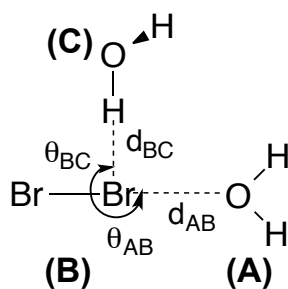


Figure 5.4. An illustration of the water-containing trimer system ($\text{Br}_2\text{-2H}_2\text{O}$), where *A* is a halogen bonding water molecule, *B* is molecular bromine, and *C* is a hydrogen bonding water molecule. The ammonia-containing trimer system ($\text{Br}_2\text{-2NH}_3$) was similarly constructed.

The APFD method was initially of interest because it is a relatively new DFT functional that explicitly includes a correction for dispersion.²⁸ However, the interaction energies and cooperativity were consistently greater using the APFD functional than when using the MP2 method. Upon closer inspection of the APFD functional, the dispersion between atoms directly involved in a halogen bond was absent from the interaction energy due to a short-distance cut-off, which is discussed in Appendix 5. The APFD functional was therefore concluded to be an inadequate method to use when studying the underlying energetic components of halogen bonding.

When optimized the non-bonding distances in the trimers contracted to less than the sum of the van der Waals radii (Table 5.2). The non-bonding distances within $\text{Br}_2\text{-2H}_2\text{O}$ and $\text{Br}_2\text{-2NH}_3$

were shorter than those of the independent hydrogen and halogen bonding dimers, which suggests the presence of a non-additive interaction. The bond distances in $\text{Br}_2\text{-2NH}_3$ contracted by a slightly larger magnitude than those of $\text{Br}_2\text{-2H}_2\text{O}$ when compared to their respective dimers, suggesting a greater cooperativity in $\text{Br}_2\text{-2NH}_3$. The hydrogen bond was more stabilized by the presence of the halogen bond than the halogen bond was by the hydrogen bond, in agreement with published reports,^{6,13,16} as evidenced by d_{BC} contracting more than d_{AB} in the trimer structure. Lastly, d_{AB} is shorter between bromine and ammonia in both of the trimer and dimer configurations, whereas d_{BC} is shorter between bromine and water in both of the trimer and dimer configurations. This implies that the halogen bond is larger between bromine and ammonia, but the hydrogen bond is larger between bromine and water.

Table 5.2. The sum of the van der Waals radii in comparison to the interaction distances, d_{AB} and d_{BC} , of the halogen and hydrogen bonding configurations of $\text{Br}_2\text{-2H}_2\text{O}$ and $\text{Br}_2\text{-2NH}_3$ along with the optimized halogen (AB) and hydrogen (BC) bonding dimers.

	$\Sigma r_{vdW,AB}$	$\Sigma r_{vdW,BC}$	d_{AB}^{trimer}	d_{BC}^{trimer}	d_{AB}^{dimer}	d_{BC}^{dimer}
H_2O	3.37	3.05	2.80	2.68	2.83	2.79
NH_3	3.40		2.57	2.79	2.61	2.96

The counterpoise corrected single point energies (ΔE_{MP2}) of the optimized trimers (ΔE_{ABC}^{opt}) and dimers (ΔE_{AB}^{opt} and ΔE_{BC}^{opt}) were calculated to calculate ΔE_{COOP} (Table 5.3) using Eqn. 5.1. The interaction energies of the halogen bonding and hydrogen bonding dimers, AB and BC , respectively, were also calculated at the optimized distances within the trimer (ΔE_{AB}^{sp} and ΔE_{BC}^{sp} , respectively). The halogen bonding energies in the optimized dimer configurations were found to be slightly less stable than their counterparts in the trimer configurations (ΔE_{AB}^{sp}). This should not be the case assuming that the dimer structures were successfully optimized. The unexpected instability of the optimized dimers was attributed to dissonance in the hybrid methodology, where the optimizations had utilized a less expansive method and basis set combination than the single

point calculations. The hybrid methodology was utilized in order to improve the cost efficiency of the calculations, and the differences of 0.02 and 0.18 kcal/mol for the water-containing and ammonia-containing dimers, respectively, were not considered to be so significant as to nullify the conclusions presented herein.

Table 5.3. The cooperativity and interaction energies of optimized trimer and dimer systems of bromine with two orthogonal water or ammonia molecules as illustrated in Fig. 5.4. Italics added for the single point energy calculations of the halogen and hydrogen bonding dimers set to the distances found in the optimized trimer structure.

	ΔE_{COOP} (kcal/mol)	ΔE_{ABC}^{opt} (kcal/mol)	ΔE_{AB}^{opt} (kcal/mol)	ΔE_{BC}^{opt} (kcal/mol)	ΔE_{AC}^{sp} (kcal/mol)	ΔE_{AB}^{sp} (kcal/mol)	ΔE_{BC}^{sp} (kcal/mol)
	<i>ΔE_{MP2}</i>						
H ₂ O	-0.088	-6.245	-3.922	-1.313	-0.922	<i>-3.948</i>	<i>-1.311</i>
NH ₃	-0.618	-10.604	-8.007	-1.026	-0.953	<i>-8.184</i>	<i>-0.991</i>
	<i>ΔE_{HF}</i>						
H ₂ O	0.417	-1.603	-1.278	0.165	-0.907	<i>-1.133</i>	<i>0.445</i>
NH ₃	0.395	-1.618	-1.562	0.355	-0.806	<i>-1.208</i>	<i>0.815</i>

The binding energies for the optimized structures of the trimer (ΔE_{ABC}^{opt}) were stronger for Br₂-2NH₃ at both the MP2 and HF levels (-10.604 and -1.618 kcal/mol, respectively) than for Br₂-2H₂O (-6.245 and -1.603 kcal/mol, respectively) at the MP2 level. The halogen bond between bromine and ammonia was also found to be stronger, both in the configuration of the optimized dimer and of the optimized trimer (-8.007 and -8.184 kcal/mol, respectively). However, the hydrogen bond between bromine and water was found to be stronger in the configuration of the optimized dimer than the optimized trimer (-1.313 and -1.311 kcal/mol, respectively). The strength of the hydrogen bonding configuration could be attributed to differences in the electrostatic attractions within the model trimers. Oxygen is more electronegative than nitrogen, leaving a greater partially positive electrostatic potential on the hydrogens in water compared to those on ammonia (see Fig. 5.5). This leads to a greater attraction between water and the partially negative coaxial region of bromine when compared to that between ammonia and bromine.

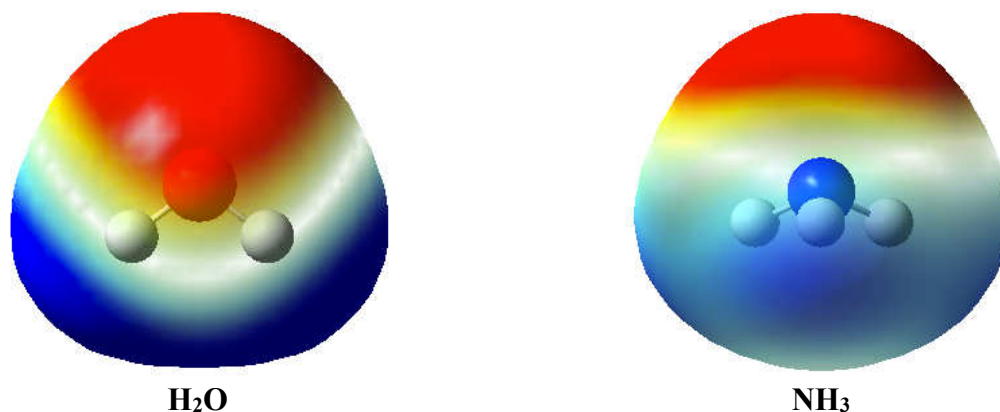


Figure 5.5. The electrostatic potential mapped onto the electron density of water (left) and ammonia (right). The hydrogen atoms covalently bound to oxygen have a greater electropositive potential than the hydrogen atoms covalently bound to nitrogen. Red represents a negative electrostatic potential (-22.0 kcal/mol) and blue represents a positive electrostatic potential (22.0 kcal/mol) between a negative point charge probe and the molecule evaluated at grid point points on the 0.0004 electron density isosurface.

A hydrogen bond in close proximity to the coaxial region of a halogen will enhance the σ -hole on the halogen, further increasing the electrostatic attraction within a model trimer.⁷ Both the ammonia- and water-containing trimer models illustrated an overall cooperative attraction at the MP2 level, -0.088 kcal/mol for $\text{Br}_2\text{-2H}_2\text{O}$ and -0.618 kcal/mol for $\text{Br}_2\text{-2NH}_3$; however, both systems illustrated an anti-cooperativity at the HF level, 0.417 kcal/mol for $\text{Br}_2\text{-2H}_2\text{O}$ and 0.395 kcal/mol for $\text{Br}_2\text{-2NH}_3$. The HF results provide a measure of the electrostatic and exchange repulsion components of the interaction energy, signifying that the non-additivity of our model trimers is not solely comprised of an electrostatic stabilization. This is not to say that a polarization enhancement of the σ -hole is not occurring on bromine, but rather that polarization enhanced electrostatics does not account for the calculated cooperativity at the MP2 level. The anti-cooperativity at the HF level can be explained by the MP2 optimized distances amplifying exchange repulsion, leading to relatively weak or even repulsive interactions. This can be seen in the weak halogen bonds between bromine and ammonia (-1.562 kcal/mol) and between bromine

and water (-1.278 kcal/mol), as well as repulsive hydrogen bonds (0.355 and 0.165 kcal/mol, respectively).

If the enhanced electrostatics cannot overcome the increased exchange repulsion in the model trimers, then one must logically conclude that energetic components not present in HF lead to the increase in stability. The difference between the MP2 and HF ΔE_{COOP} results provides a measure of the dispersive component of the non-additivity, equaling -0.505 kcal/mol for $\text{Br}_2\text{-2H}_2\text{O}$ and -1.013 kcal/mol for $\text{Br}_2\text{-2NH}_3$. However, dispersion increases as a function of decreasing interaction distance, as discussed in previous chapters; it does not lead to decreasing interaction distances. Because of the increased exchange repulsion at the short interaction distances, it must be concluded that d_{AB} and d_{BC} decreased through alternate means.

Charge Transfer in Hydrogen-Bond Enhanced Halogen Bonds

We hypothesized that the non-bonding distances contracted from those found in the optimized dimer configuration partially due to a charge transfer component in the interaction. In order to determine the relative charge transfer component, the electrostatic partial charges of the molecules in the cluster trimers (Fig. 5.6) were calculated, where a partial charge of zero suggests no charge transfer, and a partial charge of unity suggests a complete charge transfer. The partial charges of the atoms in the molecules were determined by including `pop=mk` in the command line of the input files.



Figure 5.6. The partial charges transferred in the geometrically orthogonal cluster trimers. Atomic units relative to the charge of an electron equal to -1. Arrows represent the directionality of the partial charge transfer.

The water molecule set in a halogen bonding configuration was computed to have a partial charge of 0.086. Electron density transferred to bromine, and then to the adjacent water set in a hydrogen bonding configuration. Bromine was found to have a partial charge of -0.046 and the hydrogen bonding water a partial charge of -0.040. The charge distribution across bromine and the latter water molecule is the result of oxygen being fairly electronegative and therefore capable of stabilizing a negative charge. The ammonia set in a halogen bonding had a partial charge of 0.256, which is more positive than that of the water-containing trimer, signifying a greater electron density transfer and is consistent with the greater halogen bonding interaction energy presented in Table 5.3. The electron density transferred from ammonia to bromine, and then from bromine to the adjacent ammonia set in a hydrogen bonding configuration. Bromine was found to have a partial charge of -0.245 and the hydrogen bonding ammonia a partial charge of -0.011. This result is consistent with the literature, in which the charge transfer component is reported to be larger when nitrogen is acting as the Lewis base as opposed to oxygen.²⁹⁻³¹ $\text{Br}_2\text{-}2\text{H}_2\text{O}$ was found to have a smaller magnitude of electron density transfer, which correlates to a smaller calculated cooperativity at the MP2 level. $\text{Br}_2\text{-}2\text{NH}_3$ was found to have a larger magnitude of charge transfer, which correlates to a larger calculated cooperativity at the MP2 level.

These results provide preliminary evidence that charge transfer interactions contribute to the non-additivity of model trimers. As the charge transfer component increases in a trimer, the

interaction distances are seen to decrease. This decrease in the bond distance is what proportionally leads to the increase in dispersion, and apparent dispersive cooperativity. An additional set of cluster trimers was designed to further test this correlation, where the halogen and hydrogen bonding molecules were placed on adjacent bromines in Br₂ (Fig. 5.7). The second set of trimer configurations will be referred to herein as β -trimers.

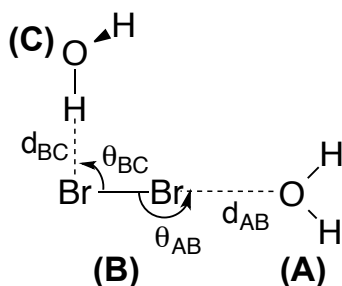


Figure 5.7. An illustration of the water-containing β -trimer system (β -Br₂-2H₂O), where *A* is the halogen bonding water molecule, *B* is bromine, and *C* is the hydrogen bonding water molecule adjacent to the halogen bond. The ammonia-containing trimer system ($(\beta$ -Br₂-2NH₃) was similarly constructed.

The energy of the β -trimers was calculated using a hybrid method, notated MP2/aug-cc-pVTZ//MP2/aug-cc-pV5Z. The interaction distances were allowed to minimize during optimization, and θ_{AB} and θ_{BC} were constrained to 180° and 90°, respectively. The interaction d_{AB} minimized to 2.79 Å and d_{BC} to 2.73 Å in the water-containing β -trimer structure, a decrease when compared to the previous trimer. This suggests an increase in the stability of the β -trimer. The non-bonding d_{AB} minimized to 2.56 Å and d_{BC} to 2.90 Å in the ammonia-containing β -trimer structure, an increase of the latter compared to the previous trimer. This suggests that the halogen bond remained as stable but the hydrogen bond in the trimer decreased in stability.

The counterpoise corrected single point energies of the optimized β -trimers and dimers were calculated (Table 5.4). Each of the β -trimer optimized energies (ΔE_{ABC}^{opt}) were found to be less than that of their previous counterparts. This was hypothesized to be due to the increased distance

between model solvent molecules in β -Br₂-2H₂O and β -Br₂-2NH₃, leading to a slight decrease in the stabilizing van der Waals interactions within the β -trimers. Additional implications of the increased distance between solvent molecules will be discussed below. The binding energy of β -Br₂-2NH₃ was found to be larger than that of β -Br₂-2H₂O (-9.937 and -5.592 kcal/mol, respectively) at the MP2 level, though not at the HF level (-1.391 and -1.464 kcal/mol, respectively). This suggests a slightly greater electrostatic component in β -Br₂-2H₂O when compared to the previous Br₂-2H₂O trimer, which can be attributed to an increase in the hydrogen-bond enhanced polarization of bromine, as suggested by Carlsson et al. in a recent publication (Ref. 7; Fig. 7). The increased polarization of bromine would lead to an increase in the σ -hole, strengthening the electrostatic interactions within β -Br₂-2H₂O measured at the HF level.

Table 5.4. The cooperativity and interaction energies of optimized β -trimer and dimer systems of bromine with two orthogonal water and ammonia molecules. Italics added to the single point energy calculations of the halogen and hydrogen bonding dimers set to the distances found in the optimized trimer structure.

	ΔE_{COOP} (kcal/mol)	ΔE_{ABC}^{opt} (kcal/mol)	ΔE_{AB}^{opt} (kcal/mol)	ΔE_{BC}^{opt} (kcal/mol)	ΔE_{AC}^{sp} (kcal/mol)	ΔE_{AB}^{sp} (kcal/mol)	ΔE_{BC}^{sp} (kcal/mol)
<i>ΔE_{MP2}</i>							
H ₂ O	-0.105	-5.592	-3.922	-1.312	-0.253	-3.956	-1.322
NH ₃	-0.967	-9.937	-8.008	-0.856	-0.106	-8.202	-0.855
<i>ΔE_{HF}</i>							
H ₂ O	-0.075	-1.464	-1.280	0.163	-0.272	-1.067	0.300
NH ₃	-0.136	-1.391	-1.561	0.388	-0.082	-1.172	0.609

The binding energy of the halogen bond between bromine and ammonia was found to be larger at the MP2 level (-8.008 kcal/mol) and at the HF level (-1.561 kcal/mol), consistent with previous trimer configurations and the literature.²⁹⁻³¹ The binding energy of the hydrogen bond between bromine and water was larger at the MP2 (-1.312 kcal/mol) and HF level (0.163 kcal/mol), consistent with the electrostatic potential argument above. Because the optimized MP2 trimer and

dimer binding energies were consistently larger than the HF results, dispersion was concluded to be present and a stabilizing energetic component as well.

Both systems were found to have a cooperative attraction, -0.105 kcal/mol for $\beta\text{-Br}_2\text{-2H}_2\text{O}$ and -0.967 kcal/mol for $\beta\text{-Br}_2\text{-2NH}_3$, a slight increase from the original trimer configurations. A cooperative attraction was also calculated at the HF level for the water- and ammonia-containing β -trimers (-0.075 and -0.136 kcal/mol, respectively). The optimized halogen and hydrogen bonding dimer energies were found to be approximately equal to those previously calculated at the HF level, suggesting little change in the electrostatic and exchange repulsion components of the interaction. The cooperativity at the HF level was therefore concluded to be due to the increased distance between model solvent molecules in $\beta\text{-Br}_2\text{-2H}_2\text{O}$ and $\beta\text{-Br}_2\text{-2NH}_3$, which led to a decrease in the magnitude of ΔE_{AC}^{SP} . The difference between the MP2 and HF ΔE_{COOP} results provides a measure of the dispersive component of the non-additivity, equaling -0.030 kcal/mol for $\beta\text{-Br}_2\text{-2H}_2\text{O}$ and -0.831 kcal/mol for $\beta\text{-Br}_2\text{-2NH}_3$, a decrease when compared to the previous trimers.

To determine the relative charge transfer component, the electrostatic partial charges of the molecules in the optimized β -trimers (Fig. 5.8) were calculated. The halogen bonding water molecule in $\beta\text{-Br}_2\text{-2H}_2\text{O}$ had a partial charge of 0.099, bromine had a partial charge of -0.053, and the hydrogen bonding water molecule had a partial charge of -0.046. Compared to the previous trimer system, the magnitude of the electron transfer increased slightly between all molecules in the β -trimer, which resulted from a resonant partial charge transfer from water to bromine, and from bromine to water. The halogen bonding ammonia molecule in $\beta\text{-Br}_2\text{-2NH}_3$ had a partial charge equal to 0.234, bromine had a partial charge equal to -0.217, and the hydrogen bonding ammonia molecule had a partial charge equal to -0.016. Compared to the previous trimer system, the magnitude of the electron density transfer between the halogen bonding molecules decreased

slightly, but that between the hydrogen bonding molecules increased slightly. Overall, the electron density transferred between the halogen bonding molecules in $\beta\text{-Br}_2\text{-2NH}_3$ is still larger than that of $\beta\text{-Br}_2\text{-2H}_2\text{O}$, and the increased charge transfer to the hydrogen bonding ammonia molecule can be hypothesized to lead to an increase in overall stability of the β -trimer.

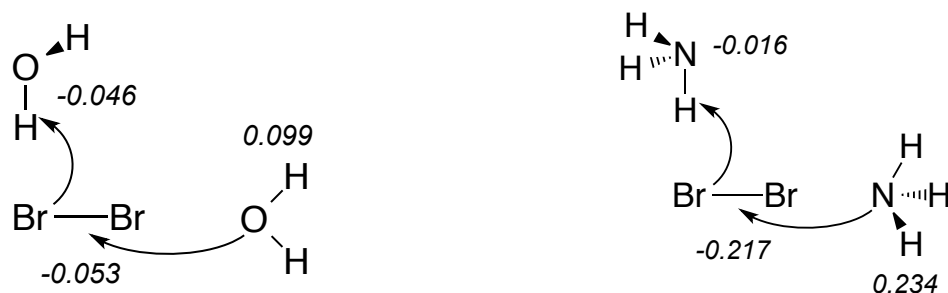


Figure 5.8. The partial charges transferred in the geometrically orthogonal β -trimers. Atomic units relative to the charge of an electron equal to -1. Arrows represent where the atom where the charge is coming from, and where it is transferring to.

Both β -trimers demonstrated an increase of charge transfer throughout the system compared to the previous trimers, ending with a negative partial charge on the hydrogen bonding model solvent molecule. The hydrogen bonding water molecule was able to stabilize a greater negative charge due to the increased electronegativity of oxygen, though ammonia was capable of a greater charge transfer when halogen bonding with bromine. The overall increase in charge transfer correlated to the increase in the cooperativity of the β -trimers. To be clear, these underlying interactions are not explicitly observables of the system, but are instead being used to understand and explain the cooperativity found in multi-molecular halogen bonding structures.

Distinguishing the Electron Correlation

In the interest of understanding more exactly how the dispersion contributed to non-additivity, the components of the electron correlation were explicitly calculated. Electron correlation can be estimated by subtracting HF from MP2 binding energies because the MP2

method³² incorporates a second order perturbation that accounts for electron correlation (ΔE_{MP2}^{corr}),^{32,33} a combination singlet (ΔE_{MP2}^S) and triplet components (ΔE_{MP2}^T) (Eqn. 5.2).

$$\Delta E_{MP2}^{corr} = \Delta E_{MP2} - \Delta E_{HF} = \Delta E_{MP2}^S + \Delta E_{MP2}^T \quad (5.2)$$

The singlet component (Eqn. 5.3) is dominantly short-range attraction caused by a stabilizing interaction between electrons of opposite spin.

$$\Delta E_{MP2}^S = \Delta E_{MP2}^{\alpha\beta} - \frac{1}{2}(\Delta E_{MP2}^{\alpha\alpha} + \Delta E_{MP2}^{\beta\beta}) \quad (5.3)$$

The triplet component (Eqn. 5.4) is a long-range attraction caused by a stabilizing interaction between two electrons of the same spin.

$$\Delta E_{MP2}^T = \frac{3}{2}(\Delta E_{MP2}^{\alpha\alpha} + \Delta E_{MP2}^{\beta\beta}) \quad (5.4)$$

The attraction found in ΔE_{MP2}^T may be somewhat counterintuitive as electrons of the same spin are often considered to behave repulsively, but the triplet component represents the dispersive correlation between atoms.

The singlet and triplet components of electron correlation for the model trimer structures were calculated using $\Delta E_{MP2}^{\alpha\alpha}$, $\Delta E_{MP2}^{\beta\beta}$, and $\Delta E_{MP2}^{\alpha\beta}$ found in the MP2 output file (Table 5.5). Electron correlation was found to be primarily comprised of the triplet component for the optimized trimers and dimers, as well as the single point calculation between water and ammonia molecules. Therefore, the electron correlation component, analogous to dispersion discussed above, is primarily dependent on ΔE_{MP2}^T . For example, ΔE_{COOP} and ΔE_{ABC}^{opt} of the ammonia-containing model trimer were -0.618 and -10.604 kcal/mol at the MP2 level, respectively. The electron correlation energy of the model trimer (-8.985 kcal/mol) was predominantly comprised

of dispersive correlation (-6.922 kcal/mol). These results can be compared to the water-containing model trimer, where ΔE_{COOP} and ΔE_{ABC}^{opt} were -0.088 and -6.245 kcal/mol, respectively, and had a weaker electron correlation (-4.642 kcal/mol) due to a weaker dispersive correlation (-3.650 kcal/mol). The magnitudes of the electron correlation components presented herein were correlated to the relative strengths of the binding energies presented in Table 5.3.

Table 5.5. The electron correlation (ΔE_{MP2}^{corr}) of the original cluster trimer systems, comprised of singlet (ΔE_{MP2}^S) and triplet (ΔE_{MP2}^T) energetic components.

	ΔE_{ABC}^{opt} (kcal/mol)	ΔE_{AB}^{opt} (kcal/mol)	ΔE_{BC}^{opt} (kcal/mol)	ΔE_{AC}^{sp} (kcal/mol)
	ΔE_{MP2}^{corr}			
H ₂ O	-4.642	-2.644	-1.478	-0.015
NH ₃	-8.985	-6.445	-1.382	-0.148
	ΔE_{MP2}^S			
H ₂ O	-0.992	-0.521	-0.369	0.032
NH ₃	-2.063	-1.438	-0.358	-0.018
	ΔE_{MP2}^T			
H ₂ O	-3.650	-2.123	-1.109	-0.047
NH ₃	-6.922	-5.008	-1.024	-0.130

The electron correlation calculations of the β -trimers approximately equaled those of the original trimers, which can be found in Appendix 6. This suggests that the changes in the interaction energies discussed above were caused by the alteration of either the electrostatics or charge transfer, in agreement with the conclusions drawn above.

The energetic non-additivity was estimated by using the cooperativity of model trimer systems, bromine with two water or ammonia molecules. Evidence supports the notion that trimers are stabilized by a combination of electrostatics, exchange repulsion, dispersion, and charge transfer, where dispersion was discussed in terms of electron correlation and charge transfer in terms of partial charges. The charge transfer component was reasoned to result in a trimer system containing shorter bond distances than in the respective dimers, increasing the non-bonding dispersive interactions and the non-additivity as calculated using cooperativity (ΔE_{COOP}). The

research presented here are our preliminary results on the charge transfer component of halogen bonding models, which will be further discussed in Chapter 6.

REFERENCES

- (1) Alkorta, I.; Blanco, F.; Deyà, P. M.; Elguero, J.; Estarellas, C.; Frontera, A.; Quiñero, D. Cooperativity in Multiple Unusual Weak Bonds. *Theor. Chem. Acc.* **2010**, *126*, 1–14.
- (2) Solimannejad, M.; Malekani, M.; Alkorta, I. Substituent Effects on the Cooperativity of Halogen Bonding. *J. Phys. Chem. A* **2013**, *117*, 5551–5557.
- (3) Lu, Y.; Li, H.; Zhu, X.; Zhu, W.; Liu, H. How Does Halogen Bonding Behave in Solution? A Theoretical Study Using Implicit Solvation Model. *J. Phys. Chem. A* **2011**, *115*, 4467–4475.
- (4) Sarwar, M. G.; Dragisic, B.; Salsberg, L. J.; Gouliaras, C.; Taylor, M. S. Thermodynamics of Halogen Bonding in Solution: Substituent, Structural, and Solvent Effects. *J. Am. Chem. Soc.* **2010**, *132*, 1646–1653.
- (5) Geballe, M. T.; Skillman, A. G.; Nicholls, A.; Guthrie, J. P.; Taylor, P. J. The SAMPL2 Blind Prediction Challenge: Introduction and Overview. *J. Comput. Aided Mol. Des.* **2010**, *24*, 259–279.
- (6) Voth, A. R.; Khuu, P.; Oishi, K.; Ho, P. S. Halogen Bonds as Orthogonal Molecular Interactions to Hydrogen Bonds. *Nat. Chem.* **2009**, *1*, 74–79.
- (7) Carlsson, A.-C. C.; Scholfield, M. R.; Rowe, R. K.; Ford, M. C.; Alexander, A. T.; Mehl, R. A.; Ho, P. S. Increasing Enzyme Stability and Activity through Hydrogen Bond-Enhanced Halogen Bonds. *Biochemistry* **2018**, *57*, 4135–4147.
- (8) Riel, A. M. S.; Decato, D. A.; Sun, J.; Massena, C. J.; Jessop, M. J.; Berryman, O. B. The Intramolecular Hydrogen Bonded–Halogen Bond: A New Strategy for Preorganization and Enhanced Binding. *Chem. Sci.* **2018**, *9*, 5828–5836.
- (9) Grabowski, S. J. Cooperativity of Hydrogen and Halogen Bond Interactions. *Theor. Chem. Acc.* **2013**, *132*, 1347.
- (10) George, J.; Deringer, V. L.; Dronskowski, R. Cooperativity of Halogen, Chalcogen, and Pnictogen Bonds in Infinite Molecular Chains by Electronic Structure Theory. *J. Phys. Chem. A* **2014**, *118*, 3193–3200.
- (11) Albrecht, L.; Boyd, R. J.; Mó, O.; Yáñez, M. Changing Weak Halogen Bonds into Strong Ones through Cooperativity with Beryllium Bonds. *J. Phys. Chem. A* **2014**, *118*, 4205–4213.
- (12) Esrafilí, M. D.; Vakili, M. Halogen Bonds Enhanced by σ -Hole and π -Hole Interactions: A Comparative Study on Cooperativity and Competition Effects Between $X\cdots N$ and $S\cdots N$ Interactions in $H_3N\cdots XCN\cdots SF_2$ and $H_3N\cdots XCN\cdots SO_2$ Complexes ($X = F, Cl, Br$ and I). *J. Mol. Model.* **2014**, *20*, 2291.
- (13) Esrafilí, M. D.; Mohammadian-Sabet, F. Halogen-Bond Interactions Enhanced by Charge-Assisted Hydrogen Bonds: An Ab Initio Study. *Bull. Chem. Soc. Jpn.* **2014**, *87*, 882–889.
- (14) Vatanparast, M. Cooperativity Between the Halogen Bonding and Halogen–Hydride Bonding in $NCX\cdots NCX\cdots HMgY$ Complexes ($X=F, Cl, Br$; $Y=H, F, Cl, Br, CH_3, Li$). *Comput. Theor. Chem.* **2014**, *1048*, 77–83.
- (15) Han, N.; Zeng, Y.; Sun, C.; Li, X.; Sun, Z.; Meng, L. $N\cdots I$ Halogen Bonding Interactions: Influence of Lewis Bases on Their Strength and Characters. *J. Phys. Chem. A* **2014**, *118*, 7058–7065.
- (16) Ji, J.; Meng, D.; Zhang, X.; Meng, L.; Zeng, Y. Enhancing Effects of Hydrogen/Halogen Bonds on σ -Hole Interactions Involving Ylide. *J. Mol. Model.* **2014**, *20*, 2282.
- (17) Dominikowska, J.; Palusiak, M. Halogen–Halogen Interaction in View of Many-Body Approach. *Chem. Phys. Lett.* **2013**, *583*, 8–13.
- (18) Mulliken, R. S. Structures of Complexes Formed by Halogen Molecules with Aromatic and with Oxygenated Solvents ¹. *J. Am. Chem. Soc.* **1950**, *72*, 600–608.
- (19) Auffinger, P.; Hays, F. A.; Westhof, E.; Ho, P. S. Halogen Bonds in Biological Molecules. *Proc. Natl. Acad. Sci.* **2004**, *101*, 16789–16794.
- (20) Riley, K. E.; Murray, J. S.; Politzer, P.; Concha, M. C.; Hobza, P. $Br\cdots O$ Complexes as Probes of Factors Affecting Halogen Bonding: Interactions of Bromobenzenes and Bromopyrimidines with Acetone. *J. Chem. Theory Comput.* **2009**, *5*, 155–163.

- (21) Albrecht, L.; Boyd, R. J. Visualizing Internal Stabilization in Weakly Bound Systems Using Atomic Energies: Hydrogen Bonding in Small Water Clusters. *J. Phys. Chem. A* **2012**, *116*, 3946–3951.
- (22) Cook, J. L.; Hunter, C. A.; Low, C. M. R.; Perez-Velasco, A.; Vinter, J. G. Solvent Effects on Hydrogen Bonding. *Angew. Chem. Int. Ed.* **2007**, *46*, 3706–3709.
- (23) Solimannejad, M.; Ramezani, V.; Trujillo, C.; Alkorta, I.; Sánchez-Sanz, G.; Elguero, J. Competition and Interplay between σ -Hole and π -Hole Interactions: A Computational Study of 1:1 and 1:2 Complexes of Nitryl Halides (O_2NX) with Ammonia. *J. Phys. Chem. A* **2012**, *116*, 5199–5206.
- (24) Adhikari, U.; Scheiner, S. Comparison of P \cdots D (D = P,N) with Other Noncovalent Bonds in Molecular Aggregates. *J. Chem. Phys.* **2011**, *135*, 184306.
- (25) Mohan, N.; Suresh, C. H. Accurate Binding Energies of Hydrogen, Halogen, and Dihydrogen Bonded Complexes and Cation Enhanced Binding Strengths. *Int. J. Quantum Chem.* **2014**, *114*, 885–894.
- (26) Woon, D. E.; Dunning, T. H. Gaussian Basis Sets for Use in Correlated Molecular Calculations. IV. Calculation of Static Electrical Response Properties. *J. Chem. Phys.* **1994**, *100*, 2975–2988.
- (27) Boys, S. F.; Bernardi, F. The Calculation of Small Molecular Interactions by the Differences of Separate Total Energies. Some Procedures with Reduced Errors. *Mol. Phys.* **1970**, *19*, 553–566.
- (28) Austin, A.; Petersson, G. A.; Frisch, M. J.; Dobek, F. J.; Scalmani, G.; Throssell, K. A Density Functional with Spherical Atom Dispersion Terms. *J. Chem. Theory Comput.* **2012**, *8*, 4989–5007.
- (29) Wang, C.; Danovich, D.; Mo, Y.; Shaik, S. On The Nature of the Halogen Bond. *J. Chem. Theory Comput.* **2014**, *10*, 3726–3737.
- (30) Amezaga, N. J. M.; Pamies, S. C.; Peruchena, N. M.; Sosa, G. L. Halogen Bonding: A Study Based on the Electronic Charge Density. *J. Phys. Chem. A* **2010**, *114*, 552–562.
- (31) Karpfen, A. Charge-Transfer Complexes between NH_3 and the Halogens F_2 , ClF , and Cl_2 : An Ab Initio Study on the Intermolecular Interaction. *J. Phys. Chem. A* **2000**, *104*, 6871–6879.
- (32) Møller, C.; Plesset, M. S. Note on an Approximation Treatment for Many-Electron Systems. *Phys. Rev.* **1934**, *46*, 618–622.
- (33) Martin, J. M. What Can We Learn about Dispersion from the Conformer Surface of N-Pentane? *J. Phys. Chem. A* **2013**, *117*, 3118–3132.

CHAPTER 6: MODEL HALOGEN BONDING VIA CHARGE TRANSFER

Halogen bonding can be used in place of hydrogen bonding found in biomolecular structures when designing novel medications with specific interaction distances, angles, and strengths.¹⁻⁸ Understanding the dependence of the underlying energetic components as a function of distance and angle is necessary to accurately predict the energy of biomolecular systems. The electrostatic component of halogen bonding has been at the forefront of most theoretical models since early 21st century. Novel electrostatic terms implemented into published force fields have incorrectly reproduced experimental energies found in halogen bonding structures.^{9,10} For example, M. A. A. Ibrahim calculated the non-bonding energies of halobenzene-formaldehyde dimers using both AMBER-PEP and MP2/aug-cc-pVDZ.⁵ The magnitude of root mean square difference between Ibrahim's calculations suggest that AMBER-PEP is capable of roughly predicting the dimer energy, but halogen bonding is dependent on more than one underlying energetic component. The purpose of using a model is to predict the real behavior of a system; if a model leads to incorrect energetics, then the real behavior can neither be predicted nor applied to the selective synthesis of novel medications.

Halogen bonding was called a "charge transfer bond" by Hassel et al.^{11,12} in reference to work done by R. S. Mulliken.¹³ Mulliken used spectroscopic methods in 1950 to study the electronic structure of a halogen molecule interacting with a Lewis base, and predict the geometry of the interaction. Specifically, he demonstrated that dissolving iodine in an aromatic solvent, such as benzene, toluene, and xylene, in a 1:1 molar ratio caused a color change from an initially purple solution to a brown solution.^{14,15} Mulliken concluded that the color change signified the presence of a charge transfer complex (Ar^+I_2^-), and proposed the electronic structure of the complex (Fig. 6.1) using molecular orbital theory.

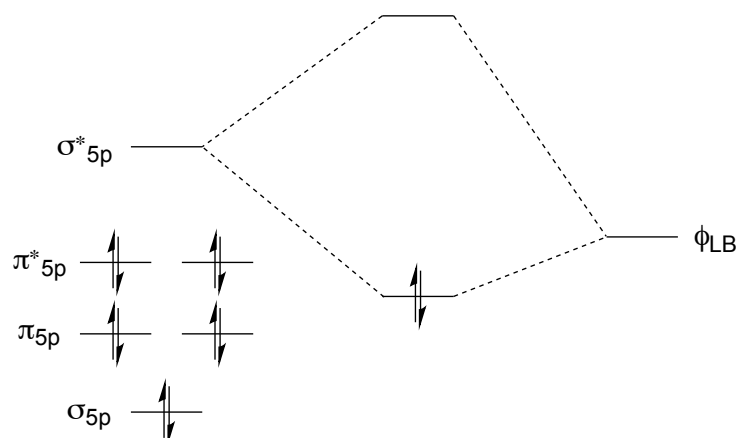


Figure 6.1. The mixing of the lowest unoccupied molecular orbital and highest occupied molecular orbital of a Lewis acid-base pair of iodine and an aromatic molecule, respectively, resulting in a charge transfer of the lone pair.

The general electronic structure proposed by Mulliken (Fig. 6.2) was supported by the presence of a strong absorption peak in the UV range near 3000 nm that had not been previously seen in spectrum for iodine, nor the aromatic solvents. The absorption peak was attributed to the broken symmetry of the molecular structures caused by orbital combination.¹¹⁻¹³

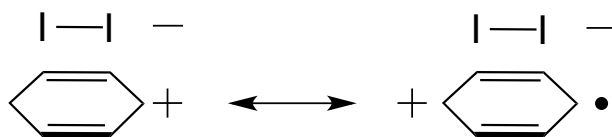


Figure 6.2. The predicted resonance geometries of an aromatic derivative in close contact with iodine, stabilized by charge transfer (adapted from *J. Am. Chem. Soc.* **1950**, 72, 600).

Interest in describing halogen bonding is shifting away from a solely electrostatic σ -hole model and returning to one that incorporates charge transfer.¹⁷ We developed a novel potential term that calculates the interaction energy of a halogen bonding structure as a function of charge transfer. To our knowledge, a similar charge transfer potential term has not been published in the literature.^{16,18,19}

Model Charge Transfer Between Borane and Ammonia

The goal of this research was to provide a fundamental explanation for the distance dependent process of charge transfer in halogen bonding. Previously developed models, such as the APT force field,²⁰ were referenced to develop a model that approximated halogen bonding strength as a function of charge transfer, dependent on the electronic structure of the reactant molecules in contrast to the charge transfer complex.²¹⁻²³ A simple “2-centre, 2-electron” charge transfer model of borane and ammonia was developed for ease of derivation. NH_3 interacts with BH_3 at close distances (Fig. 6.3), forming $\text{NH}_3^+\text{BH}_3^-$. Terms such as the ionization potential of ammonia, the electron affinity of borane, the electrostatics of the transferred electron, and a covalent bond between boron and nitrogen were incorporated into the model.^{11,21} A second charge transfer model for a, “3-centre, 4-electron” halogen bonding complex formed by bromine and ammonia was then developed, which will be discussed in the following section.

The MP2 method with an aug-cc-pvTZ basis set was used to calculate halogen bonding interaction energies, and establish the relative magnitude of the charge transfer component for two Lewis acid-base pairs. The potential term was visually matched to the interaction energy of borane and ammonia calculated at the MP2 level as a function of distance (r_{AB}).

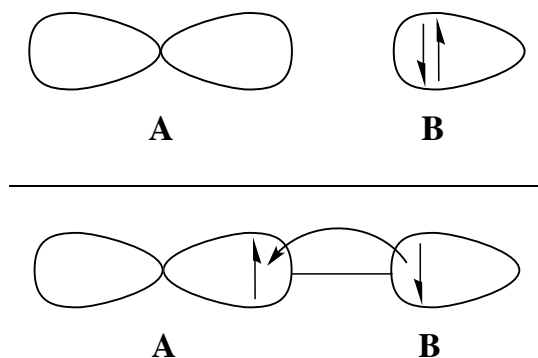


Figure 6.3. An illustration of the borane and ammonia reactant model (top) and the product model (bottom). The Lewis acid (*A*) was modeled using BH_3 and the Lewis base (*B*) was modeled using NH_3 .

The charge transfer potential model presented herein was based on the original charge transfer proposal by Mulliken,¹³ except that our model was developed using a valence bond theory model²⁴ instead of molecular orbital theory.^{13,23} The charge transfer complex was defined by two wavefunctions, a reactant wavefunction (Ψ_1) and a product wavefunction (Ψ_2). Ψ_1 consisted of the electron pair on NH_3 before the charge had transferred, and Ψ_2 consisted of a model after the charge had transferred, resulting in a weak bond between BH_3 and NH_3 . The total wavefunction (Ψ) was then defined by a linear combination of Ψ_1 and Ψ_2 (Eqn. 6.1).

$$\Psi = c_1\Psi_1 + c_2\Psi_2 \quad (6.1)$$

The resulting energy (ΔE_{CT}) of the model (Eqn. 6.2) was given by the expectation value of the Hamiltonian (\hat{H}), rearranged such that ΔE_{CT} was solved for.

$$\Delta E_{CT}\langle\Psi|\Psi\rangle = \langle\Psi|\hat{H}|\Psi\rangle \quad (6.2)$$

The energy expression of the charge transfer was derived by inserting the total wavefunction from Eqn. 6.1 into Eqn. 6.2. The left side of Eqn 6.2 was expanded (Eqn. 6.3), where \mathbf{P} was equal to twice the overlap of the reactant and product cases, $2\mathbf{S}_{12}$.

$$\Delta E_{CT}\langle\Psi|\Psi\rangle = \Delta E_{CT}(c_1^2 + 2c_1c_2\mathbf{P} + c_2^2) \quad (6.3)$$

The right side of Eqn. 6.2 was also expanded (Eqn. 6.4). ΔE_{CT} was solved for by taking the partial derivative of the expression dependent on constants, c_1 and c_2 and arranged the results in a matrix to find the determinant of the derivatives.

$$\langle\Psi|\hat{H}|\Psi\rangle = c_1^2H_{11} + 2c_1c_2H_{12} + c_2^2H_{22} \quad (6.4)$$

The energy of the charge transfer was found to be dependent on the Hamiltonian terms, H_{11} , H_{22} , and H_{12} , equal to the energies associated with the reactant, product, and cross term models of $\text{NH}_3^+\text{BH}_3^-$ respectively. Potential expressions were assigned to the Hamiltonian terms based on the interactions present in the model to approximate ΔE_{CT} . For example, H_{11} corresponded to an electronic structure where no charge had transferred yet from ammonia to borane, and was therefore approximated using a van der Waals potential (Eqn. 6.5) as a function of r_{AB} , where ε was equal to the energy at the bottom of the well and ρ the corresponding bond distance.²⁵

$$H_{11} = \varepsilon \left(\left(\frac{\rho}{r_{AB}} \right)^{12} - 2 \left(\frac{\rho}{r_{AB}} \right)^6 \right) \quad (6.5)$$

H_{22} corresponded to a system where the charge had been completely transferred from ammonia to borane (Eqn. 6.6).

$$H_{22} = -EA_{\text{BH}_3} + IP_{\text{NH}_3} + V_{\text{BB}} + V_{\text{AB}} \quad (6.6)$$

The energy of the product model was approximated using the electron affinity of borane (EA_{BH_3})^{26,27} and the ionization potential of ammonia (IP_{NH_3}).²⁸ A one-electron potential energy term, V_{BB} (Eqn. 6.7),²⁹ was used to calculate the attraction of the transferred electron to the nitrogen nucleus as a function of r_{AB} .

$$V_{\text{BB}} = \xi \left(e^{-2\xi r_{AB}} + \frac{e^{-2\xi r_{AB}} - 1}{r_{AB}} \right) \quad (6.7)$$

A Morse potential, V_{AB} (Eqn. 6.8), was used to approximate the covalent bond contribution to the energy of the bond between B and N in $\text{NH}_3^+\text{BH}_3^-$.³⁰⁻³²

$$V_{\text{AB}} = D_e \left(e^{-2\sqrt{\frac{k_e}{2D_e}}(r_{AB}-r_e)} - 2e^{-\sqrt{\frac{k_e}{2D_e}}(r_{AB}-r_e)} \right) \quad (6.8)$$

D_e corresponded to the energy at equilibrium, r_e to the equilibrium bond distance, and k_e to the force constant at equilibrium in Eqn. 6.8.³²

Values for the terms in Equations 6.5–6.8 (Table 6.1) were found in the literature.^{21,25–28,32} While adjusting the Slater exponent (ζ) of the model to visually match the calculated interaction energy between BH_3 and NH_3 at the MP2/aug-cc-pVTZ level, r_e was increased from 1.54 Å and k_e was decreased from 633 kcal/mol Å².³² The alteration of these variables signifies that the covalent bond between boron and nitrogen in a charge transfer complex is longer than that of a conventional covalent bond, and the spring constant weaker.

Table 6.1. The H_{11} , H_{22} , and H_{12} parameters for the model $\text{NH}_3^+\text{BH}_3^-$ charge transfer potential described using Equations 6.5–6.8.

BH₃—NH₃							
ε (kcal/mol)	ρ (Å)	EA_{BH_3} (kcal/mol)	IP_{NH_3} (kcal/mol)	ζ (Bohr ⁻¹)	D_e (kcal/mol)	r_e (Å)	k_e (kcal/mol Å ²)
0.125	3.00	-1.38	233	0.920	85	1.73	450

H_{12} (Eqn. 6.9) corresponded to the resonance cross term of H_{11} and H_{22} and was approximated using an expression that had been previously derived in the APT force field for a “3-centre, 2-electron” system.²⁰

$$H_{12} = \frac{V_{\text{AB}}}{\mathcal{S}_{\text{AB}} + 1} \quad (6.9)$$

The orbital overlap, \mathcal{S} (Eqn. 6.10),^{25,33} between two wavefunctions was defined as a function of ζ and r_{AB} . The Slater exponent (ζ) in Eqn. 6.10, equal to that of Eqn. 6.7, was varied to visually match the slopes of the repulsive wall and energetic well, respectively.

$$\mathcal{S}_{\text{AB}} = e^{-\zeta r_{\text{AB}}} \left(1 + \zeta r_{\text{AB}} + \frac{1}{3} (\zeta r_{\text{AB}})^2 \right) \quad (6.10)$$

The charge transfer model was visually matched to calculations at the MP2 level (Fig. 6.4), and provided an explanation for how the Lewis acid-base pair attracted and settled to its optimized bond distance. The energy of H_{11} resulted in a mostly repulsive curve shaped according to the van der Waals parameters of Eqn. 6.5. H_{22} resulted in a curve shaped according to the parameters of Eqn. 6.6, where ζ shifted the location of the repulsive wall and energetic well. An energetic minimum was found at 1.50 Å that transitioned quickly into an unfavorable interaction with increasing r_{AB} due to the ionization potential of NH_3 . H_{12} resulted in a curve shaped according to the overlap and bonding parameters of Eqn. 6.9, where ζ adjusted the slope of the repulsive wall and energetic well. An energetic minimum was found at 1.80 Å that countered the ionization potential at long distance and led to a smooth ΔE_{CT} , tending toward zero kcal/mol at infinite distance. The difference in the location of the energetic wells of H_{22} and H_{12} signified that the overlap within the cross term initially attracted the ammonia to borane at long distance, and then the exchange present in the form of a covalent bond stabilized the Lewis acid-base pair at short distance.

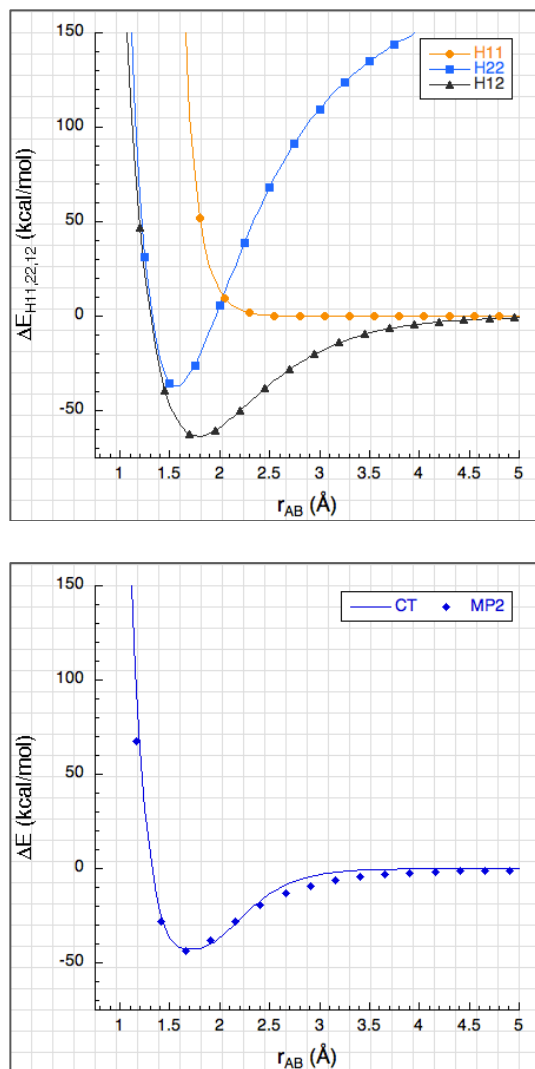


Figure 6.4. The $\text{NH}_3^+\text{BH}_3^-$ charge transfer H_{11} , H_{22} , and H_{12} components (top) and the MP2 and model charge transfer energies (bottom) as a function of r_{AB} . The charge transfer model results are seen to visually match those calculated at the MP2 level as a function of distance.

Model Charge Transfer Between Bromine and Ammonia

The non-additivity of model halogen bonding trimers was demonstrated in Chapter 5 to be in part due to the charge transfer present in the system, particularly from the lone pair of ammonia to bromine. This Lewis acid-base pair was therefore chosen to initially model the charge transfer within a halogen bonding dimer; nitrogen-containing electron donors have been found to increase the strength of the charge transfer component.^{34,35} The charge transfer potential term was modified to calculate the ΔE_{CT} of the “3-centre, 4-electron” model, where the charge from ammonia

transferred to bromine (Fig. 6.5), forming $\text{NH}_3^+\text{Br}_2^-$. The charge transfer within the complex occurred according to a valence bond resonance model as a function of distance (r_{BC}).

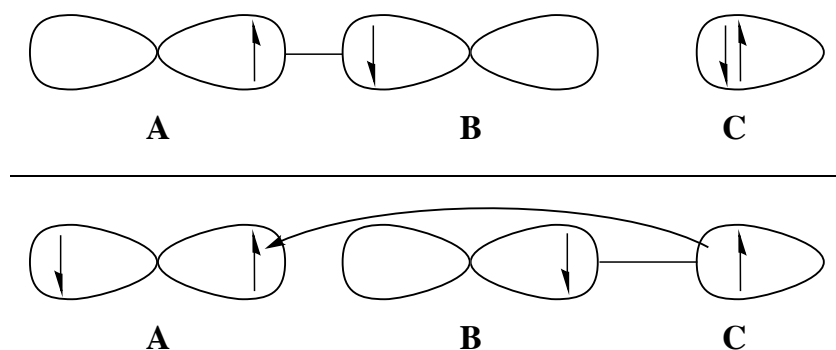


Figure 6.5. An illustration of the bromine and ammonia reactant model (top) and the product model (bottom). The Lewis acid (*A* and *B*) was modeled using Br_2 and the Lewis base (*C*) modeled using NH_3 .

The charge transfer model was defined using a reactant wavefunction (Ψ_1) and product wavefunction (Ψ_2) (Eqn. 6.11 and 6.12, respectively) modified to represent diatomic bromine in close contact with ammonia. Ψ_1 represented the covalent bond within Br_2 and the electron pair on NH_3 . Ψ_2 represented the transfer of charge to bromine, resulting in an electron pair on bromine (*A*) and a bond between bromine (*B*) and ammonia (*C*).

$$\Psi_1 = (\phi_A\phi_B + \phi_B\phi_A)\phi_C\phi_C \quad (6.11)$$

$$\Psi_2 = \phi_A\phi_A(\phi_B\phi_C + \phi_C\phi_B) \quad (6.12)$$

The total wavefunction was then defined by a linear combination of Ψ_1 and Ψ_2 , like that presented in Eqn. 6.1. The derivation of the expectation value of the Hamiltonian (\hat{H}) resulted in the same final energy expression written in Eqn. 6.3 and Eqn. 6.4, except that \mathbf{P} was found to equal a more complex product of overlaps (Eqn. 6.13).

$$\mathbf{P} = 4\mathbf{S}_{AB}\mathbf{S}_{BC} \quad (6.13)$$

The Hamiltonian terms, H_{11} , H_{22} , and H_{12} , corresponding to the energy of the reactant, product, and resonance cross term models of $\text{NH}_3^+\text{Br}_2^-$ respectively, were assigned energetic approximations similar to those in the “2-centre, 2-electron” model. H_{11} corresponded to the energy of Ψ_1 , where the electron had not yet transferred. The interaction was approximated using a van der Waals potential,²⁵ where ε was equal to the energy at the bottom of the well and ρ the corresponding bond distance. The H_{22} term corresponded to the energy of Ψ_2 , where the electron had been completely transferred (Eqn. 6.14) to form $\text{NH}_3^+\text{Br}_2^-$. The energy of the product model was approximated using the electron affinity of bromine (EA_{Br_2})³⁶ and the ionization potential of ammonia (IP_{NH_3}).²⁸ V_{CC} was an approximation of the attraction of the transferred electron to the positive nucleus in ammonia, written using Eqn. 6.7. Two potentials³⁰ were included to approximate the energy of the covalent bonds, written using the Morse potentials in Eqn. 6.8. The negative sign of V_{AB} represented the breaking of the Br—Br covalent bond, and the positive sign of V_{BC} represented the forming of the Br—NH₃ covalent bond.

$$H_{22} = -EA_{\text{Br}_2} + IP_{\text{NH}_3} + V_{\text{CC}} - V_{\text{AB}} + V_{\text{BC}} + \frac{\mathbf{S}_{\text{AB}}^2}{2 - 2\mathbf{S}_{\text{AB}}^2} \quad (6.14)$$

A final exchange repulsion term estimated by the overlap of the bromine atoms was also included due to their close contact distance in the model.²⁹ The derivation of our exchange repulsion term was discussed in Chapter 4, where \mathbf{S}_{AB} represents the overlap of orbitals ϕ_A and ϕ_B . H_{12} corresponded to the cross term of the reactant and product cases (Eqn. 6.15) equal to the complete “3-centre, 2-electron” cross term from the APT force field.²⁰ \mathbf{S} corresponds to the orbital overlap, as described above. V_{AB} and V_{BC} are the same Morse potentials described above.

$$H_{12} = \frac{\mathbf{S}_{\text{BC}}(V_{\text{AB}} + V_{\text{BC}})}{2(\mathbf{S}_{\text{AB}}\mathbf{S}_{\text{BC}} + \mathbf{S}_{\text{AC}})} \quad (6.15)$$

The construction of the charge transfer potential model was otherwise the same as the “2-centre, 2-electron” model. D_e corresponded to the energy at equilibrium, r_e to the equilibrium bond distance, and k_e to the force constant at equilibrium in Eqn. 6.8 for both V_{AB} and V_{BC} .

Values for the terms in Equations 6.7, 6.13–6.15 (Table 6.2) were found in the literature.^{25,34,36} While adjusting ζ of the model to visually match the calculated interaction energy between Br_2 and NH_3 at the MP2/aug-cc-pVTZ level, r_e of $\text{Br}-\text{NH}_3$ was increased from 1.89 Å and k_e was decreased from 162 kcal/mol Å².^{34,36} The necessity for altering these variables signifies that the covalent bond between bromine and nitrogen in a charge transfer complex is longer than expected when compared to a conventional covalent bond, and the spring constant weaker. The alterations are consistent with those necessary in the $\text{NH}_3^+\text{BH}_3^-$ model.

Table 6.2. The H_{11} , H_{22} , and H_{12} parameters for the model $\text{NH}_3^+\text{Br}_2^-$ charge transfer potential.

Br—NH₃							
ε (kcal/mol)	ρ (Å)	EA_{Br_2} (kcal/mol)	IP_{NH_3} (kcal/mol)	ζ (Bohr ⁻¹)	D_e (kcal/mol)	r_e (Å)	k_e (kcal/mol Å ²)
0.165	3.60	77.6	233	0.982	57.0	2.46	145
Br—Br							
-	-	-	-	ζ (Bohr ⁻¹)	D_e (kcal/mol)	r_e (Å)	k_e (kcal/mol Å ²)
-	-	-	-	1.30	48.5	2.28	339

The ζ -exponents in the model were varied to visually match the location and slope of the repulsive wall and energetic well of the “3-centre, 4-electron” charge transfer model to the calculated interaction energy between Br_2 and NH_3 at the MP2/aug-cc-pVTZ level. The charge transfer model visually matched calculations at the MP2 level as a function of distance (Fig. 6.6). The energy of H_{11} resulted in a mostly repulsive curve and H_{22} resulted in a generally repulsive curve shaped according to the parameters of Eqn. 6.14. The energetic minimum of the product model was found at 2.16 Å, which transitioned quickly into an unfavorable interaction due to the

ionization potential of NH_3 with increasing r_{AB} . H_{12} resulted in a curve shaped according to the overlap and bonding parameters of Eqn. 6.15. An energetic minimum was found at 2.31 Å that countered the ionization potential at long distance and led to a smooth ΔE_{CT} , tending toward zero kcal/mol at infinite distance. Unlike the borane-ammonia pair, the overall attraction in the halogen bonding dimer resulted from the cross term of the reactant and product wavefunctions, which is shown by H_{22} not dropping below zero kcal/mol. The stability of the charge transfer interaction was caused by the attractive cross-term, H_{12} , of Ψ_1 and Ψ_2 .

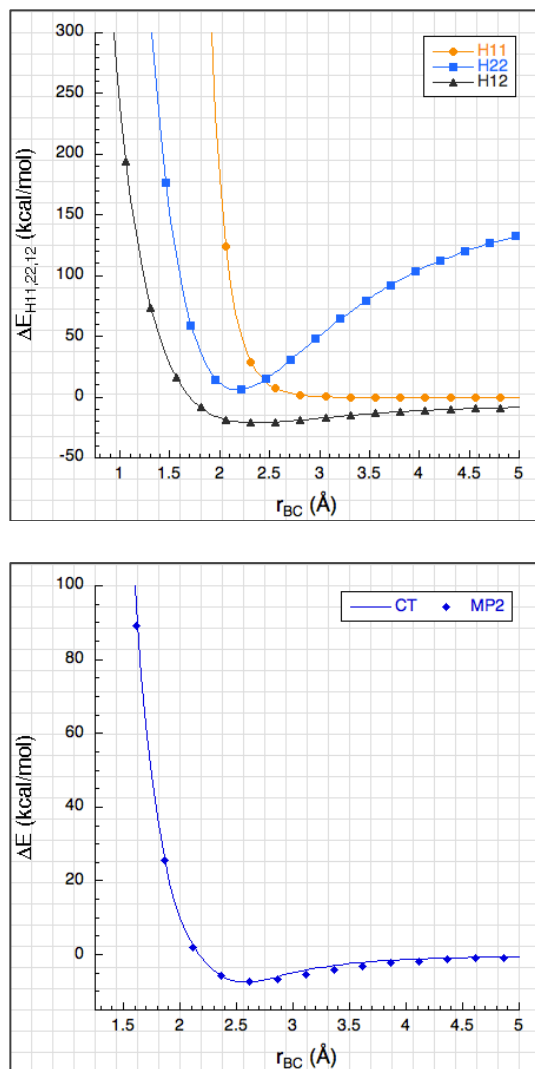


Figure 6.6. The $\text{NH}_3^+\text{Br}_2^-$ charge transfer H_{11} , H_{22} , and H_{12} components (top) and the MP2 and model energies (bottom) as a function of r_{AB} . The charge transfer model results are seen to visually match those calculated at the MP2 level as a function of distance.

In this final chapter, two novel charge transfer models were presented that use mathematic potential terms to predict the interaction energy of dimers. The goal was to provide a fundamental explanation for the process of charge transfer in halogen bonding as a function of distance. In both molecular models, H_{11} , which represented the electronic structure of the molecules before charge transfer had occurred, primarily resulted in repulsion as the interaction distance decreased. H_{12} and H_{22} of the borane-ammonia model resulted in attractive energetic minima at short interaction distances, representing the exchange of charge transfer and the interaction of the molecules after

charge transfer had occurred, respectively. This is in contrast to the bromine-ammonia model, of which the H_{22} minimum was not found to be attractive. Instead, the energetic minimum of the halogen bond resulted from the exchange of the charge transfer, measured by H_{12} as a function of distance. The sum of the H_{11} , H_{22} , and H_{12} terms well predicted a halogen bonding curve calculated as a function of distance, providing insight into the nature of the charge transfer interaction of a pairwise, halogen bonding interaction.

REFERENCES

- (1) Aakeröy, C. B.; Wijethunga, T. K.; Desper, J. Practical Crystal Engineering Using Halogen Bonding: A Hierarchy Based on Calculated Molecular Electrostatic Potential Surfaces. *J. Mol. Struct.* **2014**, *1072*, 20–27.
- (2) Zordan, F.; Brammer, L.; Sherwood, P. Supramolecular Chemistry of Halogens: Complementary Features of Inorganic (M–X) and Organic (C–X') Halogens Applied to M–X···X'–C Halogen Bond Formation. *J. Am. Chem. Soc.* **2005**, *127*, 5979–5989.
- (3) Metrangolo, P.; Resnati, G. Halogen Bonding: A Paradigm in Supramolecular Chemistry. *Chem. - Eur. J.* **2001**, *7*, 2511–2519.
- (4) Wilcken, R.; Zimmermann, M. O.; Lange, A.; Joerger, A. C.; Boeckler, F. M. Principles and Applications of Halogen Bonding in Medicinal Chemistry and Chemical Biology. *J. Med. Chem.* **2013**, *56*, 1363–1388.
- (5) Ibrahim, M. A. A. Molecular Mechanical Perspective on Halogen Bonding. *J. Mol. Model.* **2012**, *18*, 4625–4638.
- (6) Chudzinski, M. G.; McClary, C. A.; Taylor, M. S. Anion Receptors Composed of Hydrogen- and Halogen-Bond Donor Groups: Modulating Selectivity With Combinations of Distinct Noncovalent Interactions. *J. Am. Chem. Soc.* **2011**, *133*, 10559–10567.
- (7) Xu, Z.; Yang, Z.; Liu, Y.; Lu, Y.; Chen, K.; Zhu, W. Halogen Bond: Its Role beyond Drug–Target Binding Affinity for Drug Discovery and Development. *J. Chem. Inf. Model.* **2014**, *54*, 69–78.
- (8) Carlsson, A.-C. C.; Scholfield, M. R.; Rowe, R. K.; Ford, M. C.; Alexander, A. T.; Mehl, R. A.; Ho, P. S. Increasing Enzyme Stability and Activity through Hydrogen Bond-Enhanced Halogen Bonds. *Biochemistry* **2018**, *57*, 4135–4147.
- (9) Lu, Y.; Li, H.; Zhu, X.; Zhu, W.; Liu, H. How Does Halogen Bonding Behave in Solution? A Theoretical Study Using Implicit Solvation Model. *J. Phys. Chem. A* **2011**, *115*, 4467–4475.
- (10) Geballe, M. T.; Skillman, A. G.; Nicholls, A.; Guthrie, J. P.; Taylor, P. J. The SAMPL2 Blind Prediction Challenge: Introduction and Overview. *J. Comput. Aided Mol. Des.* **2010**, *24*, 259–279.
- (11) Hassel, O. Structural Aspects of Interatomic Charge-Transfer Bonding. *Science* **1970**, *170*, 497–502.
- (12) Bent, H. A. Structural Chemistry of Donor-Acceptor Interactions. *Chem. Rev.* **1968**, *68*, 587–648.
- (13) Mulliken, R. S. Structures of Complexes Formed by Halogen Molecules with Aromatic and with Oxygenated Solvents ¹. *J. Am. Chem. Soc.* **1950**, *72*, 600–608.
- (14) Guthrie, F. XXVIII.—On the Iodide of Iodammonium. *J. Chem. Soc.* **1863**, *16*, 239–244.
- (15) Remsen, I. Action of the Halogens on the Methylamines. *Am. Chem. J.* **1896**, *18*, 90–95.
- (16) Hassel, O.; Rømming, C. Direct Structural Evidence for Weak Charge-Transfer Bonds in Solids Containing Chemically Saturated Molecules. *Q. Rev. Chem. Soc.* **1962**, *16*, 1–18.
- (17) Thirman, J.; Engelage, E.; Huber, S. M.; Head-Gordon, M. Characterizing the Interplay of Pauli Repulsion, Electrostatics, Dispersion and Charge Transfer in Halogen Bonding with Energy Decomposition Analysis. *Phys. Chem. Chem. Phys.* **2018**, *20*, 905–915.
- (18) Erdelyi, M. A Big Hello to Halogen Bonding: Scientific Conferences. *Nat. Chem.* **2014**, *6*, 762–764.
- (19) Hassel, O.; Hvoslef, J. The Structure of Bromine 1,4-Dioxanate. *Acta Chem. Scand.* **1954**, *8*, 873.
- (20) Rappé, A. K.; Bormann-Rochotte, L. M.; Wisner, D. C.; Hart, J. R.; Pietsch, M. A.; Casewit, C. J.; Skiff, W. M. APT a Next Generation QM-Based Reactive Force Field Model. *Mol. Phys.* **2007**, *105*, 301–324.
- (21) Mo, Y.; Gao, J.; Peyerimhoff, S. D. Energy Decomposition Analysis of Intermolecular Interactions Using a Block-Localized Wave Function Approach. *J. Chem. Phys.* **2000**, *112*, 5530–5538.
- (22) Mo, Y.; Song, L.; Wu, W.; Zhang, Q. Charge Transfer in the Electron Donor–Acceptor Complex BH₃NH₃. *J. Am. Chem. Soc.* **2004**, *126*, 3974–3982.
- (23) Umeyama, H.; Morokuma, K. Molecular Orbital Studies of Electron Donor-Acceptor Complexes. 3. Energy and Charge Decomposition Analyses for Several Strong Complexes: Carbon Monoxide-

- Borane, Ammonia-Borane, Methylamine-Borane, Trimethylamine-Borane, and Ammonia-Boron Trifluoride. *J. Am. Chem. Soc.* **1976**, *98*, 7208–7220.
- (24) Muller, R. P.; Goddard III, W. A. Valence Bond Theory. In *The Encyclopedia of Physical Science and Technology*; Academic Press, 2002; pp 1–8.
- (25) Rappé, A. K.; Casewit, C. J.; Colwell, K. S.; Goddard III, W. A.; Skiff, W. M. UFF, A Full Periodic Table Force Field for Molecular Mechanics and Molecular Dynamic Simulations. *J. Am. Chem. Soc.* **1992**, *114*, 10024–10035.
- (26) Wu, T.-Y. Electron Affinity of Boron, Carbon, Nitrogen, and Oxygen Atoms. *Phys. Rev.* **1955**, *100*, 1195–1196.
- (27) Paduani, C.; Wu, M. M.; Willis, M.; Jena, P. Theoretical Study of the Stability and Electronic Structure of $\text{Al}(\text{BH}_4)_{n=1 \rightarrow 4}$ and $\text{Al}(\text{BF}_4)_{n=1 \rightarrow 4}$ and Their Hyperhalogen Behavior. *J. Phys. Chem. A* **2011**, *115*, 10237–10243.
- (28) Branton, G. R.; Frost, D. C.; Herring, F. G.; McDowell, C. A.; Stenhouse, I. A. The Ionization Potentials of Ammonia and Ammonia-D₃. Measured by Photoelectron Spectroscopy, and an Indo Calculation of These Values. *Chem. Phys. Lett.* **1969**, *3*, 581–584.
- (29) Goddard III, W. A. *Nature of the Chemical Bond*; California Institute of Technology: Pasadena, CA, 1986; Vol. 1.
- (30) Morse, P. M. Diatomic Molecules According to the Wave Mechanics. II. Vibrational Levels. *Phys. Rev.* **1929**, *34*, 57–64.
- (31) Kuznetsov, A. M.; German, E. D.; Masliy, A. N.; Korshin, G. V. A Density Functional Study of Dissociative Electron Transfer Reactions with Participation of Halogenated Methanes. *J. Electroanal. Chem.* **2004**, *573*, 315–325.
- (32) Huxley, P.; Murrell, J. N. Ground-State Diatomic Potentials. *J. Chem. Soc. Faraday Trans. 2 Mol. Chem. Phys.* **1983**, *79*, 323–328.
- (33) Roothaan, C. C. J. A Study of Two-Center Integrals Useful in Calculations on Molecular Structure. I. *J. Chem. Phys.* **1951**, *19*, 1445–1458.
- (34) Karpfen, A. Charge-Transfer Complexes between NH_3 and the Halogens F_2 , ClF , and Cl_2 : An Ab Initio Study on the Intermolecular Interaction. *J. Phys. Chem. A* **2000**, *104*, 6871–6879.
- (35) Wang, C.; Danovich, D.; Mo, Y.; Shaik, S. On The Nature of the Halogen Bond. *J. Chem. Theory Comput.* **2014**, *10*, 3726–3737.
- (36) Alkorta, I.; Rozas, I.; Elguero, J. Charge-Transfer Complexes between Dihalogen Compounds and Electron Donors. *J. Phys. Chem. A* **1998**, *102*, 9278–9285.

CHAPTER 7: CONCLUSION

Since its resurgence in the early 21st century, halogen bonding has found application in supramolecular and biomolecular chemistry, specifically photovoltaics, organic magnets, anion transport, protein and ligand modification, and drug design.^{1,2} The interaction distance is shorter than the sum of the species' van der Waals radii, and the bond angle is approximately 180°. ³⁻¹⁰ The geometry of a biomolecule defines its reactivity, which has been found to be dependent on the halogen atom present, the Lewis base that it is interacting with, and the geometry of the interacting pair in the overall structure.^{1,2,10-25} It is necessary to understand the underlying energetic components of the interaction in order to predict reactivity of a halogen bonding pair in a biomolecular structure. Throughout this thesis, the research that our group has completed has been demonstrated to work toward understanding the electrostatic component, as well as the exchange repulsion, dispersion, and charge transfer of halogen bonding.

The Cambridge Structural Database was used to visualize the distance and angle dependence of halogen bonding supramolecular crystal structures. The distance versus angle scatterplot illustrated a high density of crystals within the region characteristic of halogen bonding. In translating the scatterplot into a 3-D surface of crystal frequency versus distance and angle, a peak maximum was found with a $d < \Sigma r_{vdW}$ and $\theta = 180^\circ$. An increasing bias toward a halogen bonding configuration was found at a distance within the sum of the van der Waals radii as a periodic trend from fluorine to iodine. A bias away from a halogen bonding configuration was found at distances longer than the sum of the van der Waals radii for fluorine and iodine, and a random bias was found for chlorine and bromine. Together, these results suggest a combination of electrostatic and non-electrostatic effects in crystal structures that contain halogen bonds.

Molecular models of acetone interacting with the halobenzenes, halomethanes, and diatomic halogens were prepared to better understand the distance and angle dependence of halogen bonding dimers. The underlying attractive components of the interaction energy, namely electrostatics, exchange repulsion, and dispersion, were observed. The magnitude of the overall attraction increased down the periodic table from fluorine to iodine, corresponding to the increasing polarizability of the atom. The underlying electrostatic attraction was found to increase with the polarizability of the atom and electron-withdrawing strength of the organic substituent group. Similarly, the exchange repulsion decreased, which corresponded to an increase in the measured dispersion. Difference curves were then calculated by subtracting the binding energy of X_2 —acetone from that of RX —acetone at the MP2 level. The phenyl and methyl binding energies were more repulsive than the diatomic halogens as a function of distance, as expected given the observed stronger and shorter binding curves for the diatomic halogens. The interaction energy as a function of angle displayed a similar shape as a function of angle, with a minimum present generally at 180° and repulsion increased toward an angle of 90° or 270° . The depth was found to be dependent on the shape of the halogen. This correlation is dependent on the electronic structure of the halogen atom.

The purpose of constructing our electrostatic potential and exchange repulsion models was to understand the source of the observed distance-angle dependence of halogen bonding at the most fundamental (atomic) level. The electrostatics and exchange repulsion were modeled using a linear combination of atomic orbitals to explain the source of the anisotropy and evident periodic trend in halogen bonding. The magnitude of the E_{XR} could be seen to increase from fluorine to iodine, consistent with the aforementioned periodic trends. The size of the repulsive well illustrated the relative increase in size of the σ -hole due to the singly-occupied valence p_z -orbital. Lastly, the angular dependence of the E_{XR} approached zero beyond the sum of the van der Waals radii,

suggesting that our model is consistent with experimental conclusions. The attractive E_{ES} resulted in a stable model halogen bonding interaction at an angle of 180° , though it did not approach zero beyond the sum of the van der Waals radii. Additional calculations were performed where either an additional charge or dipole moment was present in the model, which resulted in an energy that approached zero at long distance. Finally, a dipole-dipole interaction was found to be essential for reproduction of the substituent effect in going from X_2 —acetone to MeX —acetone. Our model was concluded to have profound implications for halogen bonding, where the difference curves for $X = F, Cl, Br$ could be accurately modeled using the combination of $1/r^3$ dipole-dipole repulsion and exchange repulsion.

Preliminary steps were taken to model the non-additivity of multimolecular structures with the intention of understanding the underlying energetic contributions. Model trimers were useful for studying multimolecular halogen bonding systems interacting with small solvent molecules. The non-additivity of a trimer can be calculated using a measure of the cooperativity. Interaction distances within the trimer were found to be less than that of their respective dimer counterparts, reflecting an increase in stability due to cooperative effects. The non-additivity of the trimers was found to be dependent on a balance of electrostatics, exchange repulsion, dispersion, and charge transfer. Evidence was also provided that the magnitude of charge transfer found in a trimer correlated to that of the cooperativity found at the MP2 level. The triplet component of the electron correlation, was also found to comprise a majority of the dispersive component that resulted in an increased non-additivity as non-bonding distances decreased.

There is currently an increasing interest “charge transfer bond” descriptions of halogen bonding.^{26–29} A novel charge transfer model has begun development that was used to examine the process of charge transfer as a function of distance in charge transfer complexes. Initially, the charge transfer model was constructed for a borane-ammonia “2-centre, 2-electron” complex, and

then expanded to a bromine-ammonia “3-centre, 4-electron” complex. The models were visually fitted to calculated interaction energies at the MP2/aug-cc-pVTZ level. The results of the models showed that the cross-term of the charge transfer interaction between reactant and product components primarily contributed to the attraction as a function of distance. To our knowledge, a similar charge transfer potential term has not been published in the literature.^{1,30-34}

In summary, a halogenated molecule and a Lewis base at long distance begin to attract as partially positive and negative electrostatics align. Electron exchange adds to the stability of the interaction at a shorter distance and both attractive terms reach equilibrium with the exchange repulsion. The electrostatics and exchange repulsion terms are anisotropic with a minimum repulsion found at a bond angle of 180°. As the Lewis acid-base pair is forming, the electrostatics and exchange repulsion act as a funnel, optimally aligning the molecules at an R–X—O bond angle of 180°. The charge transfer contribution leads to a contraction of the bond to a distance to within the sum of the van der Waals radii of the interacting atoms. Dispersion then increases due to the shortened bond distance, further stabilizing the interaction.

Future Works

Additional steps can be taken to continue work on the theoretical studies presented throughout this thesis. First, the exchange model should be expanded to model the electrostatics and exchange repulsion of the molecular halogens as well as the atomic structures. The importance of the substituent group was emphasized in Chapter 3, but our theoretical model in Chapter 4 has thus far been developed to study the electronic structure of atomic halogens. Second, the cluster trimers that were observed in Chapter 5 should also be expanded because only bromine has thus far been studied in detail. More halogen-containing Lewis acids will need to be observed, particularly those considered to form model halogen bonds. Lastly, the charge transfer potential

term that was derived in Chapter 6 should be statistically fitted to computational calculations. Not only that, but the model itself should be expanded to predict the dependence of halogen bonding on charge transfer as a function of interaction angle and halogen type. Meeting these goals will provide further insight into the nature of halogen bonding as caused by the underlying electrostatics, dispersion, exchange repulsion, and charge transfer components.

REFERENCES

- (1) Erdelyi, M. Scientific Conferences: A Big Hello to Halogen Bonding. *Nat. Chem.* **2014**, *6* (9), 762.
- (2) Priimagi, A.; Cavallo, G.; Metrangolo, P.; Resnati, G. The Halogen Bond in the Design of Functional Supramolecular Materials: Recent Advances. *Acc. Chem. Res.* **2013**, *46* (11), 2686.
- (3) Politzer, P.; Riley, K. E.; Bulat, F. A.; Murray, J. S. Perspectives on Halogen Bonding and Other σ -Hole Interactions: Lex Parsimoniae (Occam's Razor). *Comput. Theor. Chem.* **2012**, *998*, 2.
- (4) Riley, K. E.; Hobza, P. Investigations into the Nature of Halogen Bonding Including Symmetry Adapted Perturbation Theory Analyses. *J. Chem. Theory Comput.* **2008**, *4*, 232.
- (5) Riley, K. E.; Merz, K. M. Insights into the Strength and Origin of Halogen Bonding: The Halobenzene-Formaldehyde Dimer. *J. Phys. Chem. A* **2007**, *111*, 1688.
- (6) Peebles, S. A.; Fowler, P. W.; Legon, A. C. Anisotropic Repulsion in Complexes B.Cl₂ and B.HCl: The Shape of the Chlorine Atom-in-a-Molecule. *Chem. Phys. Lett.* **1995**, *240*, 130.
- (7) Riley, K. E.; Murray, J. S.; Fanfrlík, J.; Řezáč, J.; Solá, R. J.; Concha, M. C.; Ramos, F. M.; Politzer, P. Halogen Bond Tunability I: The Effects of Aromatic Fluorine Substitution on the Strengths of Halogen-Bonding Interactions Involving Chlorine, Bromine, and Iodine. *J. Mol. Model.* **2011**, *17*, 3309.
- (8) Shields, Z. P.; Murray, J. S.; Politzer, P. Directional Tendencies of Halogen and Hydrogen Bonds. *Int. J. Quantum Chem.* **2010**, *110*, 2823.
- (9) Kolář, M.; Hobza, P. On Extension of the Current Biomolecular Empirical Force Field for the Description of Halogen Bonds. *J. Chem. Theory Comput.* **2012**, *8*, 1325.
- (10) Wilcken, R.; Zimmermann, M. O.; Lange, A.; Joerger, A. C.; Boeckler, F. M. Principles and Applications of Halogen Bonding in Medicinal Chemistry and Chemical Biology. *J. Med. Chem.* **2013**, *56*, 1363.
- (11) Aakeroy, C. B.; Wijethunga, T. K.; Desper, J. Practical Crystal Engineering Using Halogen Bonding: A Hierarchy Based on Calculated Molecular Electrostatic Potential Surfaces. *J. Mol. Struct.* **2014**, *1072*, 20.
- (12) Zordan, F.; Brammer, L.; Sherwood, P. Supramolecular Chemistry of Halogens: Complementary Features of Inorganic (M-X) and Organic (C-X') Halogens Applied to M-X--X'-C Halogen Bond Formation. *J. Am. Chem. Soc.* **2005**, *127*, 5979.
- (13) Wilcken, R.; Zimmermann, M. O.; Lange, A.; Zahn, S.; Boeckler, F. M. Using Halogen Bonds to Address the Protein Backbone: A Systematic Evaluation. *J. Comput. Aided Mol. Des.* **2012**, *26* (8), 935.
- (14) Parisini, E.; Metrangolo, P.; Pilati, T.; Resnati, G.; Terraneo, G. Halogen Bonding in Halocarbon-Protein Complexes: A Structural Survey. *Chem. Soc. Rev.* **2011**, *40*, 2267.
- (15) Ibrahim, M. A. A. Molecular Mechanical Study of Halogen Bonding in Drug Discovery. *J. Comput. Chem.* **2011**, *32*, 2564.
- (16) Metrangolo, P.; Resnati, G. Halogen Bonding: A Paradigm in Supramolecular Chemistry. *Chem. Eur. J.* **2001**, *7*, 2511.
- (17) Chudzinski, M. G.; McClary, C. A.; Taylor, M. S. Anion Receptors Composed of Hydrogen- and Halogen-Bond Donor Groups: Modulating Selectivity With Combinations of Distinct Noncovalent Interactions. *J. Am. Chem. Soc.* **2011**, *133* (27), 10559.
- (18) Xu, Z.; Yang, Z.; Liu, Y.; Lu, Y.; Chen, K.; Zhu, W. Halogen Bond: Its Role Beyond Drug-Target Binding Affinity for Drug Discovery and Development. *J. Chem. Inf. Model.* **2014**, *54* (1), 69.
- (19) Perez-Torrallba, M.; Garcia, M. A.; Lopez, C.; Torralba, M. C.; Torres, M. R.; Claramunt, R. M.; Elguero, J. Structural Investigation of Weak Intermolecular Interactions (Hydrogen and Halogen Bonds) in Fluorine-Substituted Benzimidazoles. *Cryst. Growth Des.* **2014**, *14*, 3499.
- (20) Rissanen, K. Halogen Bonded Supramolecular Complexes and Networks. *CrystEngComm* **2008**, *10* (9), 1107.

- (21) Lu, Y.; Shi, T.; Wang, Y.; Yang, H.; Yan, X.; Luo, X.; Jiang, H.; Zhu, W. Halogen Bonding--A Novel Interaction for Rational Drug Design? *J. Med. Chem.* **2009**, *52*, 2854.
- (22) Zhou, P.; Lv, J.; Zou, J.; Tian, F.; Shang, Z. Halogen-Water-Hydrogen Bridges in Biomolecules. *J. Struct. Biol.* **2010**, *169*, 172.
- (23) Matter, H.; Nazaré, M.; Güssregen, S.; Will, D. W.; Schreuder, H.; Bauer, A.; Urmann, M.; Ritter, K.; Wagner, M.; Wehner, V. Evidence for C-Cl/C-Br... π Interactions as an Important Contribution to Protein-Ligand Binding Affinity. *Angew. Chem. Int. Ed.* **2009**, *48* (16), 2911.
- (24) Kolář, M.; Hobza, P.; Bronowska, A. K. Plugging the Explicit σ -Holes in Molecular Docking. *Chem. Commun.* **2013**, *49*, 981.
- (25) Kolář, M.; Kubař, T.; Hobza, P. On the Role of London Dispersion Forces in Biomolecular Structure Determination. *J. Phys. Chem. B* **2011**, *115* (24), 8038.
- (26) Wang, C.; Danovich, D.; Mo, Y.; Shaik, S. On The Nature of the Halogen Bond. *J. Chem. Theory Comput.* **2014**, *10* (9), 3726.
- (27) Li, R.; Li, Z.; Wu, D.; Li, Y.; Chen, W.; Sun, C. Study of π Halogen Bonds in Complexes $C_2H_4 \cdot nF_n \cdots ClF$. *J. Phys. Chem. A* **2005**, *109*, 2608.
- (28) Mo, Y.; Gao, J.; Peyerimhoff, S. D. Energy Decomposition Analysis of Intermolecular Interactions Using a Block-Localized Wave Function Approach. *J. Chem. Phys.* **2000**, *112* (13), 5530.
- (29) Karpfen, A. Charge-Transfer Complexes between NH_3 and the Halogens F_2 , ClF , and Cl_2 : An Ab Initio Study on the Intermolecular Interaction. *J. Phys. Chem. A* **2000**, *104* (29), 6871.
- (30) Bent, H. Structural Chemistry of Donor-Acceptor Interactions. *Chem. Rev.* **1968**, *68*, 587.
- (31) Mulliken, R. S. Structures of Complexes Formed by Halogen Molecules with Aromatic and with Oxygenated Solvents¹. *J. Am. Chem. Soc.* **1950**, *72* (1), 600.
- (32) Hassel, O. Aspects of Interatomic Charge-Transfer Bonding. *Science* **1970**, *170*, 497.
- (33) Hassel, O.; Romming, C. Direct Structural Evidence for Weak Charge-Transfer Bonds in Solids Containing Chemically Saturated Molecules. *Q. Rev. Chem. Soc.* **1962**, *16*, 1.
- (34) Hassel, O.; Hvoslef, J.; Vihovde, E. H.; Sørensen, N. A. The Structure of Bromine 1,4-Dioxanate. *Acta Chem. Scand.* **1954**, *8*, 873.

APPENDIX 1

The primary method for calculating the energy of biomolecular systems, like ligands in the active sites of proteins, is by using a force field to approximate the interaction energy using simple potential expressions within molecular mechanics/dynamics suites.¹⁻¹¹ A force field that incorporates a van der Waals potential term has been shown to improve halogen bonding calculations,^{2,12} as introduced in Chapter 1. An updated force field was published by Scholfield et al.¹ in 2015 titled the “Force Field Model of Periodic Trends in Biomolecular Halogen Bonds,”¹ which I contributed to by obtaining the well depth (ϵ_X) and anisotropic shape (Δr_X) parameters for the van der Waals potential term (V_{LJ}) in the force field for biological halogen bonds ffBXB. I also provided an initial approximation for the average van der Waals radii of the halogens ($\langle r_{vdW(X)} \rangle$). It was my goal to understand the radial and angular dependence of the underlying van der Waals components. In doing so, I would help to expand ffBXB to include chlorine and iodine.¹³⁻¹⁶

We used CCSD(T) to calculate the energy of the interaction between X and He, where X was Cl, Br, or I. The coupled clusters with singles and doubles including perturbative triples (CCSD(T)) method¹⁷ is considered to be one of the most accurate quantum mechanical (QM) methods for calculating total interaction energy, and correlation in non-bonding structures.^{15,18-20} The method is not more widely used because it becomes computationally expensive with atom count; the limit has been found to be approximately a dozen atoms per monomer.²⁰ Dunning’s augmented correlation consistent triple zeta (aug-cc-pVTZ) basis set was supplemented with additional functions to enhance the dispersion between the halogens and helium probe. The basis set was supplemented by single p , d , and f functions for He, and d , f , and g functions for Cl, Br, and I (Table A1.1). A helium probe was used to calculate the attractive and repulsive van der

Waals interactions. Helium is a closed-shell atom with low polarizability, making it a suitable atom to measure both the exchange repulsion and dispersion of an atom or molecule.²¹⁻²⁶

Table A1.1. The exponents of the supplemental p , d , f , and g functions for Dunning's basis set.¹

Atom	p	d	f	g
He	0.2400	0.2900	0.3300	-
Cl	-	0.0300	0.1200	0.1700
Br	-	0.1200	0.2000	0.1400
I	-	0.1600	0.3700	0.2800

The helium probe was moved first as a function of distance along the direction of the singly-occupied p-orbital (p_σ) and then along the direction of a doubly-occupied p-orbital (p_π) for each halogen. Carter et al. had found that there was little to no variation in dispersion as a function of angle,² so we decided to isolate the electron correlations in both directions ($\Delta E_{corr}^{p_\sigma}$ and $\Delta E_{corr}^{p_\pi}$, respectively) by subtracting the Hartree-Fock (HF) results from the CCSD(T) results. A weighted average was calculated (Eqn. 1) of the electron correlations. $\Delta E'_{corr}$ was then added to HF, resulting in what Scholfield et al. referred to as QM(σ) and QM(π).¹

$$\Delta E'_{corr} = \left(\frac{1}{3}\right) \Delta E_{corr}^{p_\sigma} + \left(\frac{2}{3}\right) \Delta E_{corr}^{p_\pi} \quad (1)$$

We found that anisotropic exchange repulsion and isotropic dispersion accurately model the van der Waals component of halogen bonding as a function of distance and angle in a force field. The energetic well and atomic shape parameters (ϵ_X and Δr_X , respectively) were obtained by adjusting them until V_{LJ} visually matched the averaged CCSD(T) results as a function of distance (d) in the p_σ and p_π directions (Fig. A1.1).

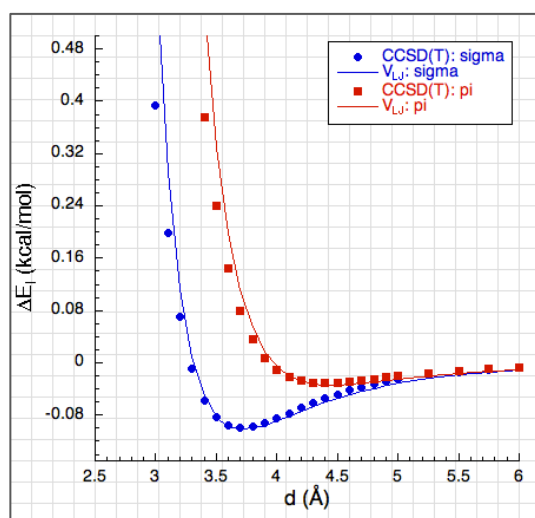
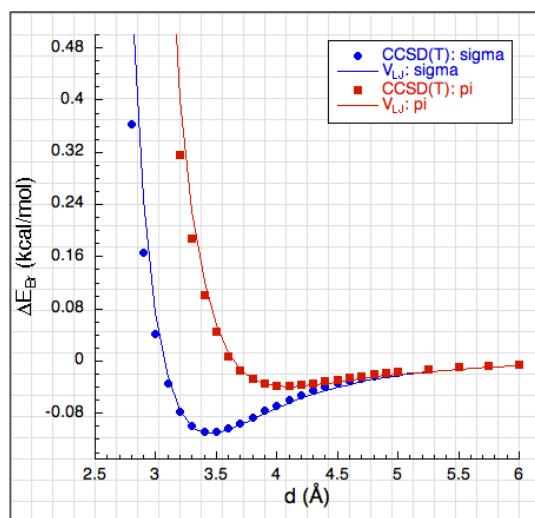
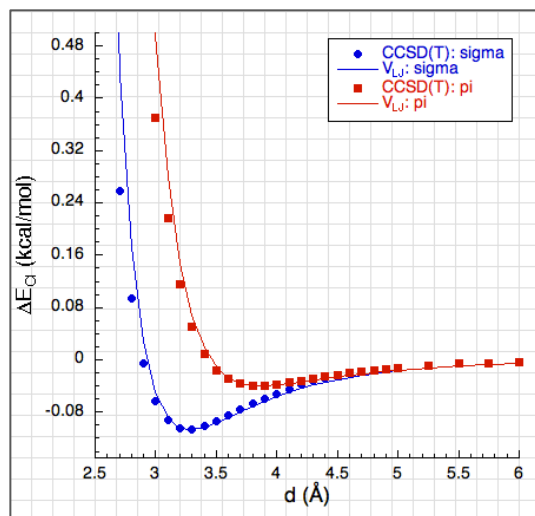


Figure A1.1. The CCSD(T) interaction energies of the halogens (Cl-top, Br-middle, and I-bottom) and helium along the p_σ and p_π orbitals (dots), and the V_{LJ} approximation (line).

The well depth parameters (ϵ_X) were similar to those presented in the Universal Force Field by Rappé et al.,²⁵ and the anisotropic shape parameters (Δr_X) were equal to the differences of the van der Waals radii of the halogens in the p_σ and p_π directions (Table A1.2).

Table A1.2. The well depth (ϵ_X) and anisotropic shape (Δr_X) parameters of the ffBXB.¹

Halogen	ϵ_X (kcal/mol)	Δr_X (Å)
Cl	0.107 ± 0.002	0.149 ± 0.001
Br	0.109 ± 0.038	0.160 ± 0.018
I	0.087 ± 0.008	0.185 ± 0.006

Scholfield et al. applied a nonlinear least-squares program to fit the remaining parameters in the ffBXB (Table A1.3).¹ The fitting process was weighted toward the potential well, as that is where a halogen bond would form.

Table A1.3. The parameters of the ffBXB parameterized by our collaborators, as presented in Scholfield et al.¹ $\langle r_{vdW(X)} \rangle$ is the average radius of the halogen, A the amplitude of the cosine function, ν the period of the cosine function, and B the baseline of the cosine function.

Halogen	$\langle r_{vdW(X)} \rangle$	A (e ⁻)	ν	B (e ⁻)
Cl	1.719 ± 0.010	0.14 ± 0.03	2.46 ± 0.05	-0.016 ± 0.005
Br	1.817 ± 0.014	0.23 ± 0.05	2.42 ± 0.04	0.15 ± 0.04
I	1.922 ± 0.015	0.46 ± 0.06	2.23 ± 0.04	0.29 ± 0.06

The researchers then examined how well the model simulated experimental measurements. The interaction energy of five different DNA junctions were determined either from a crystallographic assay or differential scanning calorimetry: C11J, C12J, Br1J, Br2J, and I2J (Table A1.4). Halouracil and hypophosphate were used to model the junctions in the QM calculations and ffBXB model. A linear correlation was calculated between the experimental and ffBXB results, showing an agreement in the interaction energies with an R^2 value of 0.97 (Ref. 1, Fig. 7).

Table A1.4. Experimental and theoretical interaction energies of model BXBs, as presented in Scholfield et al.¹

Geometry	Experimental (kcal/mol)	Theoretical (kcal/mol)	
	Crystal Assay/Calorimetric	QM	ffBxB
C11J	-0.79 ± 0.12	-0.79	-0.76
C12J	-0.79 ± 0.12	0.02	-0.01
Br1J	-2.28 ± 0.11	-2.07	-2.41
Br2J	-3.6 ± 1.3	-2.93	-2.94
I2J	-5.9 ± 1.1	-5.93	-5.96

In conclusion, the potential energy terms V_{LJ} and V_{elect} were found to be generally applicable to model the geometry and energy of biological halogen bonds.

REFERENCES

- (1) Scholfield, M. R.; Ford, M. C.; van der Zanden, C. M.; Billman, M. M.; Ho, P. S.; Rappé, A. K. Force Field Model of Periodic Trends in Biomolecular Halogen Bonds. *J. Phys. Chem. B* **2015**, *119*, 9140.
- (2) Carter, M.; Rappé, A. K.; Ho, P. S. Scalable Anisotropic Shape and Electrostatic Models for Biological Bromine Halogen Bonds. *J. Chem. Theory Comput.* **2012**, *8*, 2461.
- (3) Ibrahim, M. AMBER Empirical Potential Describes the Geometry and Energy of Noncovalent Halogen Interactions Better than Advanced Semiempirical Quantum Mechanical Method PM6-DH2X. *J. Phys. Chem. B* **2012**, *116*, 3659.
- (4) Pearlman, D. A.; Case, D. A.; Caldwell, J. W.; Ross, W. S.; Cheatham III, T. E.; DeBolt, S.; Ferguson, D.; Seibel, G.; Kollman, P. A. AMBER, A Package of Computer Programs for Applying Molecular Mechanics, Normal Mode Analysis, Molecular Dynamics and Free Energy Calculations to Simulate the Structural and Energetic Properties of Molecules. *Comput. Phys. Commun.* **1995**, *91*, 1.
- (5) Weiner, S. J.; Kollman, P. A.; Case, D. A.; Singh, U. C.; Ghio, C.; Alagona, G.; Profeta, S.; Weiner, P. A New Force Field for Molecular Mechanical Simulation of Nucleic Acids and Proteins. *J. Am. Chem. Soc.* **1984**, *106*, 765.
- (6) Weiner, S. J.; Kollman, P. A.; Nguyen, D. T.; Case, D. A. An All Atom Force Field for Simulations of Proteins and Nucleic Acids. *J. Comput. Chem.* **1986**, *7*, 230.
- (7) Wang, J.; Wolf, R. M.; Caldwell, J. W.; Kollman, P. A.; Case, D. A. Development and Testing of a General Amber Force Field. *J. Comput. Chem.* **2004**, *25*, 1157.
- (8) Jorgensen, W. L.; Schyman, P. Treatment of Halogen Bonding in the OPLS-AA Force Field: Application to Potent Anti-HIV Agents. *J. Chem. Theory Comput.* **2012**, *8* (10), 3895.
- (9) Jorgensen, W. L.; Tirado-Rives, J. The OPLS Potential Functions for Proteins. Energy Minimizations for Crystals of Cyclic Peptides and Crambin. *J. Am. Chem. Soc.* **1988**, *110*, 1657.
- (10) Brooks, B. R.; Brucoleri, R. E.; Olafson, B. D.; States, D. J.; Swaminathan, S.; Karplus, M. CHARMM: A Program for Macromolecular Energy, Minimization, and Dynamics Calculations. *J. Comput. Chem.* **1983**, *4*, 187.
- (11) Brooks, B. R.; Brooks, C. L.; Mackerell, A. D.; Nilsson, L.; Petrella, R. J.; Roux, B.; Won, Y.; Archontis, G.; Bartels, C.; Boresch, S.; et al. CHARMM: The Biomolecular Simulation Program. *J. Comput. Chem.* **2009**, *30* (10), 1545–1614.
- (12) Scholfield, M. R.; Zanden, C. M. V.; Carter, M.; Ho, P. S. Halogen Bonding (X-Bonding): A Biological Perspective. *Protein Sci.* **2013**, *22* (2), 139.
- (13) Jeziorski, B.; Moszynski, R.; Szalewicz, K. Perturbation Theory Approach to Intermolecular Potential Energy Surfaces of van Der Waals Complexes. *Chem. Rev.* **1994**, *94*, 1887.
- (14) Wilcken, R.; Zimmermann, M. O.; Lange, A.; Zahn, S.; Boeckler, F. M. Using Halogen Bonds to Address the Protein Backbone: A Systematic Evaluation. *J. Comput. Aided Mol. Des.* **2012**, *26* (8), 935.
- (15) Kolář, M.; Kubař, T.; Hobza, P. On the Role of London Dispersion Forces in Biomolecular Structure Determination. *J. Phys. Chem. B* **2011**, *115* (24), 8038.
- (16) Lu, Y.; Li, H.; Zhu, X.; Zhu, W.; Liu, H. How Does Halogen Bonding Behave in Solution? A Theoretical Study Using Implicit Solvation Model. *J. Phys. Chem. A* **2011**, *115* (17), 4467.
- (17) Pople, J. A.; Head-Gordon, M.; Raghavachari, K. Quadratic Configuration Interaction. A General Technique for Determining Electron Correlation Energies. *J. Chem. Phys.* **1987**, *87* (10), 5968.
- (18) Woon, D. E. Benchmark Calculations with Correlated Molecular Wave Functions V. The Determination of Accurate Ab Initio Intermolecular Potentials for He₂, Ne₂, and Ar₂. *J. Chem. Phys.* **1994**, *100*, 2838.
- (19) Svensson, M.; Humbel, S.; Froese, R. D. J.; Matsubara, T.; Sieber, S.; Morokuma, K. ONIOM: A Multilayered Integrated MO+MM Method for Geometry Optimizations and Single Point Energy

- Predictions. A Test for Diels--Alder Reactions and $\text{Pt}(\text{P}(\text{t-Br})_3)_2 + \text{H}_2$ Oxidative Addition. *J. Phys. Chem.* **1996**, *100*, 19357.
- (20) Zuchowski, P. S.; Podeszwa, R.; Moszynski, R.; Jeziorski, B.; Szalewicz, K. Symmetry-Adapted Perturbation Theory Utilizing Density Functional Description of Monomers for High-Spin Open-Shell Complexes. *J. Chem. Phys.* **2008**, *129*, 84101.
- (21) Peebles, S. A.; Fowler, P. W.; Legon, A. C. Anisotropic Repulsion in Complexes B.Cl_2 and B.HCl : The Shape of the Chlorine Atom-in-a-Molecule. *Chem. Phys. Lett.* **1995**, *240*, 130.
- (22) Roberts, C. S. Interaction Energy between a Helium Atom and a Hydrogen Molecule. *Phys. Rev.* **1963**, *131*, 203.
- (23) Rappé, A. K.; Bormann-Rochotte, L. M.; Wisner, D. C.; Hart, J. R.; Pietsch, M. A.; Casewit, C. J.; Skiff, W. M. APT a Next Generation QM-Based Reactive Force Field Model. *Mol. Phys.* **2007**, *105* (2–3), 301.
- (24) Muller, R. P.; Goddard III, W. A. Valence Bond Theory. *The Encyclopedia of Physical Science and Technology*, Academic Press; 2002.
- (25) Rappé, A. K.; Casewit, C. J.; Colwell, K. S.; Goddard III, W. A.; Skiff, W. M. UFF, a Full Periodic Table Force Field for Molecular Mechanics and Molecular Dynamics Simulations. *J. Am. Chem. Soc.* **1992**, *114*, 10024.
- (26) Wilson Jr., C. W.; Goddard III, W. A. Exchange Kinetic Energy, Contragradience, and Chemical Binding. *Chem. Phys. Lett.* **1970**, *5*, 45.
- (27) Møller, C.; Plesset, M. S. Note on an Approximation Treatment for Many-Electron Systems. *Phys. Rev.* **1934**, *46* (7), 618–622.
- (28) Nagels, N.; Geboes, Y.; Pinter, B.; De Proft, F.; Herrebout, W. A. Tuning the Halogen/Hydrogen Bond Competition: A Spectroscopic and Conceptual DFT Study of Some Model Complexes Involving CHF_2 I. *Chem. Eur. J.* **2014**, *20*, 8433.
- (29) Woon, D. E.; Dunning, T. H. Gaussian Basis Sets for Use in Correlated Molecular Calculations. IV. Calculation of Static Electrical Response Properties. *J. Chem. Phys.* **1994**, *100*, 2975.
- (30) Boys, S. F.; Bernardi, F. The Calculation of Small Molecular Interactions by the Differences of Separate Total Energies. Some Procedures with Reduced Errors. *Mol. Phys.* **1970**, *19*, 553.
- (31) McDowell, S. A. C. σ -Hole Cooperativity in Anionic $[\text{FX}--\text{CH}_3--\text{YF}]^-$ (X, Y = Cl, Br) Complexes. *Chem. Phys. Lett.* **2014**, *598*, 1.
- (32) Dominikowska, J.; Palusiak, M. Halogen-Halogen Interaction in View of Many-Body Approach. *Chem. Phys. Lett.* **2013**, *583*, 8.
- (33) Mohan, N.; Suresh, C. H. Accurate Binding Energies of Hydrogen, Halogen, and Dihydrogen Bonded Complexes and Cation Enhanced Binding Strengths. *Int. J. Quantum Chem.* **2014**, *114*, 885.

APPENDIX 2

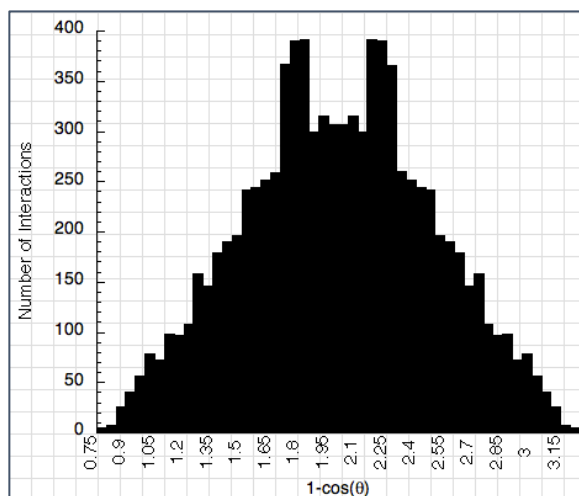


Figure A2.1a. The Cambridge Structural Database was scanned for structures with short R-X—O=C contacts to observe the distance-angle correlation of halogen bonding crystal structures. Here is presented the aggregate number of interactions as a function of X—O=C angle at a normalized distance ($d/\Sigma r_{vdW}$) less than 1.0. Maxima are found at 135° and at 225° .

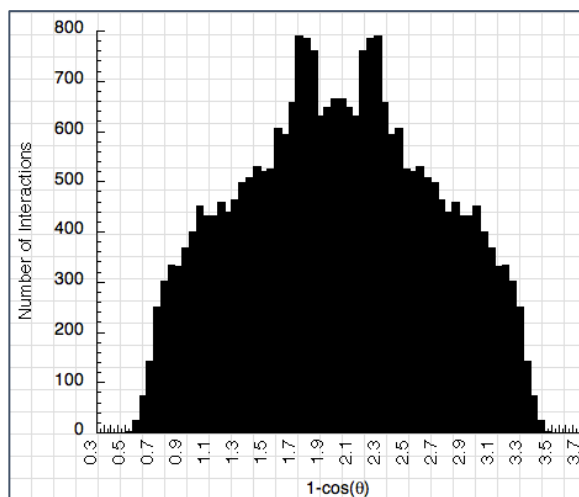


Figure A2.1b. The Cambridge Structural Database was scanned for structures with short R-X—O=C contacts to observe the distance-angle correlation of halogen bonding crystal structures. Here is presented the aggregate number of interactions as a function of X—O=C angle at all normalized distances ($d/\Sigma r_{vdW}$). Maxima are found at 145° and at 215° .

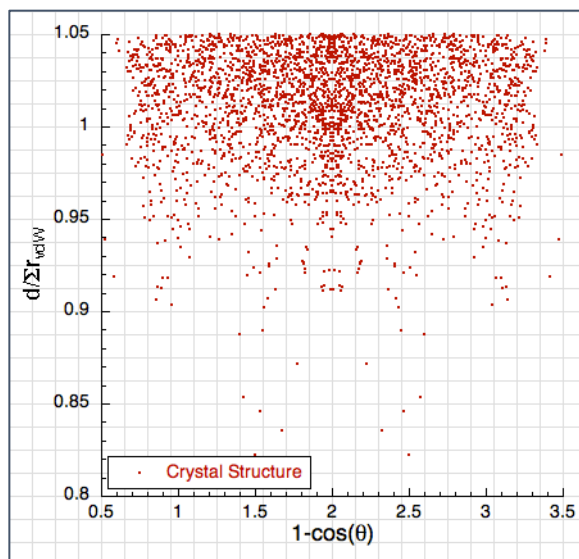


Figure A2.2a. Scatterplot of the fluorinated crystal structures displaying the correlation between normalized non-bonding distance versus redistributed angle by $1-\cos(\theta)$. It is apparent from this figure that a sizable portion of fluorinated crystal structures found in the Cambridge Structural Database exhibit non-bonding distances longer than the sum of the F—O van der Waals radii, and that there is a lack of angular specificity.

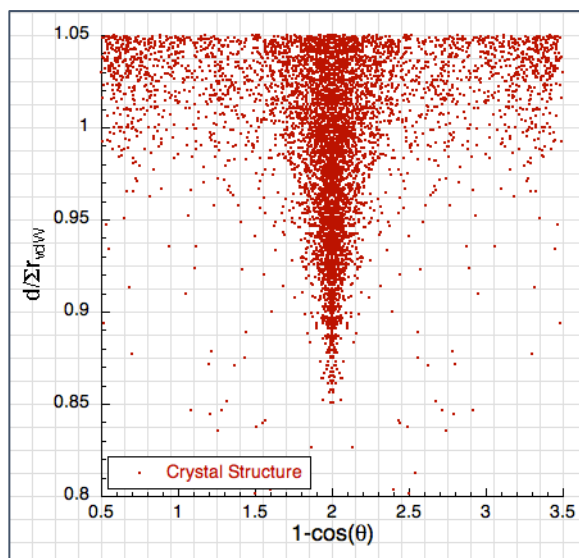


Figure A2.2b. Scatterplot of the chlorinated crystal structures displaying the correlation between normalized non-bonding distance versus redistributed angle by $1-\cos(\theta)$. It is apparent from this figure that a sizable portion of chlorinated crystal structures possess angular specificity, as illustrated by the high density of points near $\theta = 180^\circ$. The angular specificity appears to increase at non-bonding distances shorter than the sum of the Cl—O van der Waals radii.

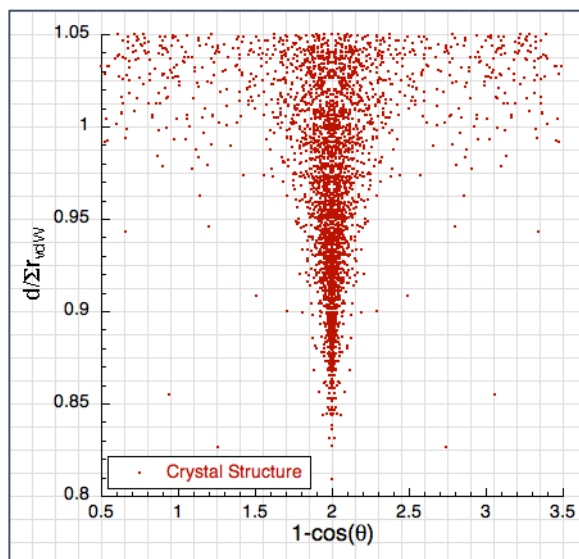


Figure A2.2c. Scatterplot of the brominated crystal structures displaying the correlation between normalized non-bonding distance versus redistributed angle by $1-\cos(\theta)$. It is apparent from this figure that a sizable portion of brominated crystal structures possess angular specificity, as illustrated by the high density of points near $\theta = 180^\circ$. The angular specificity appears to have shifted toward non-bonding distances shorter than the sum of the Br—O van der Waals radii.

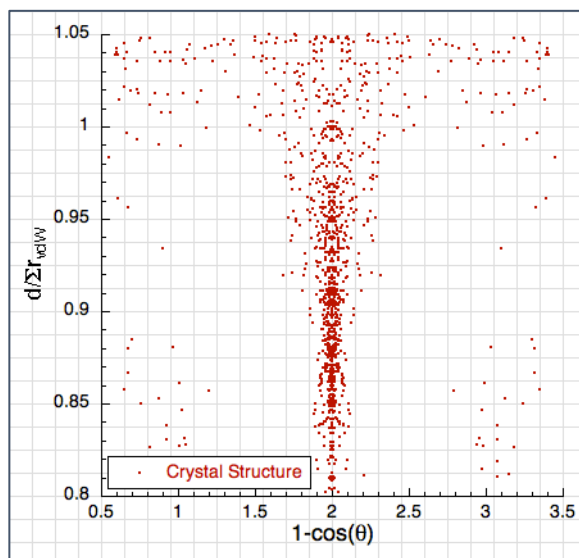


Figure A2.2d. Scatterplot of the iodized crystal structures displaying the correlation between normalized non-bonding distance versus redistributed angle by $1-\cos(\theta)$. It is apparent from this figure that iodized crystal structures possess high angular specificity at non-bonding distances shorter than the I—O sum of the van der Waals radii, and little angular specificity at non-bonding distances greater than the sum of the van der Waals radii.

APPENDIX 3

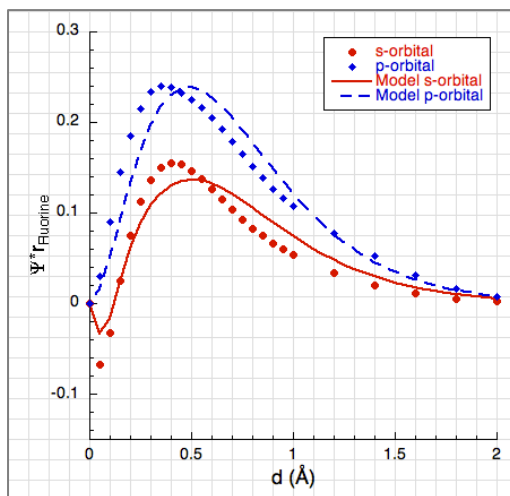


Figure A3.1a. The radial distribution of fluorine's valence s-orbital (red) and p-orbital (blue) wavefunctions. The model s-orbitals and p-orbitals were fit to the radial distributions using the Simplex algorithm.

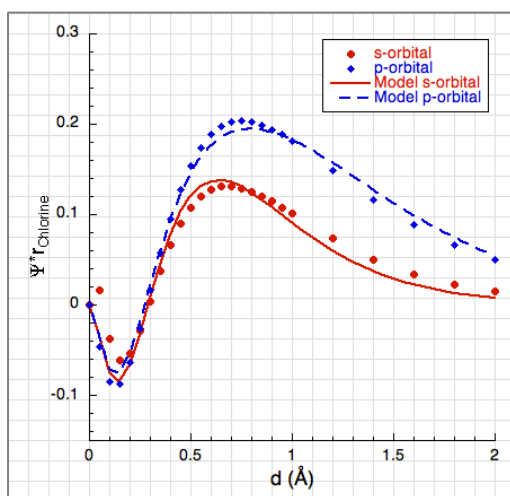


Figure A3.1b. The radial distribution of chlorine's valence s-orbital (red) and p-orbital (blue) wavefunctions. The model s-orbitals and p-orbitals were fit to the radial distributions using the Simplex algorithm.

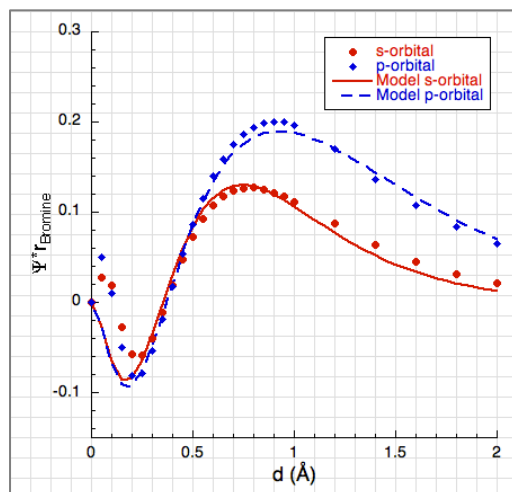


Figure A3.1c. The radial distribution of bromine's valence s-orbital (red) and p-orbital (blue) wavefunctions. The model s-orbitals and p-orbitals were fit to the radial distributions using the Simplex algorithm.

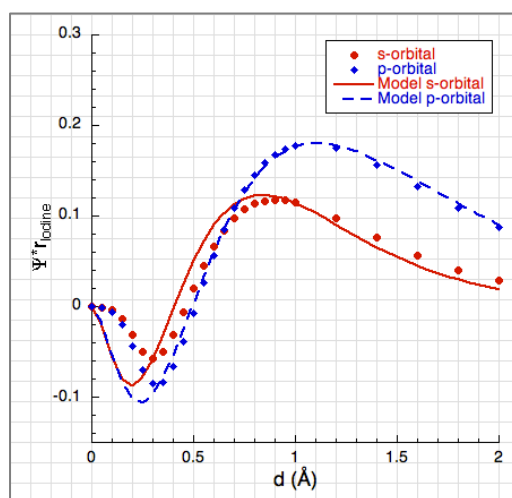


Figure A3.1d. The radial distribution of iodine's valence s-orbital (red) and p-orbital (blue) wavefunctions. The model s-orbitals and p-orbitals were fit to the radial distributions using the Simplex algorithm.

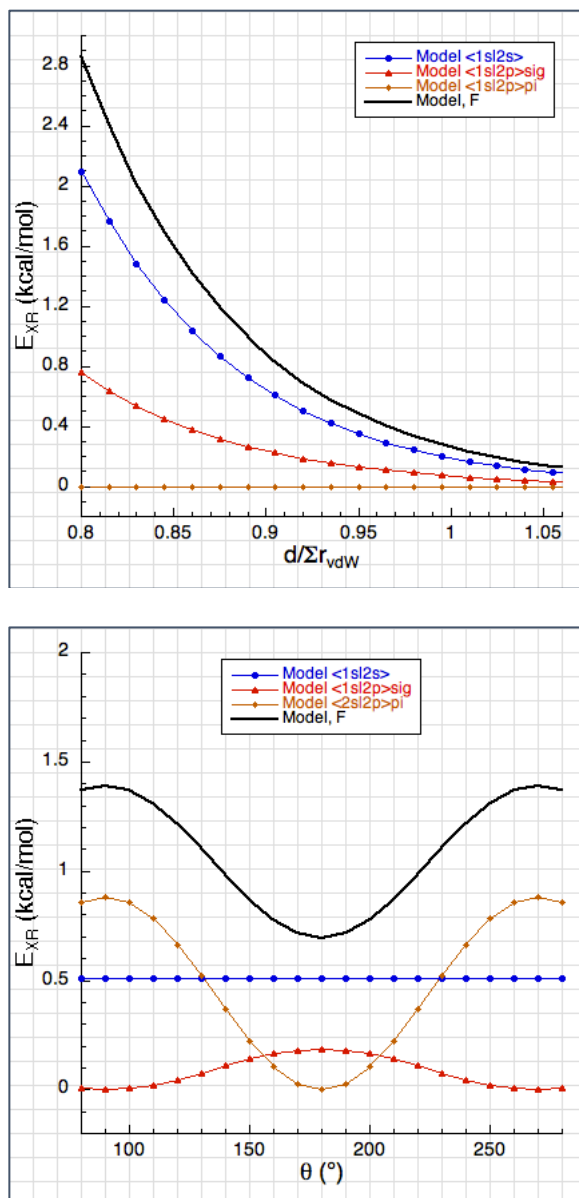


Figure A3.2a. The model s-orbital, p_{σ} -orbital, and p_{π} -orbital contributions to the E_{XR} of fluorine as a function of distance (top) and angle (bottom).

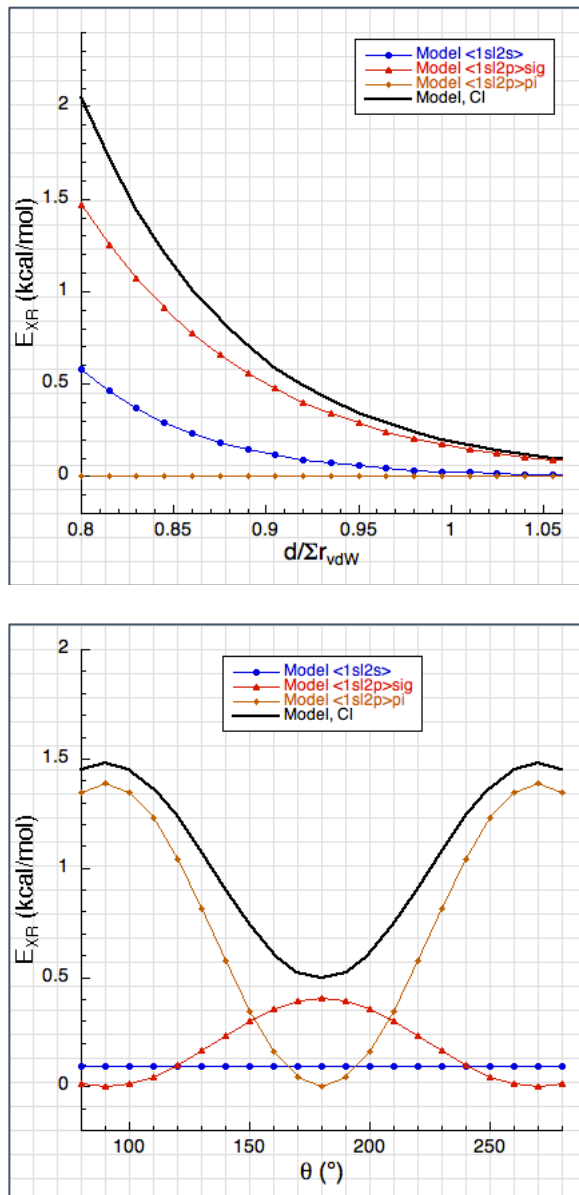


Figure A3.2b. The model s -orbital, p_{σ} -orbital, and p_{π} -orbital contributions to the E_{XR} of chlorine as a function of distance (top) and angle (bottom).

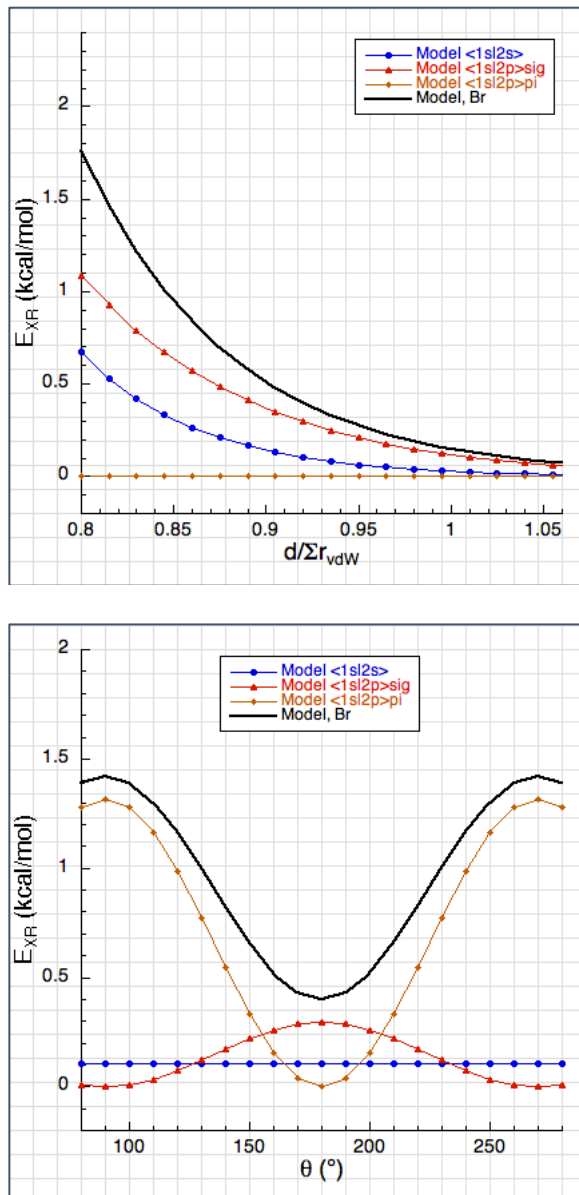


Figure A3.2c. The model s-orbital, p_{σ} -orbital, and p_{π} -orbital contributions to the E_{XR} of bromine as a function of distance (top) and angle (bottom).

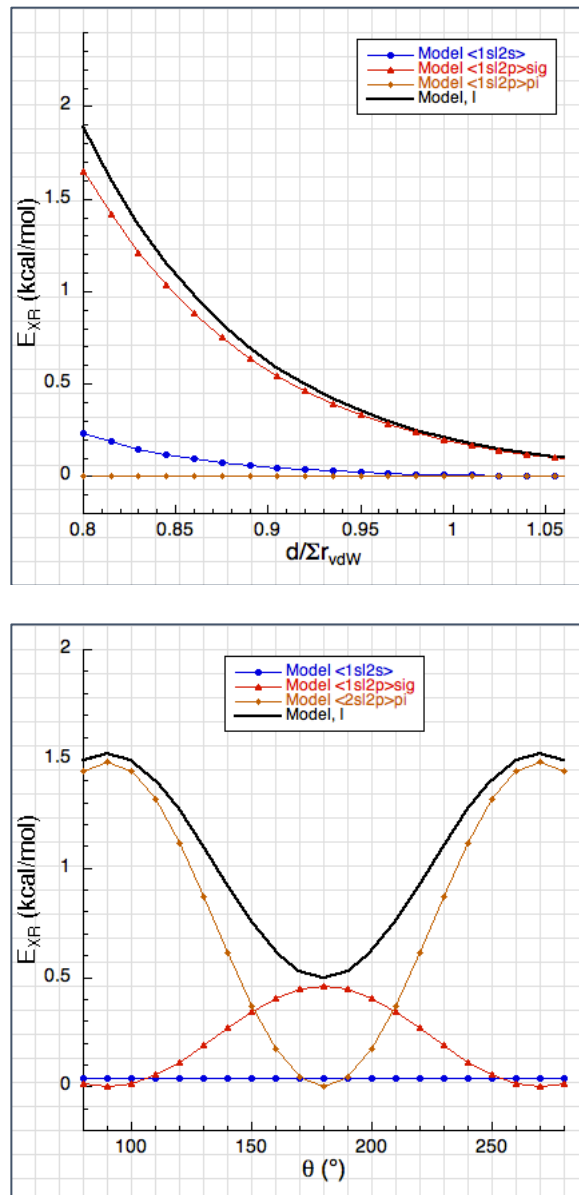


Figure A3.2d. The model s-orbital, p_σ -orbital, and p_π -orbital contributions to the E_{XR} of iodine as a function of distance (top) and angle (bottom).

APPENDIX 4

Program A4.1. The Fortran 77 programs developed to calculate the exchange repulsion of the atomic halogens as a function of atomic radii and angle relative to $\phi_{2p\sigma}$.

```
Program Overlap_F_tot

implicit none

real*8 pi,ang,boh,lam,zetHe,zet2s,zet1s,zet2p,zet1p,zH2s
real*8 zH1s,zH2p,zH1p,tH2s,tH1s,tH2p,tH1p,t12s,t12p,ovrs
real*8 ovrp,Ns,Np,xF,yF,zF,phia,the,ra,xHe,yHe,zHe
real*8 cosa,sina,rHe,rHe2,rho,rho2,rho3,rhoa,rhoa2,cont
real*8 Heter,Clter,OH2s,OH1s,S,Ts,OH2p,OH1p,Psg,Ppi
real*8 Tsg,Tpi,Exr,kH2s,kH1s,kH2p,kH1p
real*8 zero,amax,step,dist

integer*4 i,j,k

pi = 2.0d0*dacos(0.0d0)
ang = 0.5291771d0
boh = 1/ang
lam = 0.346367d0

dist=1.03d0+1.40d0
c dist=1.47d0+1.40d0

zetHe = 1.69d0
zet1s = 14.043877d0
zet2s = 2.111385d0
zet2p = 2.182682d0
zH2s = 0.5d0*(zetHe+zet2s)
zH1s = 0.5d0*(zetHe+zet1s)
zH2p = 0.5d0*(zetHe+zet2p)
tH2s = (zetHe-zet2s)/(zetHe+zet2s)
tH1s = (zetHe-zet1s)/(zetHe+zet1s)
tH2p = (zetHe-zet2p)/(zetHe+zet2p)
kH2s = (zetHe**2.0d0+zet2s**2.0d0)/(zetHe**2.0d0-zet2s**2.0d0)
kH1s = (zetHe**2.0d0+zet1s**2.0d0)/(zetHe**2.0d0-zet1s**2.0d0)
kH2p = (zetHe**2.0d0+zet2p**2.0d0)/(zetHe**2.0d0-zet2p**2.0d0)

t12s = (zet1s-zet2s)/(zet1s+zet2s)
ovrs = (1.0d0+t12s)**2.5d0*(1.0d0-t12s)**2.5d0
Ns = 1.0d0/sqrt(1.0d0-ovrs**2.0d0)

do 10 k=0,20
  i = 18
  phia = i+0.0d0
  phia = phia*10.0d0*(pi/180.0d0)
  j = 9
  the = j+0.0d0
  the = the*10.0d0*(pi/180.0d0)
  ra = k+0.0d0
```

```

    ra = ra*0.20d0+1.6d0
    cosa = cos(phia)
    sina = sin(phia)
    rHe = zetHe*ra*boh
    rHe2 = rHe**2.0d0
c   <1s|2s>
    rho = zet2s*ra*boh
    rho2 = rho**2.0d0
    rhoa = 0.5d0*(rHe+rho)
    cont = sqrt(1.0d0-tH2s**2.0d0)/(sqrt(3.0d0)*tH2s*rhoa)
    Heter = -(1.0d0-kH2s)*(2.0d0*(1.0d0+kH2s)*(2.0d0-3.0d0*
#      kH2s)+(1.0d0-2.0d0*kH2s)*rHe)*exp(-rHe)
    Clter = (1.0d0+kH2s)*(2.0d0*(1.0d0-kH2s)*(2.0d0-3.0d0*
#      kH2s)+4.0d0*(1.0d0-kH2s)*rho+rho2)*exp(-rho)
    OH2s = cont*(Heter+Clter)
c   <1s|2s'>
    rho = zet1s*ra*boh
    rho2 = rho**2.0d0
    rhoa = 0.5d0*(rHe+rho)
    cont = sqrt(1.0d0-tH1s**2.0d0)/(sqrt(3.0d0)*tH1s*rhoa)
    Heter = -(1.0d0-kH1s)*(2.0d0*(1.0d0+kH1s)*(2.0d0-3.0d0*
#      kH1s)+(1.0d0-2.0d0*kH1s)*rHe)*exp(-rHe)
    Clter = (1.0d0+kH1s)*(2.0d0*(1.0d0-kH1s)*(2.0d0-3.0d0*
#      kH1s)+4.0d0*(1.0d0-kH1s)*rho+rho2)*exp(-rho)
    OH1s = cont*(Heter+Clter)
    S = (OH2s-ovrs*OH1s)*Ns
    Ts = 4.0d0*(0.2837*S**2.0d0/(1.0d0-S**2.0d0))*
#      627.51d0
c   <1s|2p>
    rho = zet2p*ra*boh
    rho2 = rho**2.0d0
    rho3 = rho**3.0d0
    rhoa = 0.5d0*(rHe+rho)
    rhoa2 = rhoa**2.0d0
    cont = (1.0d0/(tH2p*rhoa2))*sqrt((1.0d0+tH2p)/(1.0d0-tH2p))
    Heter = -(1.0d0-kH2p)**2.0d0*(6.0d0*(1.0d0+kH2p)*(1.0d0+rHe)
#      +2.0d0*rHe2)*exp(-rHe)
    Clter = (1.0d0+kH2p)*(6.0d0*(1.0d0-kH2p)**2.0d0*(1.0d0+rho)+
#      4.0d0*(1.0d0-kH2p)*rho2+rho3)*exp(-rho)
    OH2p = cont*(Heter+Clter)
    Psg = cosa*OH2p
    Ppi = sina*OH2p
    Tsg = 0.0946d0*Psg**2.0d0/(1.0d0-Psg**2.0d0)*627.51d0
    Tpi = (0.3369d0*Ppi**2.0d0/(1.0d0-Ppi**2.0d0))*
#      627.51d0
    Exr = Ts+Tsg+Tpi
c   write(*,200) ra,ra/dist,Exr
c   write(*,200) ra/dist,Ts,Tsg,Tpi,Exr
10 continue
200 format(5f15.7)

write(*,*) ' R T Num '

do 20 i=0,20
  phia = i+0.0d0
  phia = (phia*10.0d0+80.0d0)*(pi/180.d0)
  j = 9

```

```

the = j+0.0d0
the = the*10.0d0*(pi/180.0d0)
do 15 k=0,20
c   ra = 1.826d0
    zero=0.8*dist
    amax=1.1*dist
    step=(amax-zero)/20.0d0
c   ra = k+0.0d0
    ra = ra*0.05d0+2.4d0
    ra = ra*step+zero
    cosa = cos(phia)
    sina = sin(phia)
    rHe = zetHe*ra*boh
    rHe2 = rHe**2.0d0
c   <1s|2s>
    rho = zet2s*ra*boh
    rho2 = rho**2.0d0
    rhoa = 0.5d0*(rHe+rho)
    cont = sqrt(1.0d0-tH2s**2.0d0)/(sqrt(3.0d0)*tH2s*rhoa)
    Heter = -(1.0d0-kH2s)*(2.0d0*(1.0d0+kH2s)*(2.0d0-3.0d0*
#           kH2s)+(1.0d0-2.0d0*kH2s)*rHe)*exp(-rHe)
    Clter = (1.0d0+kH2s)*(2.0d0*(1.0d0-kH2s)*(2.0d0-3.0d0*
#           kH2s)+4.0d0*(1.0d0-kH2s)*rho+rho2)*exp(-rho)
    OH2s = cont*(Heter+Clter)
c   <1s|2s'>
    rho = zet1s*ra*boh
    rho2 = rho**2.0d0
    rhoa = 0.5d0*(rHe+rho)
    cont = sqrt(1.0d0-tH1s**2.0d0)/(sqrt(3.0d0)*tH1s*rhoa)
    Heter = -(1.0d0-kH1s)*(2.0d0*(1.0d0+kH1s)*(2.0d0-3.0d0*
#           kH1s)+(1.0d0-2.0d0*kH1s)*rHe)*exp(-rHe)
    Clter = (1.0d0+kH1s)*(2.0d0*(1.0d0-kH1s)*(2.0d0-3.0d0*
#           kH1s)+4.0d0*(1.0d0-kH1s)*rho+rho2)*exp(-rho)
    OH1s = cont*(Heter+Clter)
    S = (OH2s-ovrs*OH1s)*Ns
    Ts = 4.0d0*(0.2837d0*S**2.0d0/(1.0d0-S**2.0d0))*
#           627.51d0
c   <1s|2p>
    rho = zet2p*ra*boh
    rho2 = rho**2.0d0
    rho3 = rho**3.0d0
    rhoa = 0.5d0*(rHe+rho)
    rhoa2 = rhoa**2.0d0
    cont = (1.0d0/(tH2p*rhoa2))*sqrt((1.0d0+tH2p)/(1.0d0-tH2p))
    Heter = -(1.0d0-kH2p)**2.0d0*(6.0d0*(1.0d0+kH2p)*(1.0d0+rHe)
#           +2.0d0*rHe2)*exp(-rHe)
    Clter = (1.0d0+kH2p)*(6.0d0*(1.0d0-kH2p)**2.0d0*(1.0d0+rho)+
#           4.0d0*(1.0d0-kH2p)*rho2+rho3)*exp(-rho)
    OH2p = cont*(Heter+Clter)
    Psg = cosa*OH2p
    Ppi = sina*OH2p
    Tsg = 3.0d0*0.0946d0*Psg**2.0d0/(1.0d0-Psg**2.0d0)*627.51d0
    Tpi = 4.0d0*(0.3369d0*Ppi**2.0d0/(1.0d0-Ppi**2.0d0))*
#           627.51d0
    Exr = Ts+Tsg+Tpi
c   write(*,200) ra/dist,180.0d0*phia/pi,Exr
    write(*,200) ra,180.0d0*phia/pi,Exr

```



```

c      write(*,200) cosa,Ts,Tsg,Tpi,Exr
15 continue
20 continue

stop
end

Program Overlap_Cl_tot

implicit none

real*8 pi,ang,boh,lam,zetHe,zet2s,zet1s,zet2p,zet1p,zH2s
real*8 zH1s,zH2p,zH1p,tH2s,tH1s,tH2p,tH1p,t12s,t12p,ovrs
real*8 ovrp,Ns,Np,xCl,yCl,zCl,phia,the,ra,xHe,yHe,zHe
real*8 cosa,sina,rHe,rHe2,rho,rho2,rho3,rhoa,rhoa2,cont
real*8 Heter,Clter,OH2s,OH1s,S,Ts,OH2p,OH1p,Psg,Ppi
real*8 Tsg,Tpi,Exr,kH2s,kH1s,kH2p,kH1p
real*8 zero,amax,step,dist

integer*4 i,j,k

pi = 2.0d0*dacos(0.0d0)
ang = 0.5291771d0
boh = 1/ang
lam = 0.662613d0

dist=1.62d0+1.40d0
c dist=1.75d0+1.40d0

zetHe = 1.69d0
zet1s = 5.413733d0
zet2s = 2.077413d0
zet1p = 6.093864d0
zet2p = 1.371594d0
zH2s = 0.5d0*(zetHe+zet2s)
zH1s = 0.5d0*(zetHe+zet1s)
zH2p = 0.5d0*(zetHe+zet2p)
zH1p = 0.5d0*(zetHe+zet1p)
tH2s = (zetHe-zet2s)/(zetHe+zet2s)
tH1s = (zetHe-zet1s)/(zetHe+zet1s)
tH2p = (zetHe-zet2p)/(zetHe+zet2p)
tH1p = (zetHe-zet1p)/(zetHe+zet1p)
kH2s = (zetHe**2.0d0+zet2s**2.0d0)/(zetHe**2.0d0-zet2s**2.0d0)
kH1s = (zetHe**2.0d0+zet1s**2.0d0)/(zetHe**2.0d0-zet1s**2.0d0)
kH2p = (zetHe**2.0d0+zet2p**2.0d0)/(zetHe**2.0d0-zet2p**2.0d0)
kH1p = (zetHe**2.0d0+zet1p**2.0d0)/(zetHe**2.0d0-zet1p**2.0d0)

t12s = (zet1s-zet2s)/(zet1s+zet2s)
t12p = (zet1p-zet2p)/(zet1p+zet2p)
ovrs = (1.0d0+t12s)**2.5d0*(1.0d0-t12s)**2.5d0
ovrp = (1.0d0+t12p)**2.5d0*(1.0d0-t12p)**2.5d0
Ns = 1.0d0/sqrt(1.0d0-ovrs**2.0d0)
Np = 1.0d0/sqrt(1.0d0-ovrp**2.0d0)

do 10 k=0,20
  i = 18
  phia = i+0.0d0

```

```

    phia = phia*10.0d0*(pi/180.0d0)
    j     = 9
    the   = j+0.0d0
    the   = the*10.0d0*(pi/180.0d0)
    ra    = k+0.0d0
    ra    = ra*0.20d0+1.6d0
    cosa  = cos(phia)
    sina  = sin(phia)
    rHe   = zetHe*ra*boh
    rHe2  = rHe**2.0d0
c   <1s|2s>
    rho   = zet2s*ra*boh
    rho2  = rho**2.0d0
    rhoa  = 0.5d0*(rHe+rho)
    cont  = sqrt(1.0d0-tH2s**2.0d0)/(sqrt(3.0d0)*tH2s*rhoa)
    Heter = -(1.0d0-kH2s)*(2.0d0*(1.0d0+kH2s)*(2.0d0-3.0d0*
#         kH2s)+(1.0d0-2.0d0*kH2s)*rHe)*exp(-rHe)
    Clter = (1.0d0+kH2s)*(2.0d0*(1.0d0-kH2s)*(2.0d0-3.0d0*
#         kH2s)+4.0d0*(1.0d0-kH2s)*rho+rho2)*exp(-rho)
    OH2s  = cont*(Heter+Clter)
c   <1s|2s'>
    rho   = zet1s*ra*boh
    rho2  = rho**2.0d0
    rhoa  = 0.5d0*(rHe+rho)
    cont  = sqrt(1.0d0-tH1s**2.0d0)/(sqrt(3.0d0)*tH1s*rhoa)
    Heter = -(1.0d0-kH1s)*(2.0d0*(1.0d0+kH1s)*(2.0d0-3.0d0*
#         kH1s)+(1.0d0-2.0d0*kH1s)*rHe)*exp(-rHe)
    Clter = (1.0d0+kH1s)*(2.0d0*(1.0d0-kH1s)*(2.0d0-3.0d0*
#         kH1s)+4.0d0*(1.0d0-kH1s)*rho+rho2)*exp(-rho)
    OH1s  = cont*(Heter+Clter)
    S     = (OH2s-ovrs*OH1s)*Ns
    Ts    = 2.0d0*(1.13326d0*S**2.0d0/(1.0d0-S**2.0d0))*lam*
#         627.51d0
c   <1s|2p>
    rho   = zet2p*ra*boh
    rho2  = rho**2.0d0
    rho3  = rho**3.0d0
    rhoa  = 0.5d0*(rHe+rho)
    rhoa2 = rhoa**2.0d0
    cont  = (1.0d0/(tH2p*rhoa2))*sqrt((1.0d0+tH2p)/(1.0d0-tH2p))
    Heter = -(1.0d0-kH2p)**2.0d0*(6.0d0*(1.0d0+kH2p)*(1.0d0+rHe)
#         +2.0d0*rHe2)*exp(-rHe)
    Clter = (1.0d0+kH2p)*(6.0d0*(1.0d0-kH2p)**2.0d0*(1.0d0+rho)+
#         4.0d0*(1.0d0-kH2p)*rho2+rho3)*exp(-rho)
    OH2p  = cont*(Heter+Clter)
c   <1s|2p'>
    rho   = zet1p*ra*boh
    rho2  = rho**2.0d0
    rho3  = rho**3.0d0
    rhoa  = 0.5d0*(rHe+rho)
    rhoa2 = rhoa**2.0d0
    cont  = (1.0d0/(tH1p*rhoa2))*sqrt((1.0d0+tH1p)/(1.0d0-tH1p))
    Heter = -(1.0d0-kH1p)**2.0d0*(6.0d0*(1.0d0+kH1p)*(1.0d0+rHe)
#         +2.0d0*rHe2)*exp(-rHe)
    Clter = (1.0d0+kH1p)*(6.0d0*(1.0d0-kH1p)**2.0d0*(1.0d0+rho)+
#         4.0d0*(1.0d0-kH1p)*rho2+rho3)*exp(-rho)
    OH1p  = cont*(Heter+Clter)

```

```

Psg = cosa*(OH2p-ovrp*OH1p)*Np
Ppi = sina*(OH2p-ovrp*OH1p)*Np
Tsg = 0.57601*Psg**2.0d0/(1.0d0-Psg**2.0d0)*lam*627.51d0
Tpi = 2.0d0*(0.50148*Ppi**2.0d0/(1.0d0-Ppi**2.0d0))*lam*
#      627.51d0
Exr = Ts+Tsg+Tpi
c      write(*,200) ra,Ts,Tsg,Tpi,Exr
10 continue
200 format(5f15.7)

write(*,*) ' R T Num '

do 20 i=0,20
  phia = i+0.0d0
  phia = (phia*10.0d0+80.0d0)*(pi/180.0d0)
  j = 9
  the = j+0.0d0
  the = the*10.0d0*(pi/180.0d0)
do 15 k=0,20
c      ra = 2.082d0
  zero=0.8*dist
  amax=1.1*dist
  step=(amax-zero)/20.0d0
  ra = k+0.0d0
c      ra = ra*0.05d0+2.4d0
  ra = ra*step+zero

c      ra = 2.224d0
  cosa = cos(phia)
  sina = sin(phia)
  rHe = zetHe*ra*boh
  rHe2 = rHe**2.0d0
c      <1s|2s>
  rho = zet2s*ra*boh
  rho2 = rho**2.0d0
  rhoa = 0.5d0*(rHe+rho)
  cont = sqrt(1.0d0-tH2s**2.0d0)/(sqrt(3.0d0)*tH2s*rhoa)
  Heter = -(1.0d0-kH2s)*(2.0d0*(1.0d0+kH2s)*(2.0d0-3.0d0*
#      kH2s)+(1.0d0-2.0d0*kH2s)*rHe)*exp(-rHe)
  Clter = (1.0d0+kH2s)*(2.0d0*(1.0d0-kH2s)*(2.0d0-3.0d0*
#      kH2s)+4.0d0*(1.0d0-kH2s)*rho+rho2)*exp(-rho)
  OH2s = cont*(Heter+Clter)
c      <1s|2s'>
  rho = zet1s*ra*boh
  rho2 = rho**2.0d0
  rhoa = 0.5d0*(rHe+rho)
  cont = sqrt(1.0d0-tH1s**2.0d0)/(sqrt(3.0d0)*tH1s*rhoa)
  Heter = -(1.0d0-kH1s)*(2.0d0*(1.0d0+kH1s)*(2.0d0-3.0d0*
#      kH1s)+(1.0d0-2.0d0*kH1s)*rHe)*exp(-rHe)
  Clter = (1.0d0+kH1s)*(2.0d0*(1.0d0-kH1s)*(2.0d0-3.0d0*
#      kH1s)+4.0d0*(1.0d0-kH1s)*rho+rho2)*exp(-rho)
  OH1s = cont*(Heter+Clter)
  S = (OH2s-ovrs*OH1s)*Ns
  Ts = 4.0d0*(0.5449d0*S**2.0d0/(1.0d0-S**2.0d0))*
#      627.51d0
c      <1s|2p>
  rho = zet2p*ra*boh

```

```

        rho2 = rho**2.0d0
        rho3 = rho**3.0d0
        rhoa = 0.5d0*(rHe+rho)
        rhoa2 = rhoa**2.0d0
        cont = (1.0d0/(tH2p*rhoa2))*sqrt((1.0d0+tH2p)/(1.0d0-tH2p))
        Heter = -(1.0d0-kH2p)**2.0d0*(6.0d0*(1.0d0+kH2p)*(1.0d0+rHe)
#           +2.0d0*rHe2)*exp(-rHe)
        Clter = (1.0d0+kH2p)*(6.0d0*(1.0d0-kH2p)**2.0d0*(1.0d0+rho)+
#           4.0d0*(1.0d0-kH2p)*rho2+rho3)*exp(-rho)
        OH2p = cont*(Heter+Clter)
c   <1s|2p'>
        rho = zet1p*ra*boh
        rho2 = rho**2.0d0
        rho3 = rho**3.0d0
        rhoa = 0.5d0*(rHe+rho)
        rhoa2 = rhoa**2.0d0
        cont = (1.0d0/(tH1p*rhoa2))*sqrt((1.0d0+tH1p)/(1.0d0-tH1p))
        Heter = -(1.0d0-kH1p)**2.0d0*(6.0d0*(1.0d0+kH1p)*(1.0d0+rHe)
#           +2.0d0*rHe2)*exp(-rHe)
        Clter = (1.0d0+kH1p)*(6.0d0*(1.0d0-kH1p)**2.0d0*(1.0d0+rho)+
#           4.0d0*(1.0d0-kH1p)*rho2+rho3)*exp(-rho)
        OH1p = cont*(Heter+Clter)
        Psg = cosa*(OH2p-ovrp*OH1p)*Np
        Ppi = sina*(OH2p-ovrp*OH1p)*Np
        Tsg = 3.0d0*0.0903d0*Psg**2.0d0/(1.0d0-Psg**2.0d0)*627.51d0
        Tpi = 4.0d0*(0.2336d0*Ppi**2.0d0/(1.0d0-Ppi**2.0d0))*
#           627.51d0
        Exr = Ts+Tsg+Tpi
c   write(*,200) cosa,Ts,Tsg,Tpi,Exr
        write(*,200) ra/dist,180.0d0*phia/pi,Exr

```

15 continue

20 continue

stop
end

Program Overlap_Br_tot

implicit none

```

real*8 pi,ang,boh,lam,zetHe,zet2s,zet1s,zet2p,zet1p,zH2s
real*8 zH1s,zH2p,zH1p,tH2s,tH1s,tH2p,tH1p,t12s,t12p,ovrs
real*8 ovrp,Ns,Np,xBr,yBr,zBr,phia,the,ra,xHe,yHe,zHe
real*8 cosa,sina,rHe,rHe2,rho,rho2,rho3,rhoa,rhoa2,cont
real*8 Heter,Clter,OH2s,OH1s,S,Ts,OH2p,OH1p,Psg,Ppi
real*8 Tsg,Tpi,Exr,kH2s,kH1s,kH2p,kH1p
real*8 zero,amax,step,dist

```

integer*4 i,j,k

```

pi = 2.0d0*dacos(0.0d0)
ang = 0.5291771d0
boh = 1/ang
lam = 0.729313d0

```

dist=1.80d0+1.40d0

```

c      dist=1.85d0+1.40d0

zetHe = 1.69d0
zet1s = 4.357680d0
zet2s = 1.896394d0
zet1p = 4.362203d0
zet2p = 1.272221d0
zH2s = 0.5d0*(zetHe+zet2s)
zH1s = 0.5d0*(zetHe+zet1s)
zH2p = 0.5d0*(zetHe+zet2p)
zH1p = 0.5d0*(zetHe+zet1p)
tH2s = (zetHe-zet2s)/(zetHe+zet2s)
tH1s = (zetHe-zet1s)/(zetHe+zet1s)
tH2p = (zetHe-zet2p)/(zetHe+zet2p)
tH1p = (zetHe-zet1p)/(zetHe+zet1p)
kH2s = (zetHe**2.0d0+zet2s**2.0d0)/(zetHe**2.0d0-zet2s**2.0d0)
kH1s = (zetHe**2.0d0+zet1s**2.0d0)/(zetHe**2.0d0-zet1s**2.0d0)
kH2p = (zetHe**2.0d0+zet2p**2.0d0)/(zetHe**2.0d0-zet2p**2.0d0)
kH1p = (zetHe**2.0d0+zet1p**2.0d0)/(zetHe**2.0d0-zet1p**2.0d0)

t12s = (zet1s-zet2s)/(zet1s+zet2s)
t12p = (zet1p-zet2p)/(zet1p+zet2p)
ovrs = (1.0d0+t12s)**2.5d0*(1.0d0-t12s)**2.5d0
ovrp = (1.0d0+t12p)**2.5d0*(1.0d0-t12p)**2.5d0
Ns    = 1.0d0/sqrt(1.0d0-ovrs**2.0d0)
Np    = 1.0d0/sqrt(1.0d0-ovrp**2.0d0)

do 10 k=0,20
  i    = 18
  phia = i+0.0d0
  phia = phia*10.0d0*(pi/180.0d0)
  j    = 9
  the  = j+0.0d0
  the  = the*10.0d0*(pi/180.0d0)
  ra   = k+0.0d0
  ra   = ra*0.20d0+1.6d0
  cosa = cos(phia)
  sina = sin(phia)
  rHe  = zetHe*ra*boh
  rHe2 = rHe**2.0d0
c      <1s|2s>
  rho  = zet2s*ra*boh
  rho2 = rho**2.0d0
  rhoa = 0.5d0*(rHe+rho)
  cont = sqrt(1.0d0-tH2s**2.0d0)/(sqrt(3.0d0)*tH2s*rhoa)
  Heter = -(1.0d0-kH2s)*(2.0d0*(1.0d0+kH2s)*(2.0d0-3.0d0*
#          kH2s)+(1.0d0-2.0d0*kH2s)*rHe)*exp(-rHe)
  Clter = (1.0d0+kH2s)*(2.0d0*(1.0d0-kH2s)*(2.0d0-3.0d0*
#          kH2s)+4.0d0*(1.0d0-kH2s)*rho+rho2)*exp(-rho)
  OH2s = cont*(Heter+Clter)
c      <1s|2s'>
  rho  = zet1s*ra*boh
  rho2 = rho**2.0d0
  rhoa = 0.5d0*(rHe+rho)
  cont = sqrt(1.0d0-tH1s**2.0d0)/(sqrt(3.0d0)*tH1s*rhoa)
  Heter = -(1.0d0-kH1s)*(2.0d0*(1.0d0+kH1s)*(2.0d0-3.0d0*
#          kH1s)+(1.0d0-2.0d0*kH1s)*rHe)*exp(-rHe)

```

```

      Clter = (1.0d0+kH1s) * (2.0d0 * (1.0d0-kH1s) * (2.0d0-3.0d0 *
#           kH1s)+4.0d0 * (1.0d0-kH1s) * rho+rho2) * exp(-rho)
      OH1s = cont * (Heter+Clter)
      S     = (OH2s-ovrs*OH1s) * Ns
      Ts    = 2.0d0 * (1.03426d0 * S**2.0d0 / (1.0d0-S**2.0d0)) * lam*
#           627.51d0
c    <1s|2p>
      rho   = zet2p*ra*boh
      rho2  = rho**2.0d0
      rho3  = rho**3.0d0
      rhoa  = 0.5d0 * (rHe+rho)
      rhoa2 = rhoa**2.0d0
      cont  = (1.0d0 / (tH2p*rhoa2)) * sqrt((1.0d0+tH2p) / (1.0d0-tH2p))
      Heter = -(1.0d0-kH2p) **2.0d0 * (6.0d0 * (1.0d0+kH2p) * (1.0d0+rHe)
#           +2.0d0*rHe2) * exp(-rHe)
      Clter = (1.0d0+kH2p) * (6.0d0 * (1.0d0-kH2p) **2.0d0 * (1.0d0+rho) +
#           4.0d0 * (1.0d0-kH2p) * rho2+rho3) * exp(-rho)
      OH2p  = cont * (Heter+Clter)
c    <1s|2p'>
      rho   = zet1p*ra*boh
      rho2  = rho**2.0d0
      rho3  = rho**3.0d0
      rhoa  = 0.5d0 * (rHe+rho)
      rhoa2 = rhoa**2.0d0
      cont  = (1.0d0 / (tH1p*rhoa2)) * sqrt((1.0d0+tH1p) / (1.0d0-tH1p))
      Heter = -(1.0d0-kH1p) **2.0d0 * (6.0d0 * (1.0d0+kH1p) * (1.0d0+rHe)
#           +2.0d0*rHe2) * exp(-rHe)
      Clter = (1.0d0+kH1p) * (6.0d0 * (1.0d0-kH1p) **2.0d0 * (1.0d0+rho) +
#           4.0d0 * (1.0d0-kH1p) * rho2+rho3) * exp(-rho)
      OH1p  = cont * (Heter+Clter)
      Psg   = cosa * (OH2p-ovrp*OH1p) * Np
      Ppi   = sina * (OH2p-ovrp*OH1p) * Np
      Tsg   = 0.51711d0 * Psg**2.0d0 / (1.0d0-Psg**2.0d0) * lam*627.51d0
      Tpi   = 2.0d0 * (0.45011d0 * Ppi**2.0d0 / (1.0d0-Ppi**2.0d0)) * lam*
#           627.51d0
      Exr   = Ts+Tsg+Tpi
c    write(*,200) ra,Ts,Tsg,Tpi,Exr
10 continue
200 format(5f15.7)

      write(*,*) ' R T Num '

      do 20 i=0,20
        phia = i+0.0d0
        phia = (phia*10.0d0+80.0d0) * (pi/180.d0)
        j     = 9
        the   = j+0.0d0
        the   = the*10.0d0 * (pi/180.0d0)
c      ra    = 2.356d0
c      do 15 k=0,20
c      ra    = 2.082d0
        zero=0.8*dist
        amax=1.1*dist
        step=(amax-zero)/20.0d0
        ra   = k+0.0d0
c      ra    = ra*0.05d0+2.4d0
c      ra    = ra*step+zero

```

```

    cosa = cos(phia)
    sina = sin(phia)
    rHe  = zetHe*ra*boh
    rHe2 = rHe**2.0d0
c   <1s|2s>
    rho  = zet2s*ra*boh
    rho2 = rho**2.0d0
    rhoa = 0.5d0*(rHe+rho)
    cont = sqrt(1.0d0-tH2s**2.0d0)/(sqrt(3.0d0)*tH2s*rhoa)
    Heter = -(1.0d0-kH2s)*(2.0d0*(1.0d0+kH2s)*(2.0d0-3.0d0*
#      kH2s)+(1.0d0-2.0d0*kH2s)*rHe)*exp(-rHe)
    Clter = (1.0d0+kH2s)*(2.0d0*(1.0d0-kH2s)*(2.0d0-3.0d0*
#      kH2s)+4.0d0*(1.0d0-kH2s)*rho+rho2)*exp(-rho)
    OH2s = cont*(Heter+Clter)
c   <1s|2s'>
    rho  = zet1s*ra*boh
    rho2 = rho**2.0d0
    rhoa = 0.5d0*(rHe+rho)
    cont = sqrt(1.0d0-tH1s**2.0d0)/(sqrt(3.0d0)*tH1s*rhoa)
    Heter = -(1.0d0-kH1s)*(2.0d0*(1.0d0+kH1s)*(2.0d0-3.0d0*
#      kH1s)+(1.0d0-2.0d0*kH1s)*rHe)*exp(-rHe)
    Clter = (1.0d0+kH1s)*(2.0d0*(1.0d0-kH1s)*(2.0d0-3.0d0*
#      kH1s)+4.0d0*(1.0d0-kH1s)*rho+rho2)*exp(-rho)
    OH1s = cont*(Heter+Clter)
    S     = (OH2s-ovrs*OH1s)*Ns
    Ts    = 4.0d0*(0.6130d0*S**2.0d0/(1.0d0-S**2.0d0))*
#      627.51d0
c   <1s|2p>
    rho  = zet2p*ra*boh
    rho2 = rho**2.0d0
    rho3 = rho**3.0d0
    rhoa = 0.5d0*(rHe+rho)
    rhoa2 = rhoa**2.0d0
    cont = (1.0d0/(tH2p*rhoa2))*sqrt((1.0d0+tH2p)/(1.0d0-tH2p))
    Heter = -(1.0d0-kH2p)**2.0d0*(6.0d0*(1.0d0+kH2p)*(1.0d0+rHe)
#      +2.0d0*rHe2)*exp(-rHe)
    Clter = (1.0d0+kH2p)*(6.0d0*(1.0d0-kH2p)**2.0d0*(1.0d0+rho)+
#      4.0d0*(1.0d0-kH2p)*rho2+rho3)*exp(-rho)
    OH2p = cont*(Heter+Clter)
c   <1s|2p'>
    rho  = zet1p*ra*boh
    rho2 = rho**2.0d0
    rho3 = rho**3.0d0
    rhoa = 0.5d0*(rHe+rho)
    rhoa2 = rhoa**2.0d0
    cont = (1.0d0/(tH1p*rhoa2))*sqrt((1.0d0+tH1p)/(1.0d0-tH1p))
    Heter = -(1.0d0-kH1p)**2.0d0*(6.0d0*(1.0d0+kH1p)*(1.0d0+rHe)
#      +2.0d0*rHe2)*exp(-rHe)
    Clter = (1.0d0+kH1p)*(6.0d0*(1.0d0-kH1p)**2.0d0*(1.0d0+rho)+
#      4.0d0*(1.0d0-kH1p)*rho2+rho3)*exp(-rho)
    OH1p = cont*(Heter+Clter)
    Psg  = cosa*(OH2p-ovrp*OH1p)*Np
    Ppi  = sina*(OH2p-ovrp*OH1p)*Np
    Tsg  = 3.0d0*0.0669d0*Psg**2.0d0/(1.0d0-Psg**2.0d0)*627.51d0
    Tpi  = 4.0d0*(0.2233d0*Ppi**2.0d0/(1.0d0-Ppi**2.0d0))*
#      627.51d0

```

```

      Exr      = Ts+Tsg+Tpi
      write(*,200) ra/dist,180.0d0*phia/pi,Exr
c      write(*,200) cosa,Ts,Tsg,Tpi,Exr
15 continue
20 continue

      stop
      end

      Program Overlap_I_tot

      implicit none

      real*8 pi,ang,boh,lam,zetHe,zet2s,zet1s,zet2p,zet1p,zH2s
      real*8 zH1s,zH2p,zH1p,tH2s,tH1s,tH2p,tH1p,t12s,t12p,ovrs
      real*8 ovrp,Ns,Np,xI,yI,zI,phia,the,ra,xHe,yHe,zHe
      real*8 cosa,sina,rHe,rHe2,rho,rho2,rho3,rhoa,rhoa2,cont
      real*8 Heter,Clter,OH2s,OH1s,S,Ts,OH2p,OH1p,Psg,Ppi
      real*8 Tsg,Tpi,Exr,kH2s,kH1s,kH2p,kH1p
      real*8 zero,amax,step,dist

      integer*4 i,j,k

      pi = 2.0d0*dacos(0.0d0)
      ang = 0.5291771d0
      boh = 1/ang
      lam = 0.908426d0

c      dist=1.98d0+1.40d0
      dist=1.98d0+1.40d0

      zetHe = 1.69d0
      zet1s = 3.766487d0
      zet2s = 1.739151d0
      zet1p = 3.201268d0
      zet2p = 1.165130d0
      zH2s = 0.5d0*(zetHe+zet2s)
      zH1s = 0.5d0*(zetHe+zet1s)
      zH2p = 0.5d0*(zetHe+zet2p)
      zH1p = 0.5d0*(zetHe+zet1p)
      tH2s = (zetHe-zet2s)/(zetHe+zet2s)
      tH1s = (zetHe-zet1s)/(zetHe+zet1s)
      tH2p = (zetHe-zet2p)/(zetHe+zet2p)
      tH1p = (zetHe-zet1p)/(zetHe+zet1p)
      kH2s = (zetHe**2.0d0+zet2s**2.0d0)/(zetHe**2.0d0-zet2s**2.0d0)
      kH1s = (zetHe**2.0d0+zet1s**2.0d0)/(zetHe**2.0d0-zet1s**2.0d0)
      kH2p = (zetHe**2.0d0+zet2p**2.0d0)/(zetHe**2.0d0-zet2p**2.0d0)
      kH1p = (zetHe**2.0d0+zet1p**2.0d0)/(zetHe**2.0d0-zet1p**2.0d0)

      t12s = (zet1s-zet2s)/(zet1s+zet2s)
      t12p = (zet1p-zet2p)/(zet1p+zet2p)
      ovrs = (1.0d0+t12s)**2.5d0*(1.0d0-t12s)**2.5d0
      ovrp = (1.0d0+t12p)**2.5d0*(1.0d0-t12p)**2.5d0
      Ns = 1.0d0/sqrt(1.0d0-ovrs**2.0d0)
      Np = 1.0d0/sqrt(1.0d0-ovrp**2.0d0)

      do 10 k=0,20

```



```

i      = 18
phia  = i+0.0d0
phia  = phia*10.0d0*(pi/180.0d0)
j      = 9
the   = j+0.0d0
the   = the*10.0d0*(pi/180.0d0)
ra    = k+0.0d0
ra    = ra*0.20d0+1.6d0
cosa  = cos(phia)
sina  = sin(phia)
rHe   = zetHe*ra*boh
rHe2  = rHe**2.0d0
c      <1s|2s>
rho   = zet2s*ra*boh
rho2  = rho**2.0d0
rhoa  = 0.5d0*(rHe+rho)
cont  = sqrt(1.0d0-tH2s**2.0d0)/(sqrt(3.0d0)*tH2s*rhoa)
Heter = -(1.0d0-kH2s)*(2.0d0*(1.0d0+kH2s)*(2.0d0-3.0d0*
#       kH2s)+(1.0d0-2.0d0*kH2s)*rHe)*exp(-rHe)
Clter = (1.0d0+kH2s)*(2.0d0*(1.0d0-kH2s)*(2.0d0-3.0d0*
#       kH2s)+4.0d0*(1.0d0-kH2s)*rho+rho2)*exp(-rho)
OH2s  = cont*(Heter+Clter)
c      <1s|2s'>
rho   = zet1s*ra*boh
rho2  = rho**2.0d0
rhoa  = 0.5d0*(rHe+rho)
cont  = sqrt(1.0d0-tH1s**2.0d0)/(sqrt(3.0d0)*tH1s*rhoa)
Heter = -(1.0d0-kH1s)*(2.0d0*(1.0d0+kH1s)*(2.0d0-3.0d0*
#       kH1s)+(1.0d0-2.0d0*kH1s)*rHe)*exp(-rHe)
Clter = (1.0d0+kH1s)*(2.0d0*(1.0d0-kH1s)*(2.0d0-3.0d0*
#       kH1s)+4.0d0*(1.0d0-kH1s)*rho+rho2)*exp(-rho)
OH1s  = cont*(Heter+Clter)
S      = (OH2s-ovrs*OH1s)*Ns
Ts     = 2.0d0*(0.92284d0*S**2.0d0/(1.0d0-S**2.0d0))*lam*
#       627.51d0
c      <1s|2p>
rho   = zet2p*ra*boh
rho2  = rho**2.0d0
rho3  = rho**3.0d0
rhoa  = 0.5d0*(rHe+rho)
rhoa2 = rhoa**2.0d0
cont  = (1.0d0/(tH2p*rhoa2))*sqrt((1.0d0+tH2p)/(1.0d0-tH2p))
Heter = -(1.0d0-kH2p)**2.0d0*(6.0d0*(1.0d0+kH2p)*(1.0d0+rHe)
#       +2.0d0*rHe2)*exp(-rHe)
Clter = (1.0d0+kH2p)*(6.0d0*(1.0d0-kH2p)**2.0d0*(1.0d0+rho)+
#       4.0d0*(1.0d0-kH2p)*rho2+rho3)*exp(-rho)
OH2p  = cont*(Heter+Clter)
c      <1s|2p'>
rho   = zet1p*ra*boh
rho2  = rho**2.0d0
rho3  = rho**3.0d0
rhoa  = 0.5d0*(rHe+rho)
rhoa2 = rhoa**2.0d0
cont  = (1.0d0/(tH1p*rhoa2))*sqrt((1.0d0+tH1p)/(1.0d0-tH1p))
Heter = -(1.0d0-kH1p)**2.0d0*(6.0d0*(1.0d0+kH1p)*(1.0d0+rHe)
#       +2.0d0*rHe2)*exp(-rHe)
Clter = (1.0d0+kH1p)*(6.0d0*(1.0d0-kH1p)**2.0d0*(1.0d0+rho)+

```

```

#           4.0d0*(1.0d0-kH1p)*rho2+rho3)*exp(-rho)
OH1p  = cont*(Heter+Clter)
Psg   = cosa*(OH2p-ovrp*OH1p)*Np
Ppi   = sina*(OH2p-ovrp*OH1p)*Np
Tsg   = 0.46010d0*Psg**2.0d0/(1.0d0-Psg**2.0d0)*lam*627.51d0
Tpi   = 2.0d0*(0.39962d0*Ppi**2.0d0/(1.0d0-Ppi**2.0d0))*lam*
#           627.51d0
Exr   = Ts+Tsg+Tpi
c     write(*,200) ra,Ts,Tsg,Tpi,Exr
10 continue
200 format(5f15.7)

write(*,*) ' R T Num '

do 20 i=0,20
  phia = i+0.0d0
  phia = (phia*10.0d0+80.0d0)*(pi/180.0d0)
  j     = 9
  the  = j+0.0d0
  the  = the*10.0d0*(pi/180.0d0)
c     ra  = 2.553d0
do 15 k=0,20
c     ra  = 2.082d0
  zero=0.8*dist
  amax=1.1*dist
  step=(amax-zero)/20.0d0
  ra   = k+0.0d0
c     ra  = ra*0.05d0+2.4d0
  ra   = ra*step+zero

  cosa = cos(phia)
  sina = sin(phia)
  rHe  = zetHe*ra*boh
  rHe2 = rHe**2.0d0
c     <1s|2s>
  rho  = zet2s*ra*boh
  rho2 = rho**2.0d0
  rhoa = 0.5d0*(rHe+rho)
  cont = sqrt(1.0d0-tH2s**2.0d0)/(sqrt(3.0d0)*tH2s*rhoa)
  Heter = -(1.0d0-kH2s)*(2.0d0*(1.0d0+kH2s)*(2.0d0-3.0d0*
#           kH2s)+(1.0d0-2.0d0*kH2s)*rHe)*exp(-rHe)
  Clter = (1.0d0+kH2s)*(2.0d0*(1.0d0-kH2s)*(2.0d0-3.0d0*
#           kH2s)+4.0d0*(1.0d0-kH2s)*rho+rho2)*exp(-rho)
  OH2s = cont*(Heter+Clter)
c     <1s|2s'>
  rho  = zet1s*ra*boh
  rho2 = rho**2.0d0
  rhoa = 0.5d0*(rHe+rho)
  cont = sqrt(1.0d0-tH1s**2.0d0)/(sqrt(3.0d0)*tH1s*rhoa)
  Heter = -(1.0d0-kH1s)*(2.0d0*(1.0d0+kH1s)*(2.0d0-3.0d0*
#           kH1s)+(1.0d0-2.0d0*kH1s)*rHe)*exp(-rHe)
  Clter = (1.0d0+kH1s)*(2.0d0*(1.0d0-kH1s)*(2.0d0-3.0d0*
#           kH1s)+4.0d0*(1.0d0-kH1s)*rho+rho2)*exp(-rho)
  OH1s = cont*(Heter+Clter)
  S    = (OH2s-ovrs*OH1s)*Ns
  Ts   = 4.0d0*(0.2135d0*S**2.0d0/(1.0d0-S**2.0d0))*
#           627.51d0

```

```

c      <1s|2p>
      rho  = zet2p*ra*boh
      rho2 = rho**2.0d0
      rho3 = rho**3.0d0
      rhoa = 0.5d0*(rHe+rho)
      rhoa2 = rhoa**2.0d0
      cont = (1.0d0/(tH2p*rhoa2))*sqrt((1.0d0+tH2p)/(1.0d0-tH2p))
      Heter = -(1.0d0-kH2p)**2.0d0*(6.0d0*(1.0d0+kH2p)*(1.0d0+rHe)
#         +2.0d0*rHe2)*exp(-rHe)
      Clter = (1.0d0+kH2p)*(6.0d0*(1.0d0-kH2p)**2.0d0*(1.0d0+rho)+
#         4.0d0*(1.0d0-kH2p)*rho2+rho3)*exp(-rho)
      OH2p = cont*(Heter+Clter)
c      <1s|2p'>
      rho  = zet1p*ra*boh
      rho2 = rho**2.0d0
      rho3 = rho**3.0d0
      rhoa = 0.5d0*(rHe+rho)
      rhoa2 = rhoa**2.0d0
      cont = (1.0d0/(tH1p*rhoa2))*sqrt((1.0d0+tH1p)/(1.0d0-tH1p))
      Heter = -(1.0d0-kH1p)**2.0d0*(6.0d0*(1.0d0+kH1p)*(1.0d0+rHe)
#         +2.0d0*rHe2)*exp(-rHe)
      Clter = (1.0d0+kH1p)*(6.0d0*(1.0d0-kH1p)**2.0d0*(1.0d0+rho)+
#         4.0d0*(1.0d0-kH1p)*rho2+rho3)*exp(-rho)
      OH1p = cont*(Heter+Clter)
      Psg  = cosa*(OH2p-ovrp*OH1p)*Np
      Ppi  = sina*(OH2p-ovrp*OH1p)*Np
      Tsg  = 3.0d0*0.0884d0*Psg**2.0d0/(1.0d0-Psg**2.0d0)*627.51d0
      Tpi  = 4.0d0*(0.2135d0*Ppi**2.0d0/(1.0d0-Ppi**2.0d0))*
#         627.51d0
      Exr  = Ts+Tsg+Tpi
      write(*,200) ra/dist,180.0d0*phia/pi,Exr
c      write(*,200) cosa,Ts,Tsg,Tpi,Exr
15 continue
20 continue

      stop
      end

```

Program A4.2. The Fortran 77 programs developed to calculate the ESP of the atomic halogens as a function of atomic radii and angle relative to $\phi_{2p\sigma}$.

```

Program Model_ESP_F

implicit none

real*8 pi,ang,boh,zet2s,zet1s,zet2p,zet1p,t22s,t12s
real*8 t11s,t22p,t12p,t11p,ovrs,ovrp,Ns,Np,xF,yF,zF
real*8 phi a,the,ra,xHe,yHe,zHe,cosa,cosa2,sina,sina2
real*8 nuc,rho,rho2,rho3,rho4,rho5,cont,con1,con2,con3
real*8 S3ter,D3ter,I22s,I12s,I11s,Ipsig,Ippi,Cpsig
real*8 Cppi,I22p,I12p,I11p,In2s,In2p,ESP
integer*4 i,j,k

pi = 2.0d0*dacos(0.0d0)
ang = 0.5291771d0

```

```

boh = 1/ang

zet1s = 14.043877d0
zet2s = 2.111385d0
zet2p = 2.182682d0
t22s = 0.0d0
t12s = (zet1s-zet2s)/(zet1s+zet2s)
t11s = 0.0d0
t22p = 0.0d0
ovrs = (1.0d0+t12s)**2.5d0*(1.0d0-t12s)**2.5d0
Ns = 1.0d0/(1.0d0-ovrs**2.0d0)

do 10 k=0,20
  i = 18
  phia = i+0.0d0
  phia = phia*10.0d0*(pi/180.0d0)
  j = 9
  the = j+0.0d0
  the = the*10.0d0*(pi/180.0d0)
  ra = k+0.0d0
  ra = ra*0.20d0+1.6d0
  cosa = cos(phia)
  cosa2 = cosa**2.0d0
  sina = sin(phia)
  sina2 = sina**2.0d0
  nuc = -7.0d0/(ra*boh)
c [a|2s2s]
  rho = zet2s*ra*boh
  rho2 = rho**2.0d0
  rho3 = rho**3.0d0
  cont = 1.0d0
  con1 = zet2s/rho
  S3ter = 1.0d0-(1.0d0+3.0d0*rho/2.0d0+rho2+rho3/3.0d0)*
# exp(-2.0d0*rho)
  I22s = cont*con1*S3ter
c [a|2s'2s]
  rho = (zet1s+zet2s)*ra*boh/2.0d0
  rho2 = rho**2.0d0
  rho3 = rho**3.0d0
  cont = (1.0d0+t12s)**2.5d0*(1.0d0-t12s)**2.5d0
  con1 = (zet1s+zet2s)/(rho*2.0d0)
  S3ter = 1.0d0-(1.0d0+3.0d0*rho/2.0d0+rho2+rho3/3.0d0)*
# exp(-2.0d0*rho)
  I12s = cont*con1*S3ter
c [a|2s'2s']
  rho = zet1s*ra*boh
  rho2 = rho**2.0d0
  rho3 = rho**3.0d0
  cont = 1.0d0
  con1 = zet1s/rho
  S3ter = 1.0d0-(1.0d0+3.0d0*rho/2.0d0+rho2+rho3/3.0d0)*
# exp(-2.0d0*rho)
  I11s = cont*con1*S3ter
  In2s = 2.0d0*(I22s-2.0d0*ovrs*I12s+ovrs**2.0d0*I11s)*Ns
c [a|2p2p]
  rho = zet2p*ra*boh
  rho2 = rho**2.0d0

```

```

rho3 = rho**3.0d0
rho4 = rho**4.0d0
rho5 = rho**5.0d0
cont = 1.0d0
con1 = zet2p/rho
con2 = 3.0d0*zet2p/rho3
con3 = (3.0d0/2.0d0)*zet2p/rho3
S3ter = 1.0d0-(1.0d0+3.0d0*rho/2.0d0+rho2+rho3/3.0d0)*
# exp(-2.0d0*rho)
D3ter = 1.0d0-(1.0d0+2.0d0*rho+2.0d0*rho2+4.0d0*rho3/
# 3.0d0+2.0d0*rho4/3.0d0+2.0d0*rho5/9.0d0)*
# exp(-2.0d0*rho)
Ipsig = cont*(con1*S3ter+con2*D3ter)
Ippi = cont*(con1*S3ter-con3*D3ter)
Cpsig = cosa2*Ipsig+sina2*Ippi
Cppi = sina2*Ipsig+cosa2*Ippi
I22p = 2.0d0*Ippi+Cpsig+2.0d0*Cppi
Esp = In2s+I22p+nuc
write(*,200) In2s,I22p,nuc,Esp*627.51d0
10 continue
200 format(4f13.7)

write(*,*) ' '

do 20 i=0,20
  phia = i+0.0d0
  phia = (phia*10.0d0+80.0d0)*(pi/180.0d0)
  j = 9
  the = j+0.0d0
  the = the*10.0d0*(pi/180.0d0)
  ra = 2.082d0
  xHe = xF+ra*sin(phia)*cos(the)
  yHe = yF+ra*sin(phia)*sin(the)
  zHe = zF+ra*cos(phia)
  cosa = cos(phia)
  cosa2 = cosa**2.0d0
  sina = sin(phia)
  sina2 = sina**2.0d0
  nuc = -7.0d0/(ra*boh)
c [a|2s2s]
  rho = zet2s*ra*boh
  rho2 = rho**2.0d0
  rho3 = rho**3.0d0
  cont = 1.0d0
  con1 = zet2s/rho
  S3ter = 1.0d0-(1.0d0+3.0d0*rho/2.0d0+rho2+rho3/3.0d0)*
# exp(-2.0d0*rho)
  I22s = cont*con1*S3ter
c [a|2s'2s]
  rho = (zet1s+zet2s)*ra*boh/2.0d0
  rho2 = rho**2.0d0
  rho3 = rho**3.0d0
  cont = (1.0d0+t12s)**2.5d0*(1.0d0-t12s)**2.5d0
  con1 = (zet1s+zet2s)/(rho*2.0d0)
  S3ter = 1.0d0-(1.0d0+3.0d0*rho/2.0d0+rho2+rho3/3.0d0)*
# exp(-2.0d0*rho)
  I12s = cont*con1*S3ter

```

```

c      [a|2s'2s']
      rho   = zet1s*ra*boh
      rho2  = rho**2.0d0
      rho3  = rho**3.0d0
      cont  = 1.0d0
      con1  = zet1s/rho
      S3ter = 1.0d0-(1.0d0+3.0d0*rho/2.0d0+rho2+rho3/3.0d0)*
#      exp(-2.0d0*rho)
      I11s  = cont*con1*S3ter
      In2s  = 2.0d0*(I22s-2.0d0*ovrs*I12s+ovrs**2.0d0*I11s)*Ns
c      [a|2p2p]
      rho   = zet2p*ra*boh
      rho2  = rho**2.0d0
      rho3  = rho**3.0d0
      rho4  = rho**4.0d0
      rho5  = rho**5.0d0
      cont  = 1.0d0
      con1  = zet2p/rho
      con2  = 3.0d0*zet2p/rho3
      con3  = (3.0d0/2.0d0)*zet2p/rho3
      S3ter = 1.0d0-(1.0d0+3.0d0*rho/2.0d0+rho2+rho3/3.0d0)*
#      exp(-2.0d0*rho)
      D3ter = 1.0d0-(1.0d0+2.0d0*rho+2.0d0*rho2+4.0d0*rho3/
#      3.0d0+2.0d0*rho4/3.0d0+2.0d0*rho5/9.0d0)*
#      exp(-2.0d0*rho)
      Ipsig = cont*(con1*S3ter+con2*D3ter)
      Ippi  = cont*(con1*S3ter-con3*D3ter)
      Cpsig = cosa2*Ipsig+sina2*Ippi
      Cppi  = sina2*Ipsig+cosa2*Ippi
      I22p  = 2.0d0*Ippi+Cpsig+2.0d0*Cppi
      Esp   = In2s+I22p+nuc
      write(*,200) In2s,I22p,nuc,ESP*627.51d0
20 continue

      stop
      end

Program Model_ESP_C1

implicit none

real*8 pi,ang,boh,zet2s,zet1s,zet2p,zet1p,t22s,t12s
real*8 t11s,t22p,t12p,t11p,ovrs,ovrp,Ns,Np,xCl,yCl,zCl
real*8 phi a,the,ra,xHe,yHe,zHe,cosa,cosa2,sina,sina2
real*8 nuc,rho,rho2,rho3,rho4,rho5,cont,con1,con2,con3
real*8 S3ter,D3ter,I22s,I12s,I11s,Ipsig,Ippi,Cpsig
real*8 Cppi,I22p,I12p,I11p,In2s,In2p,ESP
integer*4 i,j,k

pi   = 2.0d0*dacos(0.0d0)
ang  = 0.5291771d0
boh  = 1/ang

zet1s = 5.413733d0
zet2s = 2.077413d0
zet1p = 6.093864d0

```

```

zet2p = 1.371594d0
t22s = 0.0d0
t12s = (zet1s-zet2s)/(zet1s+zet2s)
t11s = 0.0d0
t22p = 0.0d0
t12p = (zet1p-zet2p)/(zet1p+zet2p)
t11p = 0.0d0
ovrs = (1.0d0+t12s)**2.5d0*(1.0d0-t12s)**2.5d0
ovrp = (1.0d0+t12p)**2.5d0*(1.0d0-t12p)**2.5d0
Ns = 1.0d0/(1.0d0-ovrs**2.0d0)
Np = 1.0d0/(1.0d0-ovrp**2.0d0)

do 10 k=0,20
  i = 18
  phia = i+0.0d0
  phia = phia*10.0d0*(pi/180.0d0)
  j = 9
  the = j+0.0d0
  the = the*10.0d0*(pi/180.0d0)
  ra = k+0.0d0
  ra = ra*0.20d0+1.6d0
  cosa = cos(phia)
  cosa2 = cosa**2.0d0
  sina = sin(phia)
  sina2 = sina**2.0d0
  nuc = -7.0d0/(ra*boh)
c [a|2s2s]
  rho = zet2s*ra*boh
  rho2 = rho**2.0d0
  rho3 = rho**3.0d0
  cont = 1.0d0
  con1 = zet2s/rho
  S3ter = 1.0d0-(1.0d0+3.0d0*rho/2.0d0+rho2+rho3/3.0d0)*
# exp(-2.0d0*rho)
  I22s = cont*con1*S3ter
c [a|2s'2s]
  rho = (zet1s+zet2s)*ra*boh/2.0d0
  rho2 = rho**2.0d0
  rho3 = rho**3.0d0
  cont = (1.0d0+t12s)**2.5d0*(1.0d0-t12s)**2.5d0
  con1 = (zet1s+zet2s)/(rho*2.0d0)
  S3ter = 1.0d0-(1.0d0+3.0d0*rho/2.0d0+rho2+rho3/3.0d0)*
# exp(-2.0d0*rho)
  I12s = cont*con1*S3ter
c [a|2s'2s']
  rho = zet1s*ra*boh
  rho2 = rho**2.0d0
  rho3 = rho**3.0d0
  cont = 1.0d0
  con1 = zet1s/rho
  S3ter = 1.0d0-(1.0d0+3.0d0*rho/2.0d0+rho2+rho3/3.0d0)*
# exp(-2.0d0*rho)
  I11s = cont*con1*S3ter
  In2s = 2.0d0*(I22s-2.0d0*ovrs*I12s+ovrs**2.0d0*I11s)*Ns
c [a|2p2p]
  rho = zet2p*ra*boh

```

```

rho2 = rho**2.0d0
rho3 = rho**3.0d0
rho4 = rho**4.0d0
rho5 = rho**5.0d0
cont = 1.0d0
con1 = zet2p/rho
con2 = 3.0d0*zet2p/rho3
con3 = (3.0d0/2.0d0)*zet2p/rho3
S3ter = 1.0d0-(1.0d0+3.0d0*rho/2.0d0+rho2+rho3/3.0d0)*
# exp(-2.0d0*rho)
D3ter = 1.0d0-(1.0d0+2.0d0*rho+2.0d0*rho2+4.0d0*rho3/
# 3.0d0+2.0d0*rho4/3.0d0+2.0d0*rho5/9.0d0)*
# exp(-2.0d0*rho)
Ipsig = cont*(con1*S3ter+con2*D3ter)
Ippi = cont*(con1*S3ter-con3*D3ter)
Cpsig = cosa2*Ipsig+sina2*Ippi
Cppi = sina2*Ipsig+cosa2*Ippi
I22p = 2.0d0*Ippi+Cpsig+2.0d0*Cppi
c [a|2p'2p]
rho = (zet1p+zet2p)*ra*boh/2.0d0
rho2 = rho**2.0d0
rho3 = rho**3.0d0
rho4 = rho**4.0d0
rho5 = rho**5.0d0
cont = (1.0d0+t12p)**2.5d0*(1.0d0-t12p)**2.5d0
con1 = (zet1p+zet2p)/(rho*2.0d0)
con2 = 3.0d0*(zet1p+zet2p)/(rho3*2.0d0)
con3 = (3.0d0/2.0d0)*(zet1p+zet2p)/(rho3*2.0d0)
S3ter = 1.0d0-(1.0d0+3.0d0*rho/2.0d0+rho2+rho3/3.0d0)*
# exp(-2.0d0*rho)
D3ter = 1.0d0-(1.0d0+2.0d0*rho+2.0d0*rho2+4.0d0*rho3/
# 3.0d0+2.0d0*rho4/3.0d0+2.0d0*rho5/9.0d0)*
# exp(-2.0d0*rho)
Ipsig = cont*(con1*S3ter+con2*D3ter)
Ippi = cont*(con1*S3ter-con3*D3ter)
Cpsig = cosa2*Ipsig+sina2*Ippi
Cppi = sina2*Ipsig+cosa2*Ippi
I12p = 2.0d0*Ippi+Cpsig+2.0d0*Cppi
c [a|2p'2p']
rho = zet1p*ra*boh
rho2 = rho**2.0d0
rho3 = rho**3.0d0
rho4 = rho**4.0d0
rho5 = rho**5.0d0
cont = 1.0d0
con1 = zet1p/rho
con2 = 3.0d0*zet1p/rho3
con3 = (3.0d0/2.0d0)*zet1p/rho3
S3ter = 1.0d0-(1.0d0+3.0d0*rho/2.0d0+rho2+rho3/3.0d0)*
# exp(-2.0d0*rho)
D3ter = 1.0d0-(1.0d0+2.0d0*rho+2.0d0*rho2+4.0d0*rho3/
# 3.0d0+2.0d0*rho4/3.0d0+2.0d0*rho5/9.0d0)*
# exp(-2.0d0*rho)
Ipsig = cont*(con1*S3ter+con2*D3ter)
Ippi = cont*(con1*S3ter-con3*D3ter)
Cpsig = cosa2*Ipsig+sina2*Ippi
Cppi = sina2*Ipsig+cosa2*Ippi

```



```

I11p = 2.0d0*Ippi+Cpsig+2.0d0*Cppi
In2p = (I22p-2.0d0*ovrp*I12p+ovrp**2.0d0*I11p)*Np
ESP = In2s+In2p+nuc
write(*,200) In2s,I22p,nuc,ESP*627.51d0
10 continue
200 format(4f13.7)

write(*,*) ' '

do 20 i=0,20
  phia = i+0.0d0
  phia = (phia*10.0d0+80.0d0)*(pi/180.0d0)
  j = 9
  the = j+0.0d0
  the = the*10.0d0*(pi/180.0d0)
  ra = 2.899d0
  cosa = cos(phia)
  cosa2 = cosa**2.0d0
  sina = sin(phia)
  sina2 = sina**2.0d0
  nuc = -7.0d0/(ra*boh)
c [a|2s2s]
  rho = zet2s*ra*boh
  rho2 = rho**2.0d0
  rho3 = rho**3.0d0
  cont = 1.0d0
  con1 = zet2s/rho
  S3ter = 1.0d0-(1.0d0+3.0d0*rho/2.0d0+rho2+rho3/3.0d0)*
# exp(-2.0d0*rho)
  I22s = cont*con1*S3ter
c [a|2s'2s]
  rho = (zet1s+zet2s)*ra*boh/2.0d0
  rho2 = rho**2.0d0
  rho3 = rho**3.0d0
  cont = (1.0d0+t12s)**2.5d0*(1.0d0-t12s)**2.5d0
  con1 = (zet1s+zet2s)/(rho*2.0d0)
  S3ter = 1.0d0-(1.0d0+3.0d0*rho/2.0d0+rho2+rho3/3.0d0)*
# exp(-2.0d0*rho)
  I12s = cont*con1*S3ter
c [a|2s'2s']
  rho = zet1s*ra*boh
  rho2 = rho**2.0d0
  rho3 = rho**3.0d0
  cont = 1.0d0
  con1 = zet1s/rho
  S3ter = 1.0d0-(1.0d0+3.0d0*rho/2.0d0+rho2+rho3/3.0d0)*
# exp(-2.0d0*rho)
  I11s = cont*con1*S3ter
  In2s = 2.0d0*(I22s-2.0d0*ovrs*I12s+ovrs**2.0d0*I11s)*Ns
c [a|2p2p]
  rho = zet2p*ra*boh
  rho2 = rho**2.0d0
  rho3 = rho**3.0d0
  rho4 = rho**4.0d0
  rho5 = rho**5.0d0
  cont = 1.0d0
  con1 = zet2p/rho

```

```

con2 = 3.0d0*zet2p/rho3
con3 = (3.0d0/2.0d0)*zet2p/rho3
S3ter = 1.0d0-(1.0d0+3.0d0*rho/2.0d0+rho2+rho3/3.0d0)*
# exp(-2.0d0*rho)
D3ter = 1.0d0-(1.0d0+2.0d0*rho+2.0d0*rho2+4.0d0*rho3/
# 3.0d0+2.0d0*rho4/3.0d0+2.0d0*rho5/9.0d0)*
# exp(-2.0d0*rho)
Ipsig = cont*(con1*S3ter+con2*D3ter)
Ippi = cont*(con1*S3ter-con3*D3ter)
Cpsig = cosa2*Ipsig+sina2*Ippi
Cppi = sina2*Ipsig+cosa2*Ippi
I22p = 2.0d0*Ippi+Cpsig+2.0d0*Cppi
c [a|2p'2p]
rho = (zet1p+zet2p)*ra*boh/2.0d0
rho2 = rho**2.0d0
rho3 = rho**3.0d0
rho4 = rho**4.0d0
rho5 = rho**5.0d0
cont = (1.0d0+t12p)**2.5d0*(1.0d0-t12p)**2.5d0
con1 = (zet1p+zet2p)/(rho*2.0d0)
con2 = 3.0d0*(zet1p+zet2p)/(rho3*2.0d0)
con3 = (3.0d0/2.0d0)*(zet1p+zet2p)/(rho3*2.0d0)
S3ter = 1.0d0-(1.0d0+3.0d0*rho/2.0d0+rho2+rho3/3.0d0)*
# exp(-2.0d0*rho)
D3ter = 1.0d0-(1.0d0+2.0d0*rho+2.0d0*rho2+4.0d0*rho3/
# 3.0d0+2.0d0*rho4/3.0d0+2.0d0*rho5/9.0d0)*
# exp(-2.0d0*rho)
Ipsig = cont*(con1*S3ter+con2*D3ter)
Ippi = cont*(con1*S3ter-con3*D3ter)
Cpsig = cosa2*Ipsig+sina2*Ippi
Cppi = sina2*Ipsig+cosa2*Ippi
I12p = 2.0d0*Ippi+Cpsig+2.0d0*Cppi
c [a|2p'2p']
rho = zet1p*ra*boh
rho2 = rho**2.0d0
rho3 = rho**3.0d0
rho4 = rho**4.0d0
rho5 = rho**5.0d0
cont = 1.0d0
con1 = zet1p/rho
con2 = 3.0d0*zet1p/rho3
con3 = (3.0d0/2.0d0)*zet1p/rho3
S3ter = 1.0d0-(1.0d0+3.0d0*rho/2.0d0+rho2+rho3/3.0d0)*
# exp(-2.0d0*rho)
D3ter = 1.0d0-(1.0d0+2.0d0*rho+2.0d0*rho2+4.0d0*rho3/
# 3.0d0+2.0d0*rho4/3.0d0+2.0d0*rho5/9.0d0)*
# exp(-2.0d0*rho)
Ipsig = cont*(con1*S3ter+con2*D3ter)
Ippi = cont*(con1*S3ter-con3*D3ter)
Cpsig = cosa2*Ipsig+sina2*Ippi
Cppi = sina2*Ipsig+cosa2*Ippi
I11p = 2.0d0*Ippi+Cpsig+2.0d0*Cppi
In2p = (I22p-2.0d0*ovrp*I12p+ovrp**2.0d0*I11p)*Np
ESP = In2s+In2p+nuc
write(*,200) In2s,I22p,nuc,ESP*627.51d0
20 continue

```

```
stop
end
```

```
Program Model_ESP_Br
```

```
implicit none
```

```
real*8 pi,ang,boh,zet2s,zet1s,zet2p,zet1p,t22s,t12s
real*8 t11s,t22p,t12p,t11p,ovrs,ovrp,Ns,Np,xBr,yBr,zBr
real*8 phi a,the,ra,xHe,yHe,zHe,cosa,cosa2,sina,sina2
real*8 nuc,rho,rho2,rho3,rho4,rho5,cont,con1,con2,con3
real*8 S3ter,D3ter,I22s,I12s,I11s,Ipsig,Ippi,Cpsig
real*8 Cppi,I22p,I12p,I11p,In2s,In2p,ESP
integer*4 i,j,k
```

```
pi = 2.0d0*dacos(0.0d0)
ang = 0.5291771d0
boh = 1/ang
```

```
zet1s = 4.357680d0
zet2s = 1.896394d0
zet1p = 4.362203d0
zet2p = 1.272221d0
t22s = 0.0d0
t12s = (zet1s-zet2s)/(zet1s+zet2s)
t11s = 0.0d0
t22p = 0.0d0
t12p = (zet1p-zet2p)/(zet1p+zet2p)
t11p = 0.0d0
ovrs = (1.0d0+t12s)**2.5d0*(1.0d0-t12s)**2.5d0
ovrp = (1.0d0+t12p)**2.5d0*(1.0d0-t12p)**2.5d0
Ns = 1.0d0/(1.0d0-ovrs**2.0d0)
Np = 1.0d0/(1.0d0-ovrp**2.0d0)
```

```
do 10 k=0,20
  i = 18
  phia = i+0.0d0
  phia = phia*10.0d0*(pi/180.0d0)
  j = 9
  the = j+0.0d0
  the = the*10.0d0*(pi/180.0d0)
  ra = k+0.0d0
  ra = ra*0.20d0+1.6d0
  cosa = cos(phia)
  cosa2 = cosa**2.0d0
  sina = sin(phia)
  sina2 = sina**2.0d0
  nuc = -7.0d0/(ra*boh)
```

```
c [a|2s2s]
  rho = zet2s*ra*boh
  rho2 = rho**2.0d0
  rho3 = rho**3.0d0
  cont = 1.0d0
  con1 = zet2s/rho
  S3ter = 1.0d0-(1.0d0+3.0d0*rho/2.0d0+rho2+rho3/3.0d0)*
# exp(-2.0d0*rho)
```

```

c      I22s = cont*con1*S3ter
c      [a|2s'2s]
      rho  = (zet1s+zet2s)*ra*boh/2.0d0
      rho2 = rho**2.0d0
      rho3 = rho**3.0d0
      cont = (1.0d0+t12s)**2.5d0*(1.0d0-t12s)**2.5d0
      con1 = (zet1s+zet2s)/(rho*2.0d0)
      S3ter = 1.0d0-(1.0d0+3.0d0*rho/2.0d0+rho2+rho3/3.0d0)*
#      exp(-2.0d0*rho)
      I12s = cont*con1*S3ter
c      [a|2s'2s']
      rho  = zet1s*ra*boh
      rho2 = rho**2.0d0
      rho3 = rho**3.0d0
      cont = 1.0d0
      con1 = zet1s/rho
      S3ter = 1.0d0-(1.0d0+3.0d0*rho/2.0d0+rho2+rho3/3.0d0)*
#      exp(-2.0d0*rho)
      I11s = cont*con1*S3ter
      In2s = 2.0d0*(I22s-2.0d0*ovrs*I12s+ovrs**2.0d0*I11s)*Ns
c      [a|2p2p]
      rho  = zet2p*ra*boh
      rho2 = rho**2.0d0
      rho3 = rho**3.0d0
      rho4 = rho**4.0d0
      rho5 = rho**5.0d0
      cont = 1.0d0
      con1 = zet2p/rho
      con2 = 3.0d0*zet2p/rho3
      con3 = (3.0d0/2.0d0)*zet2p/rho3
      S3ter = 1.0d0-(1.0d0+3.0d0*rho/2.0d0+rho2+rho3/3.0d0)*
#      exp(-2.0d0*rho)
      D3ter = 1.0d0-(1.0d0+2.0d0*rho+2.0d0*rho2+4.0d0*rho3/
#      3.0d0+2.0d0*rho4/3.0d0+2.0d0*rho5/9.0d0)*
#      exp(-2.0d0*rho)
      Ipsig = cont*(con1*S3ter+con2*D3ter)
      Ippi  = cont*(con1*S3ter-con3*D3ter)
      Cpsig = cosa2*Ipsig+sina2*Ippi
      Cppi  = sina2*Ipsig+cosa2*Ippi
      I22p = 2.0d0*Ippi+Cpsig+2.0d0*Cppi
c      [a|2p'2p]
      rho  = (zet1p+zet2p)*ra*boh/2.0d0
      rho2 = rho**2.0d0
      rho3 = rho**3.0d0
      rho4 = rho**4.0d0
      rho5 = rho**5.0d0
      cont = (1.0d0+t12p)**2.5d0*(1.0d0-t12p)**2.5d0
      con1 = (zet1p+zet2p)/(rho*2.0d0)
      con2 = 3.0d0*(zet1p+zet2p)/(rho3*2.0d0)
      con3 = (3.0d0/2.0d0)*(zet1p+zet2p)/(rho3*2.0d0)
      S3ter = 1.0d0-(1.0d0+3.0d0*rho/2.0d0+rho2+rho3/3.0d0)*
#      exp(-2.0d0*rho)
      D3ter = 1.0d0-(1.0d0+2.0d0*rho+2.0d0*rho2+4.0d0*rho3/
#      3.0d0+2.0d0*rho4/3.0d0+2.0d0*rho5/9.0d0)*
#      exp(-2.0d0*rho)
      Ipsig = cont*(con1*S3ter+con2*D3ter)
      Ippi  = cont*(con1*S3ter-con3*D3ter)

```

```

Cpsig = cosa2*Ipsig+sina2*Ippi
Cppi  = sina2*Ipsig+cosa2*Ippi
I12p  = 2.0d0*Ippi+Cpsig+2.0d0*Cppi
c      [a|2p'2p']
rho    = zet1p*ra*boh
rho2   = rho**2.0d0
rho3   = rho**3.0d0
rho4   = rho**4.0d0
rho5   = rho**5.0d0
cont   = 1.0d0
con1   = zet1p/rho
con2   = 3.0d0*zet1p/rho3
con3   = (3.0d0/2.0d0)*zet1p/rho3
S3ter  = 1.0d0-(1.0d0+3.0d0*rho/2.0d0+rho2+rho3/3.0d0)*
#      exp(-2.0d0*rho)
D3ter  = 1.0d0-(1.0d0+2.0d0*rho+2.0d0*rho2+4.0d0*rho3/
#      3.0d0+2.0d0*rho4/3.0d0+2.0d0*rho5/9.0d0)*
#      exp(-2.0d0*rho)
Ipsig  = cont*(con1*S3ter+con2*D3ter)
Ippi   = cont*(con1*S3ter-con3*D3ter)
Cpsig  = cosa2*Ipsig+sina2*Ippi
Cppi   = sina2*Ipsig+cosa2*Ippi
I11p   = 2.0d0*Ippi+Cpsig+2.0d0*Cppi
In2p   = (I22p-2.0d0*ovrp*I12p+ovrp**2.0d0*I11p)*Np
ESP    = In2s+In2p+nuc
write(*,200) In2s,I22p,nuc,ESP*627.51d0
10 continue
200 format(4f13.7)

write(*,*) ' '

do 20 i=0,20
  phia = i+0.0d0
  phia = (phia*10.0d0+80.0d0)*(pi/180.0d0)
  j     = 9
  the   = j+0.0d0
  the   = the*10.0d0*(pi/180.0d0)
  ra    = 3.115d0
  cosa  = cos(phia)
  cosa2 = cosa**2.0d0
  sina  = sin(phia)
  sina2 = sina**2.0d0
  nuc   = -7.0d0/(ra*boh)
c      [a|2s2s]
rho    = zet2s*ra*boh
rho2   = rho**2.0d0
rho3   = rho**3.0d0
cont   = 1.0d0
con1   = zet2s/rho
S3ter  = 1.0d0-(1.0d0+3.0d0*rho/2.0d0+rho2+rho3/3.0d0)*
#      exp(-2.0d0*rho)
I22s   = cont*con1*S3ter
c      [a|2s'2s]
rho    = (zet1s+zet2s)*ra*boh/2.0d0
rho2   = rho**2.0d0
rho3   = rho**3.0d0
cont   = (1.0d0+t12s)**2.5d0*(1.0d0-t12s)**2.5d0

```

```

        con1 = (zet1s+zet2s)/(rho*2.0d0)
        S3ter = 1.0d0-(1.0d0+3.0d0*rho/2.0d0+rho2+rho3/3.0d0)*
#         exp(-2.0d0*rho)
        I12s = cont*con1*S3ter
c   [a|2s'2s']
        rho = zet1s*ra*boh
        rho2 = rho**2.0d0
        rho3 = rho**3.0d0
        cont = 1.0d0
        con1 = zet1s/rho
        S3ter = 1.0d0-(1.0d0+3.0d0*rho/2.0d0+rho2+rho3/3.0d0)*
#         exp(-2.0d0*rho)
        I11s = cont*con1*S3ter
        In2s = 2.0d0*(I22s-2.0d0*ovrs*I12s+ovrs**2.0d0*I11s)*Ns
c   [a|2p2p]
        rho = zet2p*ra*boh
        rho2 = rho**2.0d0
        rho3 = rho**3.0d0
        rho4 = rho**4.0d0
        rho5 = rho**5.0d0
        cont = 1.0d0
        con1 = zet2p/rho
        con2 = 3.0d0*zet2p/rho3
        con3 = (3.0d0/2.0d0)*zet2p/rho3
        S3ter = 1.0d0-(1.0d0+3.0d0*rho/2.0d0+rho2+rho3/3.0d0)*
#         exp(-2.0d0*rho)
        D3ter = 1.0d0-(1.0d0+2.0d0*rho+2.0d0*rho2+4.0d0*rho3/
#         3.0d0+2.0d0*rho4/3.0d0+2.0d0*rho5/9.0d0)*
#         exp(-2.0d0*rho)
        Ipsig = cont*(con1*S3ter+con2*D3ter)
        Ippi = cont*(con1*S3ter-con3*D3ter)
        Cpsig = cosa2*Ipsig+sina2*Ippi
        Cppi = sina2*Ipsig+cosa2*Ippi
        I22p = 2.0d0*Ippi+Cpsig+2.0d0*Cppi
c   [a|2p'2p]
        rho = (zet1p+zet2p)*ra*boh/2.0d0
        rho2 = rho**2.0d0
        rho3 = rho**3.0d0
        rho4 = rho**4.0d0
        rho5 = rho**5.0d0
        cont = (1.0d0+t12p)**2.5d0*(1.0d0-t12p)**2.5d0
        con1 = (zet1p+zet2p)/(rho*2.0d0)
        con2 = 3.0d0*(zet1p+zet2p)/(rho3*2.0d0)
        con3 = (3.0d0/2.0d0)*(zet1p+zet2p)/(rho3*2.0d0)
        S3ter = 1.0d0-(1.0d0+3.0d0*rho/2.0d0+rho2+rho3/3.0d0)*
#         exp(-2.0d0*rho)
        D3ter = 1.0d0-(1.0d0+2.0d0*rho+2.0d0*rho2+4.0d0*rho3/
#         3.0d0+2.0d0*rho4/3.0d0+2.0d0*rho5/9.0d0)*
#         exp(-2.0d0*rho)
        Ipsig = cont*(con1*S3ter+con2*D3ter)
        Ippi = cont*(con1*S3ter-con3*D3ter)
        Cpsig = cosa2*Ipsig+sina2*Ippi
        Cppi = sina2*Ipsig+cosa2*Ippi
        I12p = 2.0d0*Ippi+Cpsig+2.0d0*Cppi
c   [a|2p'2p']
        rho = zet1p*ra*boh
        rho2 = rho**2.0d0

```

```

rho3 = rho**3.0d0
rho4 = rho**4.0d0
rho5 = rho**5.0d0
cont = 1.0d0
con1 = zet1p/rho
con2 = 3.0d0*zet1p/rho3
con3 = (3.0d0/2.0d0)*zet1p/rho3
S3ter = 1.0d0-(1.0d0+3.0d0*rho/2.0d0+rho2+rho3/3.0d0)*
#      exp(-2.0d0*rho)
D3ter = 1.0d0-(1.0d0+2.0d0*rho+2.0d0*rho2+4.0d0*rho3/
#      3.0d0+2.0d0*rho4/3.0d0+2.0d0*rho5/9.0d0)*
#      exp(-2.0d0*rho)
Ipsig = cont*(con1*S3ter+con2*D3ter)
Ippi  = cont*(con1*S3ter-con3*D3ter)
Cpsig = cosa2*Ipsig+sina2*Ippi
Cppi  = sina2*Ipsig+cosa2*Ippi
I11p  = 2.0d0*Ippi+Cpsig+2.0d0*Cppi
In2p  = (I22p-2.0d0*ovrp*I12p+ovrp**2.0d0*I11p)*Np
ESP   = In2s+In2p+nuc
write(*,200) In2s,I22p,nuc,ESP*627.51d0
20 continue

stop
end

```

Program Model_ESP_I

implicit none

```

real*8 pi,ang,boh,zet2s,zet1s,zet2p,zet1p,t22s,t12s
real*8 t11s,t22p,t12p,t11p,ovrs,ovrp,Ns,Np,xI,yI,zI
real*8 phi a,the,ra,xHe,yHe,zHe,cosa,cosa2,sina,sina2
real*8 nuc,rho,rho2,rho3,rho4,rho5,cont,con1,con2,con3
real*8 S3ter,D3ter,I22s,I12s,I11s,Ipsig,Ippi,Cpsig
real*8 Cppi,I22p,I12p,I11p,In2s,In2p,ESP
integer*4 i,j,k

```

```

pi = 2.0d0*dacos(0.0d0)
ang = 0.5291771d0
boh = 1/ang

```

```

zet1s = 3.766487d0
zet2s = 1.739151d0
zet1p = 3.201268d0
zet2p = 1.165130d0
t22s = 0.0d0
t12s = (zet1s-zet2s)/(zet1s+zet2s)
t11s = 0.0d0
t22p = 0.0d0
t12p = (zet1p-zet2p)/(zet1p+zet2p)
t11p = 0.0d0
ovrs = (1.0d0+t12s)**2.5d0*(1.0d0-t12s)**2.5d0
ovrp = (1.0d0+t12p)**2.5d0*(1.0d0-t12p)**2.5d0
Ns = 1.0d0/(1.0d0-ovrs**2.0d0)
Np = 1.0d0/(1.0d0-ovrp**2.0d0)

```

```

do 10 k=0,20
  i    = 18
  phia = i+0.0d0
  phia = phia*10.0d0*(pi/180.0d0)
  j    = 9
  the  = j+0.0d0
  the  = the*10.0d0*(pi/180.0d0)
  ra   = k+0.0d0
  ra   = ra*0.20d0+1.6d0
  cosa = cos(phia)
  cosa2 = cosa**2.0d0
  sina  = sin(phia)
  sina2 = sina**2.0d0
  nuc   = -7.0d0/(ra*boh)
c    [a|2s2s]
      rho   = zet2s*ra*boh
      rho2  = rho**2.0d0
      rho3  = rho**3.0d0
      cont  = 1.0d0
      con1  = zet2s/rho
      S3ter = 1.0d0-(1.0d0+3.0d0*rho/2.0d0+rho2+rho3/3.0d0)*
#          exp(-2.0d0*rho)
      I22s  = cont*con1*S3ter
c    [a|2s'2s]
      rho   = (zet1s+zet2s)*ra*boh/2.0d0
      rho2  = rho**2.0d0
      rho3  = rho**3.0d0
      cont  = (1.0d0+t12s)**2.5d0*(1.0d0-t12s)**2.5d0
      con1  = (zet1s+zet2s)/(rho*2.0d0)
      S3ter = 1.0d0-(1.0d0+3.0d0*rho/2.0d0+rho2+rho3/3.0d0)*
#          exp(-2.0d0*rho)
      I12s  = cont*con1*S3ter
c    [a|2s'2s']
      rho   = zet1s*ra*boh
      rho2  = rho**2.0d0
      rho3  = rho**3.0d0
      cont  = 1.0d0
      con1  = zet1s/rho
      S3ter = 1.0d0-(1.0d0+3.0d0*rho/2.0d0+rho2+rho3/3.0d0)*
#          exp(-2.0d0*rho)
      I11s  = cont*con1*S3ter
      In2s  = 2.0d0*(I22s-2.0d0*ovrs*I12s+ovrs**2.0d0*I11s)*Ns
c    [a|2p2p]
      rho   = zet2p*ra*boh
      rho2  = rho**2.0d0
      rho3  = rho**3.0d0
      rho4  = rho**4.0d0
      rho5  = rho**5.0d0
      cont  = 1.0d0
      con1  = zet2p/rho
      con2  = 3.0d0*zet2p/rho3
      con3  = (3.0d0/2.0d0)*zet2p/rho3
      S3ter = 1.0d0-(1.0d0+3.0d0*rho/2.0d0+rho2+rho3/3.0d0)*
#          exp(-2.0d0*rho)
      D3ter = 1.0d0-(1.0d0+2.0d0*rho+2.0d0*rho2+4.0d0*rho3/
#          3.0d0+2.0d0*rho4/3.0d0+2.0d0*rho5/9.0d0)*
#          exp(-2.0d0*rho)

```



```

Ipsig = cont*(con1*S3ter+con2*D3ter)
Ippi  = cont*(con1*S3ter-con3*D3ter)
Cpsig = cosa2*Ipsig+sina2*Ippi
Cppi  = sina2*Ipsig+cosa2*Ippi
I22p  = 2.0d0*Ippi+Cpsig+2.0d0*Cppi
c      [a|2p'2p]
rho    = (zet1p+zet2p)*ra*boh/2.0d0
rho2   = rho**2.0d0
rho3   = rho**3.0d0
rho4   = rho**4.0d0
rho5   = rho**5.0d0
cont   = (1.0d0+t12p)**2.5d0*(1.0d0-t12p)**2.5d0
con1   = (zet1p+zet2p)/(rho*2.0d0)
con2   = 3.0d0*(zet1p+zet2p)/(rho3*2.0d0)
con3   = (3.0d0/2.0d0)*(zet1p+zet2p)/(rho3*2.0d0)
S3ter  = 1.0d0-(1.0d0+3.0d0*rho/2.0d0+rho2+rho3/3.0d0)*
#      exp(-2.0d0*rho)
D3ter  = 1.0d0-(1.0d0+2.0d0*rho+2.0d0*rho2+4.0d0*rho3/
#      3.0d0+2.0d0*rho4/3.0d0+2.0d0*rho5/9.0d0)*
#      exp(-2.0d0*rho)
Ipsig  = cont*(con1*S3ter+con2*D3ter)
Ippi   = cont*(con1*S3ter-con3*D3ter)
Cpsig  = cosa2*Ipsig+sina2*Ippi
Cppi   = sina2*Ipsig+cosa2*Ippi
I12p   = 2.0d0*Ippi+Cpsig+2.0d0*Cppi
c      [a|2p'2p']
rho    = zet1p*ra*boh
rho2   = rho**2.0d0
rho3   = rho**3.0d0
rho4   = rho**4.0d0
rho5   = rho**5.0d0
cont   = 1.0d0
con1   = zet1p/rho
con2   = 3.0d0*zet1p/rho3
con3   = (3.0d0/2.0d0)*zet1p/rho3
S3ter  = 1.0d0-(1.0d0+3.0d0*rho/2.0d0+rho2+rho3/3.0d0)*
#      exp(-2.0d0*rho)
D3ter  = 1.0d0-(1.0d0+2.0d0*rho+2.0d0*rho2+4.0d0*rho3/
#      3.0d0+2.0d0*rho4/3.0d0+2.0d0*rho5/9.0d0)*
#      exp(-2.0d0*rho)
Ipsig  = cont*(con1*S3ter+con2*D3ter)
Ippi   = cont*(con1*S3ter-con3*D3ter)
Cpsig  = cosa2*Ipsig+sina2*Ippi
Cppi   = sina2*Ipsig+cosa2*Ippi
I11p   = 2.0d0*Ippi+Cpsig+2.0d0*Cppi
In2p   = (I22p-2.0d0*ovrp*I12p+ovrp**2.0d0*I11p)*Np
ESP    = In2s+In2p+nuc
write(*,200) In2s,I22p,nuc,ESP*627.51d0
10 continue
200 format(4f13.7)

write(*,*) ' '

do 20 i=0,20
  phia = i+0.0d0
  phia = (phia*10.0d0+80.0d0)*(pi/180.0d0)
  j    = 9

```

```

the = j+0.0d0
the = the*10.0d0*(pi/180.0d0)
ra = 3.396d0
cosa = cos(phia)
cosa2 = cosa**2.0d0
sina = sin(phia)
sina2 = sina**2.0d0
nuc = -7.0d0/(ra*boh)
c [a|2s2s]
rho = zet2s*ra*boh
rho2 = rho**2.0d0
rho3 = rho**3.0d0
cont = 1.0d0
con1 = zet2s/rho
S3ter = 1.0d0-(1.0d0+3.0d0*rho/2.0d0+rho2+rho3/3.0d0)*
# exp(-2.0d0*rho)
I22s = cont*con1*S3ter
c [a|2s'2s]
rho = (zet1s+zet2s)*ra*boh/2.0d0
rho2 = rho**2.0d0
rho3 = rho**3.0d0
cont = (1.0d0+t12s)**2.5d0*(1.0d0-t12s)**2.5d0
con1 = (zet1s+zet2s)/(rho*2.0d0)
S3ter = 1.0d0-(1.0d0+3.0d0*rho/2.0d0+rho2+rho3/3.0d0)*
# exp(-2.0d0*rho)
I12s = cont*con1*S3ter
c [a|2s'2s']
rho = zet1s*ra*boh
rho2 = rho**2.0d0
rho3 = rho**3.0d0
cont = 1.0d0
con1 = zet1s/rho
S3ter = 1.0d0-(1.0d0+3.0d0*rho/2.0d0+rho2+rho3/3.0d0)*
# exp(-2.0d0*rho)
I11s = cont*con1*S3ter
In2s = 2.0d0*(I22s-2.0d0*ovrs*I12s+ovrs**2.0d0*I11s)*Ns
c [a|2p2p]
rho = zet2p*ra*boh
rho2 = rho**2.0d0
rho3 = rho**3.0d0
rho4 = rho**4.0d0
rho5 = rho**5.0d0
cont = 1.0d0
con1 = zet2p/rho
con2 = 3.0d0*zet2p/rho3
con3 = (3.0d0/2.0d0)*zet2p/rho3
S3ter = 1.0d0-(1.0d0+3.0d0*rho/2.0d0+rho2+rho3/3.0d0)*
# exp(-2.0d0*rho)
D3ter = 1.0d0-(1.0d0+2.0d0*rho+2.0d0*rho2+4.0d0*rho3/
# 3.0d0+2.0d0*rho4/3.0d0+2.0d0*rho5/9.0d0)*
# exp(-2.0d0*rho)
Ipsig = cont*(con1*S3ter+con2*D3ter)
Ippi = cont*(con1*S3ter-con3*D3ter)
Cpsig = cosa2*Ipsig+sina2*Ippi
Cppi = sina2*Ipsig+cosa2*Ippi
I22p = 2.0d0*Ippi+Cpsig+2.0d0*Cppi
c [a|2p'2p]

```

```

rho   = (zet1p+zet2p)*ra*boh/2.0d0
rho2  = rho**2.0d0
rho3  = rho**3.0d0
rho4  = rho**4.0d0
rho5  = rho**5.0d0
cont  = (1.0d0+t12p)**2.5d0*(1.0d0-t12p)**2.5d0
con1  = (zet1p+zet2p)/(rho*2.0d0)
con2  = 3.0d0*(zet1p+zet2p)/(rho3*2.0d0)
con3  = (3.0d0/2.0d0)*(zet1p+zet2p)/(rho3*2.0d0)
S3ter = 1.0d0-(1.0d0+3.0d0*rho/2.0d0+rho2+rho3/3.0d0)*
#      exp(-2.0d0*rho)
D3ter = 1.0d0-(1.0d0+2.0d0*rho+2.0d0*rho2+4.0d0*rho3/
#      3.0d0+2.0d0*rho4/3.0d0+2.0d0*rho5/9.0d0)*
#      exp(-2.0d0*rho)
Ipsig = cont*(con1*S3ter+con2*D3ter)
Ippi  = cont*(con1*S3ter-con3*D3ter)
Cpsig = cosa2*Ipsig+sina2*Ippi
Cppi  = sina2*Ipsig+cosa2*Ippi
I12p  = 2.0d0*Ippi+Cpsig+2.0d0*Cppi
c      [a|2p'2p']
rho   = zet1p*ra*boh
rho2  = rho**2.0d0
rho3  = rho**3.0d0
rho4  = rho**4.0d0
rho5  = rho**5.0d0
cont  = 1.0d0
con1  = zet1p/rho
con2  = 3.0d0*zet1p/rho3
con3  = (3.0d0/2.0d0)*zet1p/rho3
S3ter = 1.0d0-(1.0d0+3.0d0*rho/2.0d0+rho2+rho3/3.0d0)*
#      exp(-2.0d0*rho)
D3ter = 1.0d0-(1.0d0+2.0d0*rho+2.0d0*rho2+4.0d0*rho3/
#      3.0d0+2.0d0*rho4/3.0d0+2.0d0*rho5/9.0d0)*
#      exp(-2.0d0*rho)
Ipsig = cont*(con1*S3ter+con2*D3ter)
Ippi  = cont*(con1*S3ter-con3*D3ter)
Cpsig = cosa2*Ipsig+sina2*Ippi
Cppi  = sina2*Ipsig+cosa2*Ippi
I11p  = 2.0d0*Ippi+Cpsig+2.0d0*Cppi
In2p  = (I22p-2.0d0*ovrp*I12p+ovrp**2.0d0*I11p)*Np
ESP   = In2s+In2p+nuc
write(*,200) In2s,I22p,nuc,ESP*627.51d0
20 continue

stop
end

```

Program A4.3. The Fortran 77 programs developed to calculate the ESP of fluorine with a partial charge and additional dipole moment as a function of atomic radii and angle relative to

$$\phi_{2p\sigma}$$

```
Program Model_ESP_F
```

```
implicit none
```

```

real*8 pi,ang,boh,zet2s,zet1s,zet2p,zet1p,t22s,t12s
real*8 t11s,t22p,t12p,t11p,ovrs,ovrp,Ns,Np,xF,yF,zF
real*8 phi a,the,ra,xHe,yHe,zHe,cosa,cosa2,sina,sina2
real*8 nuc,rho,rho2,rho3,rho4,rho5,cont,con1,con2,con3
real*8 S3ter,D3ter,I22s,I12s,I11s,Ipsig,Ippi,Cpsig
real*8 Cppi,I22p,I12p,I11p,In2s,In2p,ESP
real*8 zero,amax,step,dist
real*8 zplus,yplus,rplus,eplus
integer*4 i,j,k

pi = 2.0d0*dacos(0.0d0)
ang = 0.5291771d0
boh = 1/ang

dist=0.93d0+1.40d0
c dist=1.47d0+1.40d0

zet1s = 14.043877d0
zet2s = 2.111385d0
zet2p = 2.182682d0
t22s = 0.0d0
t12s = (zet1s-zet2s)/(zet1s+zet2s)
t11s = 0.0d0
t22p = 0.0d0
ovrs = (1.0d0+t12s)**2.5d0*(1.0d0-t12s)**2.5d0
Ns = 1.0d0/(1.0d0-ovrs**2.0d0)

do 10 k=0,20
  i = 18
  phia = i+0.0d0
  phia = phia*10.0d0*(pi/180.0d0)
  j = 9
  the = j+0.0d0
  the = the*10.0d0*(pi/180.0d0)
  ra = k+0.0d0
  ra = ra*0.20d0+1.6d0
  cosa = cos(phia)
  cosa2 = cosa**2.0d0
  sina = sin(phia)
  sina2 = sina**2.0d0
  nuc = -7.0d0/(ra*boh)
c [a|2s2s]
  rho = zet2s*ra*boh
  rho2 = rho**2.0d0
  rho3 = rho**3.0d0
  cont = 1.0d0
  con1 = zet2s/rho
  S3ter = 1.0d0-(1.0d0+3.0d0*rho/2.0d0+rho2+rho3/3.0d0)*
# exp(-2.0d0*rho)
  I22s = cont*con1*S3ter
c [a|2s'2s]
  rho = (zet1s+zet2s)*ra*boh/2.0d0
  rho2 = rho**2.0d0
  rho3 = rho**3.0d0
  cont = (1.0d0+t12s)**2.5d0*(1.0d0-t12s)**2.5d0
  con1 = (zet1s+zet2s)/(rho*2.0d0)
  S3ter = 1.0d0-(1.0d0+3.0d0*rho/2.0d0+rho2+rho3/3.0d0)*

```

```

#          exp(-2.0d0*rho)
I12s = cont*con1*S3ter
c  [a|2s'2s']
rho   = zet1s*ra*boh
rho2  = rho**2.0d0
rho3  = rho**3.0d0
cont  = 1.0d0
con1  = zet1s/rho
S3ter = 1.0d0-(1.0d0+3.0d0*rho/2.0d0+rho2+rho3/3.0d0)*
#          exp(-2.0d0*rho)
I11s = cont*con1*S3ter
In2s = 2.0d0*(I22s-2.0d0*ovrs*I12s+ovrs**2.0d0*I11s)*Ns
c  [a|2p2p]
rho   = zet2p*ra*boh
rho2  = rho**2.0d0
rho3  = rho**3.0d0
rho4  = rho**4.0d0
rho5  = rho**5.0d0
cont  = 1.0d0
con1  = zet2p/rho
con2  = 3.0d0*zet2p/rho3
con3  = (3.0d0/2.0d0)*zet2p/rho3
S3ter = 1.0d0-(1.0d0+3.0d0*rho/2.0d0+rho2+rho3/3.0d0)*
#          exp(-2.0d0*rho)
D3ter = 1.0d0-(1.0d0+2.0d0*rho+2.0d0*rho2+4.0d0*rho3/
#          3.0d0+2.0d0*rho4/3.0d0+2.0d0*rho5/9.0d0)*
#          exp(-2.0d0*rho)
Ipsig = cont*(con1*S3ter+con2*D3ter)
Ippi  = cont*(con1*S3ter-con3*D3ter)
Cpsig = cosa2*Ipsig+sina2*Ippi
Cppi  = sina2*Ipsig+cosa2*Ippi
I22p  = 2.0d0*Ippi+Cpsig+2.0d0*Cppi
Esp   = In2s+I22p+nuc
c  write(*,200) In2s,I22p,nuc,Esp*627.51d0
10 continue
200 format(4f13.7)

write(*,*) ' R T Num'

do 20 i=0,20
  phia = i+0.0d0
  phia = (phia*10.0d0+80.0d0)*(pi/180.0d0)
  j     = 9
  the  = j+0.0d0
  the  = the*10.0d0*(pi/180.0d0)
  do 15 k=0,20
c  ra   = 2.082d0
    zero=0.8*dist
    amax=1.1*dist
    step=(amax-zero)/20.0d0
    ra   = k+0.0d0
c  ra   = ra*0.05d0+2.4d0
    ra   = ra*step+zero
    xHe  = xF+ra*sin(phia)*cos(the)
    yHe  = yF+ra*sin(phia)*sin(the)
    zHe  = zF+ra*cos(phia)
    cosa = cos(phia)

```

```

        cosa2 = cosa**2.0d0
        sina  = sin(phia)
        sina2 = sina**2.0d0
        nuc   = -7.0d0/(ra*boh)
c      [a|2s2s]
        rho   = zet2s*ra*boh
        rho2  = rho**2.0d0
        rho3  = rho**3.0d0
        cont  = 1.0d0
        con1  = zet2s/rho
        S3ter = 1.0d0-(1.0d0+3.0d0*rho/2.0d0+rho2+rho3/3.0d0)*
#         exp(-2.0d0*rho)
        I22s = cont*con1*S3ter
c      [a|2s'2s]
        rho   = (zet1s+zet2s)*ra*boh/2.0d0
        rho2  = rho**2.0d0
        rho3  = rho**3.0d0
        cont  = (1.0d0+t12s)**2.5d0*(1.0d0-t12s)**2.5d0
        con1  = (zet1s+zet2s)/(rho*2.0d0)
        S3ter = 1.0d0-(1.0d0+3.0d0*rho/2.0d0+rho2+rho3/3.0d0)*
#         exp(-2.0d0*rho)
        I12s = cont*con1*S3ter
c      [a|2s'2s']
        rho   = zet1s*ra*boh
        rho2  = rho**2.0d0
        rho3  = rho**3.0d0
        cont  = 1.0d0
        con1  = zet1s/rho
        S3ter = 1.0d0-(1.0d0+3.0d0*rho/2.0d0+rho2+rho3/3.0d0)*
#         exp(-2.0d0*rho)
        I11s = cont*con1*S3ter
        In2s = 2.0d0*(I22s-2.0d0*ovrs*I12s+ovrs**2.0d0*I11s)*Ns
c      [a|2p2p]
        rho   = zet2p*ra*boh
        rho2  = rho**2.0d0
        rho3  = rho**3.0d0
        rho4  = rho**4.0d0
        rho5  = rho**5.0d0
        cont  = 1.0d0
        con1  = zet2p/rho
        con2  = 3.0d0*zet2p/rho3
        con3  = (3.0d0/2.0d0)*zet2p/rho3
        S3ter = 1.0d0-(1.0d0+3.0d0*rho/2.0d0+rho2+rho3/3.0d0)*
#         exp(-2.0d0*rho)
#         D3ter = 1.0d0-(1.0d0+2.0d0*rho+2.0d0*rho2+4.0d0*rho3/
#         3.0d0+2.0d0*rho4/3.0d0+2.0d0*rho5/9.0d0)*
#         exp(-2.0d0*rho)
        Ipsig = cont*(con1*S3ter+con2*D3ter)
        Ippi  = cont*(con1*S3ter-con3*D3ter)
        Cpsig = cosa2*Ipsig+sina2*Ippi
        Cppi  = sina2*Ipsig+cosa2*Ippi
        I22p  = 2.0d0*Ippi+Cpsig+2.0d0*Cppi
c      add in plus of the dipole
        yplus=sina*ra
        zplus=(1.35d0-cosa*ra)
        rplus=sqrt(yplus*yplus+zplus*zplus)
c      eplus=0.194937d0/(rplus*boh)

```

```

        eplus=0.194937d0*(zet2p*exp(-2.0d0*rho)
$   +(exp(-2.0d0*rho)-1.0d0)/(ra*boh)
        eplus=eplus*cosa2
        Esp   = In2s+I22p+nuc
c       Esp   = In2s+I22p+nuc-eplus
        write(*,200) ra/dist,180.0d0*phia/pi,
$   eplus*627.51d0
c       write(*,200) ra/dist,180.0d0*phia/pi,
c   $   ESP*627.51d0
c       write(*,200) In2s,I22p,nuc,ESP*627.51d0
15 continue
20 continue

        stop
        end

```

APPENDIX 5

The necessary counterpoise corrected single point energies were calculated for the water- and ammonia-containing trimers and dimers at the MP2/aug-cc-pVTZ//MP2/aug-cc-pV5Z and MP2/aug-cc-pVTZ//APFD/aug-cc-pVTZ hybrid levels in order to discern ΔE_{COOP} , the latter of which will be the focus herein. The interaction energies of the AB and BC dimers were also found in the trimer geometry (ΔE_{AB}^{sp} and ΔE_{BC}^{sp}) for a better gauge of the process with which the system stabilized. The APFD method was of interest because it is a relatively new DFT functional that explicitly includes a correction for dispersion (ΔE_{APFD}^{disp}), allegedly making it cost efficient while reducing error, although it was found that the nonbonding energies (ΔE_{APFD}) and cooperativity were consistently greater than the MP2 energies (ΔE_{MP2}) (see Table A5.1), signifying that either the APFD method naturally overestimated the interaction or the MP2 method naturally underestimated the interaction. Because an expansive basis set was used in conjunction with the MP2 method when calculating the single point energies, it was assumed that the APFD method was overestimating the energy of the trimer system, and it was decided to inspect the method with which the interactions, including the dispersion, were being calculated.

Table A5.1. The cooperativity and interaction energies of optimized β -trimer and dimer systems of bromine with two orthogonal water and ammonia molecules.

	ΔE_{COOP} (kcal/mol)	ΔE_{ABC}^{opt} (kcal/mol)	ΔE_{AB}^{opt} (kcal/mol)	ΔE_{BC}^{opt} (kcal/mol)	ΔE_{AC}^{sp} (kcal/mol)	ΔE_{AB}^{sp} (kcal/mol)	ΔE_{BC}^{sp} (kcal/mol)
	ΔE_{APFD}						
H ₂ O	-0.169	-6.821	-4.288	-1.427	-0.937	-5.332	-1.437
NH ₃	-0.689	-11.573	-8.985	-0.966	-0.933	-9.126	-0.910
	ΔE_{APFD}^{disp}						
H ₂ O	-	-2.333	-1.250	-0.904	-0.105	-	-
NH ₃	-	-1.849	-0.836	-0.836	-0.147	-	-

The dispersion calculated via APFD can be simply extracted from the output file, where specifically, the APFD method is a linear combination of the B3PW91 and PBE1PBE functionals,

$$\Delta E_{\text{APFD}} = 0.411\Delta E_{\text{B3PW91}} + 0.589\Delta E_{\text{PBE1PBE}} + \Delta E^{\text{SAM}}$$

plus a correction for the dispersion (ΔE^{SAM}), found by the Spherical Atom Model. It is for these reasons that APFD has recently gained the reputation of being a computational method that calculates interaction energies within experimental error and in a reasonable amount of time.¹ The B3PW91 and PBE1PBE functionals were chosen because the former is consistently repulsive at long distance, and the latter is consistently attractive (see *Reference 1, Figure 1*). The dispersion,

$$\Delta E^{\text{SAM}}(R_{AB}) = \frac{C_{6,AB}}{(R_{AB}^2 - R_{s,AB}^2)^3} f(R_{AB})g(R_{AB})$$

$$C_{6,AB} = P_1 \left(\frac{3}{2}\right) \left(\frac{\epsilon_{H,A}\epsilon_{H,B}}{\epsilon_{H,A} + \epsilon_{H,B}}\right) \alpha_A \alpha_B$$

where the nonbonding interaction ($C_{6,AB}$) is calculated using the energies of the highest occupied molecular orbitals ($\epsilon_{H,A}$ and $\epsilon_{H,B}$) corresponding to atoms A and B , multiplied by the isotropic atomic polarizabilities (α_A and α_B) and a scaling factor (P_1) that is equal to 1.18604. The interaction is then divided by the difference of the distance between the atomic nuclei (R_{AB}) and the difference between the atomic surfaces ($R_{s,AB}$). As can be seen, when R_{AB} approaches $R_{s,AB}$ the dispersion becomes nonsensical. Therefore, a damping function ($f(R_{AB})$) was added to ΔE^{SAM} such that the dispersion between two atoms would go to zero if R_{AB} had contracted to a given percentage of $R_{s,AB}$. Because $f(R_{AB})$ was discontinuous at higher derivatives, a switching function ($g(R_{AB})$) was added as well such that caused the damping function to behave continuously.

Upon observing the calculated dispersion according to the APFD method (see Table 1), general trends in the results lead to starkly opposing conclusions to the electron correlation found according to the MP2 method, where the dispersion is consistently weaker between bromine and ammonia than bromine and water. When dissecting the step-by-step process of how ΔE^{SAM} had been calculated, and using the equation by hand, it was surprisingly found that the damping function had nullified the dispersion between most interacting atoms, as R_{AB} had been considered to be too close in value to $R_{s,AB}$. As a result, for example, the only dispersion terms in ΔE_{AB}^{opt} between bromine and ammonia that did not go to zero was of the nitrogen with distant bromine, and the hydrogens on ammonia with bromine. The dispersion between the atoms directly involved in the Lewis acid-base pair had not been counted due to the significant contraction of d_{AB} and d_{BC} from Σr_{vdW} , and as such ΔE^{SAM} did not provide much information on the nature of halogen bonding.

REFERENCES

- (1) Austin, A.; Petersson, G. A.; Frisch, M. J.; Dobek, F. J.; Scalmani, G.; Throssell, K. A Density Functional with Spherical Atom Dispersion Terms. *J. Chem. Theory Comput.* **2012**, *8*, 4989.
- (2) Arunan, E.; Desiraju, G. R.; Klein, R. A.; Sadlej, J.; Scheiner, S.; Alkorta, I.; Clary, D. C.; Crabtree, R. H.; Dannenberg, J. J.; Hobza, P.; et al. Definition of the Hydrogen Bond (IUPAC Recommendations 2011). *Pure Appl. Chem.* **2011**, *83*, 1637.
- (3) Desiraju, G. R.; Ho, P. S.; Kloo, L.; Legon, A. C.; Marquardt, R.; Metrangolo, P.; Politzer, P.; Resnati, G.; Rissanen, K. Definition of the Halogen Bond (IUPAC Recommendations 2013). *Pure Appl. Chem.* **2013**, *85*, 1711.

APPENDIX 6

Table A6.1. The electron correlation (ΔE_{MP2}^{corr}) of the β -trimer systems, comprised of singlet (ΔE_{MP2}^S) and triplet (ΔE_{MP2}^T) energetic components.

	ΔE_{ABC}^{opt} (kcal/mol)	ΔE_{AB}^{opt} (kcal/mol)	ΔE_{BC}^{opt} (kcal/mol)	ΔE_{AC}^{sp} (kcal/mol)
	ΔE_{MP2}^{corr}			
H ₂ O	-4.487	-2.641	-1.475	0.019
NH ₃	-8.544	-6.446	-1.243	-0.024
	ΔE_{MP2}^S			
H ₂ O	-0.948	-0.521	-0.370	0.017
NH ₃	-1.942	-1.437	-0.324	-0.006
	ΔE_{MP2}^T			
H ₂ O	-3.539	-2.120	-1.105	0.002
NH ₃	-6.602	-5.009	-0.919	-0.019